

THE DEVELOPMENT OF A
CONCEPTUAL MODEL FOR
CONTAMINANT TRANSPORT
IN THE DOLOSTONE UNDERLYING
SMITHVILLE, ONTARIO

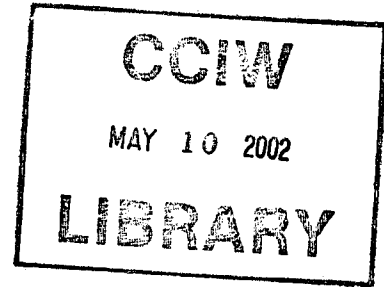
NO. 99-250 (1999)

18

Old out
maps

11 x 17

TD
226
N87
no.
99-250



THE DEVELOPMENT OF A CONCEPTUAL MODEL FOR CONTAMINANT TRANSPORT IN THE DOLOSTONE UNDERLYING SMITHVILLE, ONTARIO

by:

**Kent Novakowski¹, Pat Lapcevic², Greg Bickerton²,
John Voralek², Lavinia Zanini², and Charlie Talbot²**

©1999 Her Majesty the Queen in right of Ontario
as represented by the Minister of Environment

November 1, 1999

NWRI Cont. No 99-250

¹ Dept. of Earth Sciences, Brock University, St. Catharines, ON, L2S 3A1

² National Water Research Institute, Burlington, ON, L7R 4A6

The Development of a Conceptual Model for Contaminant Transport in the Dolostone Underlying Smithville, Ontario

MANAGEMENT PERSPECTIVE

Outcome: Conservation of biodiversity in healthy ecosystems

Results: Priority ecosystems are conserved and restored

Since 1995, the Groundwater group at NWRI has been involved in an extensive field and laboratory hydrogeological research program at the Smithville PCB site in Smithville, ON. We have completed the bulk of the field and lab work necessary to build a detailed conceptual model of the groundwater flow and contaminant transport in the fractured dolostone. This report is intended as a summary of our findings. It will be submitted to the Smithville Phase IV program as a final report and be incorporated into reports to the US EPA as required to meet our objectives for the funding received as part of multi-group study. The results of this research program will further our understanding of the hydrogeology of heterogeneous rock systems and improve our ability to predict and prevent the environmental effects of toxic substances in groundwater and help to conserve and restore priority ecosystems in the Great Lakes Basin.

The bulk of the field and lab work on this study has been completed. We are continuing monitoring of hydraulic heads in the region and are conducting some field experiments. The study has yielded a unique data set which will be amenable to further interpretations in the years to come. We expect to continue work on modelling studies and prepare journal articles on the work that has been carried out.

Développement d'un modèle conceptuel de transport des contaminants dans la dolomie sous-jacente à Smithville (Ont.)

SOMMAIRE À L'INTENTION DE LA DIRECTION

Issue : Préservation de la biodiversité dans des écosystèmes sains
Résultats : Les écosystèmes prioritaires sont préservés et restaurés

Depuis 1995, le groupe des eaux souterraines de l'INRE est engagé dans un vaste programme de recherche hydrogéologique en laboratoire et sur le terrain, au site de Smithville, en Ontario. Nous avons terminé le plus gros des travaux de laboratoire et de terrain nécessaires à l'établissement d'un modèle conceptuel détaillé de l'écoulement des eaux souterraines et du transport de contaminants dans la dolomie fracturée. Ce rapport présente un résumé de nos conclusions. Il constituera le rapport final de la phase IV de Smithville, et sera intégré comme demandé aux rapports de l'EPA des États-Unis pour que soient atteints nos objectifs aux termes du financement reçu pour l'étude pluridisciplinaire. Les résultats de ce programme de recherche feront avancer notre compréhension de l'hydrogéologie des systèmes rocheux hétérogènes et notre capacité à prévoir et éviter les effets environnementaux des substances toxiques présentes dans les eaux souterraines; de plus, ils aideront à préserver et restaurer les écosystèmes prioritaires du bassin des Grands Lacs.

L'essentiel des travaux de laboratoire et de terrain a été réalisé. Nous poursuivons la surveillance des charges hydrauliques de la région, et effectuons certaines expériences sur le terrain. L'étude a fourni un ensemble de données unique, qui se prêtera à des interprétations ultérieures dans les années à venir. Nous nous attendons à poursuivre les travaux de modélisation et préparons pour des journaux scientifiques des articles sur les travaux effectués.

ABSTRACT

Detailed characterization of the bedrock underlying the Smithville PCB site was carried out at several different scales using both laboratory and field techniques. Key to the field investigation was the installation of 18 new boreholes in and around the site. Six boreholes were instrumented with Westbay[®] multilevel instrumentation. Two cluster sites of 4-5 boreholes each were established to conduct experiments at the scale of 40-50 m. Boreholes installed 100-150 m from the South cluster site were used to investigate a larger field scale. Field testing included single and multiwell hydraulic techniques (constant head injection tests, pumping and pulse interference tests), tracer experiments and point-dilution experiments. Laboratory studies using rock core from the new boreholes included porosity measurements, diffusion experiments and the determination of organic carbon. Additionally, the Westbay[®] instrumented boreholes were used to measure the hydraulic head distribution both temporally and spatially in the study area. Inorganic and isotopic groundwater geochemistry was also investigated. The detailed data sets from both the field and lab investigations were used to develop a conceptual model for groundwater flow and solute transport in the fractured dolostone. This report presents our findings and is intended to be the final report on the study.

In summary, groundwater flow in the Lockport formation is predominated by horizontal bedding-plane fractures of significant lateral extent. Although the number of these features is not large (perhaps 5-8 depending on location), there is at least one lateral connection that allows for a continuous pathway over the regional scale. The vertical interconnection between this feature and other horizontal fractures is likely to be minimal but present with a horizon at mid-depth in the Lockport being potentially the most restrictive to vertical groundwater flow. Groundwater flowing in the fracture system above this horizon is likely recharged at specific locations up gradient from the site where the overburden thins, and perhaps elsewhere where direct contact between surface water and bedrock occurs. The groundwater velocity in the upper zone is relatively rapid (5-30 m/day), although the transport of aqueous-phase contaminants is considerably slower due to the effects of adsorption and particularly matrix diffusion. Groundwater migration in the zone below the low-permeability horizon at mid-depth, is likely to be much slower, possibly restricted by weaker interconnections in the horizontal direction. Groundwater in this zone is of poorer quality and exhibits isotopic shifts that suggest older water and slower migration. Interaction between the groundwater in this zone and Twenty Mile Creek is probably non-existent (i.e. the groundwater under-flows the Creek). The migration of aqueous phase contamination in this zone will be very restricted in comparison to the upper zone.

RÉSUMÉ

Une caractérisation détaillée du substrat rocheux du site de PCB de Smithville a été effectuée à différentes échelles, en utilisant à la fois des techniques de laboratoire et de terrain. Les travaux sur le terrain reposaient essentiellement sur l'installation de 18 nouveaux trous de forage au site et dans les alentours. Six des trous ont été équipés d'instrument multi-niveaux Westbay®. Deux sites grappés de 4 ou 5 trous chacun ont été établis pour la conduite d'expériences à l'échelle de 40-50 m. Les trous percés à 100-150 m du site grappé Sud ont servi à examiner une échelle plus grande. Les tests sur le terrain faisaient intervenir des techniques hydrauliques à trou unique ou à trous multiples (tests au perméamètre à charge constante, tests de pompage et d'interférence d'impulsions), des expériences avec traceurs et des expériences de dilution ponctuelle. Les études en laboratoire utilisant des carottes rocheuses des nouveaux trous de forage incluaient des mesures de la porosité, des expériences de diffusion et la détermination du carbone organique. En outre, les trous avec instruments Westbay® ont été utilisés pour mesurer la distribution spatiale et temporelle de la charge hydraulique dans la région d'étude. On a également examiné la géochimie inorganique et isotopique des eaux souterraines. Les ensembles de données détaillés réunis grâce aux études en laboratoire et sur le terrain ont été utilisés pour développer un modèle conceptuel de l'écoulement des eaux souterraines et du transport de solutés dans la dolomie fracturée. Ce rapport présente nos résultats et constitue le rapport final sur l'étude.

En résumé, l'écoulement des eaux souterraines dans la formation de Lockport est régie par des fractures horizontales selon la stratification et d'importante extension latérale. Bien que ces caractéristiques ne soient pas très nombreuses (peut-être 5 à 8 selon l'endroit), il y a au moins une connexion latérale qui fournit une voie continue à l'échelle régionale. L'interconnexion verticale entre cette caractéristique et d'autres fractures horizontales est probablement minimale mais présente, un horizon situé à mi-profondeur de la formation étant potentiellement le plus grand obstacle à l'écoulement vertical des eaux souterraines. L'eau circulant dans le système de fractures au-dessus de cet horizon est probablement rechargée à certains endroits en amont du site, où le manteau s'amincit, et peut-être ailleurs en des endroits où il y a contact direct entre l'eau de surface et le substrat rocheux. La vitesse de l'eau souterraine dans la zone supérieure est relativement grande (5 à 30 m par jour), mais le transport de contaminants en phase aqueuse est nettement plus lent en raison des effets d'adsorption et surtout de diffusion dans la matrice. La migration de l'eau dans la zone située sous l'horizon de basse perméabilité, à mi-profondeur, est probablement beaucoup plus lente, peut-être réduite par les interconnexions plus faibles sur l'horizontale. Les eaux souterraines de cette zone sont de moins bonne qualité, et montre des dérives isotopiques suggérant la présence d'eau plus vieille et de migration plus lente. L'interaction entre l'eau souterraine de cette zone et le ruisseau Twenty Mile est probablement nulle (c.-à-d. que l'eau souterraine coule sous le ruisseau). La migration de la contamination en phase aqueuse dans cette zone sera très réduite par rapport à la zone supérieure.

TABLE OF CONTENTS

List of Figures	ii
List of Tables	vii
List of Appendices	viii
EXECUTIVE SUMMARY	ix
1.0 INTRODUCTION	1
1.1 Background	1
1.2 Location, Physiography and Geology	3
1.3 Previous Site Investigations	7
1.4 Preliminary Conceptual Model	9
1.5 Objectives	12
2.0 METHODS	14
2.1 Field	14
2.1.1 Drilling Program	14
2.1.2 Core Logging	15
2.1.3 Vertical Fracture Orientations	15
2.1.4 Borehole Geophysics	16
2.1.5 Hydraulic Testing Program	17
2.1.5.1 Constant-head injection tests	17
2.1.5.2 Pulse Interference Tests	19
2.1.5.3 Pumping Tests	20
2.1.6 Borehole Completion and Measurements of Hydraulic Head	21
2.1.7 Geochemical Measurements	23
2.1.8 Point Dilution	25
2.1.9 Tracer Experiments	27
2.1.9.1 Injection-Withdrawal Experiments	27
2.1.9.2 Radial Divergent Experiments	29
2.2 Laboratory	30
2.2.1 Core Sampling	31
2.2.2 Measurement of Organic Carbon	33
2.2.3 Diffusion Experiments	36
2.2.4 Measurement of Total Porosity	39
3.0 RESULTS AND DISCUSSION	40
3.1 Field	40
3.1.1 Drilling and Core Analysis	40
3.1.1.1 Lithology	40
3.1.1.2 Fractures	42
3.1.2 Borehole Geophysics	44
3.1.3 Hydraulic Testing Program	46
3.1.3.1 Constant head injection tests	46

3.1.3.3 Pulse Interference Tests	53
3.1.3.4 Pumping Tests	54
3.1.4 Borehole Completions	55
3.1.5 Hydraulic Head Distribution	56
3.1.5.1 Vertical Distribution	56
3.1.5.2 Regional Direction of Horizontal Groundwater Flow	59
3.1.5.3 Transient Hydraulic Head Conditions	61
3.1.6 Aqueous Geochemistry	61
3.1.6.1 Inorganic Chemistry	61
3.1.6.2 Isotopes	63
3.1.7 Point Dilution	66
3.1.8 Tracer Experiments	67
3.1.8.1 Injection-Withdrawal Experiments	67
3.1.8.2 Radial Divergent Experiments	71
3.2 Laboratory	73
3.2.1 Rock Geochemistry	73
3.2.2 Measurement of Organic Carbon	74
3.2.2 Diffusion Experiments	77
3.2.3 Total Porosity and Bulk Density	81
4.0 CONCEPTUAL MODEL	83
4.1 Regional Scale	83
4.2 Site Scale	87
4.3 Microscopic Scale	88
5.0 RECOMMENDATIONS	89
6.0 ACKNOWLEDGMENTS	91
7.0 REFERENCES	93

List of Figures

- Figure 1.1 Location of Smithville site.
- Figure 1.2 Map illustrating topography of Smithville region.
- Figure 1.3 Physiographic features in the Smithville region.
- Figure 1.4 Map of drift thicknesses.
- Figure 1.5 Geologic map of Smithville area.
- Figure 1.6 Regional setting of Lockport Dolostone.
- Figure 1.7 Map illustrating major structural features in Southern Ontario. Note location of site in relation to Algonquin Arch and Niagara Escarpment.
- Figure 1.8 Cross-section of the Lockport dolostone following the Niagara Escarpment between Hamilton in the west and Niagara Falls in the east. (From Brett et al., 1995)
- Figure 1.9 Distribution of regional faults in southern Ontario. (From Sanford, B. V., Thompson, F. J., And McFall, G. H. 1985. Phanerozoic and recent tectonics of the Canadian Craton, in the Geoscience Program - Proceedings of the Seventeenth Information Meeting of the Nuclear Fuel Waste Management Program, Atomic Energy of Canada Limited, TR-299:334-352.)
- Figure 1.10 Diagram of vertical flow system illustrating drainage to the Upper Vinemount unit. (From McElwain et al., 1989).
- Figure 1.11 Extent of contaminant plumes (TCE, PCB and TCB) in 1988. (Modified from McElwain et al., 1989)
- Figure 1.12 Typical three-dimensional view of conceptual fracture framework for a layer-cake stratigraphy. (From Engleder, T., Fischer, M. P. And Gross, M. R. 1993. Geological Aspects of Fracture Mechanics, A Short Course Manual, Geological Society of America, Boulder, CO.)
- Figure 1.13 Diagram depicting DNAPL and aqueous phase contamination in discretely fractured rock.
- Figure 1.14 Schematic diagram depicting hypothetical transport processes at the microscopic scale.

- Figure 2.1 Location of new boreholes installed in the Smithville area as part of this study.
- Figure 2.2 Schematic showing trends of inclined boreholes.
- Figure 2.3 Schematic showing core angles measured to orient vertical fractures (after Lau(1983)).
- Figure 2.4 Schematic diagram of constant-head injection testing system.
- Figure 2.5 Schematic diagram showing field set-up for pulse interference tests. (From Novakowski, K.S., 1989)
- Figure 2.6 Type curves used to interpret pulse interference tests by graphical method when there is no observation well storage (a) curves used to calculate S and (b) curves used to calculate T. (From Novakowski, K.S., 1989)
- Figure 2.7 Set-up for pumping test in pumped borehole.
- Figure 2.8 Walton (1962) type curves used for pumping test interpretation
- Figure 2.9 Temporary monitor set up.
- Figure 2.10 Westbay multilevel instrumentation: (a) components installed permanently in borehole and (b) data acquisition instrumentation including downhole probe used to measure pressure and obtain groundwater samples.
- Figure 2.11 Map showing Westbay instrumented boreholes and multilevels used to obtain groundwater samples.
- Figure 2.12 Schematic of apparatus used to conduct point dilution experiments.
- Figure 2.13 Schematic illustrating set-up for injection-withdrawal tracer experiments.
- Figure 2.14 Schematic of diffusion cell.
- Figure 3.1 Lithology of study area: (a) Formal nomenclature (after Brett et. al, 1995) and (b) local nomenclature used in this study.
- Figure 3.2 Bedding Plane fracture spacing distributions: (a) Eramosa, (b) Gasport, (c) Upper Vinemount and (d) Lower Vinemount

- Figure 3.3 Bedding Plane fracture spacing distributions: (a) Goat Island, (b) Vinemount and Goat Island combined, (c) South Cluster Site fractures, and (d) North Cluster Site fractures.
- Figure 3.4 Rose diagram of orientations of vertical fractures in the Eramosa member.
- Figure 3.5 Rose diagram of vertical fracture orientations in the Goat Island member.
- Figure 3.6 Rose diagram of orientations of vertical fractures in the Gasport member.
- Figure 3.7 Distribution of vertical fracture spacings in the Eramosa member.
- Figure 3.8 Vertical transmissivity results for 5 boreholes using a 2-m test interval. Note that the profiles are arranged to form a cross section roughly N-S from 62 -61.
- Figure 3.9 Distributions of measured transmissivity using constant-head injection tests with a 2-m test interval: (a) Eramosa member, (b) Zones containing Eramosa/Goat Island contacts (c) Goat Island member (including Vinemount), (d) Zones containing Goat Island/ Gasport contacts and (e) Gasport member.
- Figure 3.10 Distributions of measured transmissivity using constant-head injection tests with a 0.5-m test interval: (a) Eramosa member, (b) Upper Vinemount unit (c) Lower Vinemount unit, (d) Goat Island and (e) Gasport member.
- Figure 3.11 Distributions of calculated hydraulic apertures ($2b_{eq}$) using constant-head injection tests with a 0.5-m test interval: (a) Eramosa member, (b) Upper Vinemount unit (c) Lower Vinemount unit, (d) Goat Island and (e) Gasport member.
- Figure 3.12 Vertical transmissivity profiles of south cluster boreholes determined using constant head injection tests with a 0.5-m test interval.
- Figure 3.13 Vertical transmissivity profiles of several boreholes within an area of about 10,000 m² determined using constant head injection tests with a 0.5-m test interval and illustrating possible correlation of permeable features.
- Figure 3.14 Comparison of T results for 2.0-m, 0.5-m and 0.1-m test intervals.
- Figure 3.15 (a) Distributions of measured matrix transmissivities and (b) all measurements of matrix transmissivity relative to elevation.
- Figure 3.16 Distribution of measured transmissivities where only vertical fractures were identified in the core record.

- Figure 3.17 Transmissivity measurements in zones where only vertical fractures have been identified in the core record.
- Figure 3.18 Variogram of transmissivity measurements using data from both 2.0-m and 0.5-m hydraulic tests.
- Figure 3.19 Variogram of Eramosa T measurements from south cluster site boreholes.
- Figure 3.20 Variogram of Gasport T measurements from south cluster site boreholes.
- Figure 3.21 Variogram of 0-1m T measurements over a continuous 3.4 m section of Eramosa dolostone.
- Figure 3.22 Variogram of T measurements in south cluster site. In this case, correlation is examined horizontally at all depths.
- Figure 3.23 Spring hydraulic head distribution in boreholes 11,12, 21, 53 & 65.
- Figure 3.24 Spring hydraulic head distribution in boreholes 60, 65, 53, 61 & 62.
- Figure 3.25 Spring hydraulic head distribution in boreholes 60, 62 & 63.
- Figure 3.26 Spring hydraulic head distribution in all boreholes.
- Figure 3.27 Spring and fall hydraulic head distribution in boreholes 60, 61 & 65.
- Figure 3.28 Directions of groundwater flow in most permeable and connected pathway.
- Figure 3.29 Groundwater flow directions in Upper Eramosa unit.
- Figure 3.30 Hydrograph for monitoring intervals in borehole 61.
- Figure 3.31 Hydrograph for monitoring intervals in borehole 62.
- Figure 3.32 Hydrographs for two monitoring zones in boreholes 61 and 62.
- Figure 3.33 Calculated saturation indices using PHREEQC for dolomite, gypsum and calcite calculated with groundwater chemistry from Westbay monitoring zones.
- Figure 3.34 Isotope analyses from all monitoring zones sampled.
- Figure 3.35 Breakthrough curves for the injection-withdrawal tracer experiments. Concentration in the withdrawal zone is normalized to peak concentration.

- Figure 3.36 Model fit to field breakthrough curves.
- Figure 3.37 Tracer breakthrough and model fit in borehole 58 as results of radial-divergent tracer experiment.
- Figure 3.38 Tracer breakthrough and model fit in borehole 59 as results of radial-divergent tracer experiment.
- Figure 3.39 Tracer breakthrough and model fit in borehole 64 as results of radial-divergent tracer experiment.
- Figure 3.40 Conductivity measurements of tracer input approximating a Heaviside step function.
- Figure 3.41 Modelling fit to diffusion experiment results for cell GA-1.
- Figure 3.42 Modelling fit to diffusion experiment results for cell G1-1.
- Figure 3.43 Modelling fit to diffusion experiment results for cell G1.
- Figure 3.44 Modelling fit to diffusion experiment results for cell 9.
- Figure 3.45 Gravimetric porosity measurements in borehole 64.

List of Tables

- Table 2.1 Description of samples used in diffusion experiments.
- Table 2.2 Hydraulic apertures (in μm) of the fractures used for the radial-divergent tracer experiments.
- Table 2.3 Comparison of methods (and laboratories) of organic carbon analysis.
- Table 2.4 List of samples used for the analysis of organic carbon.
- Table 2.5 Cell reservoir volumes (all volumes are in mL)
- Table 2.6 Summary of tracers used in each cell.
- Table 3.1 Summary of vertical and bedding plane fracture spacings
- Table 3.2 Fracture sets measured in the Eramosa member.
- Table 3.3 Summary of transmissivity measurements in the Lockport units using a 2-m test interval.
- Table 3.4 Summary of transmissivity measurements in the Lockport units using a 0.5-m test interval.
- Table 3.5 Summary of fracture porosity calculations using constant-head injection tests with 0-1 m and 0.5 m test intervals.
- Table 3.6 Summary of matrix transmissivity measurements in the Lockport units using a 0.5-m test interval.
- Table 3.7(a) Summary of intervals tested using pulse interference tests.
- Table 3.7(b) Summary of intervals tested using pulse interference tests.
- Table 3.7(c) Summary of intervals tested using pulse interference tests.
- Table 3.7(d) Summary of intervals tested using pulse interference tests.
- Table 3.8 Results of time-lag interpretation of pulse interference tests.
- Table 3.9 Summary of results of pumping tests conducted at south cluster site.

- Table 3.10(a) Summary of Westbay monitoring intervals.
- Table 3.10(b) Summary of multi-level monitoring intervals.
- Table 3.11 Summary of temporary monitors in new boreholes.
- Table 3.12 Summary of inorganic analyses in groundwater obtained from Westbay monitoring intervals.
- Table 3.13 Summary of isotope analyses in Westbay monitoring intervals.
- Table 3.14 Summary of isotopic analyses from multilevel monitoring intervals.
- Table 3.15 Results of point dilution experiments.
- Table 3.16 Summary of parameter values obtained for final fits to model. The fits were obtained under the constraint of a natural flow field oriented parallel to the trajectory between the two boreholes.
- Table 3.17 Calculated parameters determined from the radial-divergent tracer experiments.
- Table 3.18 Results of analyses of organic carbon on bulk rock samples.
- Table 3.19 Results of analyses of organic carbon on stylolite samples.
- Table 3.20 Results of analyses of organic carbon on samples of argillaceous layers.
- Table 3.21 Calculated retardation factors for the matrix and example fracture ($2b=500 \mu\text{m}$).
- Table 3.22 Summary of diffusion experiment results.
- Table 3.23 Summary of all measured porosity values
- Table 3.24 Summary of all bulk density measurements

List of Appendices

- Appendix A Site Chronology of Events
- Appendix B Composite Borehole Logs
- Appendix C Transmissivity profiles using 0.1 m data
- Appendix D Pumping Test Response Curves

EXECUTIVE SUMMARY

During the late 1970's and early 1980's, PCB and solvent waste destined for destruction in the United States was handled and stored at a small chemical waste management site (CWML site) located on the northern perimeter of the town of Smithville in southern Ontario. In 1985, contamination was detected at the site and in 1987 the presence of groundwater contamination had been confirmed. Over the next few years, it was discovered that PCB oils and associated solvents (DNAPL) had penetrated approximately six metres of clay-till overburden and invaded the upper horizons of the bedrock below. The uppermost formation in this area is the Lockport dolostone, which is comprised of four members totaling a thickness of approximately 40 m. Aqueous phase contamination emanating from the DNAPL source and carried by groundwater flowing in the fracture network which pervades the Lockport had traveled a distance of approximately 600 m by 1988. The discovery of the migration of contaminants in the bedrock led to the shut-down of a local municipal pumping well and the construction of a pump-and-treat system which was completed in the upper 4 m of bedrock within the assumed source area. The pump-and-treat system has been in continual operation since that time.

In October of 1995, the National Water Research Institute along with partners from the University of Waterloo, McMaster University, and the University of Utah, entered into an agreement with the Smithville Phase IV Bedrock Remediation Program to refine an existing conceptual model for groundwater flow and contaminant transport in the Lockport Formation underlying the former CWML site. Primary funding for this study was provided by the Province of Ontario. Additional funding was provided by the US Environmental Protection Agency through a research contract entitled "Groundwater Flow and Capture Zone Dynamics in Fractured Carbonate Aquifers" and by

Environment Canada through the Great Lakes 2000 program. The purpose of the present study was to define and characterize the physical hydrogeological features in the bedrock of most relevance to the groundwater flow system and to the transport of the aqueous and non-aqueous phase contaminants. This report details the studies carried out by the National Water Research Institute (NWRI) of Environment Canada and its subcontractors. Activities conducted as part of the aforementioned EPA study by the University of Waterloo, McMaster University, and the University of Utah are reported elsewhere.

The investigations were undertaken at three different scales: the regional scale, the site scale and the scale of a discrete fracture. The primary and most costly component of the investigation was the drilling and completion of eighteen new boreholes located throughout the region and within the confines of the site. The boreholes were drilled and cored through the entire section of the Lockport formation, finishing in the upper beds of the underlying Rochester shale (typical length of 55 m). Sixteen boreholes were drilled in the inclined orientation (55° - 57° from horizontal). Six of the boreholes were completed with multi-level piezometers, and the other twelve completed with temporary casing. The core from each borehole was examined in detail for both structural (horizontal and vertical fractures, stylolites, vugs etc.) and lithological features. The orientation of the vertical fractures was determined using simple trigonometric relationships with bedding. The boreholes completed with temporary casing are located within about 300 m of the contaminant source and include two borehole clusters (groups of 4-5 boreholes drilled in an approximately 50x50 m area). The overall distribution of boreholes provides a basis for a comparative statistical analysis at both the local and regional scales. The borehole clusters were also used for the completion of pumping tests and local-scale tracer experiments. Standard geophysical sondes (gamma, inductance, temperature,

caliper and inclinometer) were completed in 15 of the 18 new boreholes.

Each borehole was hydraulically tested using a straddle packer system having a packer spacing of 2 m. A complete contiguous profile was obtained for each hole. A total of approximately 360 tests were conducted using a 2-m spacing. From the results of the core logging and the initial hydraulic testing, it was determined that the packer spacing for the hydraulic tests was too large (i.e. the mean fracture spacing was less than the packer spacing for some horizons). Thus, many of the boreholes were re-tested using a packer spacing of 0.5 m. These included the boreholes from the south cluster site (55-59), boreholes 34c, 37c, 64, and the uppermost 20 m of boreholes 54A-54D. A total of 886 tests were conducted using 0.5 m spacing. In addition, as a means of locating specific fractures and fracture zones, 172 tests were conducted using 0.1 m packer spacing.

Following the completion of the hydraulic testing, temporary or permanent well completions were installed. The temporary completions consisted of two pneumatic packers spaced approximately six m apart and located at a depth that coincides with a low-permeability unit (the lower Vinemount member) which was determined from the hydraulic testing to be pervasive throughout the region. The permanent completions were constructed using Westbay multi-level piezometers. The Westbay system consists of a PVC casing linked by water-filled packer elements. A pressure-measurement and water-sampling device was used to provide access to groundwater contained in the intervals isolated exterior to the casing. The permanent completions were constructed in boreholes located regionally, with one completion in the vicinity of the site (borehole 53). A total of 42 intervals ranging in length from 2-10 m were isolated using the permanent system. The number of intervals per borehole range from 5-9.

Following the installation of the permanent casing, measurements of hydraulic head in each

interval were obtained on a weekly basis. Because the permanent completions were constructed in a phased procedure over the span of two years, a complete record of hydraulic head only exists for the period of July, 1997, to present. Measurements of hydraulic head have also been obtained over the same period from three multi-level monitoring wells (17 intervals) installed during previous studies.

Groundwater samples were collected in July and November, 1997, from the six boreholes completed with Westbay installations and three multi-level monitoring wells located in the vicinity of the site. The samples were collected from the Westbay intervals using a stainless steel sampling chamber (volume of 500 mL) connected to an electronic actuating device that draws in groundwater from the isolated zone. Samples from the multi-level monitoring wells were obtained using a Waterra hand pump. After abstracting the sample to ground surface, electrical conductivity, Eh, alkalinity, and pH were measured on the unfiltered water. Groundwater samples were also collected and filtered for measurement of inorganic constituents and dissolved organic carbon (DOC). A total of 120 samples were collected for the analysis of inorganic constituents between the two sampling events. Samples were also collected for the analysis of the environmental isotopes ^{18}O and ^2H and for tritium in July and November of 1997.

During the course of the field investigations, several measurements of groundwater velocity were obtained from discrete fractures and fracture zones in the uppermost member of the Lockport formation. The measurements were obtained in un-cased boreholes using the point dilution method. To conduct the experiment, a salt tracer is released into an isolated interval and continually mixed. The subsequent decay in concentration is directly proportional to the velocity of the groundwater passing through the borehole. Unfortunately, this experimental method is difficult to conduct and only

six reliable measurements have been obtained to date.

The vertical hydraulic properties of the fracture network were investigated by conducting several pumping tests in the south cluster site. The tests were conducted using boreholes 56 or 58 as the pumped well with the other boreholes used as observation wells. To conduct a test, a horizontal fracture located at 14 m depth was isolated using straddle packer systems in both the pumped and observation boreholes. A second horizontal fracture 2 m below the pumped fracture was also isolated with straddle packer systems. The pumping was conducted from only one isolated interval usually for a period of 15-30 hrs. A constant pumping rate of 6-8 L/min was targeted for each test. Drawdown was measured in the observation wells using pressure transducers installed in each interval. Inter-borehole distances between the pumped and observation wells ranged from 17 to 36 m.

Tracer experiments were also conducted to investigate the potential for vertical inter-connectivity within the fracture network, to evaluate the extent of horizontal fractures, and to explore the role played by matrix porosity in the transport of aqueous-phase compounds. The experiments were conducted in a variety of formats at either the north or south cluster sites. A few experiments were conducted using the injection-withdrawal format where injection was conducted in one horizontal fracture and withdrawal was conducted from another. Several experiments were conducted using the injection-withdrawal format in a single horizontal fracture where injection was conducted in one borehole and withdrawal conducted from another intersected by the same fracture. These experiments were of short duration, lasting no more than three days. Two large-scale experiments were also conducted at the south cluster site using the radially-divergent format. For these experiments, a radial flow field was established by injecting water from a nearby fire hydrant at a rate

of approximately 4-7 L/min. Following a pulse injection of tracer, arrival at the surrounding observation wells was monitored using small-volume sampling techniques. These experiments were of much longer duration requiring as much as nine days to attain peak tracer concentration at an inter-borehole distance of 125 m. The conservative tracers Lissamine FF and Bromide were employed for all experiments. Initial concentrations ranged from 100 mg/L for Lissamine FF and 1000 mg/L for Bromide.

Because it was recognized that matrix diffusion may strongly influence the transport of aqueous compounds, several elements of the study were focused on measurements of matrix porosity and diffusion in core samples. The principal element for this study was the completion of 32 radial diffusion experiments. The experiments were conducted using saturated core collected during the drilling program. Sections of core 0.10-0.20 m in length with a reservoir 12.5 mm in diameter drilled through the center, were encapsulated using a Teflon sleeve and two stainless-steel end caps. A port allowing for access to the reservoir was incorporated into one of the end caps. The experiments were conducted by mixing a known concentration of tracer into the reservoir, and monitoring the subsequent decay in concentration due to diffusion into the rock, over time. Various combinations of conservative tracers were employed during this study, including Bromide (as KBr), Lissamine FF, Nitrite (NaNO_2), and Difluorobenzoic acid (DFBA). Initial concentrations ranged from 500 $\mu\text{g/L}$ for Lissamine FF to 1000 mg/L for Bromide. Approximately 10-20 samples of tracer were obtained to define the decay in concentration over the course of each experiment. Following the completion of the experiments, the total porosity was determined for each sample using gravimetric methods.

In addition, to investigate the local-scale heterogeneity of matrix porosity within each member of the Lockport formation, approximately 10 sections of saturated core between 0.2-15.5 m in length

were sliced into discs 5-20 mm in thickness. A gravimetric measurement of total porosity was obtained from each disc. The sections were obtained from boreholes 54A, 54B, 54D, and 65, and example horizons from all members were collected. The sections were obtained from some horizons in which there were bedding-plane or vertical fractures and some in which there were none. One long section, 15.5 m in length, was also sliced into 20 mm discs. The majority of this section was obtained from the upper two members of the formation.

The transport of organic contaminants in fractured rock may be influenced by the presence of organic carbon. To explore the presence and distribution of organic carbon in the Lockport formation several types of measurement were undertaken. It was initially recognized that the stylolitic horizons observed in core may contain large amounts of organic carbon and thus act as significant sinks for the aqueous-phase contamination. During the process of core-logging, the location and physical description of stylolitic features were recorded. Approximately 20 samples of stylolitic material were collected from core and an additional 10 samples obtained from stylolites exposed in a local quarry, were analyzed for organic carbon content. The measurements were obtained using a Leco 12 Carbon Analyzer.

Although natural organic carbon is known to be present in dolostone exclusive of the presence of stylolites, measurement of the low concentrations often observed requires considerable effort. Thus, to conduct these measurements, samples were collected from several horizons distributed throughout the Lockport formation and analyzed using four different methods. The samples were pulverized and analysis for organic carbon conducted using the Leco12 Carbon Analyzer, a Leco RC412 Carbon analyzer, and a UIC Carbon Analyzer with a pre-acidification step. The latter analyses were conducted by the Department of Geology, Washington State University. Batch experiments

were also conducted using TCE as the sorbing compound. Back calculation of the percent organic carbon was determined from the batch experiments using the K_d - K_{oc} relation for TCE.

Additional laboratory studies were focused on determination of the rock composition. A total of 32 core samples, collected from the various members of the Lockport dolostone, were prepared and submitted for chemical and mineralogical analyses. The analyses were conducted using X-ray Diffraction (XRD), X-ray fluorescence (XRF) and infra-red spectrometry techniques. All analyses were conducted by the Geological Survey of Canada.

Based on the results of the core logging, hydraulic testing, measurement of hydraulic head and aqueous geochemistry obtained from the boreholes distributed regionally, a conceptual model for groundwater flow at the regional scale was developed. The Lockport formation in this area was found to be divisible into four members identified as the Eramosa, Vinemount, Goat Island, and Gasport members from uppermost to lowermost. The formation dips to the south with a mild gradient of 1-2 %. Based on observations of hydraulic head in each member, groundwater was observed to flow in the Lockport formation in an approximately southeasterly direction towards Twenty Mile Creek.

Interpretation of the lithology, the vertical distribution of transmissivity (2-m spacing), the distribution of hydraulic head, electrical conductivity (EC), ^{18}O , ^2H , tritium, and dominant ionic species for three boreholes (63, 53, 61) located along an approximately north-south transect reveals the general features of the flow system. In general, features of high transmissivity are observed to be variously prevalent in all of the members. These features are interspersed with low-T zones of unfractured rock, and with a persistently low-T feature present in the lower Vinemount member. In the up-gradient borehole (63), a substantial hydraulic gradient is present across this feature, with

uniform hydraulic head present above and below. This suggests that groundwater flow in this area is dominated by horizontal fractures in two distinct systems above and below the feature, with limited interaction in between. The distribution of EC, stable isotopes, and tritium are approximately uniform, however, across the feature, suggesting a common source of recharge, located in the up-gradient direction. Based on regional mapping of the quaternary deposits, it is surmised that the recharge occurs in areas 2-3 km to the north of the site where the overburden thins to less than a metre.

In the area immediately to the south of the CWML site (borehole 53), the topography is relatively flat-lying and the hydraulic gradient across the low-T feature in the lower Vinemount is observed to be negligible. Unlike the up-gradient borehole, the isotopic and geochemical signatures of the water in the upper and lower flow systems are quite different. Although horizontal flow likely remains dominant at this location, the rate of groundwater migration in the lower flow system is considerably diminished in comparison to that in the shallow system. Because the transmissivity remains high at this location particularly in the lowermost member, the presence of a slower flow system implies a lesser degree of horizontal fracture interconnection at depth and diminished hydraulic gradients. Although measurements of groundwater velocity obtained from point dilution experiments range from 5-30 m/day in individual fractures pervading the Eramosa member, there are no measurements obtained from the lower flow system to corroborate the interpretation that the lower flow system is slower here.

Borehole 61 is located adjacent to Twenty Mile Creek and approximately 500 m in the direction down-dip from borehole 53. There is less overburden and more thickness of the Eramosa member at this location. The highest T in the borehole occurs in the upper Vinemount member. The low T horizon is also present in the lower Vinemount. The highest hydraulic head is also associated

with the high-T zone in the Vinemount, with significant vertical gradients away from this feature both above and below. The high hydraulic head is indicative of good lateral connection with groundwater in the up-gradient direction. Based on the geochemical signature, however, it is unlikely that the source of this water is in that direction. Rather, because the EC is low, the stable isotopes approximately uniform with depth, and tritium is present in the high-T zone, it is suggested that the groundwater is freshly-recharged likely from upstream locations where the river is in direct contact with the underlying bedrock. It is important to note that groundwater flow in the system below the Vinemount appears to have a similar distribution of hydraulic head to that in the overlying upper Eramosa, suggesting that this system may underflow the creek completely.

The results of the hydraulic testing conducted using 0.5-m spacing in the boreholes of the south cluster site and vicinity show several features of the flow system that can not be interpreted from data collected at a larger packer spacing. In particular, the following observations and conclusions can be drawn: i) the low-T zone in the lower Vinemount may be several metres or as thin as one metre in thickness depending on location, ii) in some horizons, particularly at the base of the Eramosa, the average spacing of the bedding-plane fractures is less than the packer separation (thus, the need for hydraulic testing using 0.1-m spacing), iii) specific bedding-plane features both in the Eramosa and in the Gasport member can be correlated amongst the boreholes of the cluster site and with boreholes 64 and 37c (correlation over distances of as much as 125 m), iv) individual features often consist of more than one discrete horizontal fracture, and v) these features dominate the distribution of transmissivity in each borehole.

The results of the pumping tests conducted at the south cluster site showed no perceptible drawdown in the lower (un-pumped) fracture. Drawdown in the pumped fracture, however, showed

evidence of significant leakage from vertical sources (i.e. a flattening of the drawdown curve at late time). Because of the non-uniqueness of these results, it is difficult to resolve between the possible contribution of vertical fractures versus that from double porosity. The mean spacing of vertical fractures measured from drill core was approximately 0.77 m for the Eramosa member. This suggests that vertical connection through fracture pathways should exist between these two horizontal fractures. Unfortunately, the results of the inter-fracture tracer experiment were also inconclusive, as the arrival of tracer at the withdrawal borehole was not detected. These results suggest that although a vertical interconnection between the main fracture features may exist, this connection is weak, at least in the vicinity of the south cluster site.

The correlation of the upper fracture features between the south cluster site and borehole 64 was confirmed by the results of the large-scale tracer experiment conducted in the radially-divergent format. Although connection was established over this distance (i.e. south cluster to 64), further transport to either boreholes 34c or 37c was not observed. A large-scale tracer experiment conducted in the correlated feature present in the Gasport member (at approximately 41-m depth), showed direct connection only within the confines of the south cluster site. Hydraulic response to water injection during the tracer experiment was observed at borehole 64, suggesting horizontal connections at depth are present over this distance, but weaker than those observed in the Eramosa member.

The results of the diffusion experiments showed that the estimates of effective porosity determined using conservative tracers are very similar to the estimates of total porosity obtained using gravimetric methods. The range of effective porosity measured spanned 4.6% to 10.6 % with a mean of 7.1%, and the agreement between effective and total porosity was approximately equal throughout the range. The mean of the total porosity was 7.2%. Thus, measurements of total porosity provide

a good prediction of the influence that porosity will impart on the solute transport process. The range in porosity is particularly evident in the estimates obtained from the slices of the long section of core collected from borehole 64. Values as low as 2% and as high as 18% were observed to occur almost immediately adjacent one another. Although it was suspected that increases in matrix porosity occurred adjacent to fractures, this was rare and some of the zones of highest porosity were observed in intact rock. It is presumed that the zones of enhanced porosity are likely related to diagenetic processes.

The impact of matrix diffusion was directly illustrated in the results of injection-withdrawal tracer experiments conducted using tracers having different molecular diffusion coefficients (Lissamine FF and Bromide). The breakthrough curves for each tracer was shifted in time according to the degree of loss and return from the fracture to the matrix through the process of diffusion. Experiments were conducted in opposing directions and the results were found to be highly repeatable. The large-scale divergent experiments were also found to be strongly influenced by matrix diffusion, with peak tracer concentrations declining by over two orders of magnitude in only 125 m of travel distance.

The measurements of organic carbon showed that the organic carbon present in the bulk rock matrix was low in comparison to published values for carbonates. Typical values for the Eramosa, Vinemount and Goat Island members ranged from 0.00%-0.13%. The Gasport member was found to have virtually no organic carbon with the highest measured concentration at 0.04%. The stylolites were also found to contain minimal organic carbon and measurements of 0.00%-0.07% were typical. However, bituminous layers, of which only a few were noted in the core record, were found to have abundant organic carbon, with mean values of approximately 3%. The results of the batch

experiments were inconclusive and were not included in the interpretation of organic carbon content. Finally, using theoretical calculations, it was shown that even though only small percentages of organic carbon are present in the bulk rock, the effect on the retardation of migrating organic contaminants such as TCE, is significant.

In summary, groundwater flow in the Lockport formation is predominated by horizontal bedding-plane fractures of significant lateral extent. Although the number of these features is not large (perhaps 5-8 depending on location), there is at least one lateral connection that allows for a continuous pathway over the regional scale. The vertical interconnection between this feature and other horizontal fractures is likely to be minimal but present with a horizon at mid-depth in the Lockport being potentially the most restrictive to vertical groundwater flow. Groundwater flowing in the fracture system above this horizon is likely recharged at specific locations up gradient from the site where the overburden thins, and perhaps elsewhere where direct contact between surface water and bedrock occurs. The groundwater velocity in the upper zone is relatively rapid (5-30 m/day), although the transport of aqueous-phase contaminants is considerably slower due to the effects of adsorption and particularly matrix diffusion. Groundwater migration in the zone below the low-permeability horizon at mid-depth, is likely to be much slower, possibly restricted by weaker interconnections in the horizontal direction. Groundwater in this zone is of poorer quality and exhibits isotopic shifts that suggest older water and slower migration. Interaction between the groundwater in this zone and Twenty Mile Creek is probably non-existent (i.e. the groundwater under-flows the Creek). The migration of aqueous phase contamination in this zone will be very restricted in comparison to the upper zone.

Finally, it is important to note that natural gas occurs at various horizons in the Lockport

formation throughout the region and in the immediate vicinity of the site. The potential influence of the natural gas on the transport of volatile compounds may be profound, and, at present, unexplored.

1.0 INTRODUCTION

1.1 Background

Since the discovery of oil-phase chemicals in the sub-surface materials underlying Love Canal in Niagara Falls, New York, in the late 1970's our understanding of how organic contaminants are transported in hydrogeological environments has evolved substantially. Beginning with F. Schwille's quantitative studies investigating the behaviour of dense, non-aqueous phase liquids (DNAPLs) in the early to mid 1970's, numerous North American research initiatives have focused on the study of DNAPLs in both porous and fractured media. One area in which significant knowledge gaps continue to exist, is the transport of aqueous and non-aqueous phase compounds in discretely-fractured rock. This is because of the complexity of the primary groundwater conduits (i.e fractures) and the relation between the water flowing in the fractures and the immobile fluid retained in the surrounding unfractured medium. Although much recent research has focused on the transport in a discrete fracture of oil-phase compounds at the laboratory scale (Kueper and McWhorter, 1991; Reitsma and Kueper, 1994), and on aqueous phase compounds at the field scale (Raven et al., 1988; Shapiro and Nicholas, 1988; Novakowski and Lapcevic, 1994; Kuntzmann et al., 1997), little work has been conducted at the scale of a fracture network. Thus, prediction of the migration of contamination at the site and regional scales in fracture networks and the design of remedial programs remains a difficult prospect.

During the late 1970's and early 1980's, the disposal of PCB-contaminated wastes in the province of Ontario was managed through the removal of the wastes to licenced facilities in the United States. In 1978, a facility located on the northern perimeter of the town of Smithville was licenced by the Ontario Ministry of the Environment to accommodate the transfer of PCB wastes

from localities in southern Ontario to tanker trucks which would be used to ship the waste across the border. During the period 1978 to 1985, the facility operated as a collection center for PCB and other organic wastes, although little of the waste was actually shipped across the US border. In 1985, concerns raised by a local community group about the possibility of contamination emanating from the site prompted a site investigation by the Ministry of the Environment. It was subsequently discovered that oil-phase PCB and other organic contaminants had penetrated at least the upper horizons of a clay till having a thickness of approximately 6 m, underlying the site. Because a municipal well located approximately 600 m south of the site abstracted water from the bedrock aquifer underlying the clay, an investigation of the groundwater conditions in the bedrock was also initiated. Upon discovery of aqueous-phase contaminants in an off-site monitoring well completed in the bedrock, the municipal well ceased operation and a pump-and-treat system was constructed in the shallow bedrock on site. The pump-and-treat system consists of a ring of eight extraction wells within the assumed location of the DNAPL and drilled to a depth of approximately 4 m below the top of bedrock. This system has been in continual operation since 1989.

During the period 1989 to 1994, much of the activity on the site was focused on monitoring the success of the pump-and-treat system, disposing of the surface inventory of liquids and contaminated equipment, treatment of the soil contamination (by incineration) and on monitoring the general changes in the concentration of the contaminants in the bedrock. Appendix A (Golders, 1995) provides a more detailed chronology of events leading to the conditions present on the site in October, 1994. In 1993, a managing Board of Directors was formed through an agreement between the Ministry of the Environment and Energy and the Township of West Lincoln. The Board was given a mandate to manage all aspects related to the remediation of the contaminants remaining in

the ground beneath and adjacent to the former CWML site in Smithville. To assist in this process, the Smithville Phase IV Bedrock Remediation Program was established. One of the early successes of the board was the establishment of a cooperative agreement with the US Environmental Protection Agency, the National Water Research Institute of Environment Canada, the University of Waterloo, McMaster University, and the University of Utah. The partnership was formed under the aegis of a research contract entitled "Groundwater Flow and Capture Zone Dynamics in Fractured Carbonate Aquifers". A significant component of the contract was focused on the development of a conceptual model for the flow of groundwater and transport of contaminants in the bedrock underlying Smithville. The objectives in developing the conceptual model were to explore novel methods for site-characterization and to provide a rigorous data set for developing numerical capture zone models. This report summarizes the studies conducted and the results obtained in relation to the development of the conceptual model. A report describing the overall results of the study of capture zone dynamics is presently nearing completion. It should be noted that much of the data generated as part of this study and discussed in this report is included in the Smithville database (Microsoft® Access 97) and as such this report focuses primarily on the interpretation of the data.

1.2 Location, Physiography and Geology

The community of Smithville is located above the Niagara Escarpment, in the center of the Niagara Peninsula (Figure 1.1). The PCB waste site is located on the northern perimeter of the town (Figure 1.2). The topography in the vicinity of the town is dominated by the presence of Twenty Mile Creek, which drains eastward in this area. The total relief, however, is only 20 m, and the majority of the area is relatively flat-lying. A bedrock ridge oriented in the northwest-southeast direction and having a relief of approximately 8.5 m, lies approximately 4.5 km to the north of the town boundary

(immediately to the south of Spring Creek on Figure 1.2). Although not identified as such, this ridge is likely a remnant of the Eramosa Scarp observed 10 km to the west (Feenstra, 1981). In the intervening distance to the south between the ridge and the town, a low-lying draw acts as a headwaters for a tributary stream to Spring Creek which eventually discharges to Twenty Mile Creek. The Niagara Escarpment lies approximately 4 km to the north of the bedrock ridge. The relief rises approximately 6 m toward the lip of the Escarpment. A second ridge comprised of Halton Till and having a relief of approximately 7.0 m lies approximately 0.5 km to the north of the PCB site. This ridge is likely either a remnant of the Niagara Falls moraine which terminates a few kms to the west or a continuation of the Vinemount Moraine which lies immediately to the northeast. Figure 1.3 illustrates the location of these physiographic features.

The area surrounding Smithville is primarily used as farmland although the soils to the immediate north are poorly drained. These soils are classified as greysols primarily with lacustrine clay to clay-silt parent material (Kingston and Presant, 1989). In an area ranging from 1-3 km north of the town limits, the soil is predominantly clay loam till, also poorly drained. The parent material for this soil is likely the Halton Till outlier described above.

With the exception of the outlier of Halton Till and the bedrock ridge, the area is underlain by varying thicknesses of Lake Warren glaciolacustrine clay (Figure 1.3; Figure 1.4). To the north of the bedrock ridge, the drift thickness ranges from 1.0-7.5 m, with a predominant area surrounding the ridge where thicknesses are less than 1.0 m. There is also an area located 3.5 km to the northeast of the site where drift thickness is less than 1.0 m. In the southern portion of this region, the Lockport dolostone is actively quarried. In the area underlying the PCB site and to the east, the thickness of the clay increases to greater than 10 m. The clay thins towards Twenty Mile Creek to the south and

then thickens to greater than 15.0 m beyond, in the southern-most region of the map area. In the six km reach of Twenty Mile Creek which follows Highway 20 through Smithville, the creek is observed to flow directly over bedrock at several locations (Figure 1.3).

Figure 1.5 shows the topography of the bedrock surface and the stratigraphic contacts. The bedrock surface generally declines in the south-southwesterly direction, away from the promontory formed by the escarpment. The highest point in the bedrock is the ridge located to the north of the site. Low lying areas oriented in the northeast direction may be remnant channels formed on the bedrock surface during glaciation. Examples of deeper channels have been observed in the eastern area of the Niagara Peninsula (Flint and Lolcama, 1985), although these are likely related to interglacial drainage of ancestral Lake Erie.

Figure 1.5 also illustrates the contacts between the major units of the Silurian-aged stratigraphy within the vicinity of the site. The stratigraphy in this area consists of dolostone formations which dip in the southwesterly direction at an incline ranging from 0° to 2° (Figure 1.6). The CWML site is underlain by the Eramosa member of the Lockport Formation. The Eramosa member is grey to buff in color, dense and finely crystalline, and distinguished in the Niagara Region by a characteristic petroliferous odour released from a fresh surface. The contact between the Eramosa member and the overlying Guelph Dolostone lies approximately 2.0 km to the south. It is important to note that Twenty Mile Creek generally follows the northern margin of this contact. The Eramosa member is underlain by the Vinemount member, a vuggy, gypsiferous, and argillaceous dolostone, medium grey in color, and fined grained in texture. This unit is not shown on Figure 1.5, but lies to the immediate north of the contact illustrated between the Eramosa and the Gasport and Goat Island Members. This contact also appears to act as a drainage boundary (for Spring Creek) and

may have formed a discontinuous scarp, the remnants of which are represented by the bedrock ridge directly to the north of the site. The Goat Island member is sugary in texture, and exhibits white chert nodules and occasional stylolites. The Gasport member is more massive in bedding, fossiliferous, and has abundant stylolites in the Niagara Region. Underlying the Gasport member is the Rochester Shale, a massive, low-permeability dolomitic shale that acts as a regional aquitard. The Lockport Formation is approximately 40 m in thickness within the vicinity of Smithville.

The Guelph and Lockport Formations are part of the Silurian carbonate shelf sequence present on the northern margin of the Appalachian Basin. These formations form the resistant rim of the Niagara Escarpment which crosses from the Appalachian Basin over the Algonquin-Findlay Arch and encircles the Michigan Basin to the northwest (Figure 1.7). Figure 1.8 shows a cross-section of the Lockport Formation following the Niagara Escarpment between Hamilton in the west and Niagara Falls in the east.

Smithville is also located a few tens of kilometers north of the gas fields which occur along the northwest margin of the Appalachian Basin beneath Lake Erie. Structural control of the gas traps (faulting) has been postulated based on detailed mapping of the top of the Rochester Formation in southern Ontario (Sanford et al., 1985). A map of the fracture framework of southern Ontario (Figure 1.9) shows the possible presence of large through-going faults in the Smithville vicinity. Although the presence of these features has not been investigated to date, it is possible that these faults may have provided regional conduits for the emplacement of localized pockets of gas detected in the initial drilling of the bedrock at the CWML site (reported in Golders, 1988). However, based on previous drilling results, there is no evidence that these faults are present in the immediate vicinity of the site.

1.3 Previous Site Investigations

During the years prior to the discovery of the contamination at the CWML site in Smithville, the town abstracted drinking water from the Vinemount member of the Lockport Formation at two locations. Municipal Well #2 was located immediately south of the CWML site (approximately 400 m) and pumped at an average daily rate of 650 m³/day (Municipal well #1 was located to the west on the periphery of the study area). Although the water supply was abundant, the quality of the water was poor with high levels of natural sulphates. Following the initial discovery of surficial contamination on CWML site property, detailed subsurface investigations were undertaken. The majority of the investigations were focused on the groundwater contamination present in the overburden, the Eramosa member, and the Vinemount member. These investigations were very detailed and thorough, and are summarized only briefly in the following paragraph. The summary is based primarily on a conference paper published in 1989 (McIelwain et al., 1989). The reader is directed to Golder Associates (1995) for a more complete compendium and precis of all previous studies conducted on the site.

Preliminary site investigations were focused on the till overburden and the potential pathways from the surface to the top of bedrock. Based on a fracture survey conducted in an excavation adjacent to the CWML site, it was observed that some of the fractures extend through the entire thickness of the overburden. Some fractures were also filled with a fine-grained material and provided a hydraulic connection from surface to bedrock. To date, no site-specific data on the local-scale or bulk hydraulic conductivity of the till has been collected. A permeable basal till was also discovered to be pervasive in the vicinity of the site. Thus, a potential vertical and horizontal transport pathway to the top of the bedrock was established. Further investigation

of the contamination was focused on the distribution of the DNAPL and the distribution of the aqueous phase. Approximately 78 cored holes and 120 monitoring wells were installed during this phase of the investigations. The results of hydraulic testing and the measurement of hydraulic head conducted in the upper bedrock indicated the presence of two "aquifers", one in the upper weathered zone of the Eramosa and the other in a 4-m thick section of the Vinemount (the same horizon as was used for the municipal well). The average hydraulic conductivity of these "aquifers" was determined to be 5×10^{-4} m/s. Figure 1.10 shows the distribution of hydraulic head through the depth of the Lockport Formation at about the time that the municipal well discontinued operation. Note that downward vertical gradients from the top of bedrock towards low hydraulic head in the Vinemount was predominant at this time. Regional groundwater flow in the horizontal direction was estimated to be towards the south-southeast. The results of a large-scale 24 hr. pumping test conducted using the abandoned municipal pumping well showed the presence of a weak vertical connection between the upper -weathered zone in the Eramosa and the high-permeability zone in the Vinemount member (Golder Associates, 1989).

Based on drilling conducted in the vicinity of the source zone, the distribution of the DNAPL was estimated to follow an approximately circular pattern with a radius of 50 m. It was also assumed at that time that the vertical extent of the DNAPL was limited to the upper weathered zone of the Eramosa. Figure 1.11 shows the estimated distribution of the principal aqueous-phase contaminants in the upper Eramosa circa 1989. The least retarded contaminant (TCE) was estimated to travel at a velocity of 50-100 m/year, although it was assumed that velocities were likely much faster prior to the cessation of municipal pumping. Note also the skew in the concentrations towards the former municipal well, located just south of London Road. The

leading edge of the TCE plume was undefined beyond this point in 1989. A similar, but less widespread and well-defined distribution of contaminants was found in the permeable zone of the upper Vinemount. Based on these results, it was postulated at that time that the DNAPL may have penetrated to this depth in the source zone.

1.4 Preliminary Conceptual Model

To initiate the present study, a preliminary conceptual model was developed based on the results of previous research studies conducted in dolostone formations. This conceptual model is developed on the basic assumption that the groundwater flow in the Lockport dolostone is governed exclusively by fracture discontinuities located along bedding planes and perpendicular to bedding. Figure 1.12 illustrates a typical framework of fractures that might form in a flat-lying stratigraphic environment.

The fractures present in the Lockport formation underlying Smithville are exclusively extensional in origin. Those that follow bedding planes and other planes of weakness in the horizontal direction (such as stylolites or bituminous partings) either formed in recent geological time, likely syn- or immediately post-glaciation or earlier through erosional unloading. Vertical fractures which have been mapped throughout the Niagara Peninsula, follow preferred orientations usually related to paleo-stress fields associated with the Allegheny front or the directions of the contemporary stress field (Williams, et al., 1985). Trace lengths of the horizontal and vertical fractures are substantially different. Some bedding plane fractures studied elsewhere in the Niagara Region (Novakowski and Lapcevic, 1988) have been postulated to extend over distances as great as several kilometers. Conversely, as depicted in Figure 1.12, vertical fractures are usually confined to the bedding or formation thickness. In a detailed mapping study of local

quarries conducted by Gartner Lee Ltd. (1995), the majority of the lengths of the vertical fractures mapped ranged between 0.2-0.7 m. Almost all vertical fractures were observed to terminate at a bedding plane. A small number of vertical fractures, however, were observed to traverse the entire exposure, crossing bedding planes and member units. The horizontal spacing of these features was estimated to be 150 m or greater (Gartner-Lee and Associates, 1995).

Although fractures mapped in quarries often poorly represent actual subsurface flow pathways (see following discussion), it is reasonable to anticipate that fracture statistics similar to that given above will be collected from the drilling conducted in the study area.

Studies conducted in the Lockport and overlying Guelph formations at locations elsewhere in southern Ontario (Novakowski and Lapcevic, 1988; Reichart, 1992; Yager, 1996) have shown that the groundwater flow system in this environment is predominantly horizontal, governed by the bedding-plane fractures. This implies that the bulk permeability of the bedrock is less in the vertical direction. In a detailed study of the vertical hydraulic properties of the Guelph Formation (Reichart, 1992), the vertical hydraulic conductivity was found to be approximately one half to one order of magnitude less than the horizontal. Yager (1996) found that hydraulic conductivities of as much as four orders of magnitude lower in the vertical direction were required to obtain a model calibration of the Lockport Formation in the vicinity of Niagara Falls, NY.

Figure 1.13 depicts a conceptual model illustrating the fracture framework and groundwater flow system for a layered stratigraphic sequence such as the Lockport formation. The groundwater in this system flows primarily in discrete horizontal fractures of significant lateral extent. Infrequent vertical fractures connect the horizontal fractures allowing for some

vertical exchange of groundwater. A hypothetical DNAPL source is also depicted. The vertical and horizontal penetration of the source is governed by the volume and properties of the DNAPL (such as density and viscosity) and by the geometry of the fracture arrangement in the vicinity of the release. Following release into the subsurface, the initial migration of the DNAPL and redistribution to pools and residual is expected to have take place relatively quickly provided that the viscosity of the DNAPL is on the order of that of the water, and provided that its viscosity is significantly greater than that of water. For higher viscosity and/or lower density DNAPLs, however, the initial time-scale of migration is expected to be on the order of several years to possibly decades. Once the DNAPL has reached an equilibrium distribution, pools may be remobilized in response to changes in capillary pressure which can be effected by activities such as drilling, groundwater pumping, and groundwater injection. Mobilization of residual DNAPL in fractures, however, is not expected to be significant in response to such activities (Longino and Kueper, 1999). The subsequent production of aqueous-phase contamination in this environment is governed by the constituency of the DNAPL (the compounds present in the oil phase) and the geometry of the DNAPL distribution in the fracture framework. Assuming a horizontally-dominant flow system, dissolution of pooled and residual DNAPL will result in the migration of contamination in discrete horizontal fractures. It is this migration process which leads to the necessity for remedial action.

Figure 1.13 also depicts the process of aqueous-phase migration in the discrete horizontal fractures. The halo of contamination drawn around each fracture, depicts the process of matrix diffusion in this environment. This process acts to significantly slow the migration of contaminants in fractured media having moderate to large values of matrix porosity. Values of matrix porosity

over a large range have been reported for carbonate rock (Halley and Schmoker, 1983; Bloomfield, 1997), and estimates from elsewhere in the Lockport formation indicate typical porosities in the range of 5-10% (Johnston and Wilmot, 1989). Porosity of this magnitude can act as a significant sink for contaminants migrating in the fracture framework. Thus, although the TCE contamination was observed to migrate at a rate of 50-100 m/year, natural groundwater velocities can be expected to be much greater (i.e. by orders of magnitude).

In addition to matrix diffusion, the contaminants may interact with organic carbon present in the bulk rock or in carbonaceous horizons. Figure 1.14 depicts the hypothetical transport processes at the microscopic scale. The figure depicts the porosity in the form of microcracks. These are very small fractures that are often circular in shape with aperture widths of 5 μm or less. The microcracks expose any available organic carbon present in the bulk rock and provide pathways to layers of organic carbon that might be present in stylolites or bituminous partings. Stylolites often act as a plane of weakness and unloading fractures can be found adjacent to or bisecting these features (Nelson, 1985). Measurement of organic carbon in carbonate rock is difficult because of the preponderance of inorganic carbon, however, values given in the literature range from 0.06% to 0.31% with averages between 0.20-0.29% (Gehman, 1962). Thus, for those contaminants that have an affinity for the carbon phase, such as PCB and TCB, the amount of organic carbon exposed to either the contaminants in the groundwater flowing in individual fractures or to the contaminants diffusing through the matrix, will have a profound effect on the rate of migration of these compounds. This is evidenced by the limits of the contaminant plumes illustrated in Figure 1.11, which show significant retardation of the TCB and in particular the PCB concentrations. TCE will also interact with the organic carbon to a small degree, although this

process may be minor in comparison to the retarding effect of matrix diffusion.

1.5 Objectives

To refine the preliminary conceptual models described above, several specific objectives were established:

1. Develop a detailed understanding of the regional groundwater flow system to aid in defining the exchange between horizontal fracture planes through vertical fractures at the regional scale.
2. Define the specific features controlling the groundwater flow system on a discrete basis at the site scale.
3. Determine the extent of horizontal fractures and zones of low permeability using direct measurement, where possible.
4. Estimate regional and local directions of groundwater flow. Estimate groundwater velocity in specific features.
5. Determine the diffusion porosity of the individual members of the Lockport formation.
6. Measure the amount of organic carbon present in the Lockport formation.

2.0 METHODS

2.1 Field

2.1.1 Drilling Program

As a primary component of this study, sixteen inclined boreholes and two vertical boreholes were drilled through the entire Lockport Group underlying the CWML site and surrounding area (Figure 2.1). In the fall of 1995, seven boreholes were installed, eight were constructed in the spring of 1996 and the last three were constructed in the spring of 1997. The selection of drilling locations was conducted with the intention to examine the hydrogeology of the underlying rock at several scales. Four boreholes are constructed within a 30 x 30 m area to the north of the CWML property and are referred to as the North Cluster site. The South Cluster site is comprised of five boreholes constructed within a 50x50 m area in the centre of the remnant aqueous plume to the south of the source zone. Three boreholes are located down gradient of the south Cluster site, forming a triangle with the South Cluster site having sides approximately 100-125 m in length. The remaining 6 boreholes are located in areas up- and down-gradient of the site and were located to examine the regional groundwater flow at the scale of kms. The two regional boreholes (61 and 65) constructed down-gradient and cross-gradient to the site are located adjacent to Twenty Mile Creek. All of the boreholes are 76 mm in diameter and were constructed using diamond drilling techniques. In each case, steel drill collars were installed through the overburden and driven into bedrock. The inclined boreholes plunge between 55° and 57° and trend at azimuths ranging between 0° and 360° (Figure 2.2). The specific trends of the boreholes were selected to maximize the number of vertical fractures intersected and to investigate preferred fracture orientations. The boreholes were developed following drilling using a submersible pump (Grundfos®). During drilling, return water was generally

lost at less than 12 m (i.e the first encounter with a large open fracture).

2.1.2 Core Logging

Core recovery using triple tube techniques was greater than 95% in all boreholes. Immediately following removal from the core barrel, each core run was photographed and logged while still in the inner split tube. For the second and third drilling sessions (Spring 1996 and Spring 1997), the core photographs were processed digitally, producing electronic logs of the core for 11 boreholes. During core logging, all breaks in the rock were identified as either mechanical or open fractures. Open fractures were identified by the presence of infilling (generally calcite or gypsum), rough surfaces or evidence of weathering, and classified as one of three open structural features: i) a bedding-plane fracture (horizontal feature), ii) a vertical fracture or iii) a broken-core zone. Lithological features such as vuggy zones, chert or gypsum nodules were also noted in detail. All core descriptions are included in the Smithville database.

2.1.3 Vertical Fracture Orientations

The true orientations of vertical and sub-vertical fractures observed in the drill core were obtained using a geometric calculation (Lau, 1983). In this approach, the angular relationships between the apparent orientations of the fractures, the plunge and trend of the borehole and a reference line, were used to calculate the true attitudes of the fractures. The trend and plunge of each borehole was measured using a Brunton compass and the reference line was obtained using bedding-plane features observed in the core (Figure 2.3). A scribe representing the top of core was used as the reference line. Assuming that the bedding in the rock is approximately horizontal, the top of the core was determined by using features parallel to bedding such as argillaceous bands, bedding-plane

partings, or stylolites. When intersected by an inclined borehole, these features produce an elliptical outline in the core. The two points where the major axis of the ellipse intersects the circumference of the core indicates the top and bottom. The top is easily determined by orienting the core such that the bedding-plane feature is horizontal. Once the orientation of the core was determined, the true attitude of each fracture was calculated from two measured angles. The first angle is that between the core axis and the major axis of the ellipse of intersection. The second is measured from the top of core to the point where the downhole end of the major axis of the ellipse meets the core circumference. This is measured in the plane perpendicular to the core axis and clockwise from top of core when looking in the direction of drilling. Because the second angle is difficult to measure accurately, an arc length along the core circumference was measured instead. The angle was then calculated using the ratio of the arc length divided by the radius of the drill core. Strike and dip angles for individual vertical fractures were obtained using a FORTRAN program. Fracture spacings were determined for the vertical and bedding plane fractures after correcting depths for the inclination of the borehole.

2.1.4 Borehole Geophysics

Standard geophysical sondes were collected in 15 boreholes immediately following the completion of drilling. Boreholes 34C, 37C, 53, 54A, 54B, 54C and 55 were surveyed in 1995 by Gartner Lee Ltd. The boreholes were logged with 2-axis inclinometer, temperature, electromagnetic induction, natural gamma and caliper tools. Boreholes 56, 57, 58, 59, 60, 61, 62 were logged by Hyd-Eng Geophysics Inc. in July and August, 1996. In these boreholes, natural gamma, temperature, resistivity and caliper logs were collected. In addition, a natural gamma log was completed in 54B. Details of the two geophysical logging programs can be found in Gartner Lee (1996) and Hyd-Eng

(1997).

Video camera surveys were also conducted in all boreholes shortly following the development of the borehole. The NWRI video camera was used to examine the quality of the borehole wall along the length of each borehole. Observations of fractures, structural features such as breakouts and vugs, groundwater flow and the presence of natural gas were made both in a downward and upward direction of logging. A systematic log of fractures and other features was not compiled for each borehole. Rather, the video logs were used for reference when locating packers for specific programs, such as the tracer experiments. The video logs are not included in the Smithville database.

2.1.5 Hydraulic Testing Program

2.1.5.1 Constant-head injection tests

Constant-head injection tests (CHITs) were conducted in all boreholes to determine the vertical distribution of transmissivity (T) in the rock mass. The principle behind a constant-head injection test (CHIT) is to inject or withdraw water at a constant hydraulic head into an isolated portion of the borehole and measure the flow rate at steady-state conditions (Ziegler, 1976). For the present study, a series of 5 tanks ranging in diameter from 0.01 to 0.3 m, fitted with manometers and mounted on a light trailer was used to inject water over a wide range of injection flow rates (Figure 2.4). A range of T between 10^{-10} and 10^{-2} m/s² can be determined using this testing apparatus. Flowrate was measured by timing the change in water level as viewed through the tank manometers. Compressed nitrogen added above the water in each tank was used to ensure a constant flow rate. Each test interval was isolated using a pair of pneumatic packers. A pressure transducer located

down hole was used to measure the pressure changes due to water injection.

Using measurements of flowrate, Q , and the change in pressure expressed as a change in hydraulic head, ΔH , at steady conditions, the T of the tested zone is calculated using the Theim equation:

$$T = \frac{Q}{\Delta H 2\pi} \cdot \ln\left(\frac{r_e}{r_w}\right) \quad (2.1)$$

where r_w is the well radius and r_e is the radius of influence or outer flow boundary. The radius of influence can generally be assumed to be between 10 and 15 m for moderate values of T (Bliss and Rushton, 1984). While the actual radius of influence is unknown in most field situations, because it appears in a logarithmic term in (2.1), large errors in the estimation of r_e will result in only small errors in the calculation of T . In this study a value of 10 m was used for r_e in all calculations. Further discussion of this issue can be found in Doe and Remer (1980). In addition, for the case where vertical fractures intersected the test zone, the effective radius of the well is slightly increased. Again, because r_w appears in the logarithm term, the overestimation of T determined using the actual well radius is less than a few percent.

An equivalent single fracture aperture, $2b_{eq}$, can be determined from the test results by using the cubic law:

$$2b_{eq} = \left(T \cdot \frac{12\mu}{\rho g}\right)^{\frac{1}{3}} \quad (2.2)$$

Each borehole was tested systematically from bottom to top using a 2-m test interval. In eight boreholes (55-59, 64, 34C and 37C) the entire length of the borehole was re-tested using a 0.5-m test interval. In addition, the upper 15 m of the 4 boreholes in the North Cluster site were tested using the 0.5-m test interval. Selected zones in boreholes 64, 54A, 54D, 56 and 37C were also tested with a 0.1 m packer interval.

2.1.5.2 Pulse Interference Tests

Pulse interference tests were conducted using the four boreholes in the North Cluster Site (54A-54D). Single-pulse interference tests are an easy yet powerful extension to single-well slug tests. In this case, the pressure response in one or more observation zones due to the introduction of an instantaneous slug of water in a nearby source well is measured (Figure 2.5). A double packer arrangement with a 2" I.D. PVC casing was used to isolate the source zone. A mini-packer and transducer were installed in the casing to create and monitor the slug. To eliminate the effects of wellbore storage in the observation zone, only the double packer system and a transducer measuring the pressure in the isolated zone was used. Measured response in the observation zones were analysed using a graphical method (Novakowski, 1989). The graphical method is based on use of the magnitude of the peak response and time lag in the observation zone to calculate T and S. Peak response is defined as the ratio of the maximum rise in hydraulic head at the observation well (Δh), divided by the initial rise in hydraulic head in the source well (H_0). Time lag (t_l) is defined as the elapsed time between the start of the slug test in the source well and the maximum peak response in the observation well. The remaining required dimensionless parameters (r_D , t_D , and dimensionless wellbore storage coefficients in both the observation and source well (C_{DO} , C_{DS}) are defined as follows:

$$r_D = \frac{r}{r_w} \quad C_{DS} = \frac{C_s}{2\pi r_w^2 S} \quad C_{DO} = \frac{C_o}{2\pi r_w^2 S} \quad t_D = \frac{T t_L}{r_w^2 S} \quad \Delta h_{DO} = \frac{\Delta h}{H_o} \quad (2.3)$$

where r is the distance between the source and observation boreholes and C_s, C_o are the storage coefficients in the source and observation boreholes respectively. A set of graphs is used to determine T and S based on the dimensionless variables (Figure 2.6). This set of graphs can be used assuming there is no observation well storage ($C_{DO}=0$). Firstly, using h_{DO} and r_D , a value for C_{DS} is determined from the graphs in part a and S is calculated from the definition of C_{DS} given above. Secondly, using h_{DO} and r_D , a value for t_D is determined from the graphs in part b and T is calculated from the definition of t_D given above.

2.1.5.3 Pumping Tests

Pumping tests were conducted in isolated fractured zones using equipment similar to that used for the pulse interference tests. In the source (or withdrawal) zone for pumping tests, a double packer system having a submersible pump was used (Figure 2.7). Tubing (3/4" I.D.) was used to transport groundwater to the surface. Flowrate was measured using an inline flowmeter at the well head. Occasional point measurements of flowrate were obtained using a graduated cylinder. A double packer system and pressure transducer was used to measure drawdown in each observation zone. A data-logger located on ground surface was used to ensure that all data was captured electronically at an appropriate frequency.

Observation zone responses were interpreted using Walton's method (Kruseman and De Ridder, 1983). This method is based on a family of type curves in which each type curve has a unique value of r/L where r is the distance between the pumping and observation wells and L is a

leakage factor. In using this method, we assume that flow in the fracture zone is analogous to flow in a semi-confined aquifer (or 'leaky' aquifer). The drawdown, s , in a semi-confined aquifer can be described by (Hantush and Jacob, 1955):

$$s = \frac{Q}{4\pi T} \int_0^{\infty} \frac{1}{u} \exp\left(-y - \frac{r^2}{4L^2 y}\right) dy \quad (2.4)$$

where Q is the flowrate. Published tables (Kruseman and De Ridder, 1983) were used to plot $1/u$ vs $W(u, r/L)$ for different values of r/L to generate a family of type curves in log-log format (Figure 2.8). Field data in the form of drawdown, s , vs time, t , was also plotted in log-log format. By superimposing the field data on the type curves, the best match was determined visually by trial and error. From a match point the values of $W(u, r/L)$, $1/u$, s and t were noted and T is calculated from:

$$s = \frac{Q}{4\pi T} W(u, R/L) \quad (2.5)$$

and S is calculated from:

$$u = \frac{r^2 S}{4Tt} \quad (2.6)$$

2.1.6 Borehole Completion and Measurements of Hydraulic Head

Over the course of the study, either temporary or permanent instrumentation was installed in every open borehole. Temporary instrumentation consisted of two fixed-head packers (Roctest YEP® packers) separated by 1" I.D. (25.4 mm) perforated steel pipe (Figure 2.9). Water was used to inflate the packers in order to prevent leakage over long periods of time. A steel stand-pipe extending to the surface allowed for access to the test zone.

The Westbay[®] System was used in this study for permanent multilevel instrumentation. This system consists of water-filled packers connected by casing elements (Black, 1987) and specially designed pumping and measurement/sampling ports (Figure 2.10). Water pressure is measured and representative groundwater samples are obtained using a submersible probe which is lowered into the casing and connected to an electronic data acquisition device on surface. The probe has a small arm which is used to locate each measurement port inside the casing. Once positioned on the port, a mechanical foot is activated and presses the probe against the inner casing wall. This causes an O-ring on the opposite side of the probe to seal around a button valve, exposing the pressure transducer in the probe to water pressure outside the casing. Groundwater samples can be obtained using the same port by opening a valve from the surface unit and allowing water to fill a sample container attached below the probe (Figure 2.10).

The hydraulic head, h , (masl) is calculated from the pressure measurements in each Westbay zone using:

$$h = BH_{elev} - ((p_i - p_{out}) * 0.7038) \quad (2.7)$$

where BH_{elev} is the elevation of the casing top (masl), p_i is the pressure inside the casing (ie. prior to activating the shoe) (psi), p_{out} is the pressure in the monitoring interval (psi) and 0.7038 is a constant converting the pressure measured to metres of water. To use equation 2.7, the pressure measurement must be obtained with the casing completely filled with water.

Measurements of hydraulic head have been obtained on a weekly basis since the completion of each Westbay-instrumented borehole. Thus, there are varying lengths of records, some dating

back to the initial year of the study, with the most complete records available only for the years 1997 and 1998.

During the hydraulic head surveys, measurements were also obtained from multi-level boreholes 11, 12, and 21. These boreholes are completed through the entire thickness of the Lockport formation in the vicinity of the site and complement the data obtained from the more regionally-distributed Westbay completions. Use of the data from these boreholes, however, is restricted by the limited coverage (only 10-15%) of open borehole offered by traditional standpipe multi-level completions. The measurements collected from the traditional multi-level completions were obtained using an electric water level tape.

2.1.7 Geochemical Measurements

Groundwater samples were collected in three surveys in February, July and November, 1997, from the permanently-implaced packer systems. The samples were collected using the Westbay® probe which was configured with a stainless steel sampling chamber (volume of 500 mL). Because the volume of water external to the packer system is relatively small, mixing and diffusional processes equilibrate the geochemical parameters in each isolated zone over relatively short periods of time. Provided sufficient time is allowed post-installation (a few months), the need to purge the borehole of standing water is eliminated (Black et al., 1987). The packer material has been extensively tested by the manufacturer and other researchers and is not known to either leach constituents into the groundwater nor accept constituents through sorption or diffusion (Westbay Instruments Inc., personal communication). In addition, samples were also collected from boreholes 11, 12, and 21 (Figure 2.11). There are 5-6 discrete intervals in each of the boreholes, although the intervals are limited to 1.5-3.0 m in length.

The groundwater was placed in an enclosed container without filtration immediately following sampling, and electrical conductivity, Eh, and pH were measured. A combination electrode with an Ag/AgCl internal reference, calibrated against buffers 4 and 7 were used to determine pH. Eh was measured using a combination platinum redox and Ag/AgCl reference electrode. Alkalinity was measured shortly after sample collection by titrating a known volume of filtered sample with 0.16N sulfuric acid using a HACH digital titrator. Groundwater samples collected for inorganic ions and dissolved organic carbon (DOC) analyses were filtered in the field using a 0.45 μm nylon filter. Samples submitted for cation analyses were preserved at the time of collection with ultrapure HCl.

Analyses for metals were performed in the laboratory using inductively coupled plasma spectroscopy (ICP-MS). Anions (Cl , SO_4 and SiO_2) were determined using ultraviolet photometry (COBAS). Concentrations of ammonia ($\text{NH}_3\text{-N}$) and nitrate ($\text{NO}_3\text{-N}$) were analyzed using a Bran+Luebbe TRAACS-800 continuous flow analyzer. Analyses for DOC were performed using ultraviolet digestion. Charge imbalances for the inorganic ions were found to be less than 10% with the exception of 2 samples. Analyses were conducted by Environment Canada's, National Laboratory for Environmental Testing (NLET).

Samples were also collected for analyses ^{18}O , ^2H and tritium in July and November of 1997, and May, August and October of 1998. Analyses were performed using standard CO_2 /water and H_2 /water equilibration techniques. $\delta^{18}\text{O}$ and $\delta^2\text{H}$ data were normalized to VSMOW/SLAP and are reported relative to VSMOW with reproducibility of ± 0.1 and ± 2.0 respectively. Samples were analyzed for ^3H by using direct scintillation methods obtaining a detection limit of 6TU, with a reproducibility of $\pm 8\text{TU}$. A total of 25 selected zones were re-sampled for enriched ^3H analyses

in order to refine the estimate of concentration of ^3H in the groundwater at a few locations. The enriched ^3H analyses has a reproducibility ranging between ± 0.6 to ± 1.3 TU. All ^2H and ^{18}O analyses were conducted by the National Hydrology Research Institute (NHRI) while the ^3H analyses were conducted by the Isotope Lab at the University of Waterloo.

2.1.8 Point Dilution

Estimating groundwater velocity in discrete fractures is often difficult due to the large uncertainty associated with estimates of low-hydraulic gradient (ie. hydraulic head varies by only centimetres over distances of many metres). The point dilution method may be employed to determine direct measurements of groundwater velocity. This method is based on the decay of tracer concentration with time in an isolated section of a single well, due to dilution caused by the natural groundwater flow through the section (Drost et al., 1968; Grisak et al., 1977).

The point dilution experiments were conducted in this study using apparatus designed and built by NWRI for use specifically in fractured rock systems. The point-dilution probe consists of a set of two pneumatic packers which isolate a zone of 0.25m in length resulting in a volume between the packers and tubing of 736 mL (Figure 2.12). A conductivity probe is mounted in the top of the mixing zone while a pressure transducer is located above the top packer. A 12V electric motor installed below the bottom packer drives a propeller to continually mix the test zone. Prior to the start of an experiment, the probe was located over a specific zone and the inflation pressure allowed to dissipate. Background pressure and conductivity were monitored until steady conditions were achieved. Experiments were initiated by the instantaneous injection of a small volume of conservative tracer (KBr) into the test zone. Following the introduction of the tracer, the change in conductivity of the groundwater in the test zone was monitored until more than 50% of the initial

tracer slug had dissipated. A data logger was used to record conductivity and pressure at frequencies ranging from 1 s to 10 min.

The decay in tracer concentration in the test zone is interpreted using (Drost et al., 1968):

$$\frac{dc}{dt} = -Av_a \frac{c}{V} \quad (2.8)$$

where A is the cross-sectional area available to flow, v_a is the apparent velocity of groundwater flowing through the wellbore and V is the volume of the isolated zone in the borehole. Solving this equation for the case of an instantaneous injection, and relating the apparent velocity in the test section to the true formation velocity, v_f , yields (Drost et al., 1968):

$$v_f = -\frac{V}{\xi A t} \ln \frac{c}{c_0} \quad (2.9)$$

where c_0 is the initial concentration at $t=0$, c is the concentration at time t following tracer injection and ξ is a dimensionless correction factor accounting for additional flow captured by the open well due to the convergence of flow lines in the neighbourhood of the well bore. Groundwater velocity in a single fracture intersecting the test zone (v_f) is determined from the measurements of dilution of tracer in the sealed-off portion of the borehole by plotting the results in the form of $\ln c$ vs t and fitting a linear regression line to the data. Using the time (t_m) at $c/c_0=0.5$ obtained from the regression line, the previous equation reduces to:

$$v_f = \frac{0.693V}{\xi A t_m} \quad (2.10)$$

In the case of a zone containing a single fracture, A is equal to $1/2$ the circumference of the borehole times the hydraulic aperture and $\xi=2$ is used. Hydraulic aperture for each zone tested was determined after the completion of the point dilution experiment by conducting a constant-head injection test through the point-dilution apparatus and using the methodology outlined in Section 2.1.5.1 and Equation 2.2. For this interpretation it is assumed that the time-scale of the test is sufficiently small such that accounting for mass loss due to matrix diffusion is not necessary.

2.1.9 Tracer Experiments

Tracer experiments conducted during the course of these field investigations were completed either in injection-withdrawal format or in radial-divergent format. The injection-withdrawal experiments were conducted in the north cluster site, between boreholes interconnected by the same fracture and between fractures where a presumed vertical interconnection was present. The radial divergent experiments were conducted in discrete features in the south cluster site which were presumed to interconnect between the south cluster site and boreholes 64, and 37C over a distance of approximately 225 m. The purpose of the tracer experiments was to i) investigate the process of matrix diffusion at the scale of a single fracture, ii) explore the potential vertical interconnections established from pumping and pulse interference tests, and iii) investigate the scale at which discrete features are continuous in the horizontal direction.

2.1.9.1 Injection-Withdrawal Experiments

The injection-withdrawal experiments were conducted between a pair of boreholes (54A and 54D) in the north cluster site. The experiments were conducted in a discrete fracture located at a depth of approximately 17.0 m below ground surface. These boreholes were drilled in an inclined orientation and, at the depth the tracer experiments were conducted, the borehole separation is 9.5

m. The trajectory between the boreholes is oriented approximately parallel with the regional hydraulic gradient at this depth. The regional gradient has a magnitude of approximately 0.001 based on measurement of hydraulic head in the regional monitoring well system.

The location of the fracture was determined using hydraulic testing methods and video camera inspection. The hydraulic testing was conducted using the standard constant-head method (Novakowski, 1988) in open-hole conditions with a packer spacing of 0.50 m. Test intervals both above and below the fracture in both boreholes indicated the presence of unfractured rock. From video inspection, the expression of the fracture in borehole 54D was clearly observed to be discrete. Such was not the case in 54A due to the presence of vuggy texture. Based on inspection of the drill core, there was no evidence of infilling material or increased porosity as a result of weathering along the fracture walls. The effective single fracture aperture determined from the hydraulic tests for the intervals in 54A and 54D, are 648 μm and 510 μm , respectively.

Figure 2.13 illustrates schematically the configuration of the equipment used for these experiments. The first experiment was conducted by injecting water into the upgradient borehole, 54A, and withdrawing water at the same rate from borehole 54D. The water was not re-circulated between boreholes. The fracture was isolated in each borehole using pneumatic packers having a 0.5 m spacing. Total volume including the injection and withdrawal tubing for each interval was 5.71 and 9.66 L, respectively. The injection and withdrawal flow rates were maintained during the experiment at a constant rate of 2.5 ± 0.1 L/min.

After establishing a steady flow system between the injection and pumping boreholes, tracer was introduced into the injection tubing as an instantaneously-injected slug of approximately 0.098 L volume. To assist in studying the effects of matrix diffusion, two tracers were used, each having

a different coefficient of free-water diffusion. These were KBr ($D_0=1.9\times 10^{-9}$ m²/s) and Lissamine FF ($D_0=4.5\times 10^{-10}$ m²/s). The total mass of tracer injected was 112 mg of Lissamine and 334 mg of KBr. Samples were obtained from the withdrawal tubing at a frequency such that the peak of the tracer concentration was well defined. This resulted in the collection of about 50 samples. All samples were analyzed for Lissamine concentration while only ten samples, selected at even time intervals along the curve, were analyzed for Br⁻ concentration. Analysis for Lissamine and Br⁻ was conducted using a fluorometer and ion chromatograph, respectively.

The second experiment was conducted by reversing the injection-withdrawal flow field. The volumetric flow rate, tracer mass injected, sample frequency and analyzes were the same as for the previous experiment.

An injection-withdrawal experiment was conducted using the same methodology between the fracture located at 17.0 m depth and another located approximately 2 m lower. In this case, water was injected into the upper fracture and groundwater was pumped from the lower fracture. This experiment was unsuccessful and no direct connection was detected between these two horizontal fractures. A similar experiment was attempted at the south cluster site and was equally unsuccessful.

2.1.9.2 Radial Divergent Experiments

The radial-divergent experiments were conducted using equipment similar to that presented in Figure 2.13 for the injection-withdrawal experiments. Discrete fractures located at approximately 11 m and 41.5 m depth were isolated using straddle packers in each borehole, during two separate experiments. The experiments were conducted in boreholes 56, 58, 59, 64, and 37c, using borehole 56 as the injection well for the first experiment (shallow fracture) and borehole 59 for the second (deep fracture). The intersection of the fractures in the boreholes not used as observation wells were

blocked with single packers. Table 2.1 shows the hydraulic apertures in the injection and observation boreholes for both the upper and lower fractures. An aperture is not reported for the lower fracture in borehole 37c, because the interconnection between 64 and 37c is not clearly identified in the hydraulic testing results.

In both experiments, a steady flow field was established by injecting water from a nearby fire hydrant at a rate between 4-7 L/min (4.1 L/min for the first experiment and 7.0 L/min for the second). The flow field was established for a period of a few days prior to the injection of tracer. Tracer was introduced as a rectangular pulse of approximately 2.5 min in duration for both experiments. Bromine in the form of KBr and Lissamine FF were used as tracers. Concentrations in the tracer source were 1.5 g/L for the KBr and 1.0 g/L for the Lissamine, for both experiments. A down-hole conductivity meter was used to measure the input function of the Br in the isolated injection zone. This provided for a very accurate mathematical estimate of the inlet source function for the purpose of modeling. Because the range of measurement of the concentration of the Br is limited to slightly greater than 1.5 orders of magnitude, all samples obtained from the observation wells were analyzed for Lissamine only. Samples were obtained from the boreholes in the south cluster site once every half-hour to once every two hours. Samples from borehole 64 were obtained once every 4-12 hours.

2.2 Laboratory

The focus of the laboratory study was to utilize core samples obtained from the new boreholes in the determination of the geochemical and diffusional properties of the intact, unfractured component of the rock. No pre-existing Smithville core was available for this research and it was discovered using core from borehole 54B, that complete re-saturation of core that had

been actively dried or stored under arid conditions, was impossible (Langer, 1997). Therefore, all core samples used for measurement of porosity and for diffusion experiments were obtained and maintained under saturated conditions. Samples used for rock geochemistry, mineralogy and the measurement of organic carbon were not constrained by the requirement for saturation.

2.2.1 Core Sampling

During the 1995, and 1996 drilling programs, specific sections of core were sampled during the drilling program. The intention of the sampling program was i) to provide examples of core both adjacent to and at distance from open fractures, ii) to obtain representation from each of the members of the Lockport formation, and iii) preserve the sub-surface geochemical conditions, including full saturation of the pore space. The sampling process adhered to the following protocol:

Immediately following the arrival of the core barrel at ground surface, the section of rock to be sampled was identified. Within no more than 5 minutes following recovery of the rock from the core barrel, the samples were placed in a 1 L Nalgene® bottle filled with local groundwater. This procedure insured the core samples remained saturated. The groundwater was pre-treated with sodium azide (0.03-0.04% w/w) to inhibit bacterial growth during the storage of the samples. At some time during the 24-hour period prior to sampling, argon was bubbled through the water in each Nalgene® bottle for a minimum of 15 minutes in order to remove the dissolved oxygen. The bottles were then capped until required for sampling. Immediately after a sample was deposited in the Nalgene® bottle, the bottle was recapped and placed inside a GasPak® anaerobic system. Before the lid was sealed on the system, a GasPak® disposable gas generator envelope was placed inside. Approximately 10 mL

of groundwater was then added to the envelope with a syringe to initiate the generation of hydrogen and carbon dioxide. A BBL[®] dry anaerobic indicator strip was then taped inside the anaerobic system and the lid (with attached palladium catalyst) was then sealed in place. The indicator strips confirmed the presence of anaerobic conditions within 3 hours. At the end of each day, the samples were transported to the National Water Research Institute for longer term storage in an anaerobic glove box.

A total of 38 samples were obtained from boreholes 54A, 54B, 54D, 56, 58, 59, 60, 61, and 62 in this fashion. The samples range in length from 0.10 m to 0.20 m and are all of 45 mm diameter. Table 2.2 lists the dimensions, lithology and location from which each core sample to be used in the diffusion experiments, was obtained.

During the final drilling program conducted in 1997, the entire length of core obtained from boreholes 63, 64, and 65 were immersed in water immediately following collection. Rather than storing the core in core boxes, the core was placed in flat-lying plastic containers approximately one meter in length and 0.5 m in width. The boxes were filled with tap water, covered and sealed. Subsequent sub-sampling of the core was conducted on several occasions. At no time has the core been exposed to the air for a duration sufficient to initiate de-saturation, although no attempt was made to preserve anaerobic conditions with these samples.

Samples collected for determination of the rock geochemistry and for measurement of organic carbon need not have a saturated pore space. These samples were obtained from specific horizons after the core had been dried and stored. The samples collected for rock geochemistry were selected to maximize both areal and stratigraphic coverage of the study area. A total of 32 sub-

samples were obtained from core for chemical and mineralogical analysis. These samples were submitted to the Analytical Chemistry Laboratories of the Geological Survey of Canada for preparation, whole rock analysis and X-ray diffraction (XRD) analysis. Approximately 162 samples of stylolitic and bulk rock were obtained for measurement of organic carbon (not all were analyzed). In addition, 10 hand samples of pure stylolite material were collected for organic carbon analysis from the Goat Island member exposed in a local quarry.

2.2.2 Measurement of Organic Carbon

The transport of organic solutes in groundwater can be strongly influenced by organic carbon present in geological material. It is generally accepted that for hydrophobic organic compounds (e.g. chlorinated solvents), the degree of sorption experienced by the solute is proportional to the quantity of organic carbon in the surrounding materials. Consequently, accurate measurements of organic carbon are required to properly describe the transport behavior of the principal contaminants present in the groundwater underlying the CWML site. The measurement of organic carbon in a rock type of which the principal constituent is inorganic carbon, however, is a difficult problem for which there are no established procedures.

In this study, several methods for the measurement of organic carbon were used and compared. The methods include i) the Loss-on-Ignition (LoI) technique, ii) Walkley-Black wet oxidation (titration), iii) Leco Carbon Analyser, iv) Carbon Analyser with a pre-acidification step, and v) batch experiments conducted using a hydrophobic compound (TCE). The majority of the measurements were conducted by NWRI, with the exception of the measurements obtained using the pre-acidification step which were conducted by the Dept. of Geology, of Washington State University, and several comparative analyses conducted by Leco Corporation in St. Joseph,

Michigan.

The initial measurements were conducted primarily using the LoI method, Walkley-Black titration, and the Leco Carbon Analyser. Using the same homogenized rock samples and several standards containing pure calcite and known percentages of organic carbon, it was found that the LoI and Walkley-Black titration methods consistently overestimated the organic carbon content determined using the Leco Carbon Analyser. On this basis, further calibration of the Leco CR12 instrument was conducted by cross-laboratory comparison to the method used by the Dept. of Geology at Washington State University and to a more accurate instrument operated by Leco Corporation. The results of this comparison are given in Table 2.3. The agreement between the results obtained using the Leco CR12 and the UIC Carbon Analyser (Washington State) is very good, suggesting that the Leco will provide accurate estimates of organic carbon in the range typical of what might be expected for carbonate rock (0.0%-0.3%). Although the comparison between the Leco CR12 and RC412 was only obtained for a layer of high organic content (an argillaceous band), other measurements conducted using the RC412 fell within the lower ranges obtained using the CR12 and the Washington State method. Thus, all results reported in the following chapter are those obtained using the Leco CR12.

Preparation of the samples for analysis with the Leco CR12 was conducted by milling and pulverizing the sample to produce a fine-grained mass. The pulverizing process was undertaken using a tungsten-carbide shatter-box to prevent the artificial introduction of organic carbon from a regular steel source. Several samples consisting of pure glass beads were also prepared as blanks. These were powdered in the same fashion as the rock samples.

Batch experiments were also conducted to estimate the percentage of organic carbon present

in the Lockport formation. Batch experiments are conducted to measure the equilibrium exchange of a given compound between an aqueous solution and the solid phase. To conduct the batch experiments, several samples of powdered material were split into vials. Each vial was filled with water and spiked with a different concentration of contaminant. After allowing for equilibration, the concentration left in the aqueous phase was measured and C_s (the concentration of the sorbed compound on the solid phase) and C_w (the concentration of the compound remaining in the water phase) were calculated. The resulting values of C_s and C_w are plotted to produce an isotherm based on the observed data. Because trichloroethylene (TCE) has a well-defined affinity for organic carbon, this compound was chosen for this study.

The batch experiments were conducted using 40 mL glass vials capped with Teflon coated silicone septa. Three vials containing standards were also prepared for use during concentration analysis. For each of the four study materials, namely stylolitic material and separate host rock from the Goat Island and Gasport members, three vials were prepared, each containing approximately 1.0 gram of solid mass for the stylolitic materials and 3 grams for the host rock material. Exactly 40 mL of de-ionized water was then added to each vial and the vial was subsequently capped. A stock TCE solution of 800 ppm was prepared by mixing 22 μ L of neat TCE with 40 mL of MeOH. From the stock solution 0.015 mL, 0.030 mL and 0.045 mL were added to separate vials using Gastight[®] syringes to produce a set of three vials for each sample material containing approximately 300 ppb, 600 ppb and 900 ppb solutions of TCE, respectively. These sets were replicated twice to provide a total of three sets of three vials each for Goat Island host rock material, Goat Island stylolite material, Gasport host rock material and Gasport stylolite material.

To obtain estimates of C_s and C_w , headspace analysis was used. This technique has been

shown to be viable with nonionic volatile organic compounds, such as TCE, and allows for collection of concentration measurements throughout the duration of the experiments without substantial loss of mass in the aqueous-phase solution. In this case, gas-phase samples are obtained from the headspace above the batch sample in the experimental vial. It is assumed that the concentration in the aqueous phase and the gas phase can be related by Raoult's Law. This method allows for the frequent monitoring of concentrations during the course of a batch experiment as C_s and C_w achieve equilibration. Analysis of the gas-phase TCE was conducted using a Photovac® 10s Plus gas chromatograph. Each standard was analyzed prior to analysis of the actual samples and re-analyzed afterwards. The vials were stored in an inverted position to prevent any possible escape of gas-phase TCE through the septum.

For the preliminary conceptual model of the micro-scale processes, as described in the Introduction, it was assumed that the organic carbon might be distributed relatively randomly in the bulk rock and may concentrate in the stylolitic and argillaceous bands. Thus, the samples collected from the core were classified as to presence or absence of these features. Table 2.4 provides a list of the samples for which the analysis of organic carbon was obtained. The location of the sample and a brief description are also provided. The additional 10 samples collected from a local quarry were almost purely comprised of stylolitic material from the Goat Island and Gasport members.

2.2.3 Diffusion Experiments

The two most significant parameters which govern the transfer of aqueous phase contaminants from fracture to rock matrix are the effective porosity of the rock, and the effective diffusion coefficient of the contaminant. Most methods for measuring diffusion using core samples can not distinguish between these parameters. A recently-developed method (Novakowski and

vanderKamp, 1996) based on the process of radial diffusion within an intact core sample, however, has been shown to provide independent estimates of effective porosity and the effective diffusion coefficient. Thus, radial diffusion cells were constructed for the diffusion experiments. This was accomplished by drilling a 1.25 mm diameter reservoir through the center of the core samples, parallel to the core axis (Figure 2.14). The drilling was conducted using a diamond core bit, cooled with groundwater obtained from the site. Saturation was maintained at all times. An Argon-filled tent was used to minimize contact with the aerobic environment. Each end of the sample was planed to 90° and then the entire sample was encapsulated in a Teflon® sleeve and sealed with two stainless steel end caps. One end cap contained a sampling port through which samples were extracted from the reservoir. The Teflon® coating was heat sealed to minimize leaking and evaporation of the liquid phase.

The diffusion experiments were conducted in both forward (from the reservoir) and reverse (to the reservoir) directions. To initiate the forward diffusion experiments, groundwater in the reservoir was removed and replaced with groundwater containing initial tracer concentrations. The exact volume of tracer solution introduced to each reservoir is given in Table 2.5. The subsequent decrease in tracer concentration in the reservoir was monitored by periodic sampling. The sampling was conducted so as to minimize the volume of sample abstracted and at a frequency that well-defines the decline in concentration. It was assumed that free water diffusion maintained uniform concentrations in the reservoir at all times. For comparative purposes, a control cell was constructed using a stainless steel blank of dimensions similar to the rock core.

Table 2.6 lists the tracers used for the experiments. These included bromide (as KBr), Lissamine FF (a conservative organic dye), Nitrite (as NaNO_2) and Difluorobenzoic acid (DFBA).

Initial concentrations established in the reservoir ranged from 500 ppb for Lissamine to 1000 ppm for Bromide (Br), Nitrite (NO_2) and DFBA. Only tracers assumed to be conservative were chosen so as to eliminate other potential sources of mass loss, such as decay and adsorption. Previous experiments (Shackelford et al., 1989) have shown that Br will behave conservatively in most soils and rock types. Although some organic dyes are known to interact with geological materials (Smart and Laidlaw, 1977), Lissamine was observed to behave conservatively in field-scale tracer experiments conducted in rock similar to that used for the present experiments (Novakowski and Lapcevic, 1994) and in field experiments conducted at the Smithville site (Novakowski et al., 1999). Difluorobenzoic acid has recently been observed to behave conservatively in bench scale studies as well as in aquifer tracer tests (Bowman and Gibbens, 1992).

Following the initiation of the experiment, the reservoir was periodically measured for tracer concentration. A thirty to forty day period was required for the experiments to reach equilibrium (concentration within the reservoir equal to the concentration in the rock). For each Br, NO_2 or DFBA sample obtained, 0.1 to 0.45 mL was abstracted from the reservoir and replaced with de-ionized water. Lissamine analysis is non-destructive and sample volumes abstracted were immediately returned to the reservoir following analysis. Lissamine was analyzed using a Turner fluorometer. Concentrations of Br^- and NO_2^- were analyzed, after diluting the sample in distilled water, using a Waters WISP 712 ion chromatograph. In some cases, Br was analyzed along with DFBA using high performance liquid chromatography (HPLC) having a variable wavelength UV detector and a strong anion exchange column (Bowman and Gibbens, 1992). Initially, DFBA was analyzed using ion chromatography (for cells, G1, E1, E2, E3 and G3), however this analytical procedure was found to lack adequate sensitivity and later analyses for DFBA were performed

exclusively with the HPLC.

Once the forward diffusion experiments were completed, reverse diffusion experiments were conducted using some of the cells. These experiments were conducted by replacing the reservoir fluid with de-ionized water after equilibration and then monitoring Lissamine and Br tracers as they diffused back into the reservoir in a fashion following that of the forward diffusion experiments.

The weight of the cells was monitored over the entire experimental period. Diffusion cells showed an average mass loss equivalent to 0.01 mL per day. Mass loss may have occurred from non-visible leaks or evaporation.

For comparison to the results of the diffusion experiments, a gravimetric porosity (total porosity) measurement of the entire sample was obtained after the diffusion experiments were completed. To conduct this measurement, the wet weight of each sample was recorded. Samples were then placed in a drying oven at 50°C for 18 hours and allowed to cool in a desiccator before re-weighing. Porosity was calculated by converting the weight of water lost to volume and dividing this by the volume of the sample.

2.2.4 Measurement of Total Porosity

In addition to the diffusion experiments, several saturated samples were obtained from boreholes 54A, 54B, and 54D specifically for the measurement of total porosity. A total of 9 sections of saturated core approximately 0.2 m in length were sub-sampled by cutting 3-4 discs 5-20 mm in thickness. The samples were taken from all members of the Lockport and from horizons adjacent to fractures and horizons at distance from potentially-open features. In addition, a section of core from borehole 64, approximately 15.5 m in length was completely sectioned into 20 mm discs. This section straddled the lower Eramosa and upper Vinemount members ranging in depths below ground

surface from 12.4-27.9 m.

To estimate porosity, the dimensions of the discs were measured accurately and then placed in an oven to dry following the procedure outlined above. Both total porosity and dry bulk density were determined from the results. It should be noted that the gypsum present in the Vinemount, Goat Island, and Gasport members will also de-hydrate during the drying process. Using theoretical calculations, this will lead to an overestimate of porosity by as much as approximately 1.0-1.5% for very gypsiferous samples. Because the exact content of gypsum in the individual samples was unknown, correction for this effect was not conducted. In general, it is believed that the error introduced by gypsum dehydration was less than 0.5% for the majority of the samples. Because gypsum is not present in the samples obtained from the Eramosa, the porosity estimates from this member are unaffected by this process.

3.0 RESULTS AND DISCUSSION

3.1 Field

3.1.1 Drilling and Core Analysis

3.1.1.1 Lithology

The Smithville area is underlain by the Lockport Formation, a near flat-lying dolostone of Silurian age. The formation ranges in thickness between 26 and 40 m in the study area and dips gently to the south. It is overlain by 2.14 m of overburden and underlain by the Rochester Shale. Detailed descriptions of the regional geology and depositional history of the strata can be found in Gartner- Lee Associates Ltd. (1995). The Lockport Formation is generally subdivided into three members: Eramosa, Goat Island and Gasport (Figure 3.1) (Brett et al., 1995). While there continues to be debate and confusion on the formal nomenclature of the strata, in this study subdivisions were

adopted which are consistent with previous site specific and local studies.

In the Smithville area, the Eramosa dolostone is frequently subdivided into the Upper and Lower Eramosa units. The upper part of the Goat Island Dolostone is referred to as the Vinemount member and usually subdivided further into the Upper and Lower Vinemount units. The Ancaster Chert beds and Niagara Falls submember collectively form the remainder of the Goat Island Member. In this study, we focus on the following subdivisions: Eramosa, Upper and Lower Vinemount, Goat Island and Gasport (Figure 3.1). The stratigraphic contacts at each borehole were determined by visual examination of the core and are consistent with previous work by Blair and McFarland (1992). The uppermost member is the Eramosa dolostone, which is a brownish-grey to medium-grey unit characterized by frequent bedding plane fractures, variable porosity, and occasional gypsum and dolomite-filled vugs. In the Smithville area, the thickness of this unit ranges from 5.9-18.6 m based on the drilling results.

The Vinemount member transitionally underlies the Eramosa. This member is a vuggy, gypsiferous, and argillaceous dolostone, medium grey in color, and fined grained in texture. In the upper portion of the Vinemount, the gypsum-filled vugs have been weathered out. This portion is also highly fractured and was the horizon used as the source for the town water supply. In the lower half of the Vinemount, the gypsum is unweathered and bedding plane fractures are much less common. This horizon is of very low permeability and is observed to be persistent throughout the study area. Based on drilling, the upper and lower Vinemount members range in combined thickness from 3.4 to 14.1 m.

The underlying Goat Island member is a chert-rich dolostone, fine to medium grained with less frequent bedding-plane partings. This member is 4.6 to 6.8 m in thickness within the study area.

The lowermost member of the Lockport formation is the Gasport dolostone, a fine-to-medium grained unit, light grey in color, having slightly less frequent bedding plane partings than the Eramosa. The Gasport member ranges in thickness from 6.6 to 16.0 m in the study area. All of the eighteen boreholes used in this study intersect the total length of the Lockport and end in the underlying Rochester Shale.

3.1.1.2 Fractures

Both horizontal bedding-plane fractures (BPFs) and vertical fractures (VFs) were identified in the rock core. The total number of BPFs identified ranges from 410 in the Gasport member to 588 in the Eramosa member. Fracture logs are included as part of the composite borehole logs in Appendix B. While fewer BPFs were noted in the Vinemount member, core for the Upper Vinemount unit tends to be shattered making fracture identification difficult. BPF fracture spacings range from 0.01 m to 3 m with average spacings ranging from 0.2-0.7 m in the different units (Table 3.1). Average spacing in the Eramosa member is 0.39 m. The average spacing decreases to 0.22-0.27 m in the Vinemount member and increases to 0.7 m in the Goat Island member. The average spacing in the Gasport member is 0.38 m, similar to that for the Eramosa member. Based on these results, there is no evidence for an increase in the fracture spacing with depth. In addition, since the total length of core in the Eramosa is greater than that for the Gasport (Table 3.1) there appears to be a relative uniformity in fracturing between the two units, which are separated by a less fractured unit.

Fracture spacing distributions (Figures 3.2 and 3.3) show strongly skewed distributions in all members. Both power and exponential theoretical distribution types can be fit to the spacing data. Power distributions better simulate the spacing distributions in most fracture groupings except the Eramosa member where the exponential distribution shows a slightly higher R^2 . Microsoft Excel®

built-in statistical and graphing routines were used to fit the spacing data to theoretical distributions.

Vertical fractures were noted in all horizons, with the majority (~ 75%) observed in the Eramosa member. About 80% of the VFs were oriented. Fractures could not be oriented if a suitable indicator of bedding in the same core run was not noted. In the Eramosa member, VFs can be roughly subdivided into 5 different sets (Table 3.2 and Figure 3.4). The grouping of vertical fractures into sets is somewhat arbitrary considering the small number of fractures, but nevertheless helps to compare the observed orientations to results obtained from surface mapping. Set I appears to be the most dominant and roughly corresponds to a dominant orientation observed in the Paleozoic rocks in the Niagara region by other researchers (e.g., Williams et al., 1985; Ruddy, 1993). Set II is roughly orthogonal to Set I and is similar to N-S sets observed in previous regional studies. The orientation of Set III also agrees with regional trends and is believed to be formed in the neotectonic stress field (Gartner-Lee Associates Ltd., 1995). Orientation data from the Goat Island member, indicate that Set II is the only major set observed (Figure 3.5). Finally in the Gasport member, Sets I, II, and III are evident, although Set II is rotated about 10° relative to the orientation observed in the Eramosa member (Figure 3.6).

The general consistency in observed VF sets between the various units suggests that the vertical fractures predominantly originated from paleo-stress fields. This is in contrast to orientations observed in the near-surface which are often dominated by orientations related to the contemporary stress field. While it is unlikely that many of the vertical fractures extend through the different units, the length of the vertical fractures is not discernable from subsurface core measurements and remains an uncertainty.

Mean vertical fracture spacings range from 0.77 m to 1.5 m, depending on the unit (Table

3.1). In the Eramosa member, mean VF spacing is 0.77 m. In the Gasport member, the mean spacing increases to 1.5 m. The distribution of vertical fracture spacings in the Eramosa can be fit to exponential and power distributions (Figure 3.7).

The frequency of BPFs in the Eramosa member is about 5 times greater than that of the VFs. Similarly, the frequency of the VFs is only 5% of the BPFs, in the Gasport member. While both horizontal bedding plane fractures and vertical fractures combine to form a three-dimensional network of interconnected fractures, the differences in the frequencies of the individual sets suggests a predominance of breaks in the horizontal direction.

It is important to note that core analysis is subjective. It is often difficult to identify natural fractures and aperture cannot be measured from the core due to the changes in confining stress imposed by retrieving core from the subsurface. In addition, the hydrogeologically important fractures are usually not evident from purely physical inspection. The relationship of core to in-situ hydraulic measurements is discussed further in a following section.

3.1.2 Borehole Geophysics

The geophysical logs are included in the composite borehole logs in Appendix B. Details of the two geophysical logging programs can be found in Gartner Lee (1996) and Hyd-Eng (1997). Because of the uniform nature of the lithology, several of the geophysical logs were observed to be relatively featureless. The natural gamma logs were useful, however, for picking the contact between the Decew and Rochester Formations. The electric logs did exhibit correlatable signatures in the Vinemount, although these were used only qualitatively in selecting the member contacts.

Because there are no geophysical logs that can directly detect fractures that are open to groundwater flow, obtaining this information using geophysical means, must be done by inference.

The logs most useful for this are conductivity, caliper, temperature, differential temperature, and in-hole flow meter. All of these, with the exception of the latter, were obtained for two or more boreholes in the study area.

The caliper logs were uniformly observed to respond to locations where spalling of the borehole wall had occurred. In most cases, the occurrence of spalling was directly associated with fractures and vugs. In addition, the occurrence of a zone of spalling can sometimes be directly associated with zones of high transmissivity. The most notable examples of this are the zone of vuggy texture in the upper to middle Vinemount, and a fracture zone at the base of the Gasport, where high T in some boreholes is prevalent in both cases. It is important to note, however, that much of the bulk rock where the caliper log showed little if any response, may also have significant, if not greater, transmissivity in comparison to the spalled zones. Thus, the caliper log is a useful reconnaissance tool, but should not be used as a means for hydraulic characterization.

The conductivity and temperature logs are also a useful reconnaissance tool, although extreme care is required in interpreting these logs in the search for hydraulically active zones. In many cases, signals in the differential temperature log in conjunction with the a caliper response, suggested the presence of hydraulically-active fractures. However, comparison with the transmissivity profile shows only minor T present in these zones (bottom of BH 57, for example).

Calibration experiments conducted with the video equipment in the laboratory suggest that the depth resolution of noted features using the video log is within about 10 cm. The clarity of the images in the boreholes were negatively influenced by rock flour, biological growth and the presence of natural gas in the borehole. The video logs vary greatly in their quality and should be considered overall as qualitative in nature.

3.1.3 Hydraulic Testing Program

3.1.3.1 Constant head injection tests

Each of the 18 boreholes constructed for this study was hydraulically profiled using a test interval of 2-m. A total of 375 tests (not including duplicates) were conducted at this scale. Examples of the results obtained from 5 boreholes are shown in Figure 3.8. In most boreholes there is a 6-8 order of magnitude variation in transmissivity, T , over the borehole depth. The variation of T within the three major members of the Lockport Formation (Eramosa, Goat Island (including Vinemount) and Gasport) is shown with histograms of the distribution of $\log(T)$ in Figure 3.9. Distribution statistics are summarized in Table 3.3.

Twelve of the boreholes were hydraulically tested either partially or in their entirety using a 0.5 m test interval. Boreholes 55-59, 34C, 37C and 64 were tested entirely while boreholes 54A-D were partially tested. The results of this testing is summarized in Table 3.4 and Figure 3.10. With the exception of the Goat Island member and Upper Vinemount unit, the T measured in these tests show a range between the upper and lower measurement limits of the system (10^{10} and 10^{-2} m²/s). For the purpose of calculating distribution statistics, measurements at the upper and lower limits of the testing system were set as the detection limits. The statistics of the equivalent single fracture apertures ($2b_{eq}$) calculated from this data are also summarized in Table 3.4. Figure 3.11 shows aperture distributions for the various subgroups of Figure 3.10.

The geometric mean transmissivity (T_G) for the Eramosa Unit is about 1.5 orders of magnitude lower than the T_G determined from the 2-m tests (6×10^{-7} m²/s vs 1×10^{-5} m²/s). A similar difference in the T_G of the Gasport is observed between the two test interval sizes (6×10^{-6} vs 2×10^{-7} m²/s). In addition, larger standard deviations in $\ln(T)$ are calculated for the smaller test intervals.

These differences simply illustrate that the shorter test interval captures more of the variability in the T distribution than that observed with the larger test section. These results are to be expected, given that a single large open fracture will dominate the T measurement of a given zone, and since the average fracture spacings determined from the core are generally less than 2 m. It should be noted that the separation of the T distributions by geological unit is based on the lithology as determined from the core analysis. From a hydrogeological perspective the lithological classifications are rather arbitrary and only serve to assist in comparison. Based on the results of the hydraulic testing, it is evident that there are no constraints to the fracture framework and groundwater flow system, imparted by the lithology. This is with the exception perhaps of the low-permeability horizon which seems to be pervasively associated with the lower Vinemount.

Figure 3.12 shows the vertical profiles of transmissivity for the 5 boreholes in the south cluster site. Distinct high permeability features can be identified and correlated between the different boreholes at this scale (over 10–40 m). The majority of these features are located in the Eramosa and Upper Vinemount units. Correlations at a horizontal scale of 100–150 m can also be postulated (Figure 3.13). The testing conducted in the south cluster site using 0.1-m packer spacing indicate that high T features observed with the 0.5-m spacing are generally dominated by one BPF fracture.

Figure 3.14 shows a comparison between the hydraulic testing results for the 2.0 m packer spacings, the 0.5 m packer spacings and the 0.1 m packer spacings over a 5 m section of borehole. This data was collected from the Eramosa Member in borehole 37C. This figure clearly illustrates the degree of heterogeneity typically present in this rock and the degree of integration imparted by the use of 2.0-m packer spacings. In addition, because we observe that the data at the 0.5-m scale is only slightly less uniform than the 2.0-m data, it is implied that the high T features observed in the

0.10-m data occur at an average spacing of less than 0.5 m (as is also evidenced in the core record). Thus, it is suggested that a considerable number of the bedding plane fractures observed in core are permeable to groundwater flow in this horizon. Additional 0.1-m test data from boreholes 37C, 64, 56, 54A and 54D is plotted in Figures C1-C8 in Appendix C. In borehole 64, two continuous sections of the borehole in the Eramosa and Gasport units respectively were characterized with the 0.1 m test interval. The latter was 2.82 m in length (corrected for dip) and the former, 4.23 m in length.

Fracture porosities were also calculated from the results of the hydraulic testing data using the 0.1-m test interval data in 64 and all of the 0.5-m test interval data (Table 3.5). A range of fracture porosities between 6×10^{-4} and 2×10^{-5} is noted for the different units in the Lockport dolostone. The lowest fracture porosities are noted in the Lower Vinemount and Goat Island units while the Eramosa and Gasport units show similar bulk fracture porosities an order of magnitude higher. It is important to note that fracture porosity is an integrated parameter normally used to equate transport in fractured media with porous media having similar hydraulic properties. The meaning and use of the parameter for fractured media remains under scientific debate.

To examine the contributions of the different hydraulic elements to the transmissivity profile, each of the 0.5 m test zones was compared to the core log. For each test zone the number of BPF, VF, machine breaks, and broken core zones were tabulated. From this, zones which contained only machine breaks and no other features were defined. These zones were assumed to have transmissivity representative of the rock matrix. The initial interpretation of the distribution of these zones resulted in a ranges of T from 10^{-2} to 10^{-10} m²/s. Core measurements can easily be in error by up to 20 cm per 10 foot core run, however, so high permeability zones that have no associated features but are

surrounded by other high T zones or close to vertical fractures, BPFs or BC, were censored from the data set. This eliminated approximately 15% of the no-feature zones and reduced the range in T to 10^{-6} - $<10^{-10}$ m²/s. Data from boreholes 55-59, 37C, 34C and 64 were used in this analysis. While recognizing the limitations of this interpretation, the 161 zones which remained following the censoring can be used to examine the variation in the matrix T of the rock.

When classified according to lithology, average matrix transmissivities range over two orders of magnitude between the units (Table 3.6). The Eramosa unit has an average Ln (T) of 10^{-8} m²/s. This decreases to 10^{-10} m²/s in the Vinemount member and increases to 10^{-9} m²/s in the Goat Island. Matrix T in the Gasport member is about half an order of magnitude lower than that measured in the Eramosa Member. In approximately 25% of these zones, T was below the lower measurement limit of 10^{-10} m²/s (Figure 3.15(a)). Most of these zones occur in the Vinemount and Goat Island units. A plot of all the measurements shows a larger spread in values in the Eramosa member than the Gasport member (Figure 3.15(b)). The distribution and statistics of the matrix T are consistent with the other permeability measurements of the dolostone and suggests that the Lockport Formation can be subdivided into 3 zones, with 2 high permeability zones separated by a lower permeability zone. These zones are largely independent of lithology. Table 3.6 also show the associated values of hydraulic conductivity (K), m/s, converted from T using the packer spacing.

The properties of vertical fractures are important to the connectivity of the three dimensional fracture framework of the Lockport Formation. To examine this component of the flow system, a subset of the hydraulic test zones was examined in which the only structural feature noted in the corresponding core are vertical fractures. In general, the distribution of T in the vertical fractures ranges between 10^{-6} and 10^{-9} m²/s (Figure 3.16). A few measurements are higher, although these are

likely to be related to zones which contain both BPFs and VFs. This analysis is limited by core measurement error in the same manner as the analysis of matrix T zones. In addition, where both BPFs and Vfs have been identified in a single interval, there is no way of distinguishing which is the greater contributor to the permeability.

Figure 3.17 illustrates that zones in which only the vertical fractures are contributing to the permeability occur mostly in the Eramosa and Gasport Members and there is very little vertical permeability in the middle section of the Lockport Formation (Vinemount and Goat Island members). About 6% of all zones tested contain only vertical fractures, while zones which contain vertical fractures and other features make up about 17% of the total data set.

The spatial correlation of the T measurements in both horizontal and vertical directions was investigated using experimental variograms. The experimental variogram is a basic tool in geostatistics which can be used to summarize information on the spatial relationship between data points. In this analysis, it is assumed that data measurements are not random but instead are related in some manner within a certain scale (limit of which is referred to as "range"). Beyond the range, measurement points are uncorrelated. The range is identified on variograms as the point at which the variance in the data stabilizes. Each variogram was estimated using the following equation (David, 1977) for a variety of lag distances:

$$\gamma(h) = \frac{1}{2N(h)} \sum_{i=1}^{N(h)} (z(x_i+h) - z(x_i))^2 \quad (3.1)$$

Where h is lag distance, $z(x_i)$ is the property value at given point (in this study, the property is $\ln(T)$)

at the elevation of the midpoint of test interval), $z(x_i+h)$ is the property value at a given point separated by one lag distance from x_i , and $N(h)$ is the total number of pairs at a given lag distance. The interactive program VARIOWIN (Pannatier, 1996) was used to fit theoretical models to the variograms generated with the experimental data. This program uses an indicative goodness of fit (IGF) to measure the quality of the fit. The IGF is calculated at each match and allows the user to adjust model parameters until a best fit is obtained.

In interpreting data using a geostatistical approach, specifically in this variogram analysis, the manner in which the individual data measurements are grouped is critical. Utilizing data from various locations (ie. different boreholes) implies 'stationarity'. Assuming stationarity suggests that the mean and variance of the measured parameter (in this case transmissivity measurements in a given borehole or rock formation) does not vary spatially. In some of the variograms in this study a rigorous drift analysis (ie. checking for and filtering the data for stationarity) was not carried out. In addition, much of the data used in this study was obtained from inclined boreholes, suggesting that the distance between measurement points will have a horizontal component that has not been accounted for in the analysis of vertical heterogeneity. The following discussion is presented primarily as examples of how the data can be used. More rigorous variogram analysis is planned for a future study.

The transmissivity measurements as obtained from complete lengths of the boreholes using both a 0.5-m and 2-m test interval were used to construct two variograms (Figure 3.18). The variogram obtained using 0.5 m data shows evidence for multiple structures, with a rapid rise to a sill at a variance of about 17 at a range of 2 m. Beyond lag distances of 6 m, this variogram exhibits a continued rise in variance suggesting a geological influence on the transmissivity. It is important

to note, however, that if each lithological unit has a distinct transmissivity distribution then it is not appropriate to combine all data into one set. Although we have previously suggested that the flow system should be defined on an hydraulic rather than lithological basis, it is evident from these statistics that there may be some lithologic control to the development of the fracture framework.

The 0.5-m data obtained from only the Eramosa unit in the South cluster boreholes was used in constructing the variogram in Figure 3.19. This variogram shows "pure nugget" behaviour suggesting that there is no vertical correlation at this scale or correlation is at a scale below the smallest lag distance. The sill (or nugget in this case) is about a half that of the cumulative variogram (Figure 3.18) suggesting much lower variance for the Eramosa alone. Stationarity is not an issue in this variogram as the mean T in each of these boreholes spaced 10- 50 m apart are similar. In comparison, data from the Gasport unit (Figure 3.20.) illustrates a variogram with clearer structure. In this case a spherical model can be fit to the variogram (David, 1977):

$$\gamma(h) = C \left(\frac{3|h|}{2a} - \frac{1}{2} \left(\frac{|h|}{a} \right)^3 \right) + C_0 \quad h \leq a$$

$$= C + C_0 \quad h > a \quad (3.2)$$

A range of about 1.4 m and a sill of 18.4 fits the data for the Gasport member.

The variogram shown in Figure 3.21 was constructed using transmissivity data collected from 0.1 m tests over a continuous 3.4 m section of Eramosa dolostone in borehole 64. The natural cyclicity of this geological system can be simulated using a "hole effect" model. In this case the variogram was fit to a combination of linear and hole effect models (modified from Rea and Knight, 1998):

$$\gamma(h) = mh + c \left\{ 1 - \left[\exp\left(-\frac{h}{\delta}\right) \cos\left(\frac{2\pi h}{\lambda}\right) \right] \right\} + C_0 \quad (3.3)$$

where m is the slope of the linear model, c is the sill, δ is a factor to model damping of the hole effect amplitude with increasing lag, λ is the hole effect amplitude and C_0 is the nugget. In this case the model was fit to the experimental data visually by 'trial and error'. At this scale the hydraulic tests measure the T of individual fractures as well as interweaved non-fractured zones. The cyclicity in the correlation structure arises from repeated sections of fractured and non-fractured zones. The superposition of the linear model suggests an underlying trend is also influencing the vertical distribution of permeability in this rock. This trend is likely related to depositional or diagenetic processes.

In Figure 3.22, a variogram is presented which illustrates the horizontal correlation across the study site. An exponential model fit is shown with a range of about 22 m and sill of about 10. In this variogram, true three-dimensional coordinates for each measurement point were used and as such both the horizontal and vertical components of the variation in transmissivity are accounted for. The lower variance and higher range suggests that transmissivity is correlated over a much greater distance horizontally as opposed to vertically. This is consistent with a groundwater flow system that is predominantly horizontal.

3.1.3.3 Pulse Interference Tests

A total of 52 pulse interference tests were conducted using zones in 54D as the source injection zone with monitoring in observation zones located in boreholes 54A, 54B and 54C. The tests can be grouped into four different sets. In each set, a specific zone in 54D was isolated as the source interval while in each of the other boreholes the observation zone was systematically altered for each test in the set. An initial position relative to the source was determined in each of the observation boreholes. This position (marked as 0.00 in Table 3.7) is the best direct connection

between the source and observation zones. In subsequent tests within a set the position of the source zone was not altered but the observation zones were systematically modified by moving packers fixed distances up and down the borehole. The distances noted in Table 3.7 refer to true straight line distances between the observation and source zones (ie. calculated from x,y,z coordinates incorporating the dip and plunge of the inclined boreholes). A summary of all tests conducted is included in Table 3.7. The objective of these tests was to investigate the interconnectivity of the fractures both horizontally and vertically. In over 80 % of the observation intervals no response was measured. Observation zones in which response was measured are either in direct horizontal connection with the source zone or ± 0.5 m in elevation. This suggests that the vertical connectivity in this system is limited while horizontal connectivity is confirmed at a scale ranging from 8-15 m.

The results from two different source zones, interpreted using time-lag analysis, are summarized in Table 3.8. In some zones response to the pulse was detected but not interpretable. In Set #1, the source zone has a fracture aperture measured from the constant head injection tests of about 500 μm while in Set #2 the source zone fracture aperture is about 225 μm . In the Set #1 tests, the T and 2b calculated from the pulse interference tests are higher than that of the constant head injection tests. A difference in T of an order of magnitude is noted between the two test types. In the Set #2 tests, the pulse and single well numbers are roughly equal. Measured storativity (S) ranges from 10^{-4} to 10^{-6} in all tests. The measured values of storativity are similar to that obtained from other studies conducted in the same rock type (Novakowski and Lapcevic, 1988).

3.1.3.4 Pumping Tests

Two pumping tests were conducted using the south cluster boreholes (55-59). In the first test the pumping rate was 6.2 L/min out of borehole 56. In the second test, the pumping rate was

8 L/min out of borehole 58. Both tests were conducted over 24-28 hours. The zone tested corresponds to Feature D identified in the constant-head injection data (Figure 3.12). The results of both pumping tests indicate a T of 5×10^{-5} m²/s and range in S of 2×10^{-5} to 5×10^{-6} (Table 3.9). The calculated transmissivities from the pumping tests are about half an order of magnitude lower than the transmissivities calculated from the constant-head injection tests ($\sim 1 \times 10^{-4}$ m²/s). This difference is likely due to the larger radius of influence of the multiwell test. Assuming a value for the distance between major horizontal features (~ 4 m), vertical transmissivity (T_v) was determined from the leakage factors to range between 6×10^{-8} to 3×10^{-9} m²/s. From the results of the pumping tests we are able to confirm inter-well connectivity at a scale up to 36 m and surmise that the contribution of the vertical fractures to the flow system is not significant at this scale. Caution must be taken in comparing the three hydraulic testing types since the multiwell tests were designed to assess very specific features and not capture the bulk properties of the rock.

3.1.4 Borehole Completions

Permanent Westbay instrumentation was installed in 4 boreholes in August 1996 (Westbay, 1996) and in an additional two boreholes in July 1997 (Voralek, 1997). In all cases, the configuration of the isolated intervals was based on the results of the 2-m constant-head injection tests. Six to nine intervals are isolated in each borehole. Seventeen intervals in the permanent multilevel completions previously installed in boreholes 11, 12 and 21 were also used to monitor hydraulic head and obtain groundwater samples over various intervals in the Lockport. Boreholes at the North and South cluster sites, 34C, 37C and 64 were completed with temporary packer installations when not used for other testing purposes. Once installed, water level measurements were obtained from the temporary monitor installations. The location and geology for the 76 monitoring zones described above are

summarized in Table 3.10.

3.1.5 Hydraulic Head Distribution

In the following section, the distribution of hydraulic head, both spatially and temporally, is discussed. In addition to determining the directions of groundwater flow, detailed information on hydraulic head can be a valuable tool for estimating the degree of interconnection in a complicated fracture network. It is for this purpose that the vertical and three-dimensional distribution is discussed. Two measurement dates were selected to represent conditions where i) piezometric levels might be high (i.e. March 4, 1998), and ii) where the opposite is prevalent (i.e. Oct. 7, 1997).

3.1.5.1 Vertical Distribution

In reviewing all of the available information on the distribution of hydraulic head in the study area, it became evident that there are two specific groups of data. In one group, the distribution of hydraulic head is virtually uniform with respect to depth, and in the other, there are significant vertical gradients present in some or all of the stratigraphy.

Figure 3.23 illustrates the distribution of hydraulic head in those boreholes where only minor vertical gradients are observed. Note that the overall spread in hydraulic head amongst all of these boreholes is no greater than one metre. Considering the spatial distribution, substantial interconnection between these boreholes in the horizontal direction is implied. In addition, the uniformity of the hydraulic head implies that i) the horizontal features in these holes are well-interconnected in the vertical direction, or ii) a strongly-stratified horizontal flow system is predominant with virtually no vertical driving forces (i.e. sinks), present. Based on the contiguous hydraulic testing results obtained for these holes, low-permeability horizons are observed to be present in various units. Considering the results of the pumping tests conducted in the south cluster

site located nearby, which imply only minor vertical interconnection, it is more likely that the uniformity in the vertical distribution of hydraulic head is a reflection of a horizontally-dominated flow system.

Figure 3.24 shows the vertical distribution of hydraulic head along a cross-section between borehole 62 in the north to borehole 61, located adjacent to Twenty Mile Creek. Note the similarity of the hydraulic head at an elevation of approximately 160 masl amongst all boreholes. The hydraulic head at this elevation in borehole 62 is the lowest in the borehole by a significant margin. In borehole 61, the hydraulic head at this elevation is the highest by a significant margin (artesian, in fact). In both cases, the transmissivities measured at this elevation are also the highest measured in the boreholes. These zones of high T and common hydraulic head do not occur in the same lithology, however, as a result of the dip to the stratigraphy in this area. For example, the low-head interval in 62 occurs over the contact between the Goat Island and Gasport members, while the corresponding interval in 61 occurs in the lower Vinemount. Thus, although a strong horizontal interconnection across the region is implied by the similarity of the hydraulic head in these high T, low head zones, this interconnection is not lithology dependent. Also, to determine the horizontal direction of flow in the most permeable regional flow pathway, it is necessary to use the hydraulic head from the appropriate interval, rather than that from each lithological horizon.

The vertical distribution of hydraulic head in borehole 61 is unique amongst the data set, in several respects. Of particular note is the downward vertical gradient below the artesian interval. There is substantial permeability to the rock at depth at this location and this is separated from the high-head zone by low-permeability horizons. Thus, the lower features must be interconnected to a hydraulic drain located further down the flow system, resulting in two separate flow systems here.

Because downward driving gradients are not observed at the bottom of BH 53, this lower flow system does not appear to be interconnected as far north as this location. More likely the lower flow system follows the direction of the drainage basin with the hydraulic drain outcropping somewhere downstream.

Figure 3.25 shows the vertical distribution of hydraulic head in the up-gradient boreholes (60, 62, and 63). These boreholes exhibit a common form to the profile, all having a significant break in hydraulic head at approximately 175 masl. This break occurs across the low-permeability horizon which is prevalent in the lower Vinemount across the site. There is as much as 5-m drop in hydraulic head over a 2-m vertical span, in these boreholes. Clearly this indicates very poor vertical connection between the flow system above the Vinemount and that below, in the up-gradient area of the flow system. This also suggests that recharge occurs in the vicinity of these boreholes, perhaps along the bedrock ridge located immediately to the north and through the thick sequence of overlying Halton Till.

Figure 3.26 shows all of the multi-level data for the March, 1998, measurements plotted simultaneously. With the exception of BH 60, the maximum difference in hydraulic head across the site in the permeable-connected zone is no greater than 2 m, with the majority of the readings falling within a 1-m range. Again, this implies a well-connected horizontal flow system over the scale of the regional investigation. Whether this flow system is divided into two, above and below the Vinemount, is difficult to determine using only the hydraulic data. Certainly, the data from BH 61 suggests that the most well-connected component of the flow system must cross the low-permeability unit in the Vinemount at some location. It is important to note, however, that because the stratigraphy dips to the south, the permeable pathway must cross the Vinemount in an upward direction (possibly

following en-echelon fracture development) at some location, because the pathway begins in the Gasport/Goat Island to the north.

The dependence of the hydraulic head on seasonal influence is illustrated in Figure 3.27 for boreholes 60, 61, and 65. The measurements of hydraulic head in Spring were obtained during a period of maximum snowmelt and likely represent a transient condition. Conversely, the measurements representing the Fall condition, likely reflect a static low in hydraulic head, just prior to the onset of Fall recharge. Thus, the maximum range in hydraulic head over the site is as much as 2 m in the area nearest to the recharge and no more than 1 m in the majority of the flow system to the south. Note that a uniform change in hydraulic head is observed with the seasons. Transients pulsing through the system as are commonly observed in porous media, are not recognized here. This is because the storativity of the system is very low in comparison to porous media, which results in rapid, if not virtually instantaneous, propagation of changes in hydraulic head. Further discussion of this issue can be found in the second section to follow.

3.1.5.2 Regional Direction of Horizontal Groundwater Flow

As aforementioned, a defensible flow map at the regional scale can only be constructed for the most permeable and connected pathway. Thus, the directions of groundwater flow depicted in Figure 3.28 are interpreted from hydraulic heads obtained from the interconnected horizon described in the previous section. Because the data is sparse, an equipotential map is not constructed. Rather, flow directions are given as arrows located at the center of three-point calculations. All three-point calculations were conducted using data from the Westbay-completed boreholes. For example, the arrow drawn at the center of the trio of wells, 60, 53, and 65, reflects the direction of flow in this vicinity based on the hydraulic head measured in those holes only. To help clarify this interpretation,

one equipotential (185 masl) was drawn on this figure.

The results show a generally south-south-easterly flow in the southern portion of the study area with a more easterly direction in the northern portion. The equipotential suggests a split in the direction in the vicinity of the CWML site. This split, however, is determined based on the hydraulic head measured in BH 53 only. When the measurements from 11, and 21 are considered, the equipotential is more regular in shape and doesn't suggest as much of a flow divide. In either case, the distribution of hydraulic head in the permeable feature suggests flow in the easterly direction in the vicinity of the site. The flow direction in the vicinity of the site will be discussed further in a report describing the most recent drilling program during which additional Westbay-completed boreholes were constructed immediately to the south and east of the site boundary.

Referring to Figure 3.28, it is also important to note the general distinction in hydraulic head exhibited by BH 60. This is also illustrated in the vertical profiles, where the hydraulic head in BH 60 appears as an anomaly, having values much higher than any of the other boreholes. Although this borehole is undoubtedly on the upgradient side of the flow system, values of hydraulic head as high as observed in 60, would not be anticipated in a well-connected flow system. Thus, it likely that groundwater from the north-westerly portion of the study area does not contribute significantly to the flow in the rest of the area.

Groundwater flow directions can also be constructed for the flow system in the Upper Eramosa. Figure 3.29 shows the estimated directions of flow based on the Spring measurements of hydraulic head in all boreholes. In comparison to the case for the permeable feature, the directions of flow for the Upper Eramosa are more uniform and oriented in a more southerly direction. Again, more detail of the flow direction in the immediate vicinity of the site will be provided in a separate

report.

3.1.5.3 Transient Hydraulic Head Conditions

As aforementioned, changes in hydraulic head appear to propagate quickly as a result of the low storativity of the medium. To illustrate this, the entire data record of hydraulic head measurements from boreholes 61 and 62 are plotted on Figures 3.30 and 3.31, respectively. In both cases, large vertical gradients are present, thus, were one horizon or flow domain to act independently of another, considerable cross-over of records and reversals of gradients would be evident across limiting horizons (i.e. the lower Vinemount). Because this is not observed in general, it can be concluded that the entire Lockport Formation behaves as a unified fracture network in the horizontal direction. That is, the fracture network responds to a change in piezometric surface more dominantly in the horizontal rather than the vertical direction. Figure 3.32 shows the hydrographs for 62-2 and 61-5, representing the permeable pathway at northern and southern margins of the study area, respectively. These also respond simultaneously to changes in loading. Because some areas of the flow system are known to have limited vertical flux of groundwater, this provides further support to the argument that low storativity dominates the transient nature of groundwater flow.

3.1.6 Aqueous Geochemistry

3.1.6.1 Inorganic Chemistry

Three groundwater sampling surveys were conducted in February, July and November 1997. This report will focus mainly on the results of the November survey. The complete results for all three surveys can be found in Zanani et al. (1997) and Zanani et al. (1998). The results of the analyses of the November 1997 survey of groundwater for inorganic constituents are presented in Table 3.12. The groundwater underlying the Smithville site was found to be mainly reducing ($E_h < 0$) at depths

greater than 20 to 30 m below ground surface (mbgs). At shallow depths, conditions are more aerobic ($E_h > 0$ mV). Increasing concentrations of HS^- in solution and subsequent decreases in Fe concentrations, suggest that redox conditions change from iron reducing to sulfate reducing with increasing depth. The pH of the groundwater is near neutral (6.8) to slightly alkaline (7.6). Temperature of the groundwater ranges from approximately 10 to 11 °C. The concentrations of several ions increase with depth (Ca, Na, K, HS^- , Cl and SO_4) and only two decrease (Mg and Fe), correspondingly. Alkalinity also decreases slightly with depth.

Major ion analyses of the groundwater samples indicate that three chemically distinct zones are present in the flow system. At shallow depths (elevations > 170 masl), Mg and SO_4 are observed to be the highest concentration of ions in solution. At elevations between approximately 150 to 170 masl, Ca and SO_4 enriched waters dominate. At greatest depth (elevations < 150 masl), particularly in boreholes 53, 61, 63 and 65, the groundwater chemistry approaches brine conditions, characterized by high concentrations of Na and Cl.

The location of these chemical zones can be readily explained as a consequence of mineral dissolution and precipitation reactions. For instance, saturation indices calculated using PHREEQC indicate that groundwater in most boreholes is undersaturated (SI ~ -0.5 to -1.0) with respect to gypsum at shallow depths (~ 20 to 30 m bgs or > 165 masl). Below this, groundwater is observed to be close to equilibrium with gypsum (SI ~ 0) suggesting that the amount of Ca in the groundwater is controlled by chemical equilibration reactions with gypsum. At all depths groundwater tends to be undersaturated or near saturation with respect to both dolomite and calcite (Figure 3.33).

Mineralogical studies (see results described below) indicate that the geological members in the lower units contain a small percentage of gypsum whereas no gypsum was observed in the upper

Eramosa member. Thus, the dissolution of dolomite and calcite alone will control the amount of Ca concentrations in the groundwater located in this upper unit. The presence of gypsum in the lower members indicates that undersaturated water (i.e. recharge water) has not extensively reached this horizon. The high Na concentrations and overall salinity observed in groundwater at greater depth (elevations of approximately 150 masl or less) indicates high residence time and therefore sluggish groundwater velocity.

3.1.6.2 Isotopes

The results of the analysis of the groundwater for ^{18}O , deuterium, and tritium are presented in Table 3.13. The values of $\delta^{18}\text{O}$ range from -6.9 to -16.07 and the values of $\delta^2\text{H}$ range from -52.08 to -105.97. Average $\delta^{18}\text{O}$ and $\delta^2\text{H}$ values in precipitation collected at Simco, Ontario, (located approximately 100 km to the east) during the period from 1975 to 1982, are approximately -10‰ and -70‰ , respectively (IAEA/WMO). Variations in the isotopic content of precipitation over the seasons can be significant ($\pm 5\text{‰}$ $\delta^{18}\text{O}$, for example), however, it is well recognized (Clark and Fritz, 1997), that even in fractured media, these variations are damped-out over small (20-40 m) transport distances. Therefore, the extreme variations in $\delta^{18}\text{O}$ and $\delta^2\text{H}$ values observed in this data set are likely to be a function of either groundwater mixing processes, or a reflection of paleo-climate change, with the exception of a few sampling zones which clearly represent fluctuations due to annual precipitation.

The $\delta^{18}\text{O}$ and $\delta^2\text{H}$ results for boreholes 60 and 62 both reflect averages of modern precipitation, with the exception of the two uppermost zones in both holes which are slightly enriched with both isotopes. This implies a modern source of recharge for the entire Lockport in this area. Considering that there are limiting vertical hydraulic connections across the Vinemount and only

minimal downward hydraulic gradients within the major units here, it is surmised that the source of recharge is located in the up-gradient direction for the deeper zones, and occurs locally for the uppermost zones.

Borehole 63, which is the most westerly-situated borehole, exhibits similar uniformity to the isotopic signature with slight enrichment to the $\delta^2\text{H}$ content. No evidence of local recharge is present at this borehole. The magnitude of $\delta^2\text{H}$ enrichment is approximately 15-20 ‰ and is difficult to explain without assuming an exchange reaction of some type. The most likely candidate reactions are based on gas-water exchange with H_2S or methane (Clark and Fritz, 1997). In both cases, a very large concentration of these gases are required to generate an enrichment to the degree observed at BH 63. In all of the other boreholes, the $\delta^{18}\text{O}$ and $\delta^2\text{H}$ contents are generally depleted in comparison to the precipitation average. The magnitude of the depletion is quite significant, and in some cases, may be as much as 6 ‰ for $\delta^{18}\text{O}$ and 30-35 ‰ for $\delta^2\text{H}$ (eg. results for BH 65). With a few exceptions (i.e. possibly related to gas-water exchange), the depletions occur concomitantly. The most obvious trend in this data, is the increase in depleted values with depth. In most boreholes, BH 65 for example, the depleted values occur below the low-permeability zone in the lower Vinemount. It is probable that the value of the $\delta^{18}\text{O}$ and $\delta^2\text{H}$ at these depths is related to paleo-climatic conditions. Whether this indicates recent glacial meltwater or much older water, can not be discerned on the basis of this data alone. None-the-less, this suggests that the rates of groundwater migration are considerably more sluggish in the lower flow system than in the upper horizons.

Figure 3.34 shows a plot of the entire data set versus the Local Meteoric Water Line for data collected from Ottawa, Ont. Note that the outliers on the extreme high side of the data set are the values obtained from those intervals that might be influenced by gas-water interaction. Besides the

lower two intervals in BH63, two intervals in BH 53 and one in BH 62 appear to be influenced by this process. In addition, a general trend in slight enrichment of $\delta^2\text{H}$ is observed in those samples which yield values of $\delta^{18}\text{O}$ near the precipitation average. The reason for this is unknown, and will require further research.

The distribution of the $\delta^{18}\text{O}$ and $\delta^2\text{H}$ along the Local Mean Water Line in Figure 3.34 is similar to the grouping of these types of data observed by Noll (1988) in a geochemical study of groundwater in the Niagara Falls area. In a plot of his data versus the Global Mean Water Line, Noll observed similar outliers above the line and a grouping of data indicating recharge at lower temperatures. The latter samples were obtained from the deeper part of the Lockport Formation, as was the case for the Smithville study. This suggests that the older water at the base of the Lockport is regionally distributed and not a phenomenon local to Smithville.

Table 3.13 also shows the results of the tritium analysis. It is immediately evident that ^3H is detectable in almost every interval, but abundant and absent in only a few. The abundance of tritium at the top of boreholes 11, 60, 61, 62, and 65, coincides with variations in $\delta^{18}\text{O}$ and $\delta^2\text{H}$ which suggest a local source of recently-recharged groundwater. In all likelihood, this is water that has migrated through the overburden following heterogeneous pathways.

Using the enriched tritium results, we can safely conclude that tritium is absent in only two intervals, one near the bottom of BH 61, and the other near the bottom of BH 53. Virtually everywhere else, small concentrations of tritium are observed. Because of the ubiquitous appearance of ^3H , it is suggested that these results may represent remnant drill water which was rich in tritium, and may presently reside primarily in the rock matrix. The tritium in the matrix, if in large enough concentration, will slowly diffuse back into the fractures. The presence of trace concentrations of

tritium, however, have been observed in other fractured rock environments where the other isotopic data also indicate much older water. In a modeling study conducted by Cook et al. (1999), it was shown that tritium could be found in groundwater that had been carbon age-dated at 1000 years. This contradiction was attributed to the enhanced matrix diffusion of ^{14}C in comparison to ^3H which imparted an apparent retardation on the migration of the ^{14}C . A third possible explanation would be the potential mixing of groundwater recharged at the top of the Lockport with older groundwater (i.e. $\delta^{18}\text{O}$ and $\delta^2\text{H}$ depleted) carried along horizontally at depth. Considering the presence of contaminants at depth (Brown et al., 1997), it is the latter hypothesis which is supported by the evidence.

There is also one anomalously-high occurrence of tritium in the third lowermost interval in BH 53. This interval has been sampled several times and continually returns a high value for ^3H . This interval is permeable, has values of hydraulic head similar to those above and below, and has an isotopic signature (^{18}O and ^2H) that is similar to the surrounding intervals. This borehole is also located along the edge of the thickening wedge of glaciolacustrine silt and clay, and shows no evidence of local recharge near the top of bedrock. Because the tritium concentration is so high (31 TU enriched), it is suggested that the connection to ground surface is very strong. This also implies that the values of $\delta^{18}\text{O}$ and $\delta^2\text{H}$ observed are reflective of variation in precipitation. An additional sampling for these isotopes would resolve this issue.

3.1.7 Point Dilution

Point dilution experiments were conducted in borehole 37C in 1996 and in boreholes 54A, 56 and 59 in 1998. In 37C, experiments were conducted in both single fracture and dual fracture zones. The groundwater velocity determined from a single fracture about 425 μm in width was 33-35

m/day (Table 3.15). Duplicate tests conducted in March and December 1996 show less than 10% difference in measured groundwater velocity. The dual fracture experiment is more difficult to interpret as it is impossible to discern how the flux is partitioned between the two fractures. Assuming that the flux in each fracture is somewhere between 0-100% of the total flux, then the range of possible velocity in each fracture is 0-20 m/day. In Table 3.15, it was assumed that the velocity was equal in both fractures. Note that in this case the difference between the duplicate measurements is about 40%.

In 1998, a second series of point dilution experiments were conducted. For this series, while the equipment differed from the 1996 experiments, the methodology used was identical. The results of five different tests are presented in Table 3.15. In all of these experiments a single fracture was isolated. Fracture apertures ranged from 136-2444 μm . Measured groundwater velocities range from 3 m/day to 40 m/day. While only a few measurements of groundwater velocity were obtained using this method and all the measurements were obtained from the Eramosa member, the results nevertheless indicate a large range in velocity between the single fractures at the site. It is interesting to note that there is no direct correlation between fracture aperture and velocity. For example, the two lowest velocities were obtained in 136 μm and 1400 μm fractures approximately 20 cm apart suggesting poor vertical connection. The results of laboratory experiments addressing various issues related to the equipment are discussed in Radcliffe (1997) and Uhlman et al. (1998).

3.1.8 Tracer Experiments

3.1.8.2 Injection-Withdrawal Experiments

In the following, the results of the successful injection-withdrawal and radial-divergent tracer experiments are discussed and interpreted. For the injection-withdrawal experiments, concentrations

were not determined directly at the inlet and outlet points of the fracture, thus, there is some uncertainty as to the exact distribution of these concentrations. Therefore, the interpretation of the breakthrough curves was conducted using either concentrations normalized to an estimate of the initial inlet concentration, or concentrations normalized to the peak breakthrough concentration. To estimate the initial inlet concentration, the mass injected was assumed to distribute evenly into the isolated injection interval over a specified period of time. In the case of the radial divergent experiments, the temporal distribution of the inlet concentration was measured directly.

Figure 3.35 shows the breakthrough curves for the injection-withdrawal experiments plotted against peak-normalized concentration. Note that the breakthrough curve for bromide in each experiment is shifted backwards in time relative to the curve for Lissamine. This can be attributed to the difference in free-water diffusion coefficient which, as it is larger for bromide, results in a deeper penetration of the matrix and thus a delayed return to the fracture. This provides direct evidence that the exchange of solute between the fracture and the surrounding medium is governed by diffusive processes.

The mass recovery of tracer during each experiment was estimated by integrating the measured concentration with respect to time and multiplying by the volumetric flow rate. Because sampling was discontinued prior to the complete return to background concentration, total mass recovery can not be determined directly. Mass recovery to the last sample for each tracer as determined from the results of both experiments ranges from 37% for Expt II to 62% for Expt I. Extrapolation beyond the last sample using an exponentially decaying function will improve these estimates by a maximum of only 3-5%.

The mass recovery for both tracers during Experiment I is typical of tracer experiments of this

type when conducted in fractured rock (e.g. Leonhart et al., 1985; Novakowski et al., 1985; Raven et al., 1988). However, the mass recovery was substantially less for Experiment II. This can be attributed to either: i) heterogeneity in the distribution of aperture in the plane of the fracture; or ii) to the presence of the natural flow field. In both cases the effect will be to divert some tracer away from the withdrawal well.

To interpret the tracer experiments a hybrid-analytical numerical model was developed which accounts for the dipole nature of the flow field, the presence of natural groundwater flow, and incorporates mass transfer using an analytical solution for advection-dispersion with matrix diffusion in a single fracture. The model was thoroughly tested and verified (Novakowski et al., 1999) and then incorporated into an inverse routine to facilitate the simulation of the field data. For a more complete description of the model development and the simulation of the field experiments, refer to Novakowski et al. (1999).

The results of the combined fit to the field data are shown in Figure 3.36. Table 3.16 shows the values of the parameters used to achieve the fits. The parameter $\theta_m (D^*)^{1/2}$ represents the product of matrix porosity and the effective diffusion coefficient as used in the model. It is from this term that matrix porosity is calculated assuming a geometric factor of 0.1 from the results of the diffusion experiments described below. Because the geometric factor appears in a square root, the calculation of porosity is not sensitive to this value.

Note that a disparity is observed between the 2b estimates obtained for each experiment. Because the direction and magnitude of natural groundwater flow is considered in the simulations, this effect can not be attributed solely to the influence of the natural flow field. Rather, because the advective flow field for the injection-withdrawal experiment is extensive, the disparity is likely the

result of heterogeneity in the distribution of aperture within the domain of the flow field. Because a plug flow formulation is used for the definition of $2b$, the result suggests that an area of the fracture having larger aperture was encountered during the experiment conducted against the gradient.

The estimates of fracture aperture also exceed the values for hydraulic aperture determined using the constant-head tests by as much as 40% or greater in the case of Experiment II. This has been observed in the results of other experiments of this type and is also a reflection of the heterogeneity of the aperture distribution. The hydraulic apertures are representative of conditions immediately adjacent to the borehole, whereas the tracer-determined aperture is more representative of the integrated region between the boreholes and is sensitive to regions of enhanced or larger aperture.

Referring again to Table 3.16, the estimates of matrix porosity are observed to be identical between the experiments. On the basis of these results, an estimate of 11% is assumed to be representative of the rock matrix adjacent to the fracture used for the experiments. It is important to note that this agreement was only achieved after all relevant processes were accounted for (i.e. natural groundwater flow, matrix diffusion, advection-dispersion). This value of porosity also agrees well with independent estimates of matrix porosity determined from core obtained from these boreholes (see following section).

Finally, if matrix diffusion is not accounted for in this interpretation, a reasonable match to the field data can not be achieved (Novakowski et al., 1999). The results of the fitting process yield estimates of fracture aperture and dispersivity that are completely unrealistic, and the shape of the simulated breakthrough curves are not anywhere similar to the shape of the field curves. Thus, these results provide further evidence that matrix diffusion is a dominant exchange mechanism that

influences even short-term transport in this type of media. For further discussion of conduct and interpretation of these experiments, refer to Novakowski et al. (1999).

3.1.8.2 Radial Divergent Experiments

The tracer injected during the radial-divergent experiment conducted in the shallower fracture was observed to arrive at all of the observation boreholes, while the arrival in the experiment conducted in the lower fracture was limited to the extent of the south cluster site. The results of the radial-divergent experiment conducted in the upper fracture are shown in Figures 3.37 to 3.39. Although breakthrough was detected in all of the observation boreholes in the south cluster site, migration away from these boreholes was only observed as far as borehole 64. Arrival at borehole 37c was not detected, although hydraulic response to water injection was observed. To provide a preliminary interpretation of the results, only the breakthrough at boreholes 58, 59, and 64 were simulated.

Measurements obtained from the conductivity probe located in the injection interval showed that the inlet concentration is successfully approximated by a Heaviside step function having a duration of approximately 2.5 min (Figure 3.40). A dimensionless concentration of 1.0 was established for the duration of the square wave (real concentrations of 1.5 g/L for Br and 1.0 g/L for Lissamine).

To conduct the preliminary interpretation, a semi-analytical model based on a modification to the solution of Chen (1986) was developed (Glöckner, 1999). The model accounts for a square wave input concentration, radial advection-dispersion in a single fracture, and diffusion from the fracture to the matrix. The presence of a natural flow system is not considered. The model was imbedded in an inverse routine to facilitate the interpretative process. To conduct the fitting process,

fracture aperture, dispersivity, and matrix porosity were allowed to vary. The radial distance, injection rate, volumes of the source and observation intervals, the tracer input pulse, and the radii of the source and observations wells were fixed.

Figures 3.37 to 3.39 also show the model fits for each of the data sets. The simulations of the data obtained from the observation wells located in the vicinity of the injection well (BH 58 and 59) show an excellent match. The quality of the fit to the data set from BH 64 is not as good, slightly underestimating the rising limb of the curve and crossing over the tail. Further adjustment of the fits by manual means would probably improve the fits in all cases, although very little change in fitting parameters would be observed. The values of the three fitting parameters are given in Table 3.17 for each of the three boreholes.

As was the case with the injection-withdrawal experiments, the apertures determined from the tracer experiments overestimate the hydraulic apertures by a small proportion. For the boreholes closer to the injection well, the degree of overestimation is probably governed by the fact that the natural groundwater flow is not accounted for. At greater travel distances, the influence of natural flow is averaged out, and the estimated tracer aperture diminishes towards the hydraulic estimate. Further interpretation of these experiments is required to determine if this is a defensible argument.

The value of the dispersivity interpreted from the simulations are in the same order as were determined from the injection-withdrawal experiments, at least for the observation wells closest to the injection well. Peclet numbers (distance over dispersivity) for these results range from 295-343. These numbers are very high in comparison to tests of this type conducted at a similar scale (Novakowski and Lapcevic, 1994), suggesting that the another process may be influencing the shape of these curves. The Peclet number for the breakthrough curve at BH 64 is much smaller at

approximately 32, which intuitively seems too low for results at this scale. Unfortunately, there are no other experiments that are known to have been conducted at this scale, so comparison is impossible. Again, further simulation with a model which more completely accounts for all of the transport processes may provide additional insight.

The values determined for matrix porosity (Table 3.17), fall directly into the range of what has been determined for the Eramosa member from diffusion and gravimetric measurements. Values significantly different than these (i.e. $\pm 20\%$) led to simulations that would not converge. Thus, it is probable that these measurements are representative of the properties of the rock and will not change significantly through re-interpretation with a new model.

3.2 Laboratory

3.2.1 Rock Geochemistry

The results of the XRD analyses showed that three principal minerals were found in the samples provided. These minerals were dolomite, quartz and gypsum. The composition of the stratigraphic units was found to be variable. However, all samples ranged between 86-98% (by weight) dolomite, 2-15% quartz and 3-8% gypsum (when detected). Examination of the whole-rock chemistry suggested that clay minerals may also be present in significant quantities. Using a normative mineral calculation approach, it was estimated that clay minerals may account for 0.3-13.1% of the rock. Normative calculations for carbonates were generally consistent with the XRD analysis. However, the abundance of several accessory minerals detected in the XRD analysis, appear to be significantly overestimated when reconciled against the corresponding chemical analysis. Therefore, it is suspected that the XRD values for dolomite and quartz may slightly overestimate the actual amounts present. In general, the Eramosa and Goat Island members were

found to have a more uniform, dolomite rich and clay poor composition. The Rochester formation showed an opposite trend and the composition of the remaining units was found to lie between these groups. Gypsum was detected in 8 samples, although it was not found in any of the samples collected from the Eramosa or Rochester. For more detail on the results of the geochemical and mineralogical analyses, see Bickerton (1997)

3.2.2 Measurement of Organic Carbon

The results of the analysis of organic carbon on the bulk rock samples are summarized in Table 3.18. In several of the samples, no organic carbon was detected. The mean percentage of organic carbon ranges from 0.027 to 0.072 for the entire Lockport formation. There does not appear to be a significant distinction between any of the members, although a downwardly decreasing trend might be speculated. In comparison to published estimates of organic carbon from other carbonate rocks, these values are in the lower end of the range, perhaps more typical of carbonates that have been deposited at significant distance from terrestrial sources of organic carbon. Note that the mean estimate of organic carbon obtained using the blanks is 0.005%, suggesting that the mean error on the estimates for the bulk rock is no greater than this.

Table 3.19 shows the results of the analysis of the stylolite material for the percentage of organic carbon. These results suggest that contrary to what was anticipated, the stylolites in this rock contain minimal organic carbon. There is no significant difference between the results obtained from the core-sized samples versus those from the larger hand samples obtained from the quarry. In both cases, the percent organic carbon is very similar to the values obtained for the bulk rock.

Table 3.20 also shows the results of the analysis of the argillaceous bands obtained from the core samples. These features were observed to be physically similar to stylolites in core, only thicker,

often 5 mm or greater, and with virtually no curvature to the contact surfaces. The argillaceous bands also occur much less frequently in the core record. Only six samples were analyzed, and four of the six showed organic carbon at much greater than one percent. Thus, the only horizons in the Lockport formation that contain any significant amount of organic carbon, are the sparsely-distributed argillaceous layers.

Although the levels of organic carbon in the majority of the rock are relatively low, differences in the rate of migration of the contaminants, particularly between the TCB and TCE, suggest that retardation processes are significant. To explore the potential retardation imparted by the organic carbon in the rock, a hypothetical value of the retardation factor can be calculated using the percent organic carbon and published estimates of the octanol-water partitioning coefficient, K_{ow} . Using the following equation (Jackson and Hoehn, 1987), an estimate of the distribution coefficient, K_d , is obtained:

$$\text{Log } K_d = 0.72 \text{ Log } K_{ow} + \text{Log } f_{oc} + 0.49 \quad (3.4)$$

where f_{oc} is the weight fraction of organic carbon. To calculate the retardation factor, R , for the rock matrix, the standard expression for the retardation equation is used:

$$R = 1 + \frac{\rho_b}{\theta} K_d \quad (3.5)$$

where ρ_b is the bulk density of the rock, and θ is the porosity. The distribution coefficient, K_d , is usually expressed in mL/g or cm³/g. To calculate the equivalent retardation factor for the fracture walls, R_f , the internal specific surface area must be defined and a new retardation equation, used. The

retardation equation is given by:

$$R_f = 1 + \frac{2K_f}{2b} \quad (3.6)$$

where $2b$ is the aperture of the fracture and the K_f is the distribution coefficient for the fracture, which is related to K_d by the internal specific surface area of the porous medium, γ :

$$K_d = \gamma K_f \quad (3.7)$$

The coefficient, γ , can be defined using a simple conceptual model (Bickerton and Novakowski, 1993), as:

$$\gamma = \frac{2\theta}{\alpha\rho_b} \quad (3.8)$$

where α is the geometric factor which defines the arrangement of the pore space. The geometric factor is described and discussed more completely in the following section on the diffusion experiments.

Table 3.21 shows the results of the calculations for TCE and TCB using the equations given above. The retardation factors for TCE in the bulk rock range from 3-8 and for TCB, the range is broader, between 23-86. For both the TCE and the TCB the R_f is about twice the value of the R for each rock unit. For fractures of smaller aperture (i.e. less than the example 500 μm used), the value of R_f will increase proportionally. In comparison to sand aquifers, these estimates of retardation fall in the range typically measured from calculations of plume migration and batch experiments (Jackson and Hoehn, 1987). Theoretical calculations such as conducted above tend to yield much lower estimates of R , in the range of 1.3-1.4, for TCE and PCE in the sand aquifers at Gloucester and Base Borden. In these studies, the larger estimates obtained from field measurements were attributed to other sorption processes, such as ionic exchange with the mineral fraction of the aquifer. Thus, the

actual field migration of chlorinated compounds at Smithville may undergo even greater degrees of retardation than suggested by these theoretical calculations.

It would be most helpful were additional estimates of the distribution coefficient or actual field measurements of R , available. Unfortunately, the batch experiments conducted using the powdered samples led to inconclusive results. Estimates of exchange ranged from 0% to almost 100% with virtually zero reproducibility, suggesting that considerable research is required in the development of a proper experimental method for conducting batch experiments with crushed-rock samples. Field-based measurements of R have also not been calculated. To do so would require a considerable inverse modeling effort, and it is unclear as to whether sufficient historical plume data was collected to support such an exercise.

Thus, there remains some uncertainty as to the exact nature of the sorption process controlling the transport of the most mobile of the chlorinated hydrocarbons at Smithville. If we can accept the measurements of organic carbon as reasonable, however, then the theoretical calculations should provide a conservative estimate of retardation, allowing for equivalently conservative predictions of future contaminant transport.

3.2.2 Diffusion Experiments

To display the results of the diffusion experiments, the concentrations of each tracer (C) were plotted relative to the initial concentrations (C_0) against time. The relative tracer concentrations were modeled using RADIF2 (Novakowski and van der Kamp, 1996) to obtain estimates of the effective diffusion coefficient and effective porosity. RADIF2 is a semi-analytical model that accounts for radial diffusion, mass balance in the reservoir, linear adsorption, decay, and periodic volume extraction of reservoir samples. The model was incorporated in an inverse routine to facilitate the

simulation process.

Figures 3.41 and 3.42 illustrate two examples (GA-1, GI-1) of the model fits (using the inverse routine) to both the DFBA and Bromide concentrations. The quality of these fits are very high although this was not the case with all experimental results. In most cases where poor fits or poor agreement between fits occurred, the experiments were not completely equilibrated at the time sampling was discontinued. Figure 3.43 is an example of this (cell G1), where the simulation of the Bromide decay leads to a higher porosity estimate than is indicated by the final Bromide concentrations.

In addition, simulations of the Bromide and Lissamine experiments conducted in the forward direction indicates that, compared to Br, Lissamine interacted significantly with the rock material (Figure 3.44). Model-predicted porosity for the Lissamine results were also found to be as much as four times as high as that predicted using Br. Because Bromide is well known to be conservative in most types of geological materials, Lissamine is assumed not to behave conservatively during these experiments. The explanation for this behavior, however, is not readily apparent. Adsorption to the matrix material, either by binding to the organic matter in the rock or to clay particles, represents one possibility. Because measurements of organic carbon and clay content were not obtained for these specific samples, however, it is difficult to conclude that either of these processes were responsible for the observed retardation. It is important to note that Lissamine is not retarded compared to Br in the reverse radial diffusion experiments, suggesting that the Lissamine adsorbed in the forward direction was irreversible. In addition, the loss and potential adsorption was not observed in field-scale experiments (Novakowski et al., 1998), thus the mechanism of mass loss observed during the forward diffusion experiments remains unclear. Because uncertainty remained, however, Lissamine

was not employed as a tracer for use in further forward radial diffusion experiments. An alternative tracer, DFBA, was used instead.

The results of the diffusion experiments are shown in Table 3.22. These results are those that were judged to have properly reached equilibrium without any apparent retardation, and for which the simulations appeared defensible and unique. The results are grouped according to lithology, and values are provided for the effective porosity, the effective diffusion coefficient, and the geometric factor, as determined using each tracer. The gravimetric porosity and the porosity calculated from the equilibrium mass balance of the Br tracer (see explanation below) for each sample are also presented. Nitrate was used as an alternate tracer in cells 6, A, B, and V1. DFBA was used as the alternate for all others.

On average, effective porosity predicted from the forward diffusion experiments conducted using Br, over-predict gravimetric porosity by approximately 0.6%. Although not presented here, the results from the reverse diffusion experiments conducted with Br agreed almost identically with the gravimetric porosity (Zanini et al., 1999). So too do the results using the alternate tracers (nitrate and DFBA) in the forward direction (Table 3.22). In this case the porosities obtained from the simulations agree to within 0.1% in comparison to the gravimetric-based results.

Porosity estimates calculated using equilibrium tracer concentrations are also given in Table 3.23. In this case, effective porosity is calculated using tracer concentrations obtained at equilibrium and using the following equation (Novakowski and van der Kamp, 1996):

$$\beta_1 = \frac{V_r}{R\theta_e\delta_r r_r} \quad (3.9)$$

where β_1 is the dimensionless mixing coefficient calculated using the cell radius versus the radius

of the reservoir and the equilibrium concentration at the end of the experiment (this value may also incorporate a correction in the equilibrium concentration to account for mass loss during sampling events), V_r is the reservoir volume, R is the dimensionless retardation factor (1.0 for a conservative tracer), θ_e is the effective porosity, δ_r is the cross-sectional area through which diffusion occurs, and r_r is the radius of the reservoir. The calculated effective porosities for the forward diffusion experiments conducted using Br agree to within 0.2%. Therefore, considering the general agreement between all results, it is reasonable to assume that the measurements of gravimetric porosity can be used as a direct estimate of effective porosity for the purpose of model prediction.

Values of the effective diffusion coefficient are also shown in Table 3.24. These values are estimated from simulation of the amount of curvature in the concentration versus time curves (Figures 3.44). Larger values of the effective diffusion coefficient result in more rapid decline in the concentration over time. The effective diffusion coefficient, D_e is directly related to the free-water diffusion coefficient, D_0 through the following expression:

$$D_e = \alpha D_0 \quad (3.10)$$

where α is the geometric factor as introduced in the previous section. The geometric factor is a lumped-parameter which represents the arrangement of the pore space and the manner in which the pore space intersects the wall of the reservoir (or a fracture). Conceptual models have been developed for this (Walsh and Brace, 1984), although common practice is to estimate this parameter from direct measurements of the effective diffusion coefficient. Freeze and Cherry (1979) report a wide range in values for the geometric factor from unconsolidated media (0.01-0.4). It is likely that this range results from the uncertainties inherent in corresponding estimates of effective porosity. One of the

advantages of the radial diffusion method, is that the effective porosity and the effective diffusion coefficient are distinguished, unlike the traditional transient diffusion methods.

To calculate the geometric factor, estimates of D_0 for each tracer are required. The value of D_0 for Lissamine is estimated to be $4.5 \times 10^{-9} \text{ m}^2/\text{s}$ (Novakowski and van der Kamp, 1996) by comparison to a similar compound, Uranine (Skagius and Neretnieks, 1986). The free-water diffusion coefficients for Br, NO_2 , and DFBA are $2.08 \times 10^{-9} \text{ m}^2/\text{s}$ (Lide, 1992), $1.91 \times 10^{-9} \text{ m}^2/\text{s}$ for (Lide, 1992), and $7.6 \times 10^{-9} \text{ m}^2/\text{s}$ (Bowmans and Gibbens, 1992), respectively.

Because the geometric factor is a property of the matrix, comparison between tracers should result in similar numbers. The mean values illustrated in Table 3.24, in fact, do not agree, although the discrepancy is not wide. Note, however, that the averages are strongly biased by a few outliers in both columns. For example, cell E2-3 exhibits geometric factors for both tracers which are almost four times the mean geometric factor. Similarly, the estimate for cell 10, might also be cast in doubt. If we remove any value greater than 0.20, the mean values are significantly adjusted to 0.078 for the Br, and 0.108 for the alternate tracers. Thus, the geometric factor for the alternate tracers remains slightly larger than the value for Br. In addition, no distinction is apparent between the nitrite and DFBA results. Considering that the Br ion is much smaller than DFBA, it is surmised that other processes (such as surface diffusion or a small amount of sorption) may have played a role. In addition, the values collected for this study agree well with geometric factors collected by Barone et al. (1989) from diffusion experiments conducted in the Queenston shale (lower in the stratigraphic sequence underlying Smithville) using a chloride tracer. Thus, for the purpose of model prediction, a value of approximately 0.10 for the geometric factor is a reasonable and defensible estimate.

3.2.3 Total Porosity and Bulk Density

Because we can assume that total and effective porosity are equivalent, detailed measurements of total porosity can help to illustrate the structure of the porosity distribution. In porous media, porosity tends to be relatively uniform over alike formations. For example, the porosity of lacustrine clays and sand aquifers probably only vary over a few percentage points in each case. To explore the distribution of porosity in the Lockport formation, several discrete core samples and one continuous core sample were analyzed for gravimetric porosity.

Table 3.23 shows the average values of porosity measured for each member of the formation. Note that the sample n is very large for the Eramosa member. This reflects the large number of samples generated during the dissection of the continuous core from borehole 64. The mean porosity for the Eramosa member and the Rochester formation are about equal at 0.065 and 0.061, respectively. The Goat Island and Gasport members have higher porosities at 0.082 and 0.088, respectively. The lowest mean porosity was obtained from the Vinemount member. Several of the sections in the Vinemount Unit 2 showed consistently low porosity, typically around 2-3%. The upper Vinemount exhibited much higher porosity, in the order of 10-11%. The range in porosity was widest in the Eramosa (see discussion below), and narrowest in the Rochester formation. These distinctions in porosity may be related to either depositional history, weathering, the stress relief associated with fracturing, or combinations thereof. Because of the difficulties associated with incorporating variation in the porosity on a member-by-member basis, use of the averages for each member is recommended.

To explore the danger in using averages, Figure 3.45 was constructed to show the distribution of porosity over the Eramosa and upper Vinemount in borehole 64. The gaps illustrate the location of fractures, fracture zones, core breaks, machine breaks, and vuggy zones. Some gaps are too small

to be visible in this Figure. The range in measured porosity is very broad, with extremes observed over very short vertical distances (i.e. a few cm). For example, at about 180 masl, the porosity ranges from approximately 2% to 18% over the span of 0.08 m. The occurrence of high porosity is generally limited to thin bands, several cm in thickness. In several locations, machine breaks appear in association with zones of high porosity, likely occurring as a result of poorer strength to the rock in these zones.

Comparison of the location of the high porosity bands and the location of fractures identified during core logging shows no direct correlation. Thus, the origin of the porosity-enhanced zones is likely related to diagenetic processes (dolomitization) and not to weathering by groundwater flow through open fractures. Because these zones do not correspond with the major groundwater pathways, it is not necessary to consider these in formulating an understanding of the matrix diffusion process. Rather the use of the averages indicated previously will suffice, recognizing that the averages for the Eramosa are biased slightly to the high side by the presence of the high porosity bands.

Estimates of bulk density were also obtained from the calculations conducted in the interpretation of gravimetric porosity. Bulk density is the dry weight divided by the sample volume. Because both sample weight and sample volume were determined accurately, the estimates of bulk density are commensurately accurate. In Table 3.24, the range and average bulk density is presented according to lithology. The overall mean bulk density was 2.57 g/cm^3 . It is this figure that was used in all calculations requiring bulk density.

4.0 CONCEPTUAL MODEL

4.1 Regional Scale

Groundwater flow systems over the regional scale in fractured rock are frequently dominated

by large-scale structural elements and local-scale fracture inter-connectivity. Because of relatively thick overburden cover in the study region, determining the presence of regional structural elements was not possible through direct methods. Based on the measurement of hydraulic properties and through inference from geochemical results, however, a conceptual model for regional groundwater flow can be formulated. The discussion is developed around two distinct sets of geochemical and hydraulic results, one set from the up-gradient boreholes (60, 62, and 63) and the other from the downgradient boreholes (53, 61, and 65).

Although the overburden is thick in the vicinity of boreholes 60, 62 and 63, it was initially surmised that these boreholes are situated immediately downgradient from a potential zone of recharge. These boreholes are located approximately 1 km south of a swale and bedrock ridge which trends approximately east-west. The distribution of hydraulic head indicates a persistently downward gradient with increasing depth in all three boreholes. In each case, the transition between higher and lower hydraulic head occurs at the base of the Eramosa member or top of the Vinemount member, across a discrete zone of low transmissivity. In the case of borehole 60 and 63, the hydraulic head below the low transmissivity zone is uniform. The steady decrease in hydraulic head with depth observed in borehole 62 may indicate vertical fracture connection through these units within the immediate vicinity of this borehole.

Electrical conductivity is relatively uniform with depth in these boreholes, ranging from ~2000 μs to 4000 μs . Similarly, the stable isotopic composition of the groundwater sampled is also uniform with depth. Thus, the groundwater is of recent origin with variation from precipitation evident in some of the uppermost intervals. In addition, most of the sampled zones contain measurable concentrations of ^3H indicating that groundwater in these zones is of post WWII age. In

boreholes 60 and 62, ^3H concentrations are highest in the shallow depths (elevations >165 masl). However, high transmissivity zones in the lower Vinemount and Goat Island to upper Gasport also exhibit moderate to very high ^3H concentrations, particularly in borehole 62.

The fact that there is little change in electrical conductivity and in the stable isotopic signature with respect to depth suggests that in the upgradient boreholes, groundwater in both the upper Eramosa member and the in the lower members are of a common origin. The presence of ^3H at various depths (i.e. shallow and deep) further indicates that younger water is infiltrating the entire flow system. As the clay till overburden is thick and relatively impermeable overlying these boreholes, this suggests that recharge is localized to the swale and bedrock ridge which lies immediately to the north of the site. As previously described, overburden thickness in the swale/ridge complex is minor and ranges from 1 to 2 m in thickness. North of the ridge towards the escarpment, overburden thickness increases. Thus, the source of the water in the Eramosa is most likely the ridge and swale area. Also, although there are obvious limits to the vertical connection across the lower Eramosa/Vinemount members, a connection does exist, allowing for some freshly-recharged water in the Eramosa to mix with water at greater depth.

In the up-gradient area, the predominant horizon conducting groundwater occurs in the Goat Island/Gasport members. The thickness of the zone of high T is 6-8 m, although the specific number of fractures open to groundwater flow in these boreholes is unknown, as no small-packer spacing measurements were conducted here. Between these boreholes and the CWML site, a distance of only 400-600 m, the flow systems seem to merge, hydraulically, yet remain distinct geochemically. Defining an upper and lower flow system for the up-gradient area, is a reasonable approach. To do the same in the vicinity of the site, is more difficult to defend on the basis of hydraulics. However,

on the basis of pumping test results and the isotopic and inorganic geochemistry which indicate poor vertical connection between horizontal bedding planes and geochemical zonation above and below the Vinemount member, it is likely that such a division is possible.

Inorganic ion concentrations suggests that these regimes are physically and chemically related to the bedrock composition. Shallow groundwater is found to be dominated by high Mg concentrations due to equilibrium reactions with dolomite which control the amount of Ca and Mg in solution. However, in the lower flow regime, groundwater is dominated by high Ca and SO_4 concentrations due to the higher amount of gypsum minerals present in the rocks.

Transmissivity measurements in the lower flow regime are observed to be just as high as that in the upper flow regime. Thus, calculations based on equivalent aperture width would suggest that groundwater velocity in both flow regimes should be similar. However, the high electrical conductivity observed in the downgradient boreholes 53 and 65 at depth indicates that groundwater residence time in this zone is much greater than in the upper zone. Also, the observed depletion in stable oxygen and hydrogen isotopes at depth in these boreholes suggest that there is relatively less dilution from younger recharge water. As recharge is observed to occur in both regimes in the upgradient boreholes, it is therefore implied, through geochemical observation, that groundwater velocity in the lower flow regime is considerably slower than that in the upper flow regime. Because the lower flow system is not part of the most permeable pathway as observed from the hydraulic head measurements, it is suggested that although copious horizontal permeability is present in this system, horizontal interconnection of these fractures is not as prevalent as in the upper flow system. This conclusion is also supported by the results of the radial-divergent tracer experiment conducted in the lower flow system which showed horizontal interconnection only within the south cluster site.

Groundwater discharge from the flow system is less well defined. At borehole 65, groundwater in both the upper and lower flow systems appears to completely underflow the river. At borehole 61, groundwater from the upper flow system (i.e. the most permeable pathway) also appears to underflow the river. The groundwater in the artesian zone is of recent origin, having significant tritium concentrations and exhibiting the isotopic signature of recent precipitation. This suggests that this water may originate at depth, perhaps upgradient along the stream bed. The high transmissivity zone in the Goat Island/Gasport, however, exhibits the lowest hydraulic head at depth in any of the boreholes. This indicates significant underflow of the lower flow system.

4.2 Site Scale

At the scale of the CWML site (i.e. conditions local to the site), groundwater flow is primarily horizontal with virtually no vertical hydraulic gradients. Borehole 53 is an exception to this and shows a persistently-low hydraulic head in the second to uppermost interval (middle Eramosa). The elevation of this hydraulic head is just below (approximately 0.3 m) the top of rock in the site area and probably reflects the ongoing pumping in the pump-and treat system. Based on the dip of the stratigraphy, and following this fracture or fracture zone back to the CWML site, it would be reasonable to expect that this fracture sub-crops near the top of rock in this location. Thus, this particular fracture zone is extremely well-connected over a substantial horizontal distance and would have been a primary conduit for the migration of contaminants away from the site.

The diagram which best illustrates the fracture distribution at the site scale is Figure 3.11, which shows the results of the hydraulic testing conducted using 50 cm packer spacing. In this data set, it is possible to identify specific fractures or fracture zones that can be correlated over at least the local scale. To predict contaminant migration using a numerical model, it is probably only necessary

to identify these features, and to treat the vuggy zone in the upper Vinemount discretely. Thus, 8 specific features are identified in this data set, and 5 of these can be traced at least a distance of 125 m in the subsurface. Unfortunately, extrapolation of fracture trace lengths beyond this scale is impossible with this data. It is known, however, that the fractures continue through interconnection, over great distances, on the basis of hydraulic head measurements and geochemical results.

Note that interpretation of the fracture spacing data obtained from the core logs would lead to a much higher estimate of potentially open fractures for the section of rock covered by Figure 3.11 (from south cluster). This illustrates the risk in only using fracture statistics to construct a conceptual model. In addition, estimates of vertical fracture spacing would also lead to the impression that the bulk vertical permeability might be greater than the values obtained by direct hydraulic measurement and pumping test. Clearly not all fractures interpreted as open features in the core record, contribute to the groundwater flow system.

4.3 Microscopic Scale

Groundwater migration and solute transport at the scale of a discrete fracture is equally as complicated a process as that at larger scales. In this case, large variability in properties can contribute to very heterogenous flow and transport patterns. Porosity, in particular was observed to vary significantly over the scale of few cm. Much of the variability appears to be related to diagenetic processes, such as stylolitization, which are specific to individual bedding planes. Although, difficult to measure accurately, organic carbon was also found to be prevalent in the bulk rock. Concentration in stylolitic horizons was not observed, but accumulation of organic carbon in infrequent bituminous layers, was. Considering the variability of both porosity and organic carbon, use of averages for different lithologies is probably the only means by which to approximate the property for modeling

or predictive purposes.

Because the porosity of the bulk rock can be as much as 18-20% in some thin horizons, hydraulic measurements conducted using 0.10 m packer spacing also yielded some high values of T, for these unfractured zones. Although, these zones may be permeable, many are not connected to fractures or don't contribute to the flow system directly. Rather, the porosity when adjacent to a fracture, acts as a sink for the contaminants passing through the fracture.

Using theoretical calculations, it was shown that values of retardation as a result of the interaction between the organic carbon and organic contaminants will be significant. In conjunction with the loss of solute through matrix diffusion, the transport rate of the organic compounds can be expected to be orders of magnitude less than the velocity of the groundwater. Groundwater velocities measured in the Eramosa member can be as high as 30 m/day.

5.0 RECOMMENDATIONS

One of the objectives related to the EPA Capture Zone study was to make specific recommendations related to the characterization of groundwater systems in carbonate rock. While the data and interpretations outlined in this report have direct application to the remediation of the bedrock at the Smithville site, the work will also be of interest to other site characterization studies. The following recommendations are intended to examine in a general way the application of this study to other characterization studies in carbonate rock.

1) In a flat-lying stratigraphic sequence, fractures open to groundwater flow may not be confined to specific lithological units. Although appealing to conduct investigations and present results in a form constrained by lithology, this should be used as only a guideline. To develop statistical interpretations, it is more defensible to interpret the fracture occurrence holistically.

2) Although the Lockport Formation is approximately 40 m in thickness, only a small proportion of that thickness contributes to a connected flow system over the regional scale. Whether this is particular to this rock type and setting, or is common to all dolomitic rock, is unknown. Therefore in constructing conceptual models for large-scale contaminant transport in rocks of this type, it is necessary to treat even what are believed to be homogenous units, as stratified and discontinuous. Thus, investigations should include measurement of transmissivity and hydraulic head at a scale that will allow for differentiation of the potential pathways within the unit. Failure to do so will result in a complete mis-interpretation of the flow system.

3) Although a considerable effort was undertaken in this study to obtain detailed hydraulic measurements at a very fine scale, the results illustrate the necessity of conducting at least some of this kind of work. Clearly, if hydraulic testing were conducted at only the 2-m packer spacing, and these data used to compile statistics to be used in a numerical model, the results would substantially over-predict the true mean permeability. Moreover, unless the properties of specific fractures are determined directly, the use of T and an estimate of the number of open fractures intersecting an interval, will lead to extreme errors in the prediction of velocity. Because the cost to obtain this type of information is significant, it is recognized that studies as detailed as reported here are unlikely to be conducted. Rather, it is recommended that a small portion of a few boreholes be tested with small-packer-spacing, simply to provide a general sense of the relation between fractures observed in core and those open to groundwater flow.

4) The results of this study illustrate the variable nature of the fundamental properties of the bulk rock such as porosity, permeability, and occurrence of organic carbon. In conjunction with estimates of the discrete fracture pathways, it is necessary to include these properties to properly predict the rate

of migration of contaminants. In particular, very large values of effective porosity were discovered in this rock, which may act as a substantial sink, retarding the migration of contaminants. It is necessary, therefore, to consider porosity in the development of a conceptual model for carbonate rock. Because effective and total porosity are equivalent, measurement of porosity using gravimetric methods are sufficient. These measurements must be obtained using naturally-saturated rock samples. Measurement using re-saturated samples will not provide accurate estimates of porosity.

5) Because estimating groundwater velocity using the cubic law at the site scale depends on the degree of hydraulic characterization and detailed knowledge of the distribution of hydraulic head, accurate estimates are difficult to obtain without considerable effort. Direct measurement conducted using point dilution methods offer an attractive alternative. To conduct successful measurements, some detailed hydraulic testing is required, along with use of the appropriate equipment. The location of the detailed testing could be governed by the use of borehole geophysics.

6) In a horizontally stratified flow system such as that underlying Smithville, boreholes drilled through the entire formation must be completed with care. It is uncertain as to whether traditional multilevel piezometers will be sufficient in environments where very aggressive vertical gradients are prevalent (i.e. in the up-gradient portion of the study area). In addition, because a copious thickness of bentonite is required between each interval in traditional installations, information from considerable portions of the borehole are lost. Clearly, in an environment where only thin strata exhibit low permeability, to correctly interpret the flow system, borehole instrumentation must be designed to maximize the access to permeable features.

6.0 ACKNOWLEDGMENTS

This project was funded by the Ontario Provincial Government through the auspices of the Smithville Phase IV Bedrock Remediation Program (Phase IV), the US Environmental Protection Agency, through the RS Kerr Laboratories and Environment Canada. Funding management, assistance, and kind advice were provided by Ted O'Neill, Dave Ketcheson, Gregg Zwiers and Kathie Bedard, of the Phase IV team, and by Steve Kraemer of the US EPA. Dr. Ed Sudicky of the University of Waterloo ably provided overall management of the EPA component of the Project as the Principal Investigator of the EPA Capture Zone Study. We appreciate the assistance and support provided by Rick Binek, Gary Brooks, Garry Sack and Kent Tran of the Ontario Clean Water Agency (OCWA) and Jim Marshall of Sanexen Ltd. during our work at the Smithville site. The composite borehole logs were completed by Earthfx Ltd. This report benefitted from detailed reviews by Bernard Keuper and Ted O'Neill. Lastly, we could not have completed this study without the capable and enthusiastic assistance of summer and graduate students who provided support in the field, lab and office. These individuals include Jody Addah, Andrea Brown, Mark Hilverda, Vera Langer, Sandra Lortie, Nadia Marengo, Stuart Rutledge, Tony Radcliffe, Bill Uhlmann and Donna Welch.

7.0 REFERENCES

- Barone, F. S., R. K. Rowe, and M. Quigley. Laboratory determination of chloride diffusion coefficient in an intact shale, In: *Canadian Geotechnical Journal* 27, 177-184, 1990.
- Bickerton, G., Chemical and mineralogical composition of the Lockport and Rochester Formations, Smithville, Ontario, NWRI Contribution No. 97-130, 1997.
- Bickerton, G., and K. Novakowski, Measuring adsorption in low porosity rock, unpublished manuscript, 1993.
- Black, W. H., H. R. Smith, and F. D. Patton, Multiple-level groundwater monitoring with the MP system, In: *Proceedings NWWA-AGU Conf. Surface and Borehole Geophysical Methods and Groundwater Instrumentation*, NWWA, Dublin, Ohio, 1987.
- Blair, R., and S. McFarland, Regional correlation of the Middle and Lower Niagara Escarpment Area, proceedings of the 1992 Conference of the Canadian National Chapter, International Association of Hydrogeologists, Hamilton Ontario, 659-696, 1992.
- Bliss, J. C., and K. R. Rushton, The reliability of packer tests for estimating the hydraulic conductivity of aquifers, *Q. J. Engrg. Geol.*, 17, 81-91, 1984.
- Bloomfield, J., The role of diagenesis in the hydrogeological stratification of carbonate aquifers: an example from the Chalk at Fair Cross, Berkshire, UK, *Hydrology and Earth System Sciences*, 1, 19-33, 1997.
- Bowman, R. S., and J. F. Gibbens, Difluorobenzoates as non-reactive tracers in soil and groundwater, *Groundwater*, 30(1), 8-14, 1992.
- Brett, C. E., D. H. Tepper, W. M. Goodman, S. T. LoDuca, and B. H. Eckert, Revised Stratigraphy and Correlations of the Niagaran Provincial Series (Medina, Clinton and Lockport Groups) in the Type Area of Western New York, U.S. Geological Survey Bulletin 2086, U.S. Government Printing Office, Washington, D.C., 66pp., 1995.
- Brown A., P. Lapcevic, K. Novakowski, S. Lesage, S. Brown, K. Millar, J. Voralek, and L. Zanini, Characterization of Trichloroethylene Contamination in the fractured bedrock at the Smithville, Ontario Site, NWRI Contribution No. 97-140, 1997.
- Chen, C. S., Solutions for radionuclide transport from an injection well into a single fracture in a porous formation, *Water Resources Research*, 22(4), 508-518, 1986.
- Clark, I., and P. Fritz, *Environmental Isotopes in Hydrogeology*, Lewis Publishers, Boca Raton, FL, 328 pp., 1997.

- Cook, P., C. Simmons, and A. Love, Groundwater age in fractured rock aquifers, Clare Valley, South Australia, Unpublished manuscript, 14 pp., 1999.
- David, M., Geostatistical ore reserve estimation, Elsevier Scientific Publishing Company, Amsterdam, 364pp., 1977.
- Doe, T., and J. Remer, Analysis of constant-head well tests in non-porous fractured rock, In: Third Invitational well-testing symposium - "Well testing in Low Permeability Environments", Berkeley California, 84-89, 1980.
- Drost, W., D. Klotz, A. Koch, H. Moser, F. Neumaier, and R. Werner, Point dilution methods of investigating ground water flow by means of radioisotopes, *Water Resources Research*, 4(1), 125-146, 1968.
- Engelder, T., M. P. Fischer, and M. R. Gross, Geological Aspects of Fracture Mechanics, A short course manual, Geological Society of America, 281pp., 1993.
- Flint, J.-J., and J. Lolcama, Buried ancestral drainage between Lakes Erie and Ontario, *Geol. Soc. Am. Bull.*, 97, 75-84, 1985.
- Freeze, R. A., and J. A. Cherry, *Groundwater*, Prentice-Hall, New Jersey, 604 pp., 1979.
- Gartner Lee Limited, Geophysical Report for Project 95-426 Borehole Geophysics-Geology, 1996.
- Gartner Lee Limited and Acres International Ltd, Regional geologic model: Smithville Phase IV, Report No. 95-160, 75pp., 1996.
- Gehman, H. M., Jr., Organic matter in limestones, *Geochimica et Cosmochimica Acta*, 26, 885-897, 1962.
- Glöckner, M., Simulation of a radial divergent tracer experiment using a semi-analytical model, BSc. Thesis, Brock University, St. Catherines ON, 31pp., 1999.
- Golder Associates Limited, Results of geological and hydrogeological investigations and contaminated plume delineation study 1987, Clean-up of abandoned PCB storage facility, Smithville, Ontario, Ref. 871-1156, June 1988.
- Golder Associates Limited, Report on: Hydrogeologic data compilation and assessment CWML site Smithville, Ontario, Project No. 94-106, 52pp., 1995.
- Grisak, G.E., W. F. Merritt, and D. W. Williams, fluoride borehole dilution apparatus for groundwater velocity measurements, *Can. Geotech. J.*, 14, 554-561, 1977.

- Halley, and Schmoker, High porosity Cenozoic carbonate rocks of South Florida: progressive loss of porosity with depth, *AAPG Bulletin*, 67(2), 191-200, 1983.
- Hantush, M.S., and C. E. Jacob, Non-steady radial flow in an infinite leaky aquifer, *Am. Geophys. Union Trans.*, 36, 95-100, 1955.
- Hyd-Eng Geophysics Inc., 1996 Geophysical Borehole Surveys at the Smithville Phase IV Site Smithville, Ontario, Project I10 for Environment Canada, 1997.
- IAEA/WMO, Global Network for Isotopes in Precipitation, The GNIP database, Release 2 May, 1998, Simco, Ontario, www.iaea.org. 1998.
- Jackson, R., and E. Hoehn, A review of processes affecting the fate of contaminants in groundwater, *Water Pollution Research J. Can.*, 22(1), 1-20, 1987.
- Johnston, H. M. and D. J. Wilmot, Sedimentary sequence study: Results of laboratory sorption and diffusion experiments, Ontario Hydro Research Division Report No. 88-85-K, Toronto, Ontario, 201pp., 1988.
- Kueper, B. H., and D. B. McWhorter, The Behaviour of Dense, Nonaqueous Phase Liquids in Fractured Clay and Rock, *Groundwater*, 29(5), 1991.
- Kunstmann, H., W. Kinzelbach, P. Marschall, and G. Li, Joint inversion of tracer tests using reversed flow fields, *J. Contam. Hydrol.*, 26, 215-226, 1997.
- Langer, V., Resaturation and hydraulic conductivity of rock samples from the Lockport Formation at Smithville, southern Ontario, Canada, Unpublished report, National Water Research Institute, 7 pp., 1997.
- Lapcevic, P.A., The results of constant head injection tests using variable packer spacings to characterize permeable fractures in the Lockport dolostone, Niagara Falls, N.Y. NWRI Contribution 90-97, 41 pp., 1990.
- Lau, J. S. O., The determination of true orientations of fractures in rock cores, *Canadian Geotech. J.*, 20, 221-227, 1983.
- Leonhart, L. S., R. L. Jackson, D. L. Graham, L. W. Gelhar, G. M. Thompson, B. Y. Kanehiro, and C. R. Wilson, Analysis and interpretation of a recirculating tracer experiment performed on a deep basalt flow top, *Bull. Assoc. Eng. Geologists*, 22(3), 259-274, 1985.
- Lide, D.R., *CRC Handbook of Chemistry and Physics*. 73rd edition. CRC Press, Ann Arbor, 1992.
- Longino, and Kueper, Non-wetting phase retention and mobilization in rock fractures, *Water Resources Research*, 35(7), 2085-2093, 1999.

- McElwain, T. A., D. W. Jackman, P. Beukema, Characterization and remedial assessment of DNAPL PCB Oil in fractured bedrock: A case study of the Smithville, Ontario Site, In: "Contamination by Immiscible Fluids and Remediation", NWWA Conference, Kitchener, Ontario, October 1989, 303-315, 1989.
- Montgomery, J., and L. Welkom, Groundwater Chemicals Reference, Lewis Publishers Inc., Chelsea, Michigan, 1990.
- Nelson, R. A., Contribution in Petroleum Geology and Engineering, 1: Geologic Analysis of Naturally Fractured Reservoirs, Ed. G. V. Chilingar, Gulf Publishing Company, Houston, 320 pp., 1985.
- Noll, R. S., Geochemistry and hydrology of groundwater flow systems in the Lockport Dolomite, near Niagara Falls, New York. MSc. Thesis, 143pp., 1989.
- Novakowski K. S, Analysis of pulse interference tests, Water Resources Research, 25(11), 2377-2387, 1989.
- Novakowski, K. S., P. A. Lapcevic, Field Measurement of Radial Solute Transport in Fractured Rock, Water Resources Research, 30(1), 37-44, 1994.
- Novakowski, K. S., Comparison of fracture aperture widths determined from hydraulic measurements and tracer experiments, In Proc: 4th Canadian/American Conference on Hydrogeology, Ed: B. Hitchon and S. Bachu, Nat. Water Well Assoc., Dublin, Ohio, 68- 80, 1988.
- Novakowski, K. S., and P. A. Lapcevic, Regional hydrogeology of the Silurian and Ordovician sedimentary rock underlying Niagara Falls, Ontario, Canada, J. Hydrol., 104, 211-236, 1988.
- Novakowski, K. S., and G. van der Kamp, The radial diffusion method. 2. A semi-analytical model for the determination of apparent diffusivity, porosity and adsorption, Water Resources Research, 32(6), 1823-1830, 1996.
- Novakowski, K. S., G. Bickerton, and P. A. Lapcevic, Interpretation of injection-withdrawal tracer experiments conducted in a large single fracture: exchange of solute between mobile and immobile zones or matrix diffusion?, Water Resources Research, 1998.
- Novakowski, K. S., G. V. Evans, D. A. Lever, and K. G. Raven, A field example of measuring hydrodynamic dispersion in a single fracture, Water Resources Research, 21(8), 1165-1174, 1985.
- Pannatier, Y., VARIOWIN: Software for spatial data analysis in 2D, Springer-Verlag, New York, 91pp., 1996.

- Radcliffe, A., Determination of Groundwater Velocities in Discrete Fractures using Point Dilution Methods, University of Waterloo, B. Sc. Thesis, Department of Earth Sciences (Thesis), 1997.
- Raven, K. G., K. S. Novakowski, and P. A. Lapcevic, Interpretation of field tracer tests of a single fracture using a transient solute storage model, *Water Resources Research*, 24(12), 2019-2032, 1988.
- Rea, J., and R. Knight, Geostatistical analysis of ground-penetrating radar data: A means of describing spatial variation in the subsurface. *Water Resources Research*, 34(3), 329-339, 1998.
- Reichart, T. M., Influence of vertical fractures in horizontally-stratified rocks, Unpublished M.Sc. Thesis, University of Waterloo, Waterloo, Ontario, Canada, 92 pp., 1992.
- Reitsma, S., and B. H. Kueper, Laboratory measurements of capillary pressure-saturation relationships in a rock fracture, *Water Resources Research* 30(4), 865-878, 1994.
- Rutty, A. L., The basement fracture pattern of Southern Ontario: A tectonic interpretation based on Landstat TM imagery, airphotos and field data, MSc. Thesis, University of Toronto, 177pp., 1993.
- Sanford, B. V., F. Thompson, and G. McFall, Plate Tectonics - a possible controlling mechanism in the development of hydrocarbon traps in southwestern Ontario, *Bull. Can. Pet. Geol.*, 33(1), 52-71, 1985.
- Shackelford, C. D., D. E. Daniel, and H. M. Liljestrand, Diffusion of inorganic species in compacted clay soil, *Journal of Contaminant Hydrology*, 4, 241-273, 1989.
- Shapiro, A. M., and J. R. Nicholas, Assessing the validity of the channel model of fracture aperture under field conditions, *Water Resources Research*, 25(5), 817-828, 1989.
- Skagius, K., and I. Neretnieks, Porosities and diffusivities of some nonsorbing species in crystalline rocks, *Water Resources Research*, 22(3), 389-398, 1986.
- Smart, P. L., and I. M. S. Laidlaw, An evaluation of some fluorescent dyes for water tracing, *Water Resources Research*, 13(1), 15-33, 1977.
- Uhlman, W., J. Voralek, and P. Lapcevic, The Use of Point-Dilution Techniques for Determining Groundwater Velocity in Fractured Bedrock, Smithville, Ontario, NWRI Contribution No. 99-202., 29pp., 1999.
- Voralek, J. W., Westbay Completion Report for MP38 Monitoring Wells, No. 63 and 65, NWRI, 1997.

- Walsh, J. B., and W. F. Brace, The effect of pressure on porosity and the transport properties of rock, *Journal of Geophysical Research*, 89(B11), 9425-9431, 1984.
- Walton, W. C., Selected analytical methods for well and aquifer evaluation. *Illinois State Water Survey Bull.*, 49, 81 pp., 1962.
- Westbay Instruments Inc., Westbay Completion Report for MP38 Monitoring Wells No. 53, 60, 61, 62 Smithville Site, Project No. WB761-96, 1996.
- Williams, H. R., D. Corkery, and E. G. Lorek, A study of joints and stress-release buckles in Palaeozoic rocks of the Niagara Peninsula, southern Ontario, *Can. J. Earth Sci.*, 22, 296-300, 1985.
- Yager, R. M., Simulated three-dimensional groundwater flow in the Lockport Group, a fractured-dolomite aquifer near Niagara Falls, New York, U.S. Geological Survey Water Supply Paper, W 2487, 1996.
- Zanini, L., K. Novakowski, and P. Lapcevic, Inorganic Geochemistry of the Groundwater at the Smithville Site – Phase I Investigation, NWRI Contribution No. 97-123, 39 pp., 1997.
- Zanini, L., K. Novakowski, P. Lapcevic, G. Bickerton, J. Voralek, and C. Talbot, Regional groundwater flow in the fractured carbonate aquifer underlying Smithville, Ontario, inferred from combined hydrogeological and geochemical measurements, *J. Groundwater*, 1998.
- Zanini, L., K. Novakowski, P. Lapcevic, G. Bickerton, J. Voralek, and C. Talbot, Inorganic Geochemistry of the Groundwater at the CWML Site, Smithville, Ontario – Phase II and III Investigation, 1997, NWRI Contribution No. 98-243, 45 pp., 1998.
- Zeigler, T. W., Determination of rock mass permeability, Waterways Experiment Station, Technical Report S-76-2, Vicksburg, Mississippi, 1976.

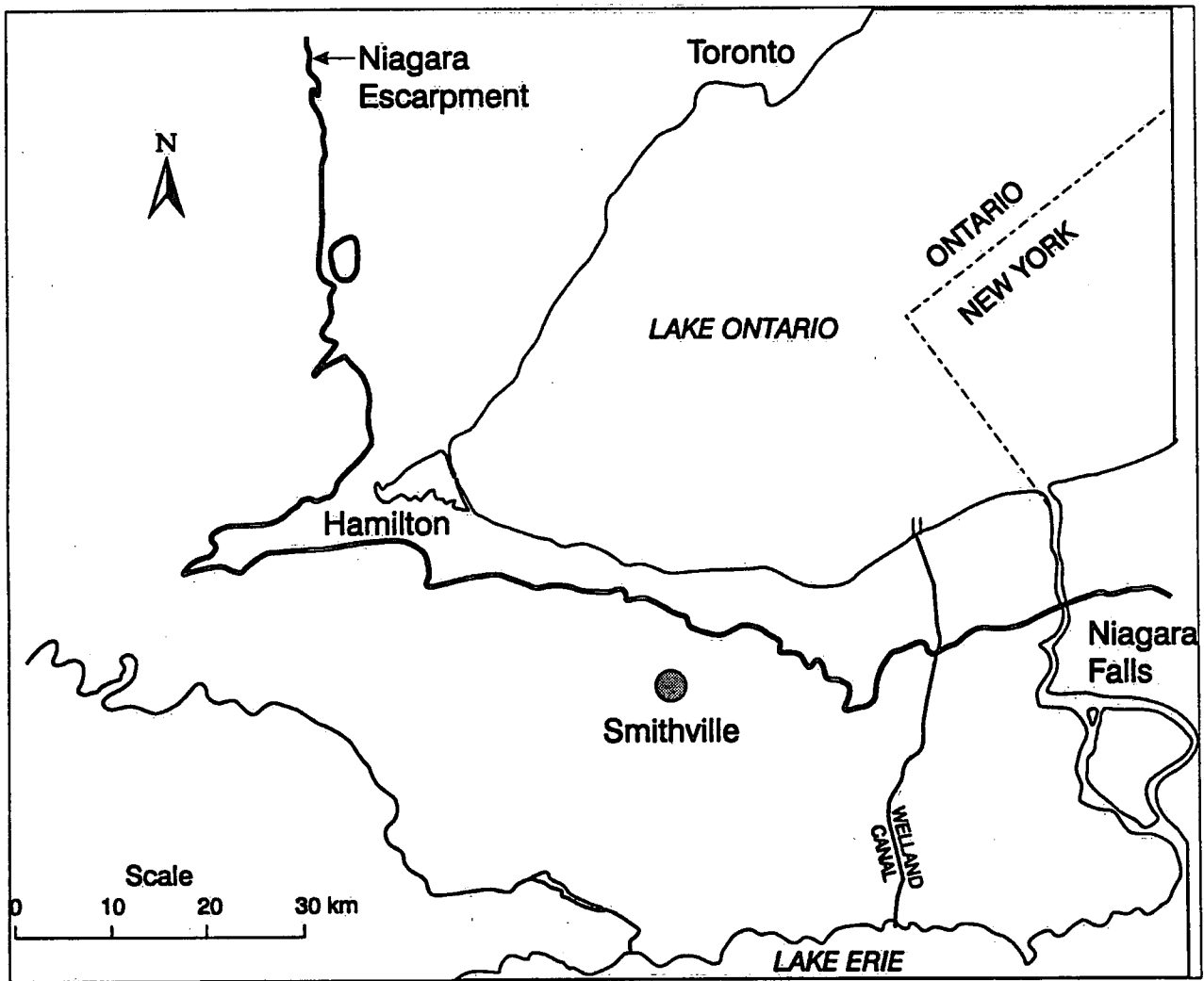


Figure 1.1 Location of Smithville site.

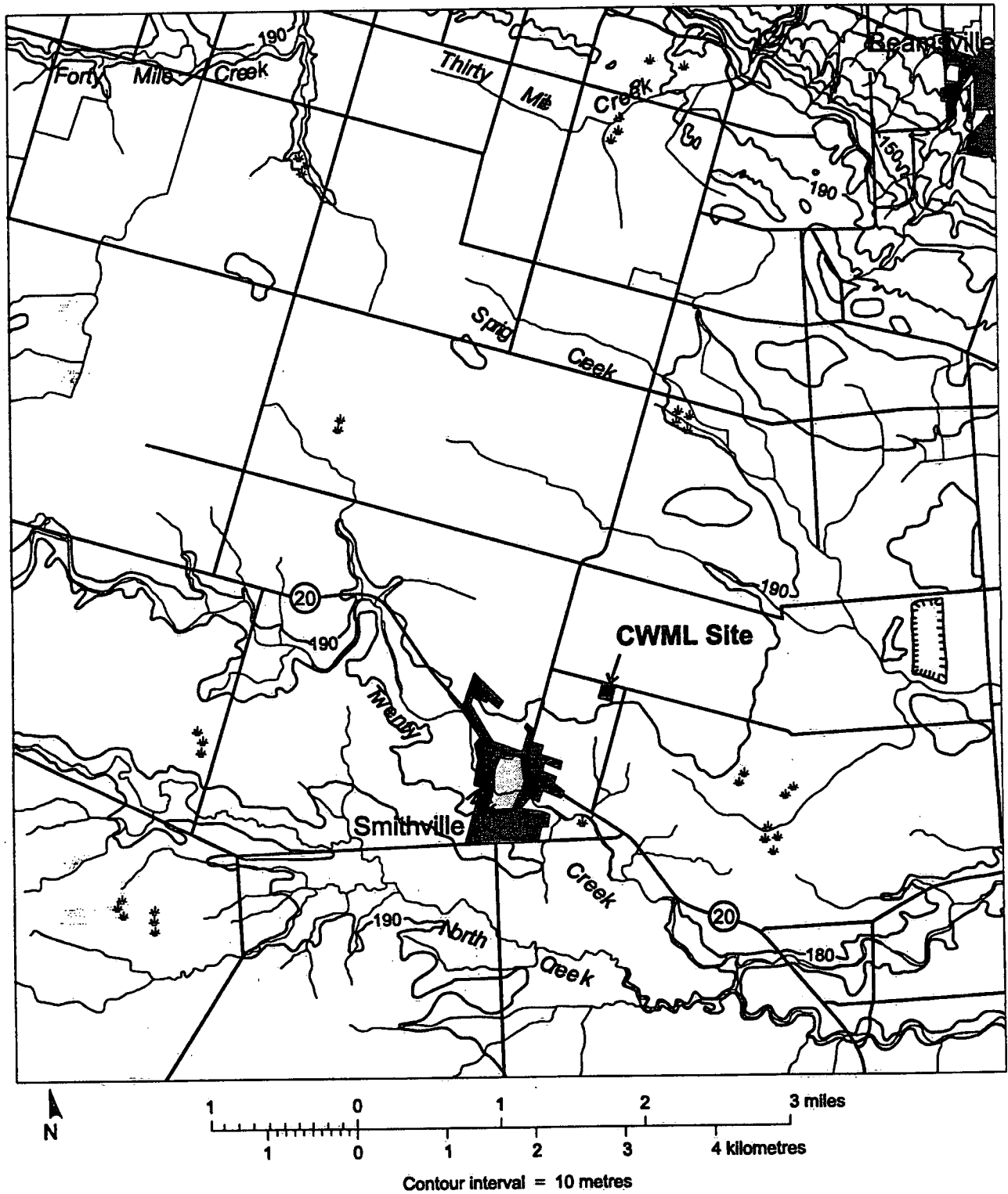


Figure 1.2 Map illustrating topography of Smithville region.

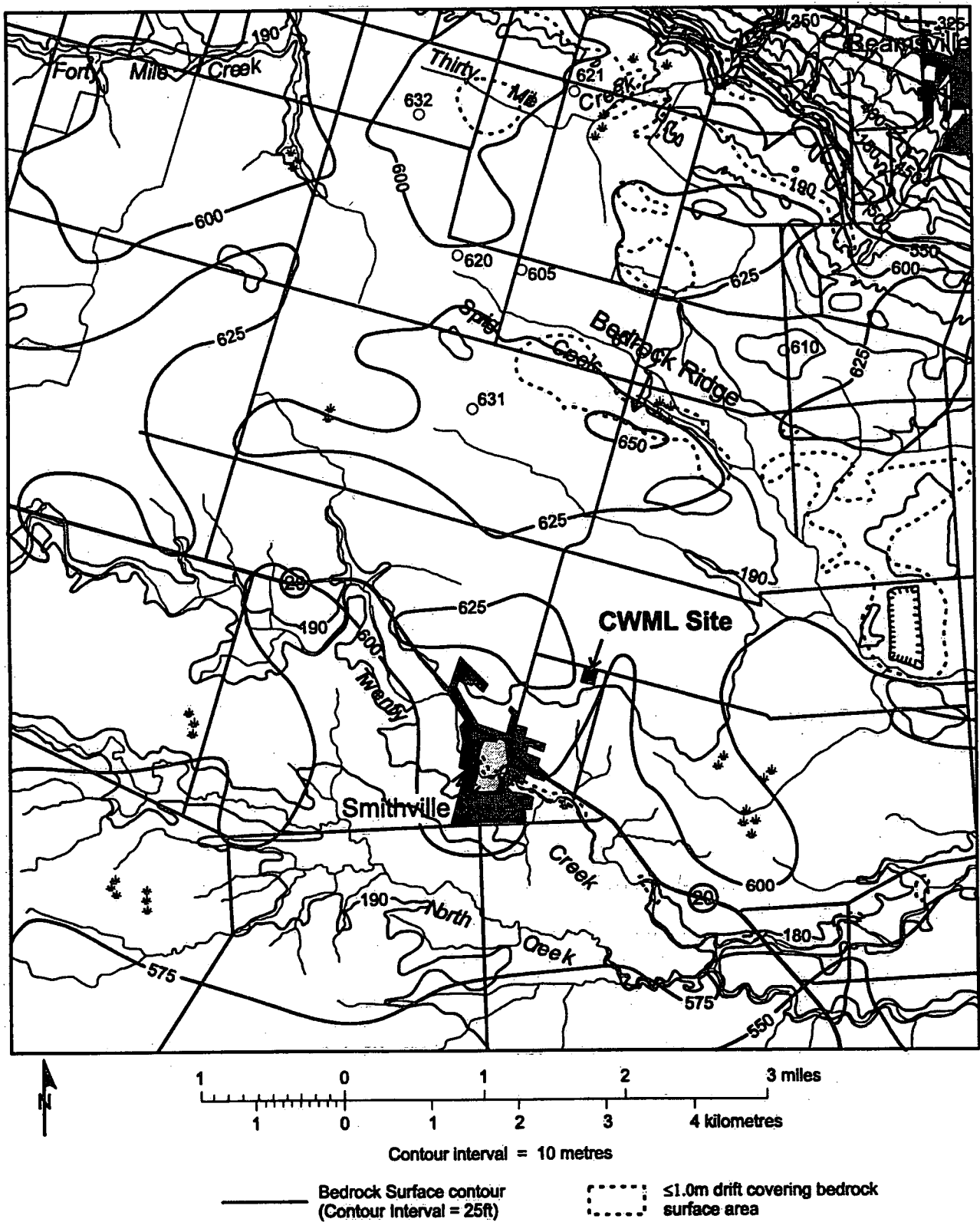


Figure 1.3 Physiographic features in the Smithville region.

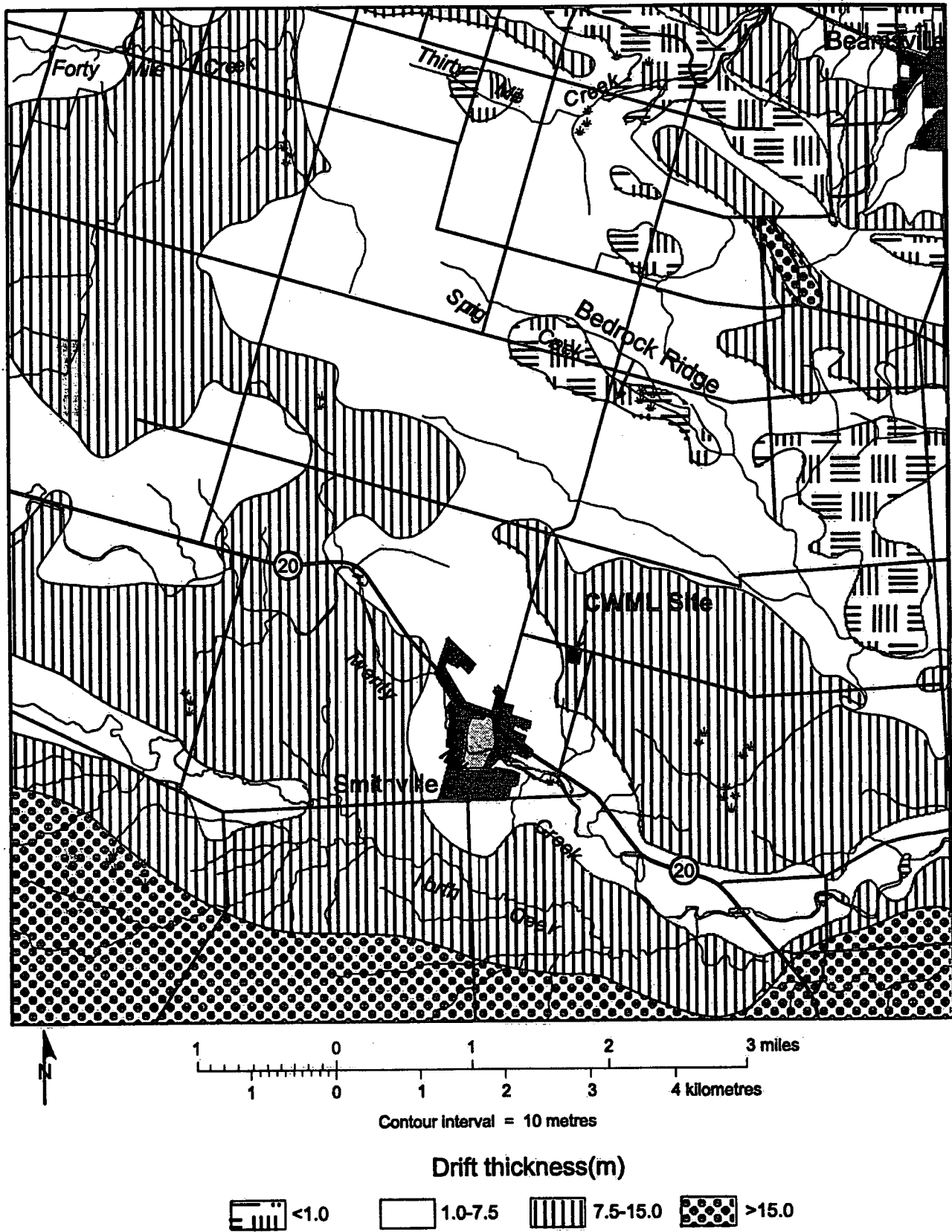
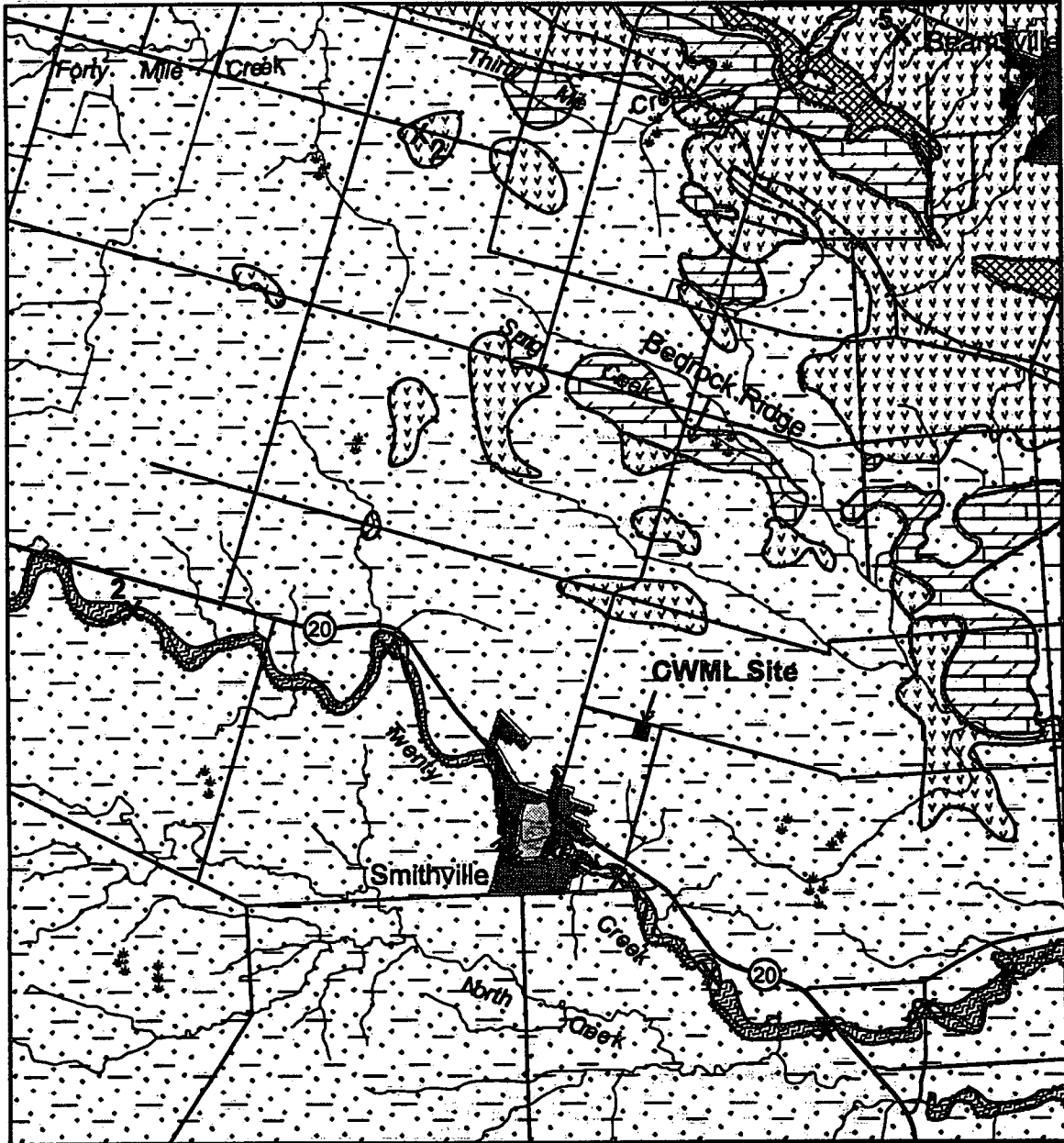


Figure 1.4 Map of drift thicknesses.










- | | |
|--|---|
|  Halton Till |  Clinton & cataract groups |
|  Lockport Formation |  Queenston Fm. Shale |
|  Glaciolacustrine clay & silt |  Stream deposits |
|  Vinemount Moraine | X Bedrock outcrop |

Figure 1.5 Geologic map of Smithville area.

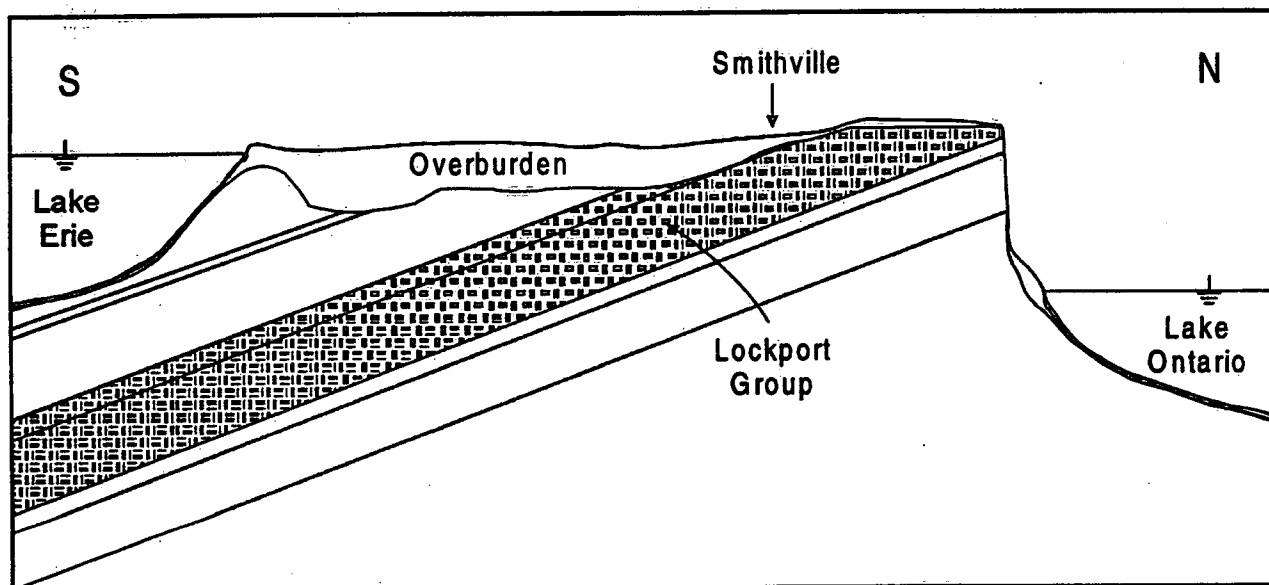


Figure 1.6 Regional setting of Lockport Dolostone.

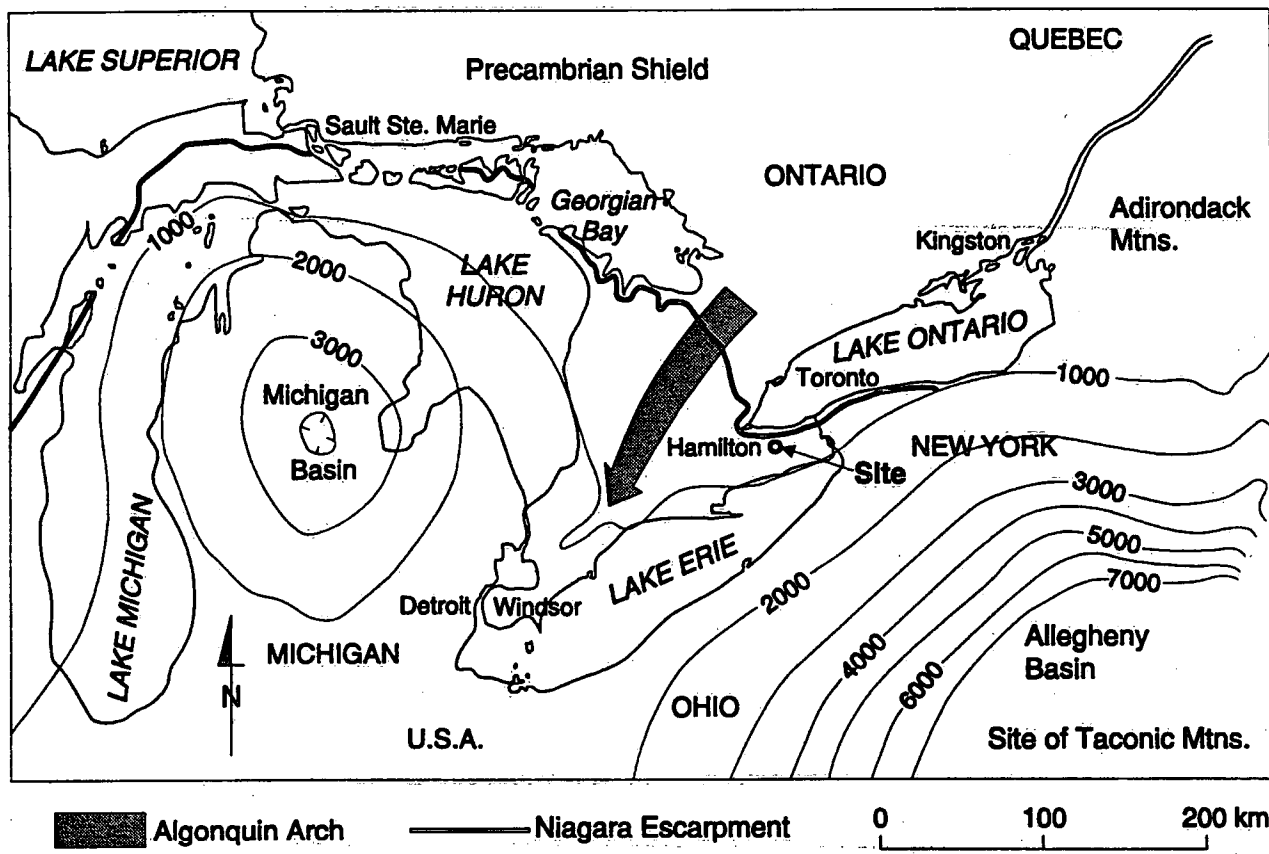


Figure 1.7 Map illustrating major structural features in Southern Ontario. Note location of site in relation to Algonquin Arch and Niagara Escarpment (modified after Gartner Lee, 1995)

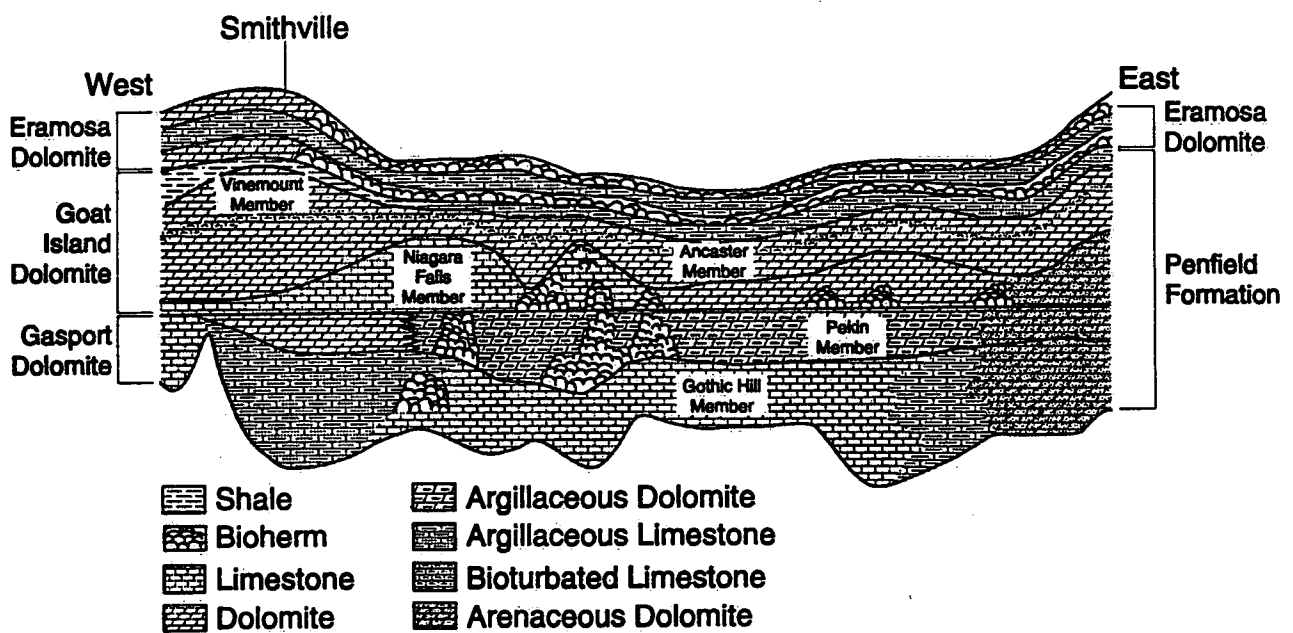


Figure 1.8 Cross-section of the Lockport dolostone following the Niagara Escarpment between Hamilton in the west and Niagara Falls in the east. (Modified from Brett et al., 1995)

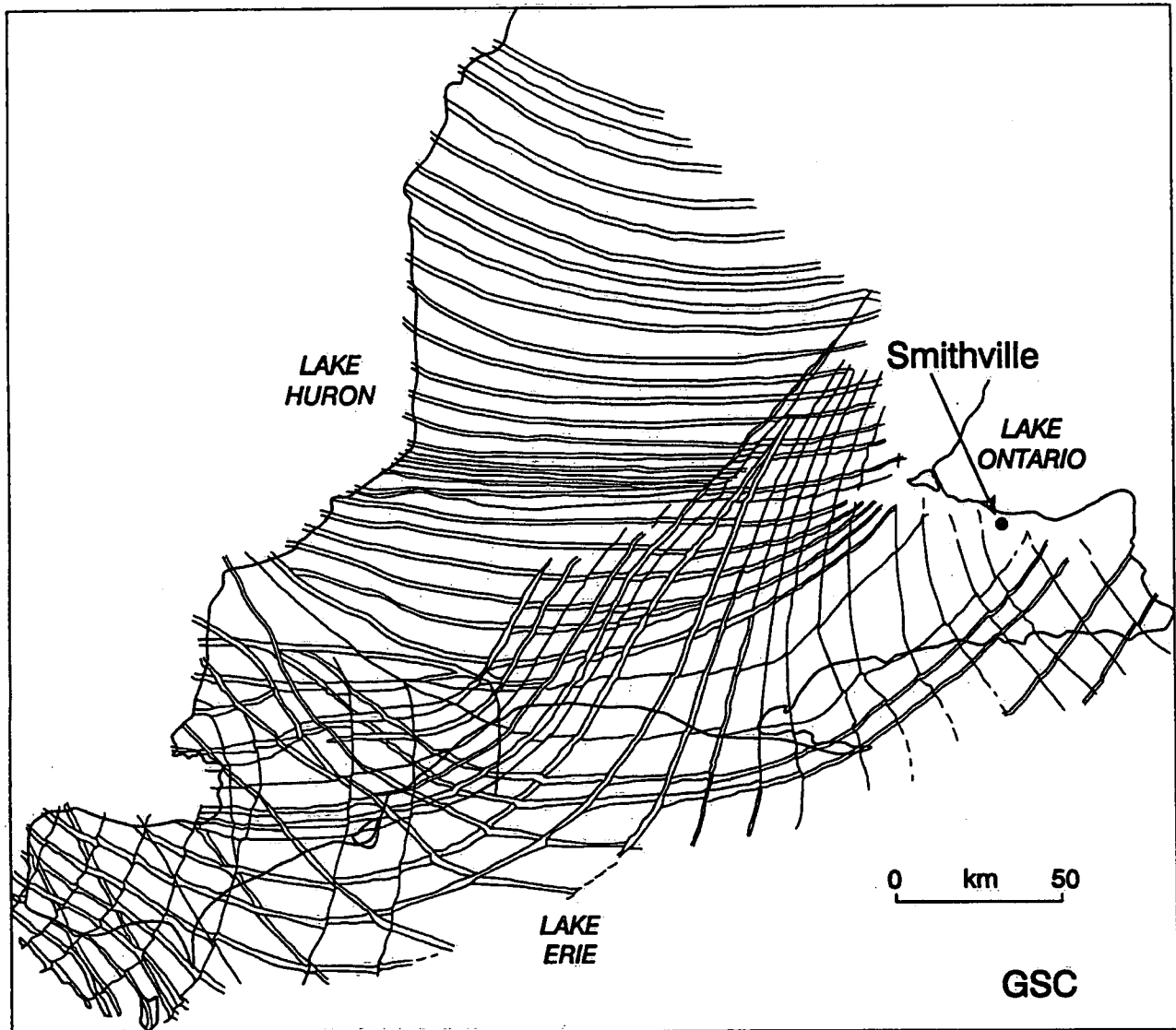


Figure 1.9 Distribution of regional faults in southern Ontario. (From Sanford, B. V., Thompson, F. J., And McFall, G. H. 1985. Phanerozoic and recent tectonics of the Canadian Craton, in the Geoscience Program - Proceedings of the Seventeenth Information Meeting of the Nuclear Fuel Waste Management Program, Atomic Energy of Canada Limited, TR-299:334-352.)

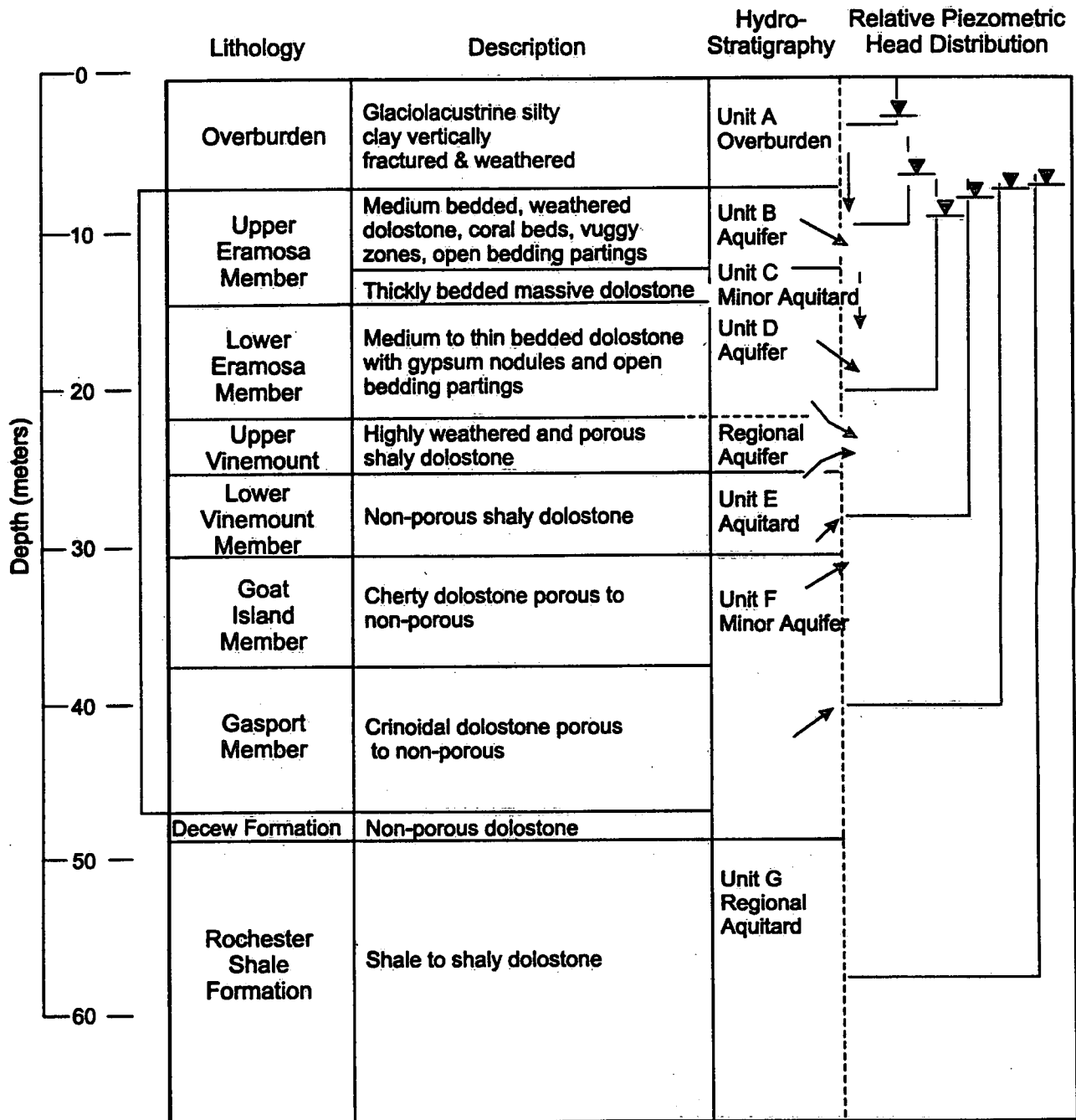


Figure 1.10 Diagram of vertical flow system illustrating drainage to the Upper Vinemount unit. (Modified from McElwain et al., 1989).

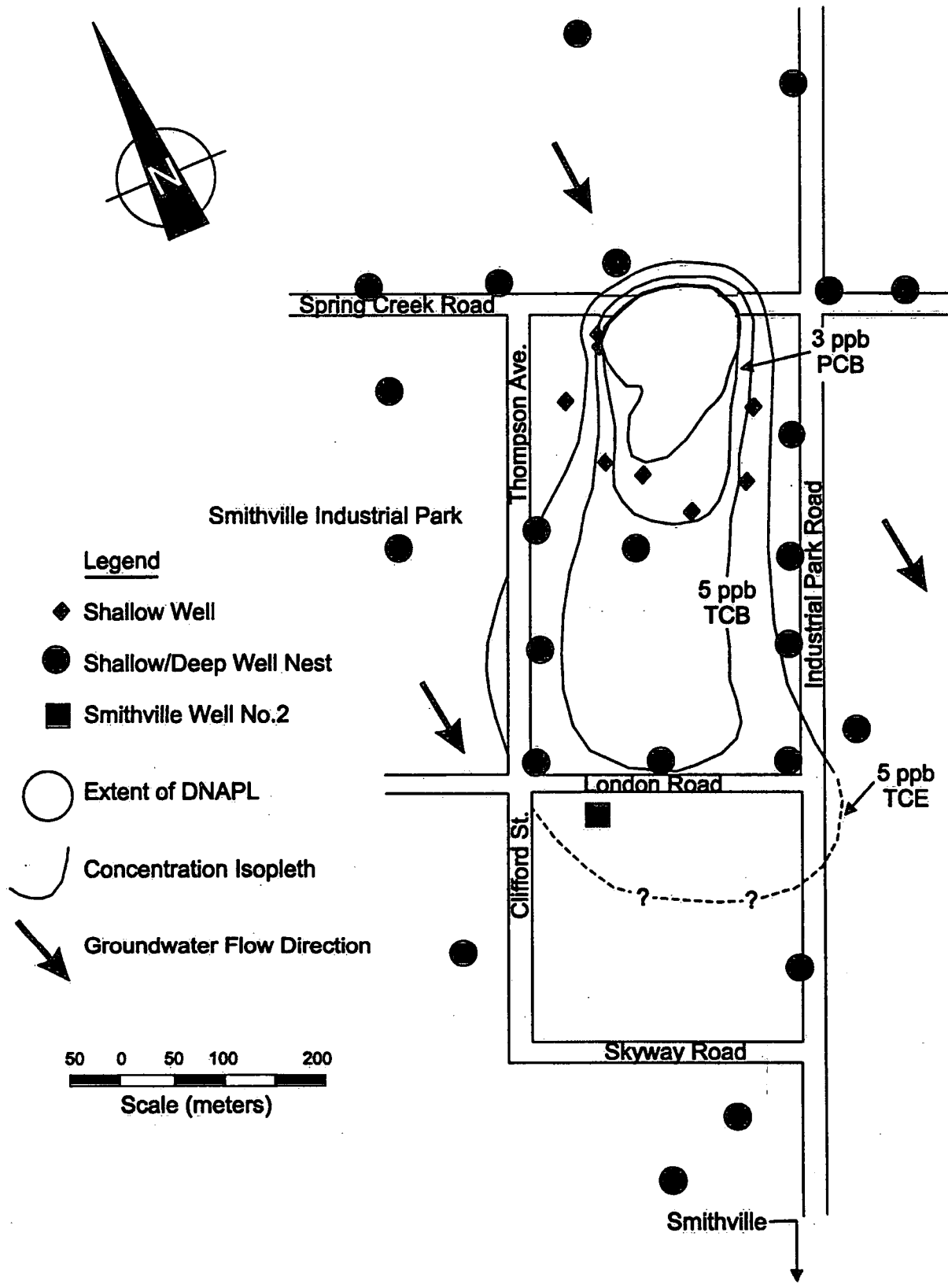


Figure 1.11 Extent of contaminant plumes (TCE, PCB and TCB) in 1988. (Modified from McIelwain et al., 1989)

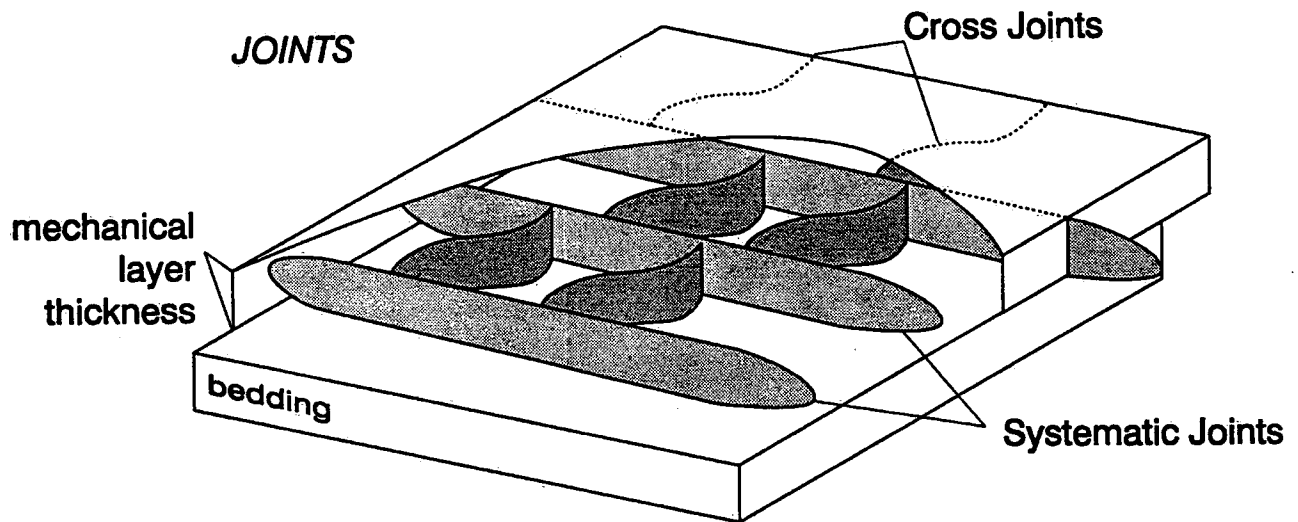


Figure 1.12 Typical three-dimensional view of conceptual fracture framework for a layer-cake stratigraphy. (From Engleder, T., Fischer, M. P. And Gross, M. R. 1993. Geological Aspects of Fracture Mechanics, A Short Course Manual, Geological Society of America, Boulder, CO.)

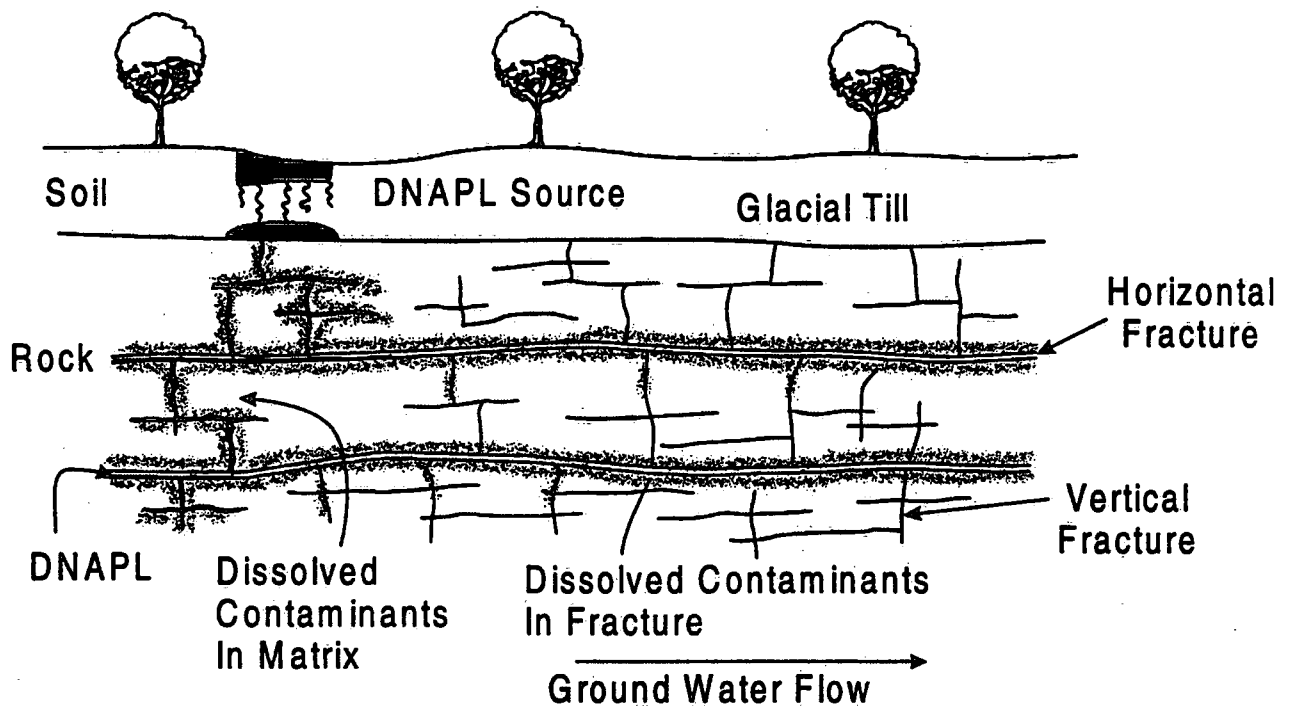


Figure 1.13 Diagram depicting DNAPL and aqueous phase contamination in discretely fractured rock.

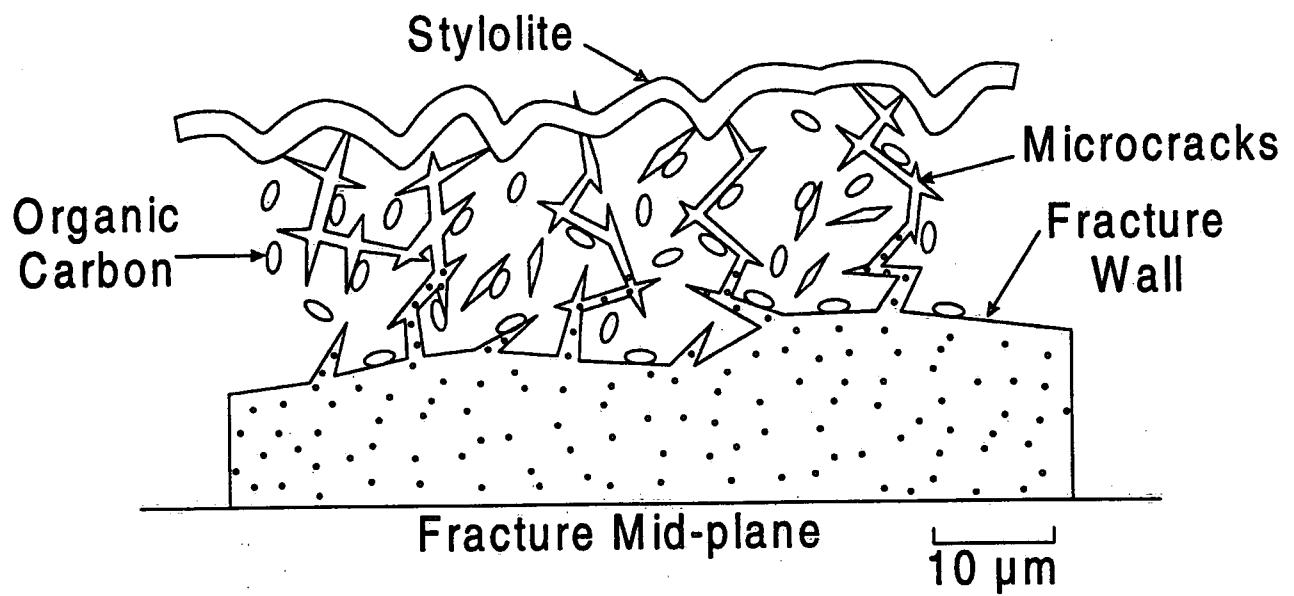


Figure 1.14 Schematic diagram depicting hypothetical transport processes at the microscopic scale.

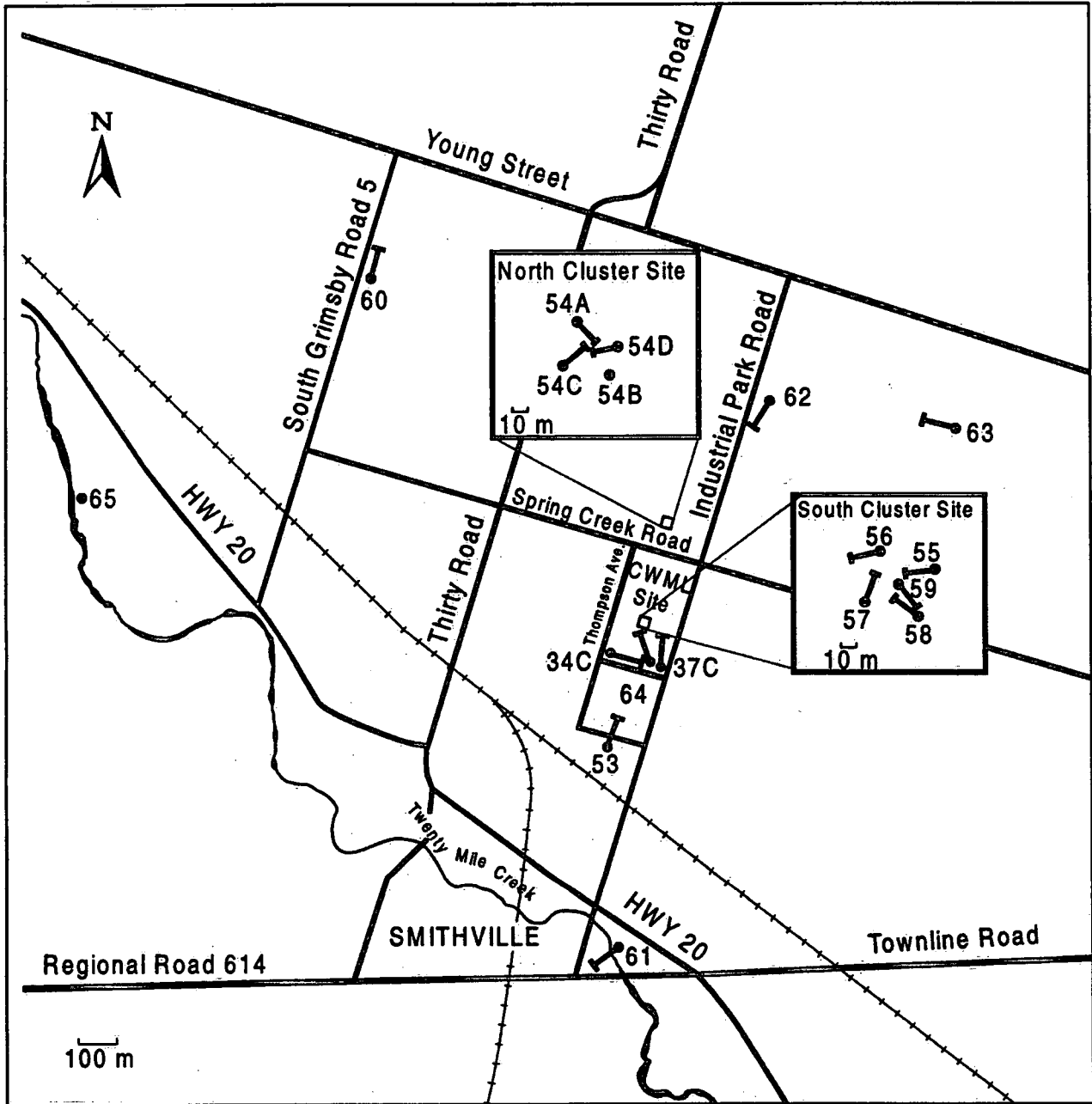


Figure 2.1 Location of new boreholes installed in the Smithville area as part of this study.

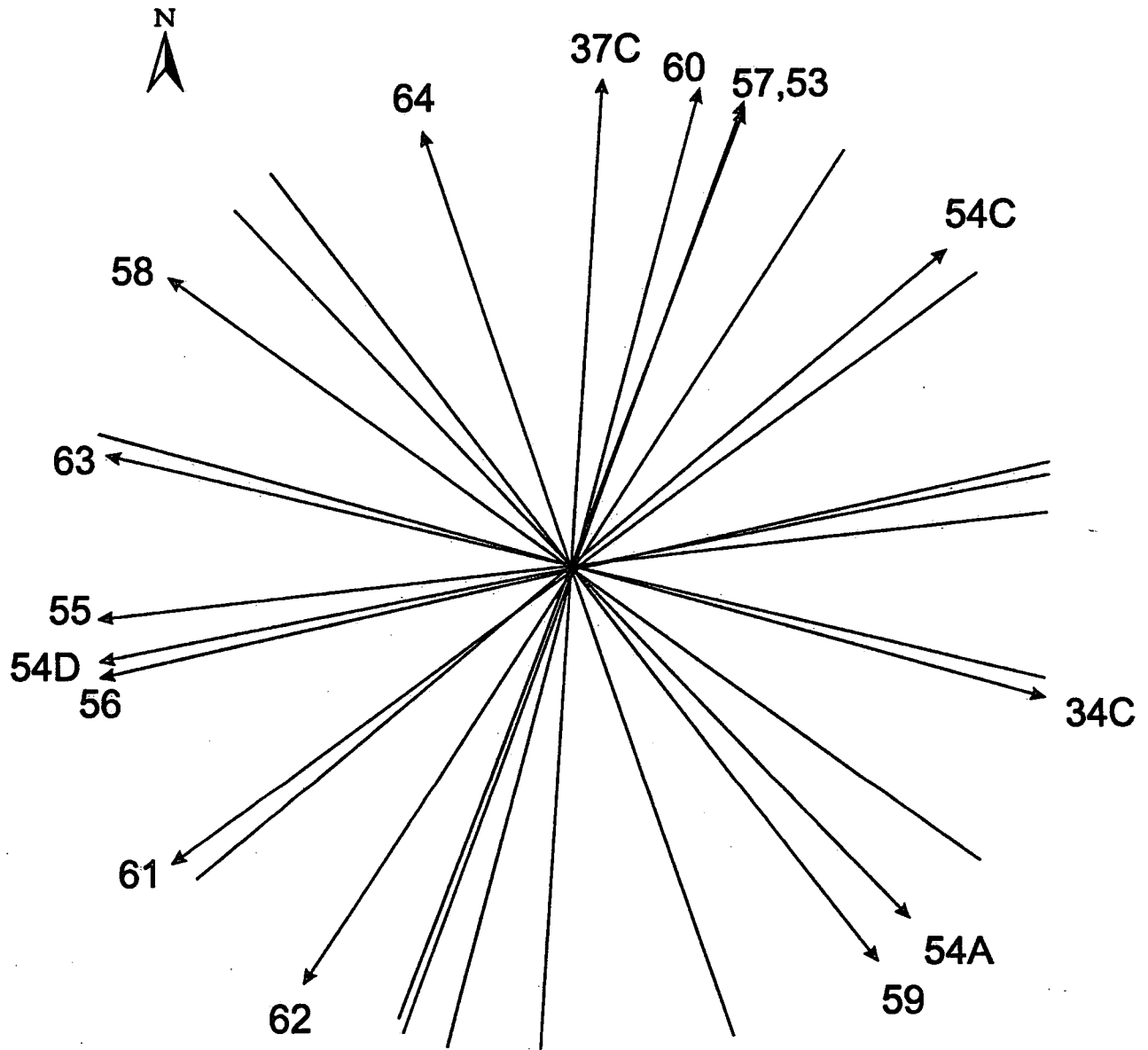


Figure 2.2 Schematic showing trends of inclined boreholes.

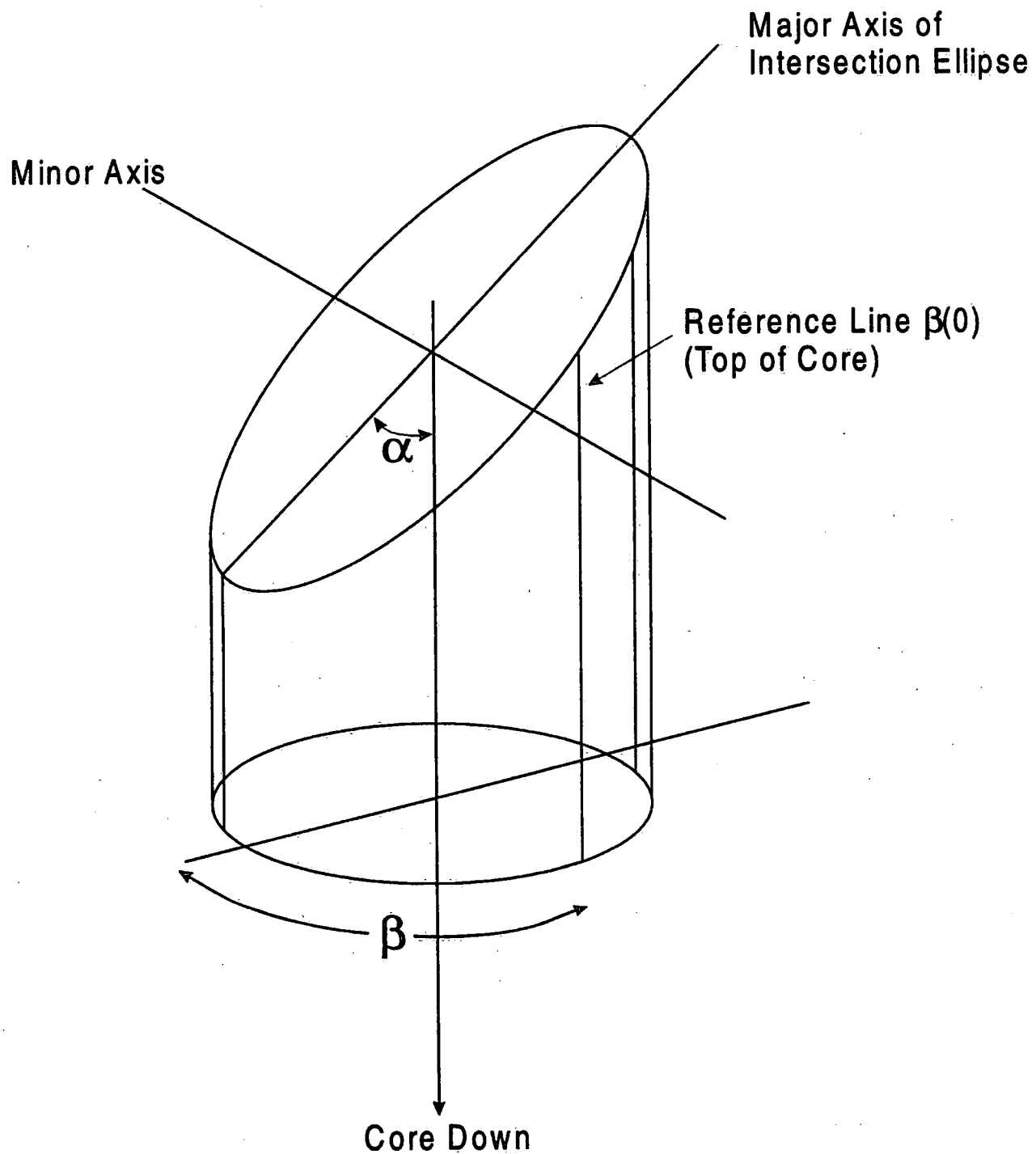


Figure 2.3 Schematic showing core angles measured to orient vertical fractures (after Lau(1983)).

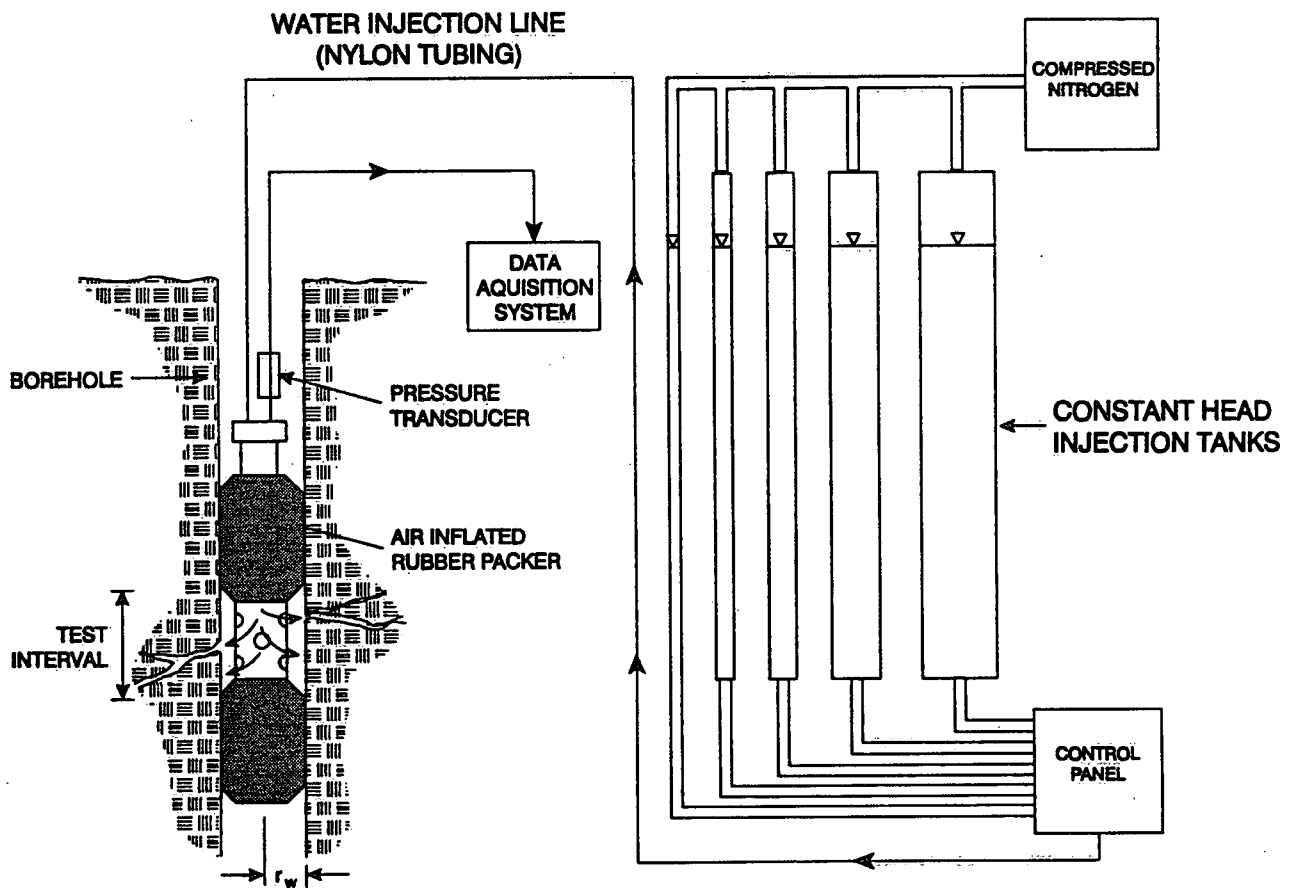


Figure 2.4 Schematic diagram of constant-head injection testing system.

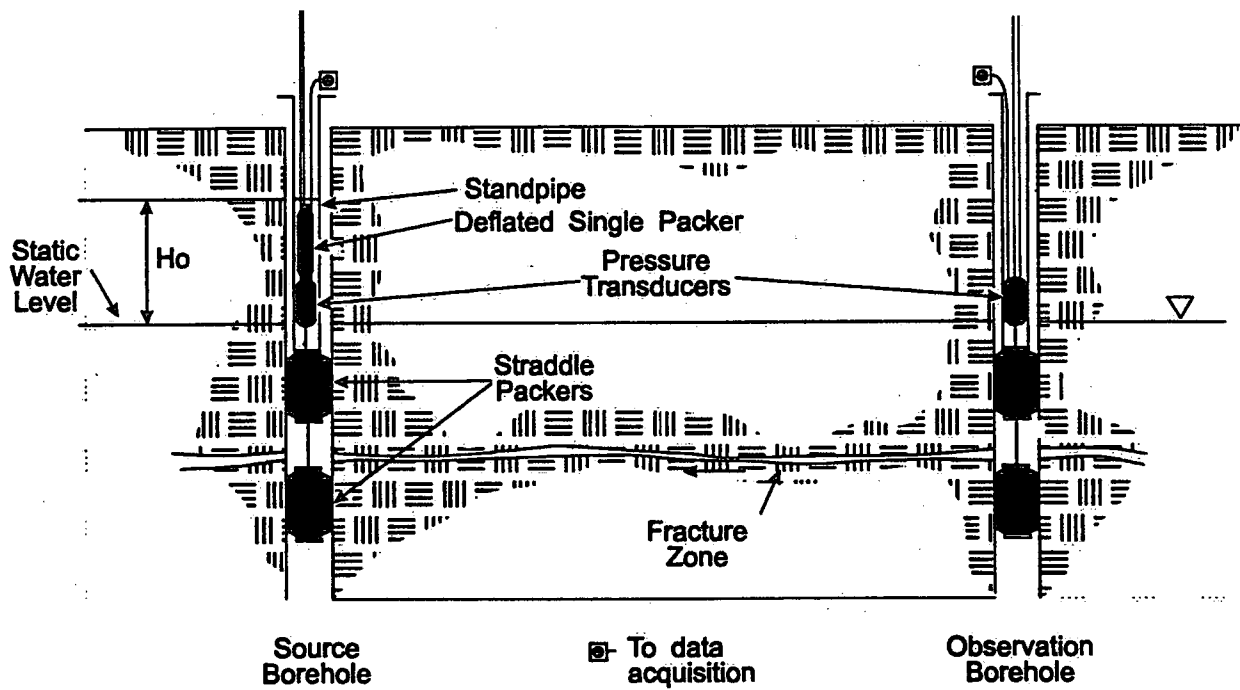


Figure 2.5 Schematic diagram showing field set-up for pulse interference tests. (From Novakowski, K.S., 1989)

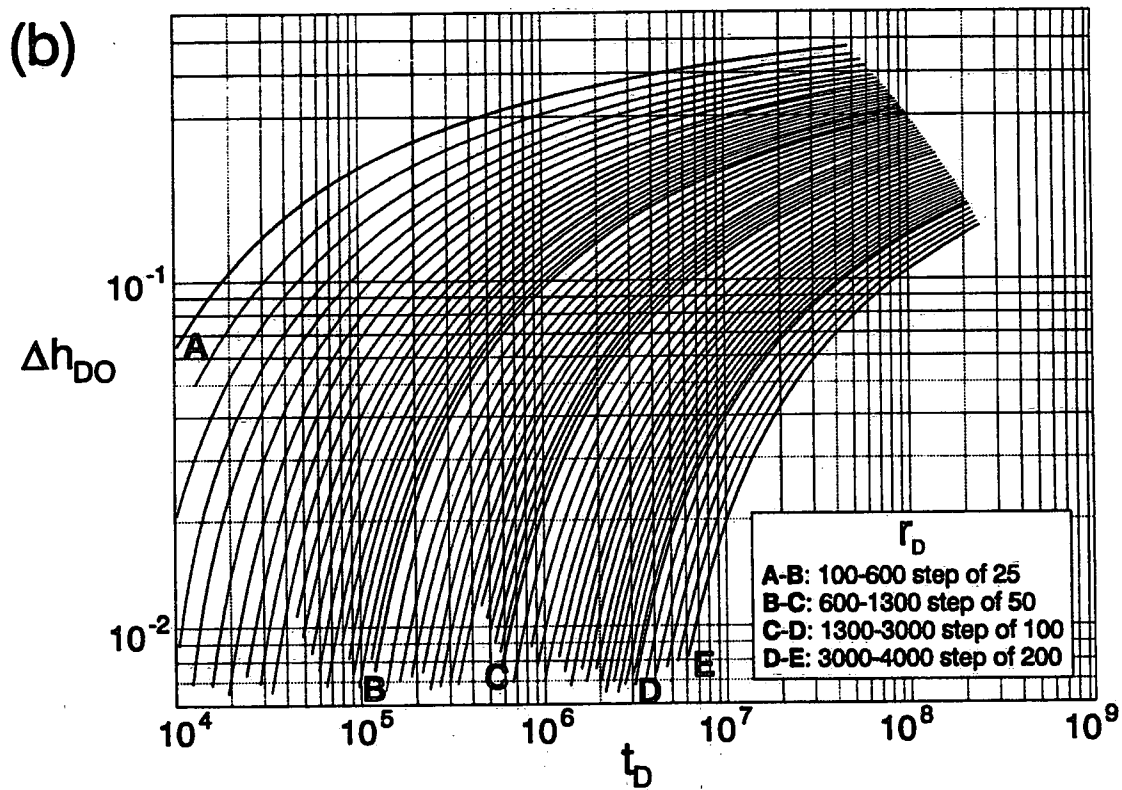
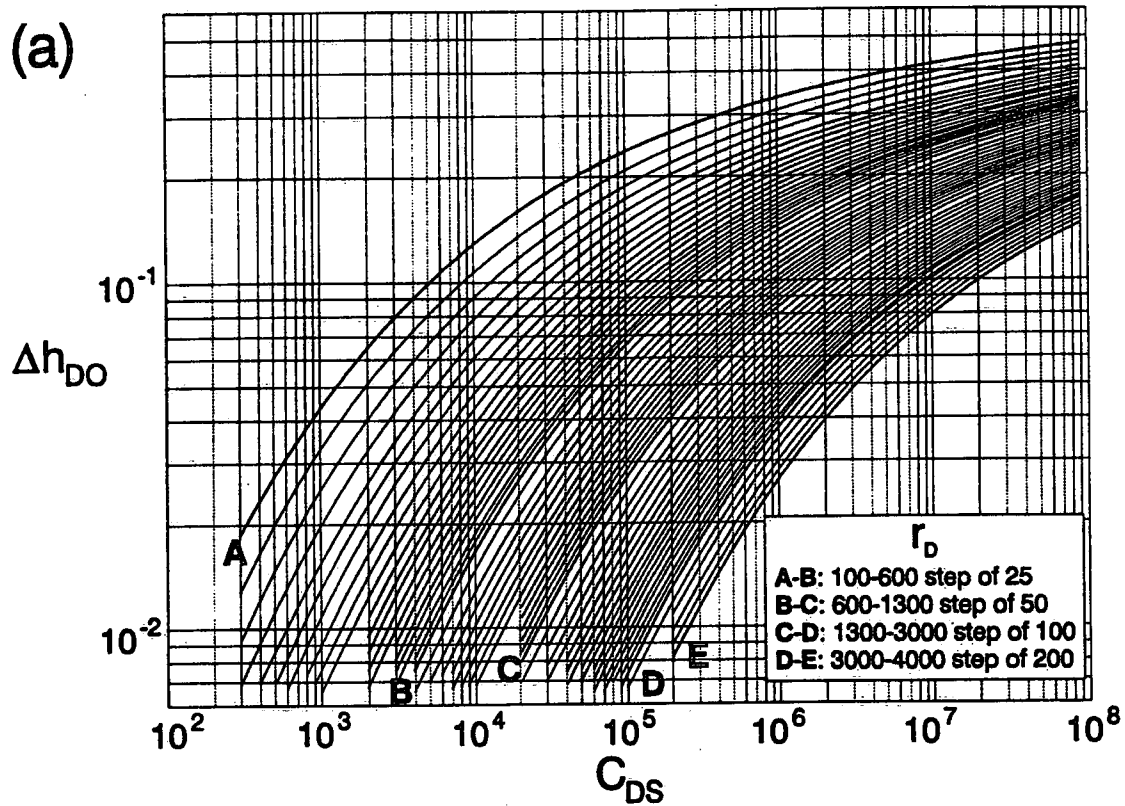


Figure 2.6 Type curves used to interpret pulse interference tests by graphical method when there is no observation well storage (a) curves used to calculate S and (b) curves used to calculate T . (From Novakowski, K.S., 1989)

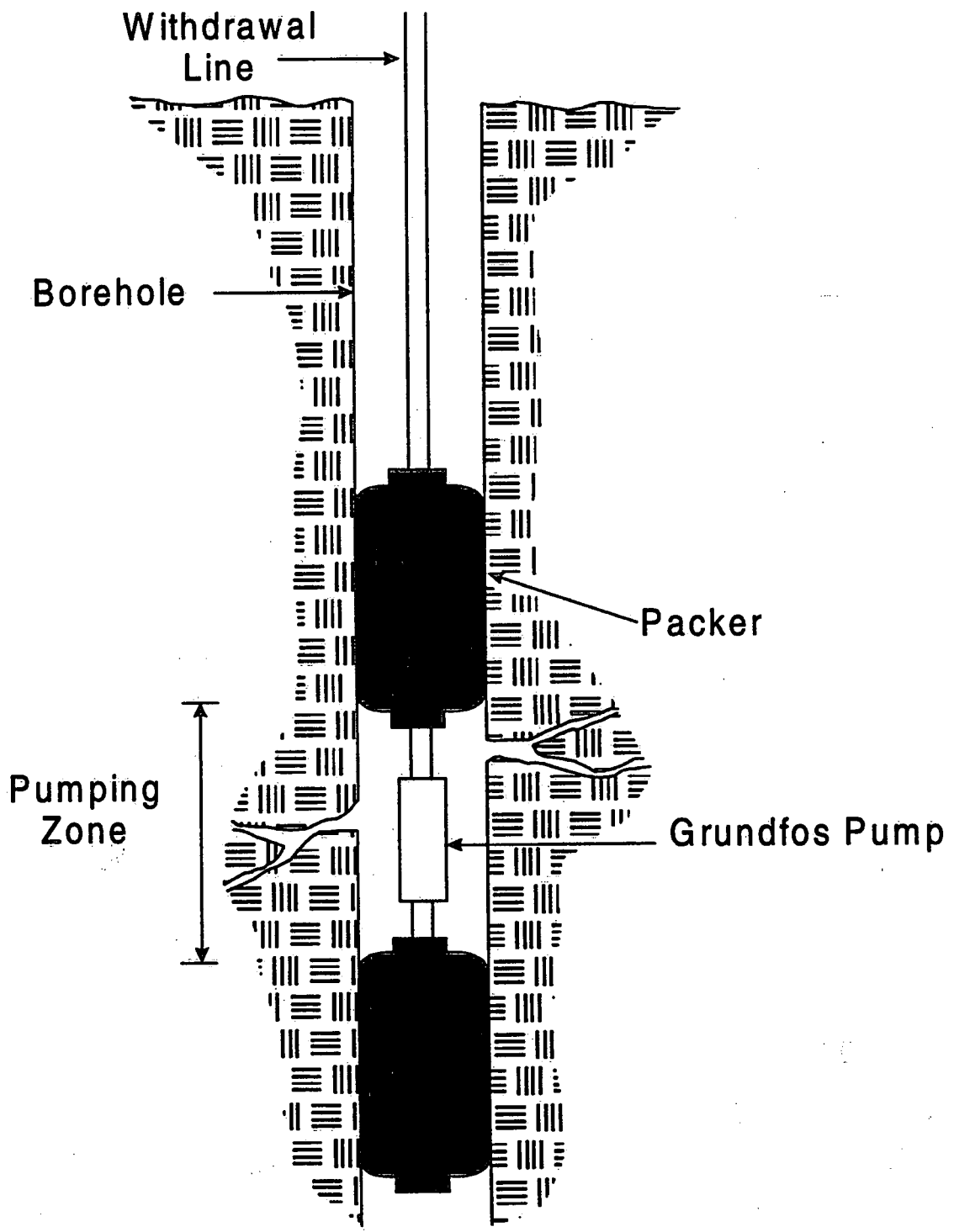


Figure 2.7 Set-up for pumping test in pumped borehole.

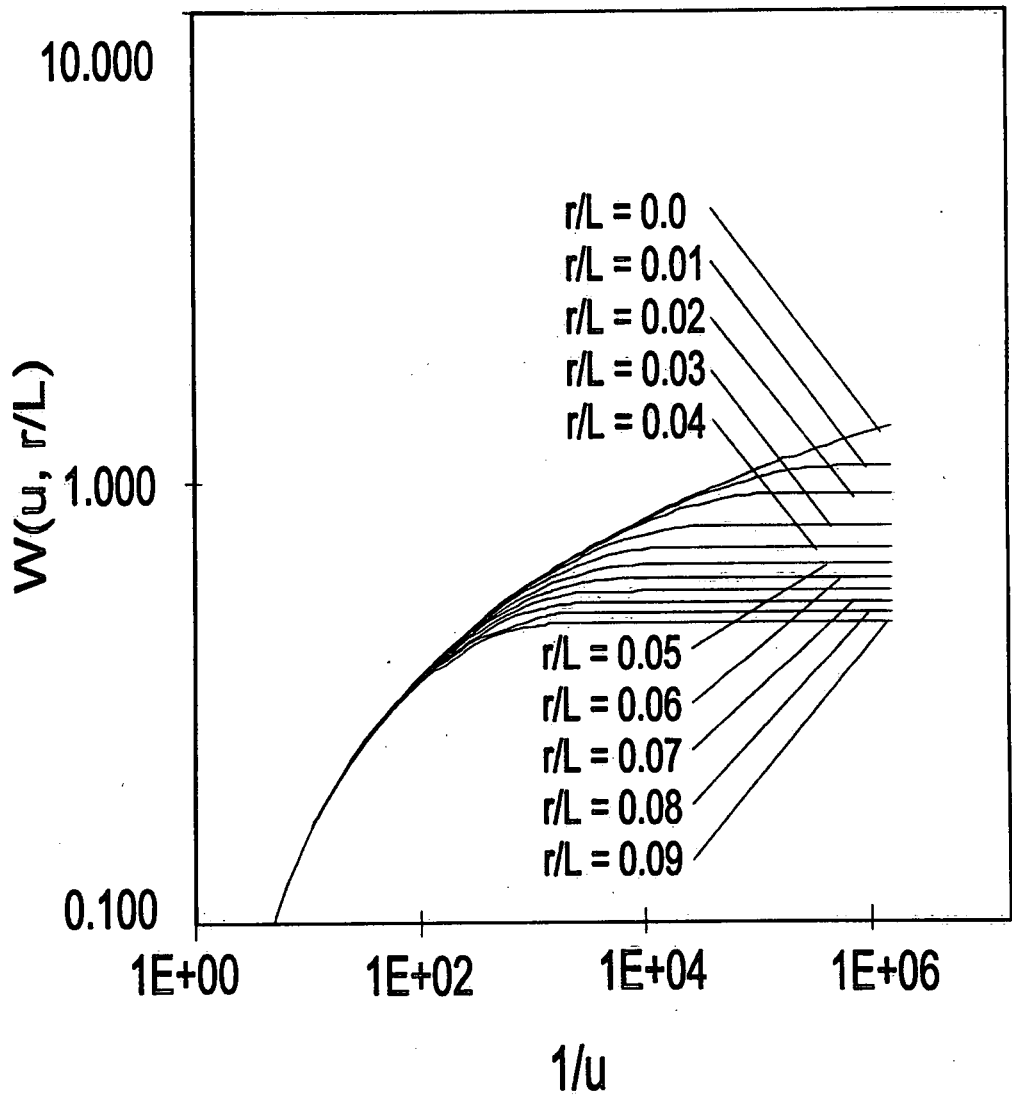


Figure 2.8 Walton (1962) type curves used for pumping test interpretation.

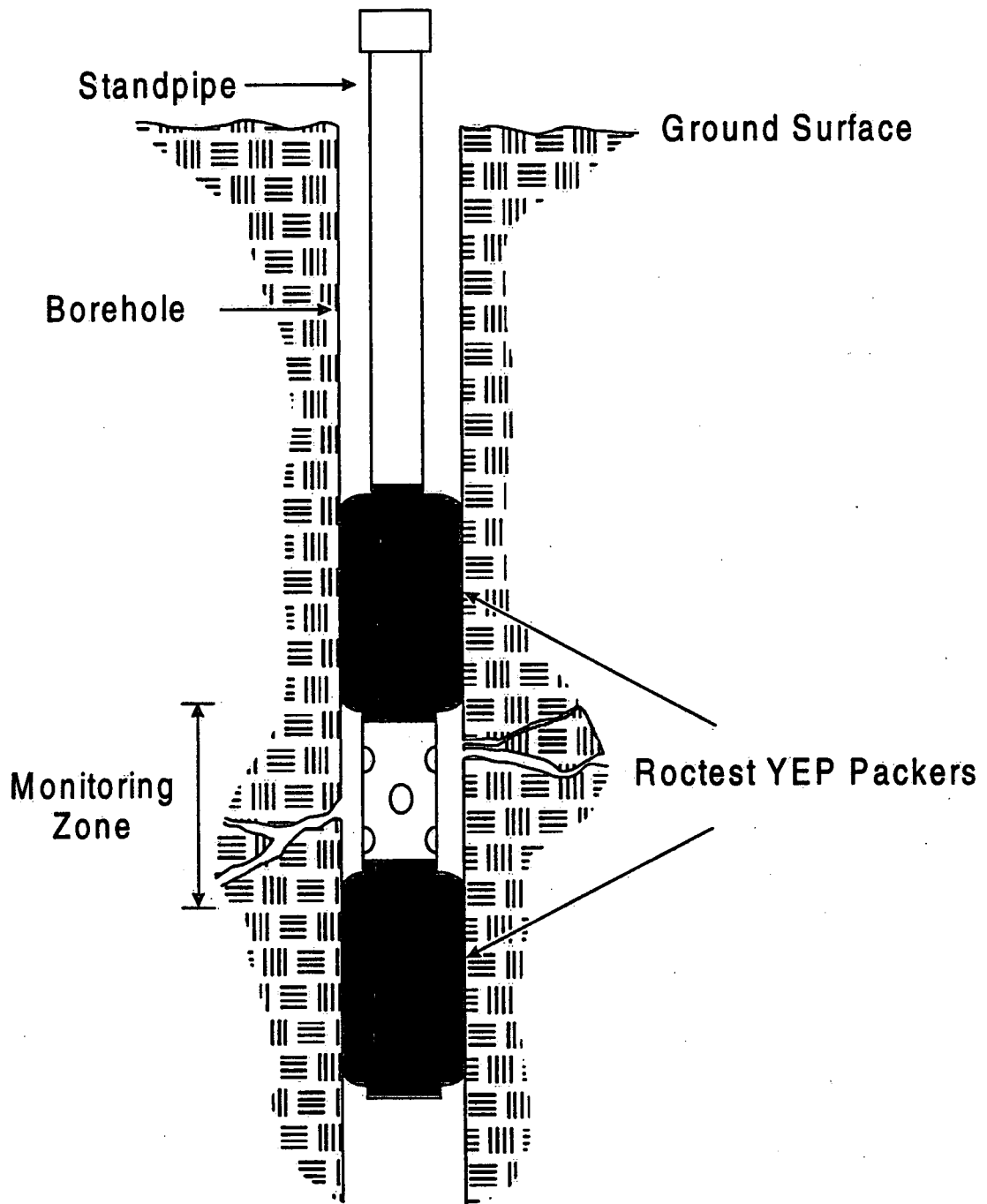


Figure 2.9 Temporary monitor set up.

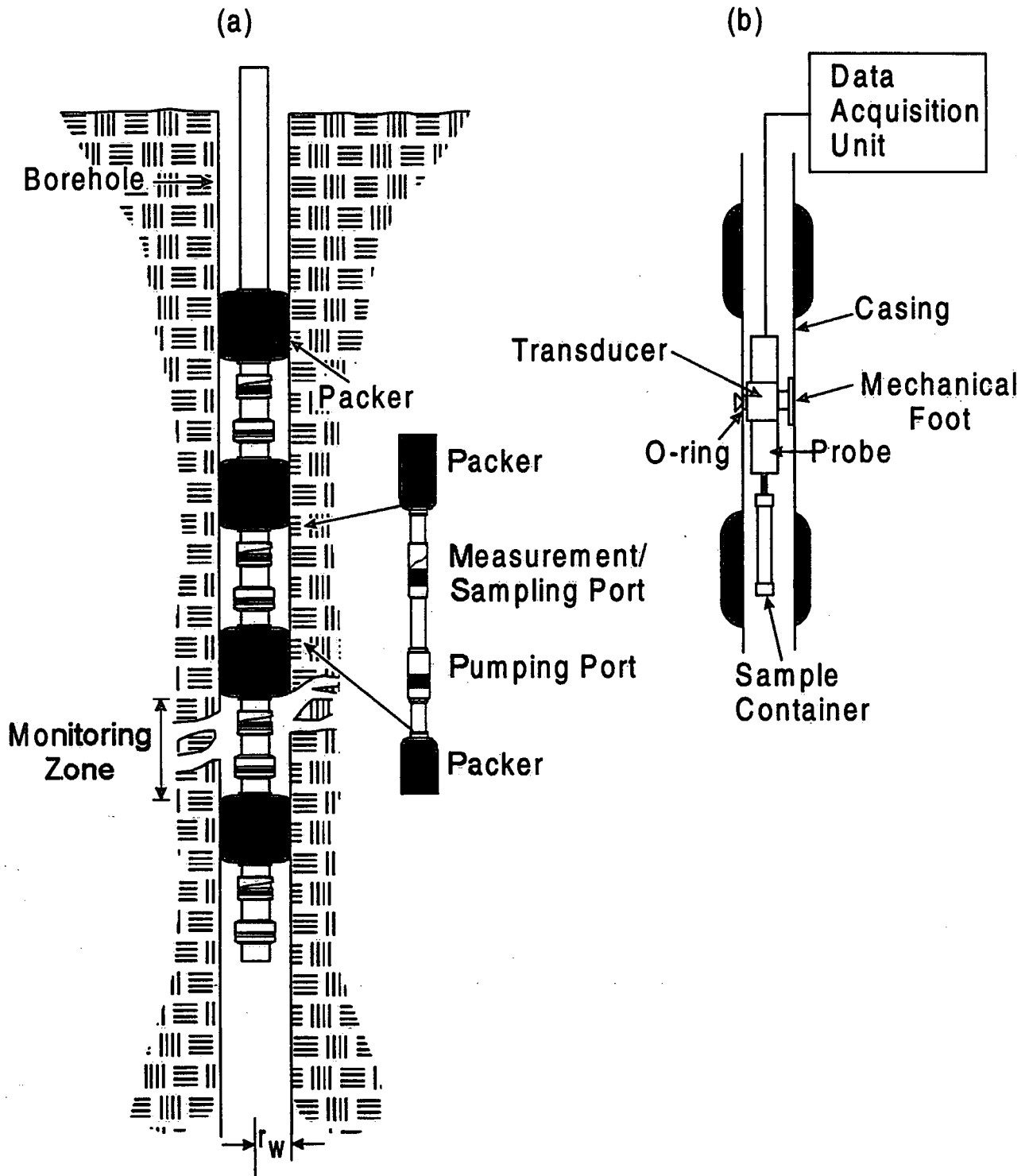


Figure 2.10 Westbay multilevel instrumentation: (a) components installed permanently in borehole and (b) data acquisition instrumentation including downhole probe used to measure pressure and obtain groundwater samples.

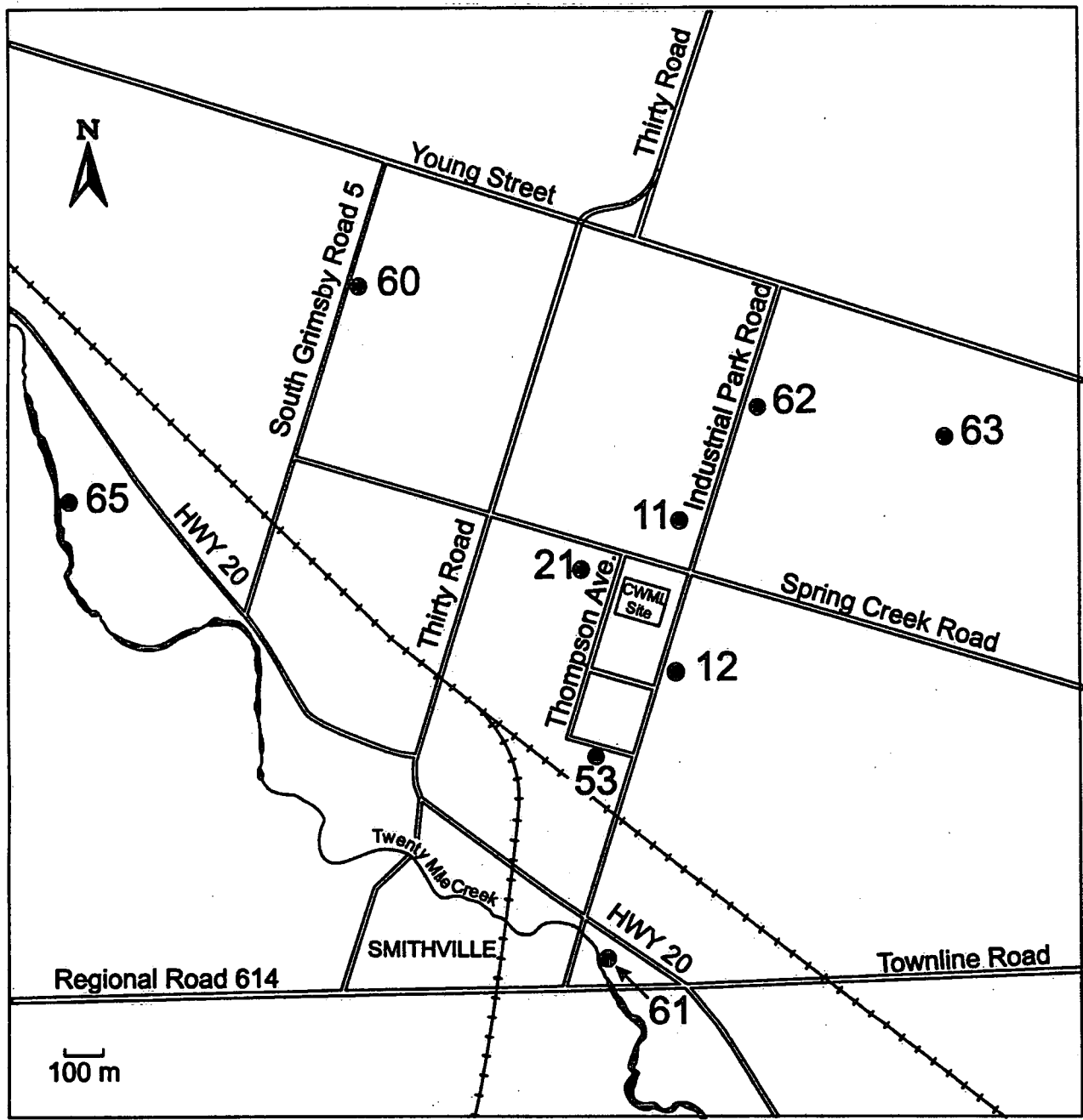


Figure 2.11 Map showing Westbay instrumented boreholes and multilevels used to obtain groundwater samples.

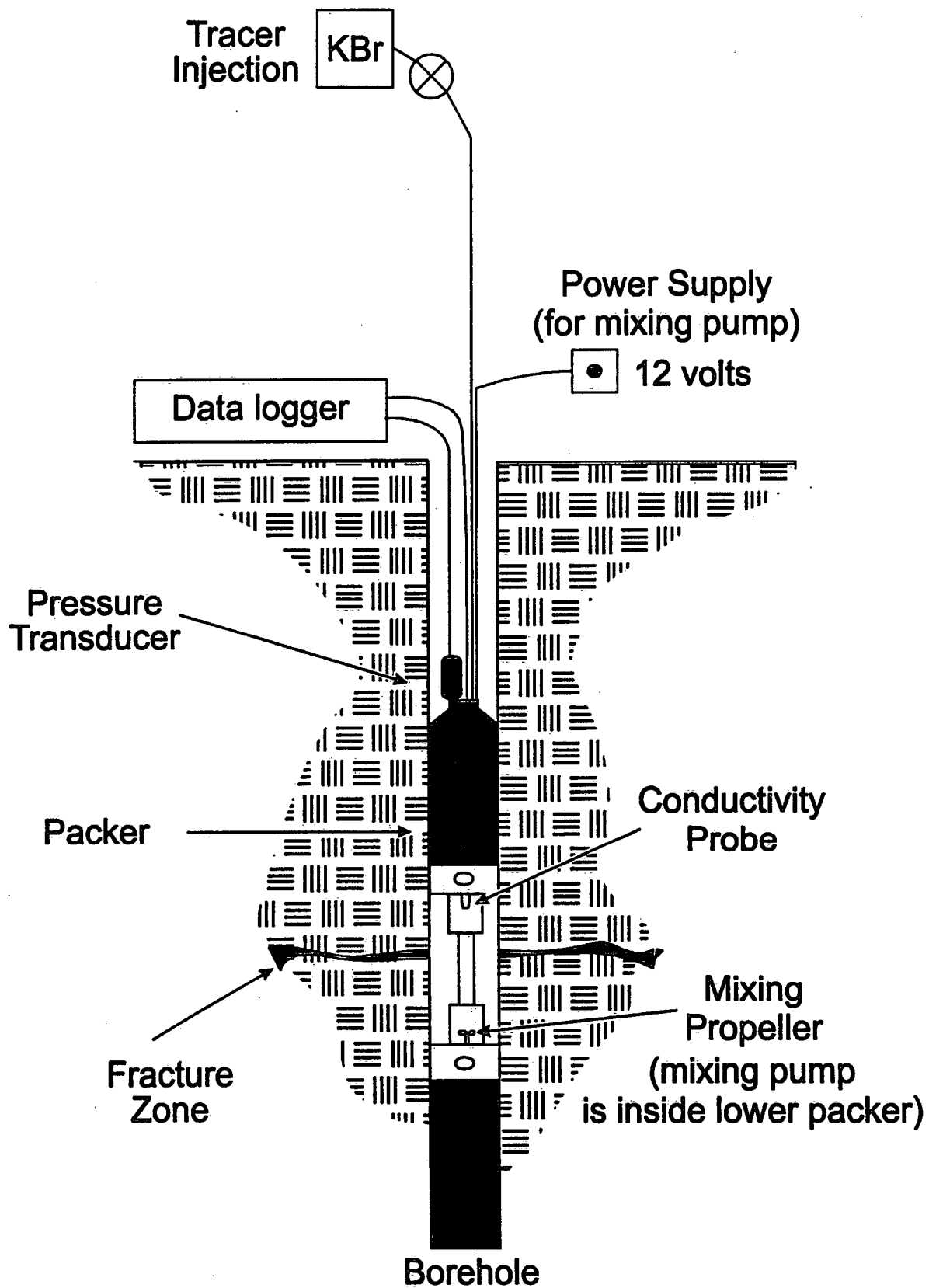


Figure 2.12 Schematic of apparatus used to conduct point dilution experiments.

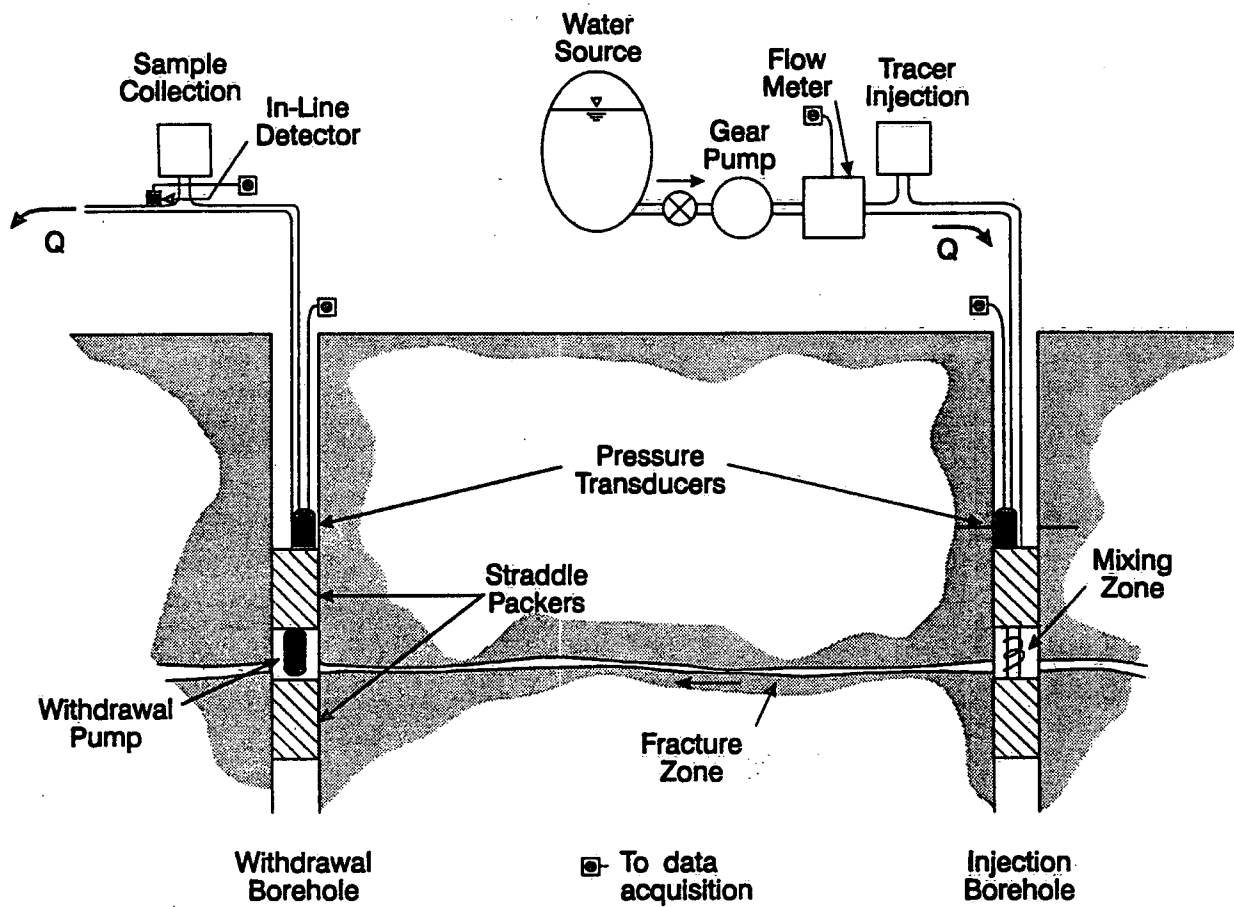


Figure 2.13 Schematic illustrating set-up for injection-withdrawal tracer experiments.

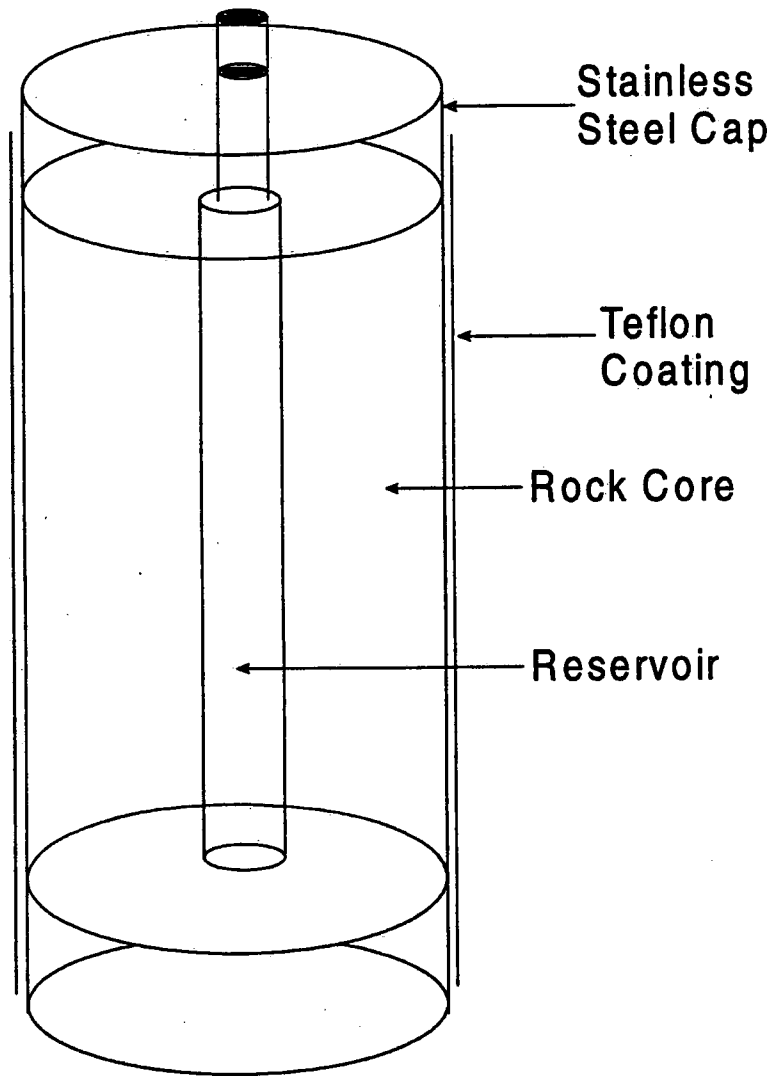


Figure 2.14 Schematic of diffusion cell.

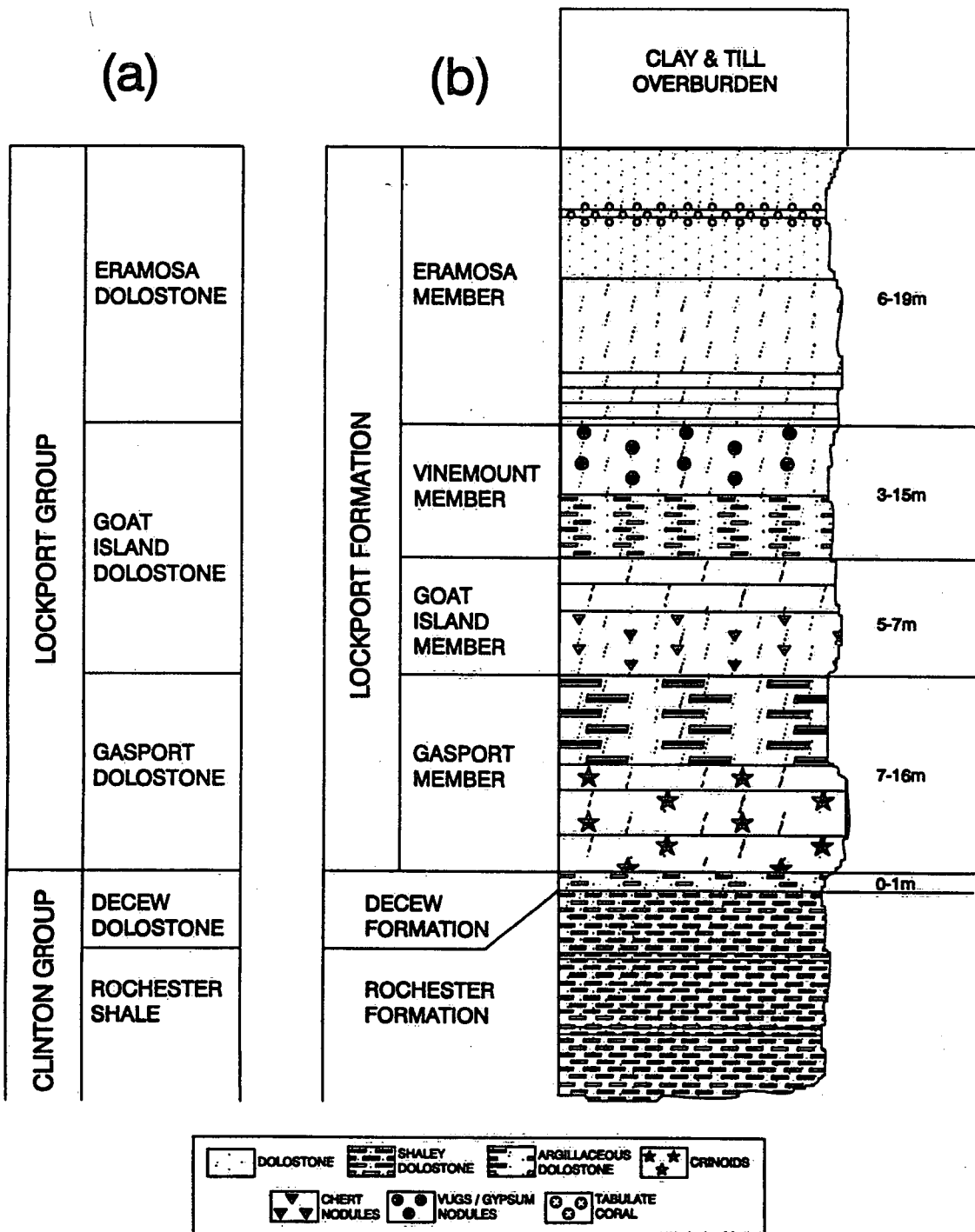


Figure 3.1 Lithology of study area: (a) Formal nomenclature (after Brett et. al, 1995) and (b) local nomenclature used in this study.

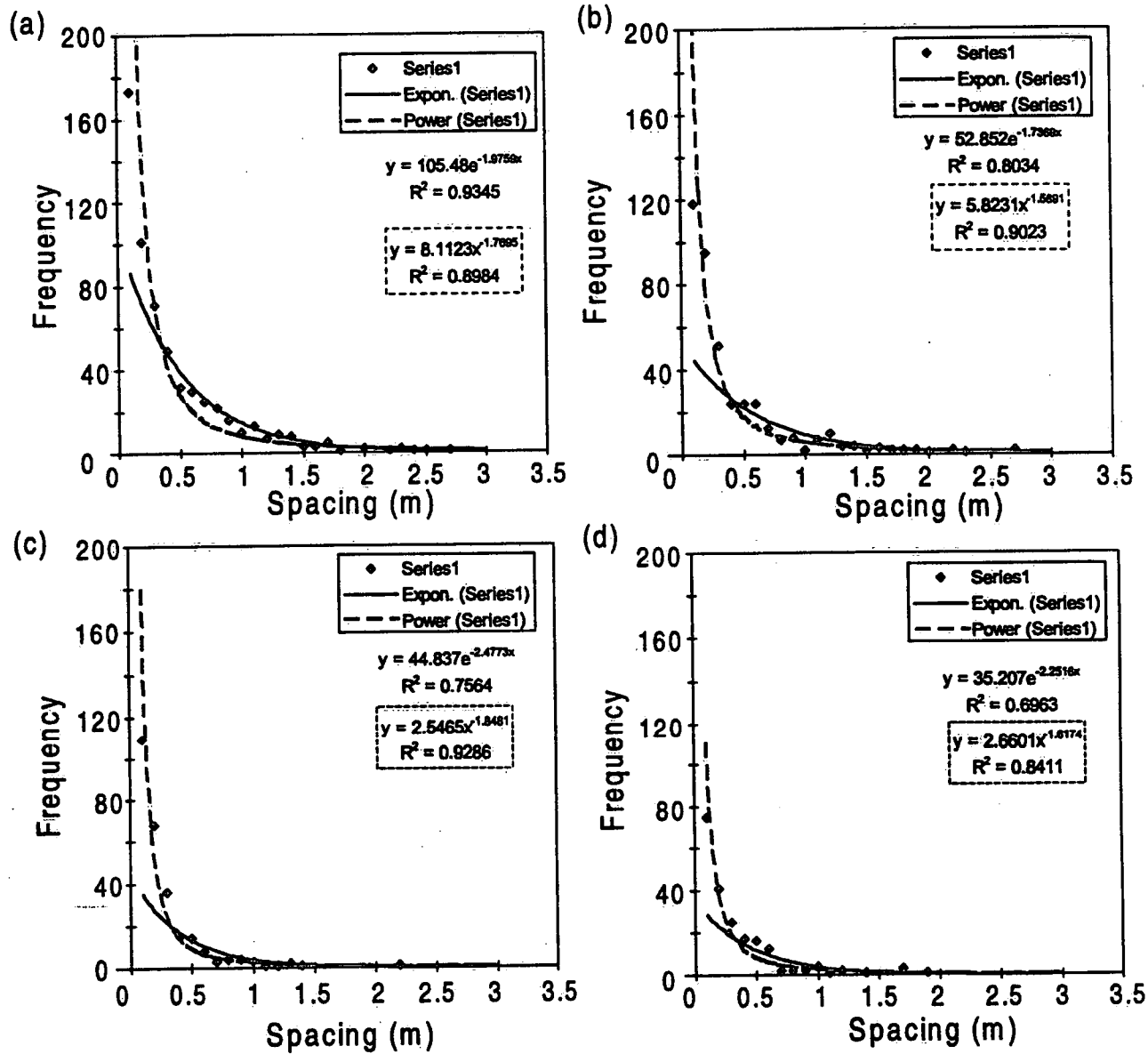


Figure 3.2 Bedding Plane fracture spacing distributions: (a) Eramosa, (b) Gasport, (c) Upper Vinemount and (d) Lower Vinemount.

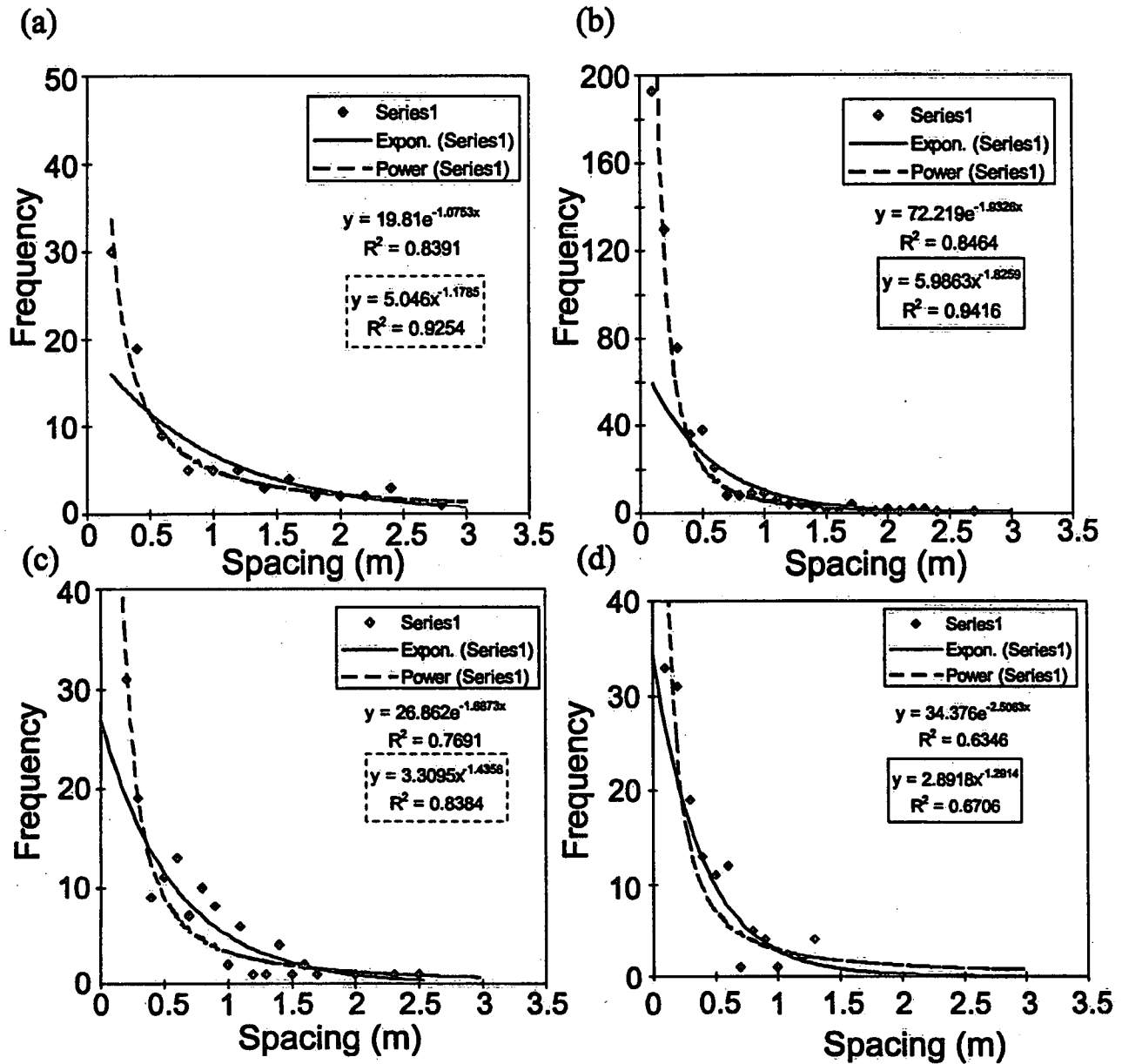


Figure 3.3. Bedding Plane fracture spacing distributions: (a) Goat Island, (b) Vinemount and Goat Island combined, (c) South Cluster Site fractures, and (d) North Cluster Site fractures.

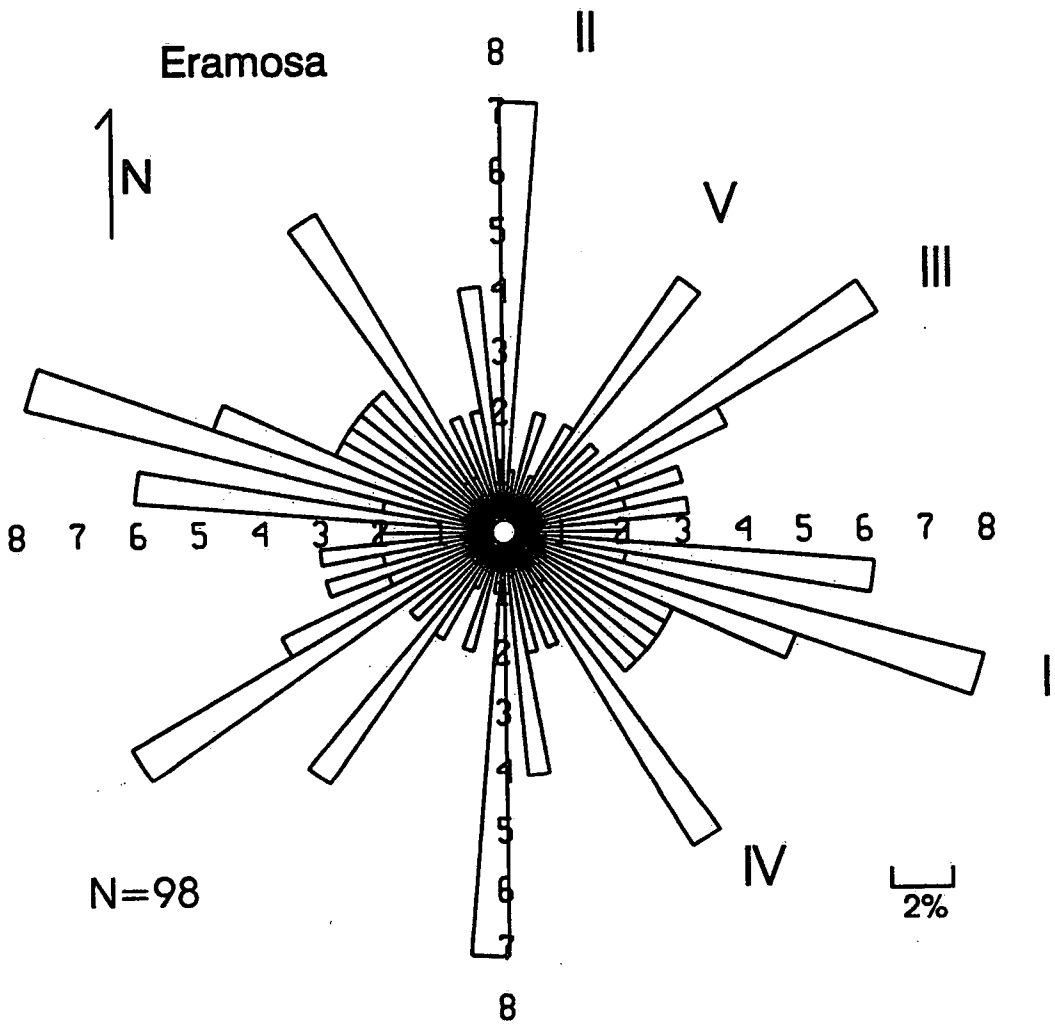


Figure 3.4 Rose diagram of orientations of vertical fractures in the Eramosa member.

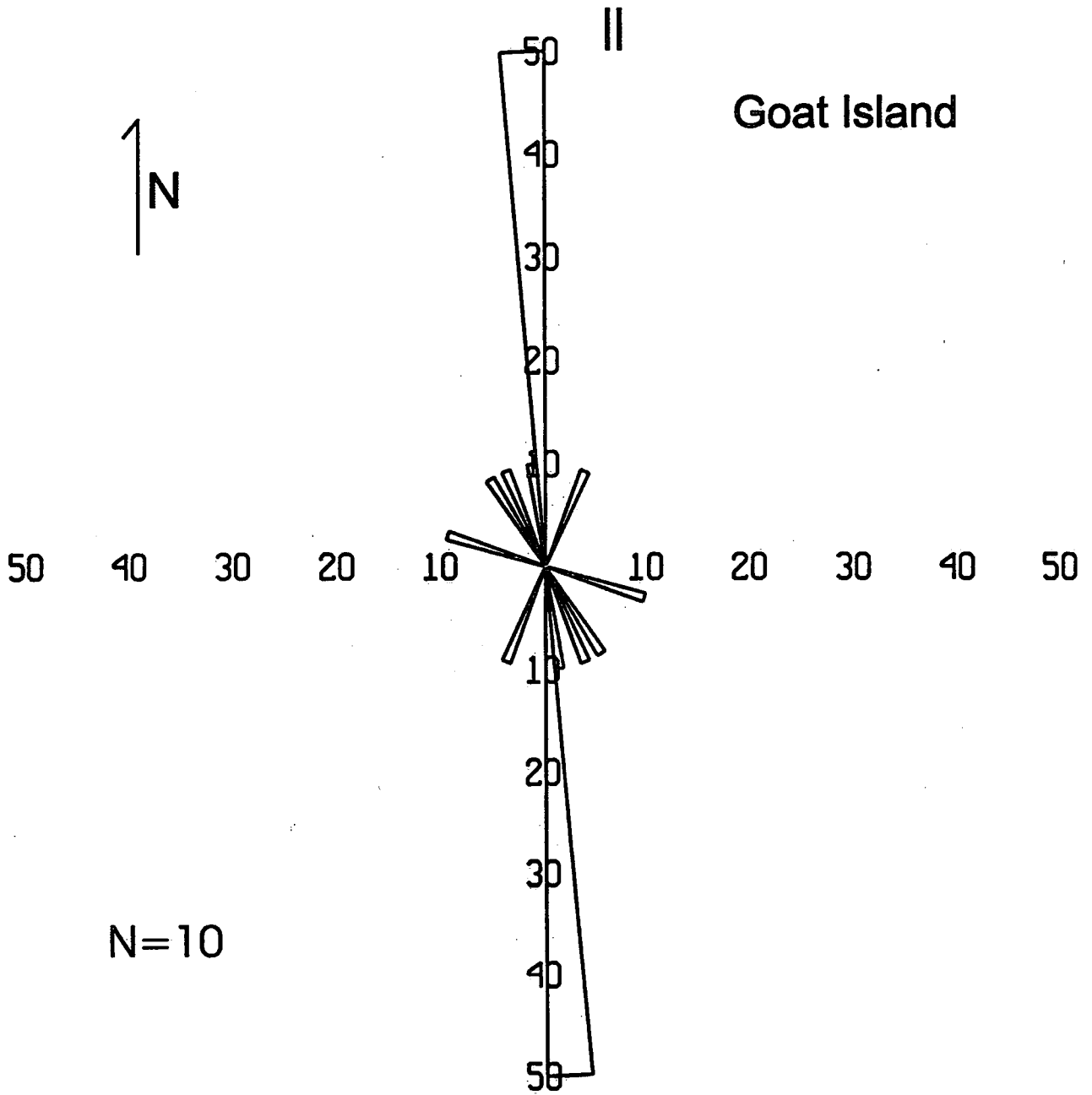


Figure 3.5 Rose diagram of vertical fracture orientations in the Goat Island member.

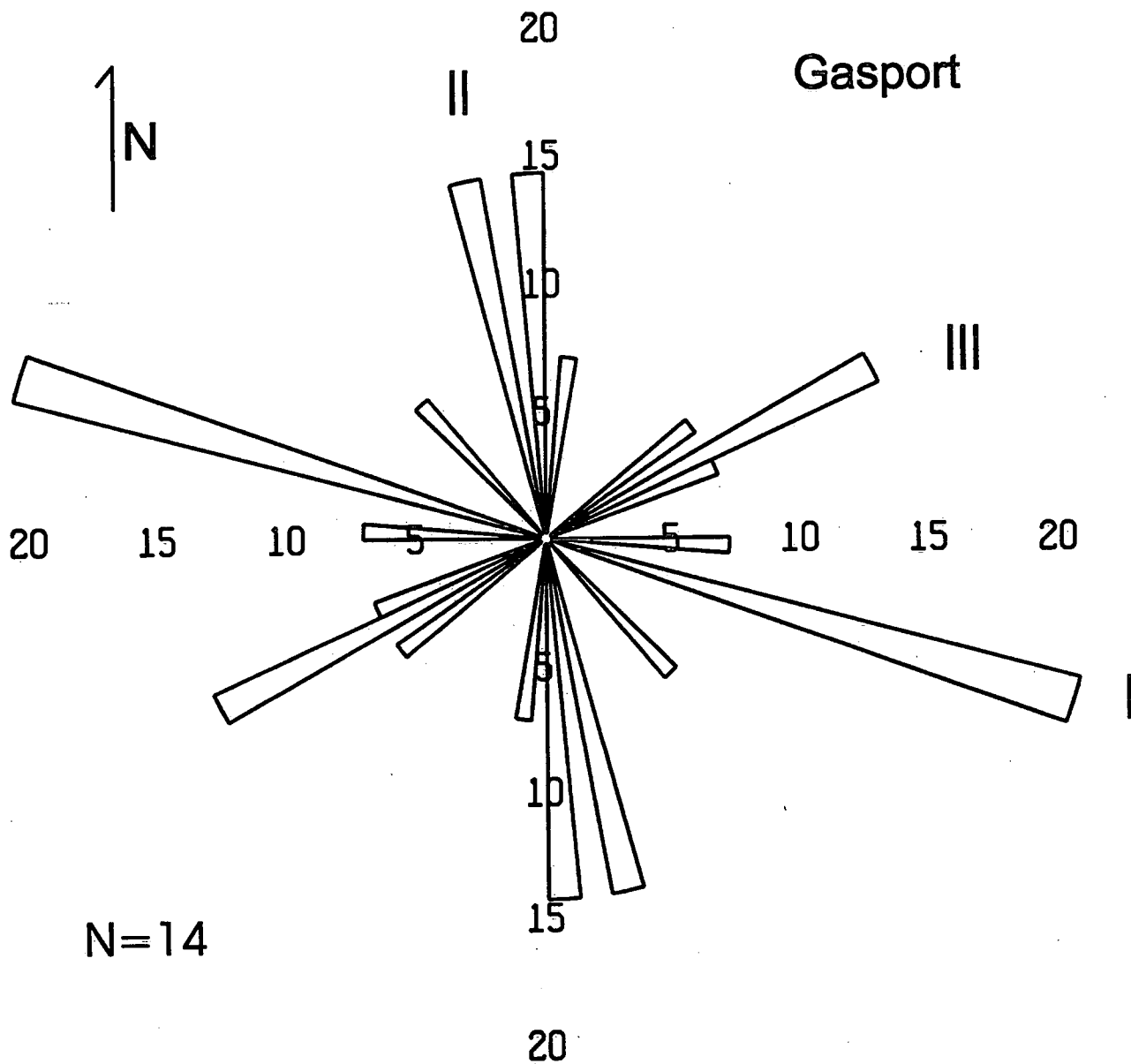


Figure 3.6 Rose diagram of orientations of vertical fractures in the Gasport member.

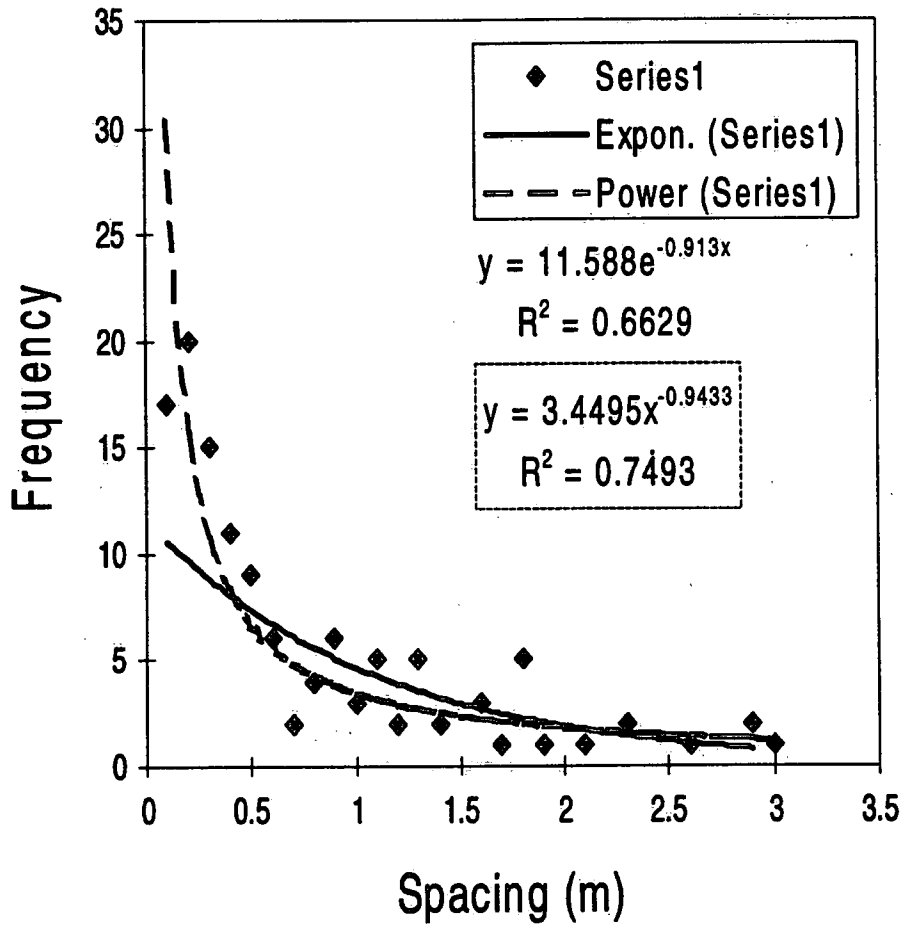


Figure 3.7 Distribution of vertical fracture spacings in the Eramosa member.

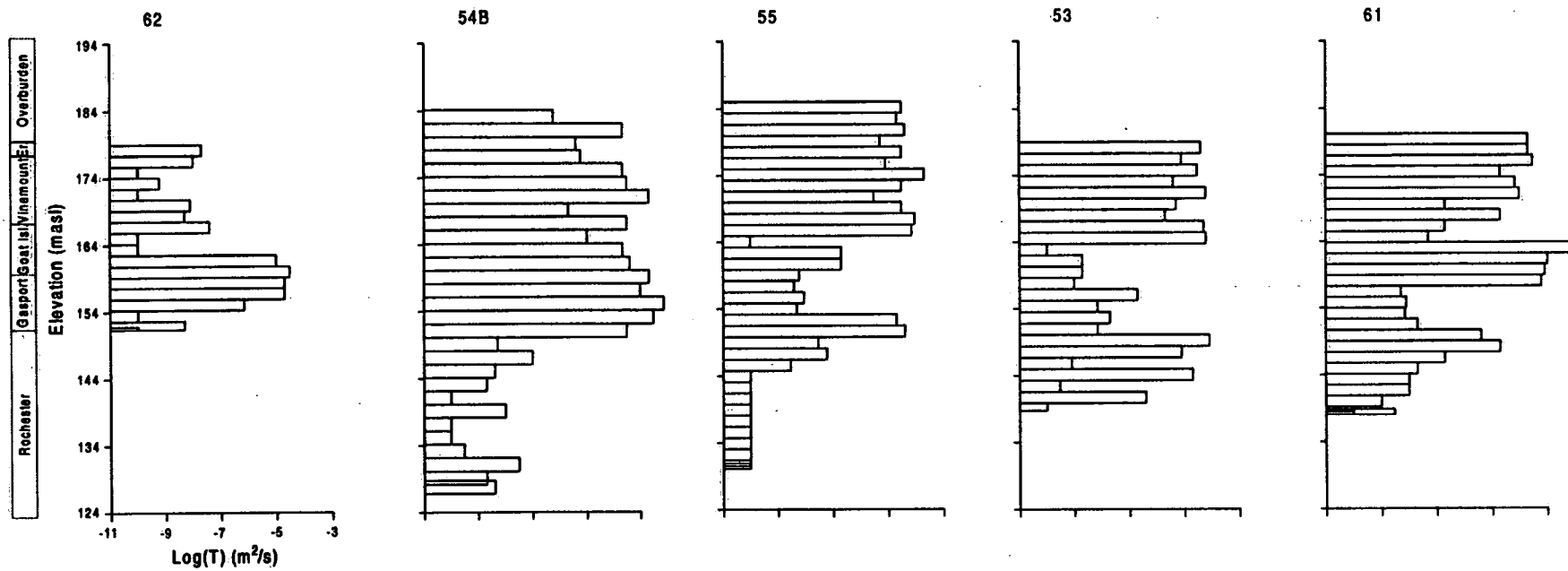


Figure 3.8 Vertical transmissivity results for 5 boreholes using a 2-m test interval. Note that the profiles are arranged to form a cross section roughly N-S from 62 -61.

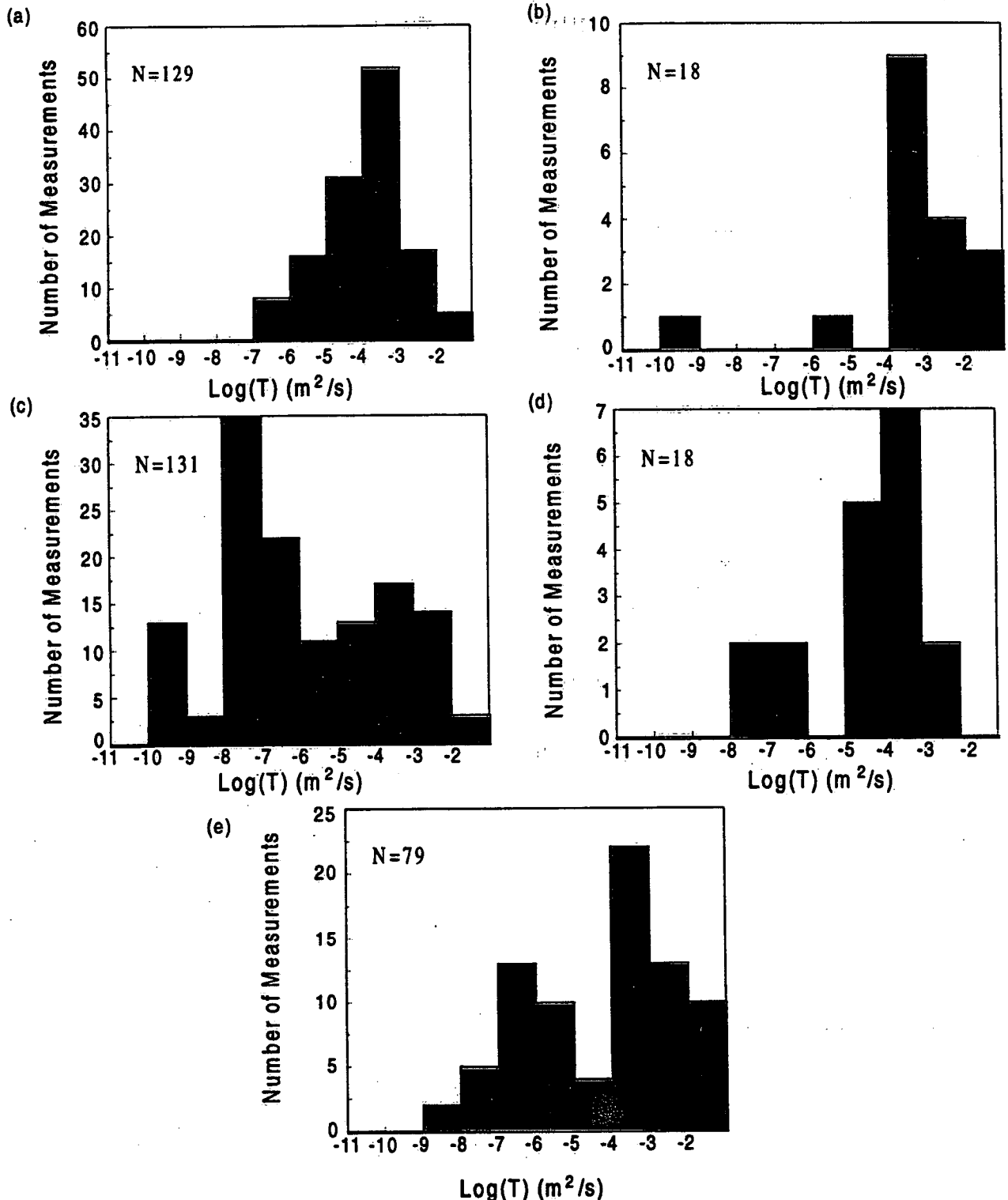


Figure 3.9 Distributions of measured transmissivity using constant-head injection tests with a 2-m test interval: (a) Eramosa member, (b) Zones containing Eramosa/Goat Island contacts (c) Goat Island member (including Vinemount), (d) Zones containing Goat Island/ Gasport contacts and (e) Gasport member.

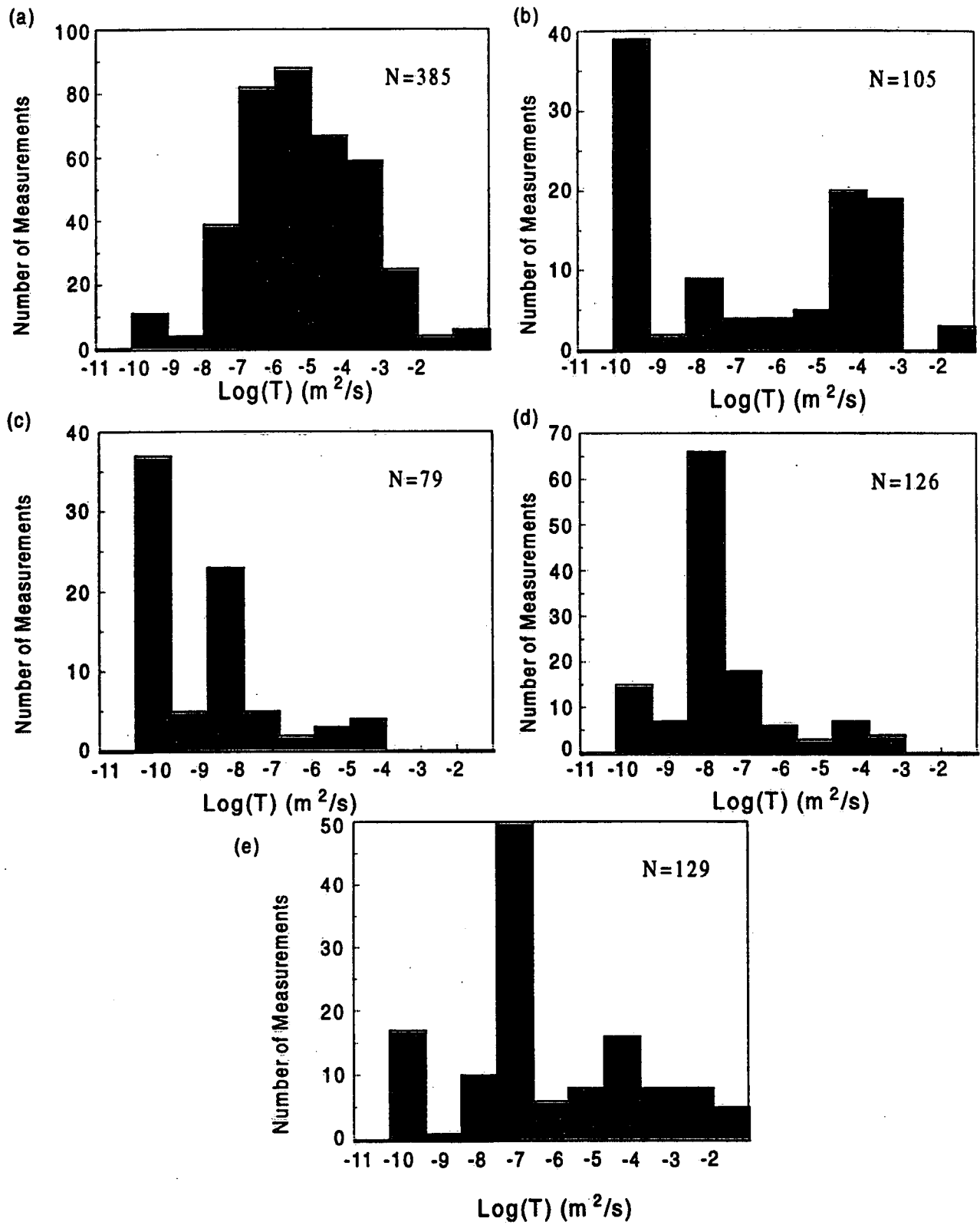


Figure 3.10 Distributions of measured transmissivity using constant-head injection tests with a 0.5-m test interval: (a) Eramosa member, (b) Upper Vinemount unit (c) Lower Vinemount unit, (d) Goat Island and (e) Gasport member.

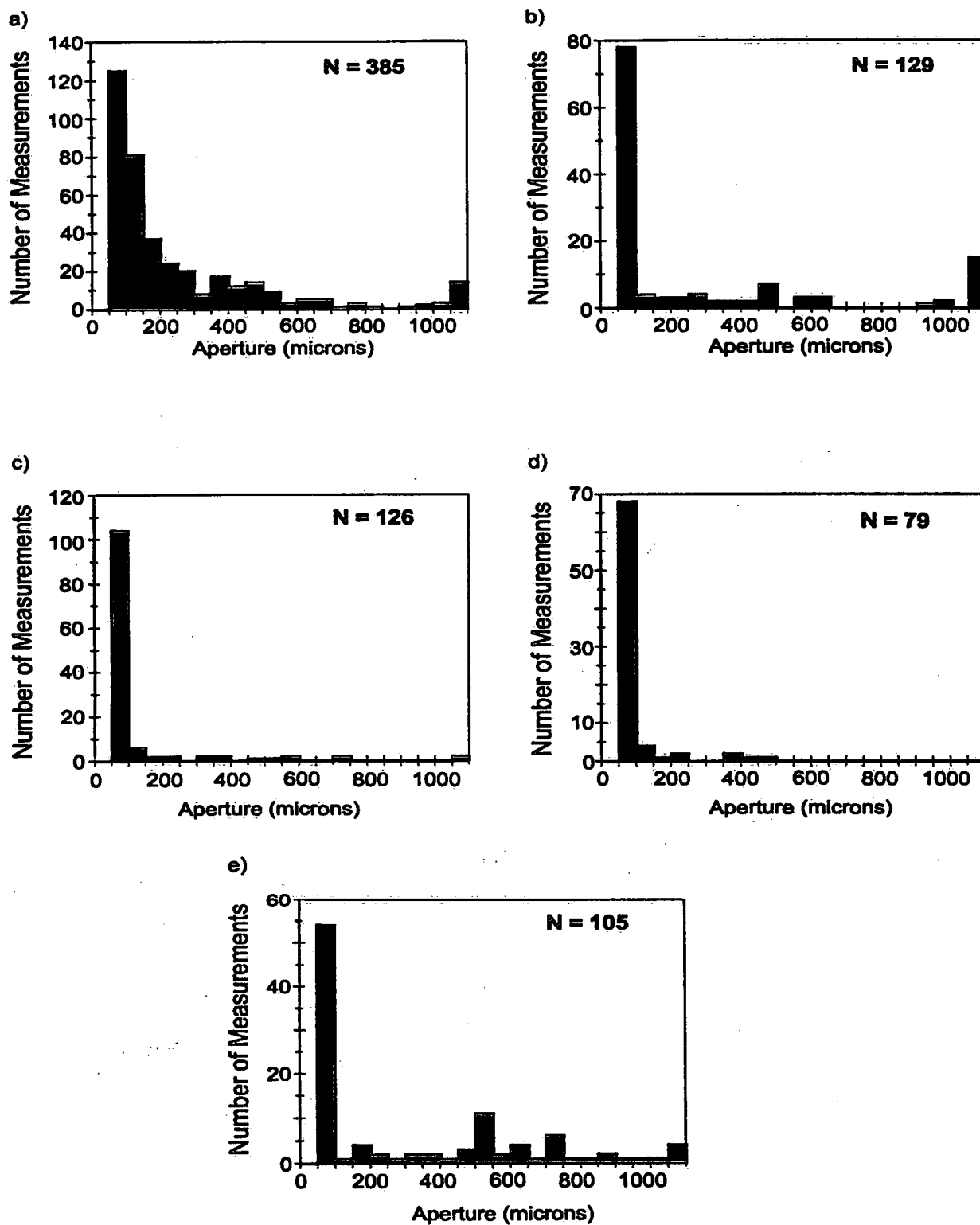


Figure 3.11 Distributions of calculated hydraulic apertures ($2b_{eq}$) using constant-head injection tests with a 0.5-m test interval: (a) Eramosa member, (b) Upper Vinemount unit (c) Lower Vinemount unit, (d) Goat Island and (e) Gasport member.

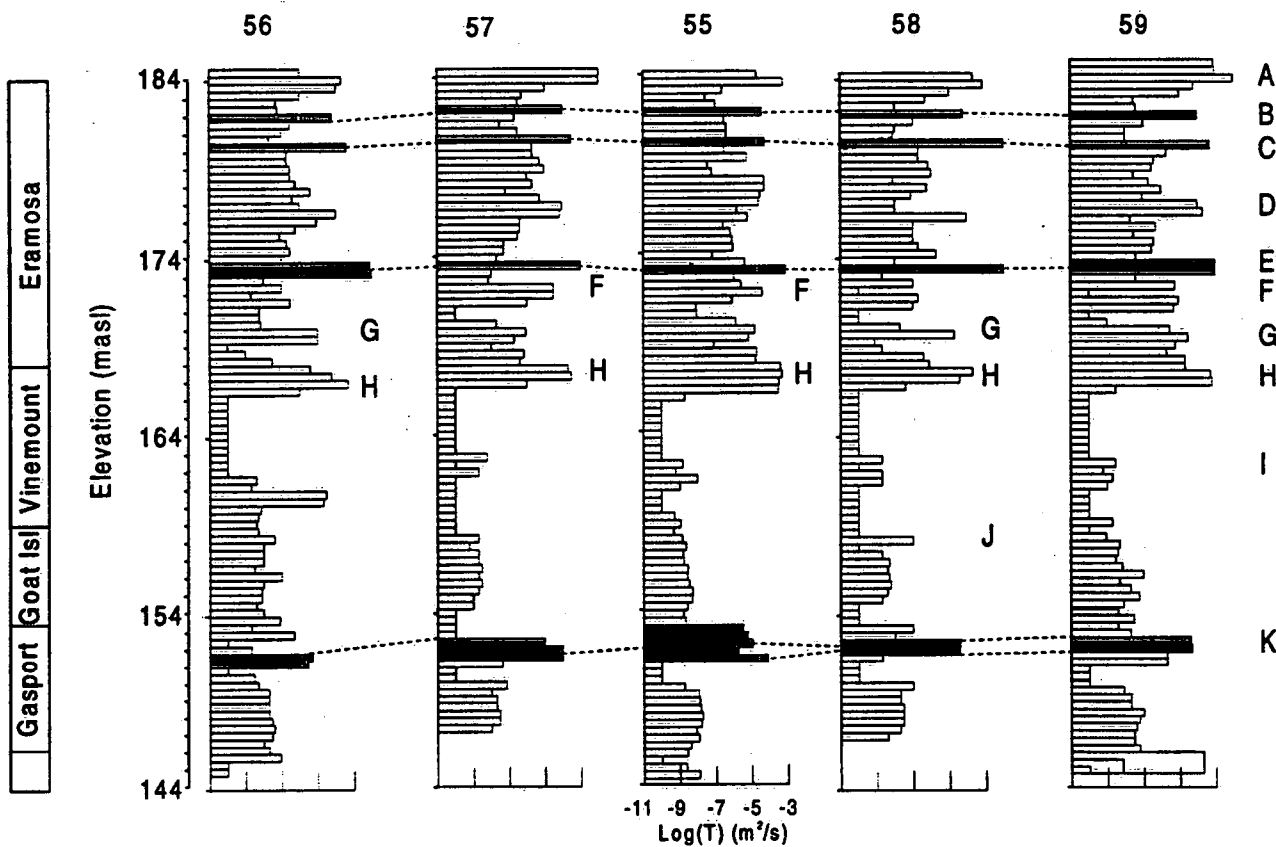


Figure 3.12 Vertical transmissivity profiles of south cluster boreholes determined using constant head injection tests with a 0.5-m test interval.

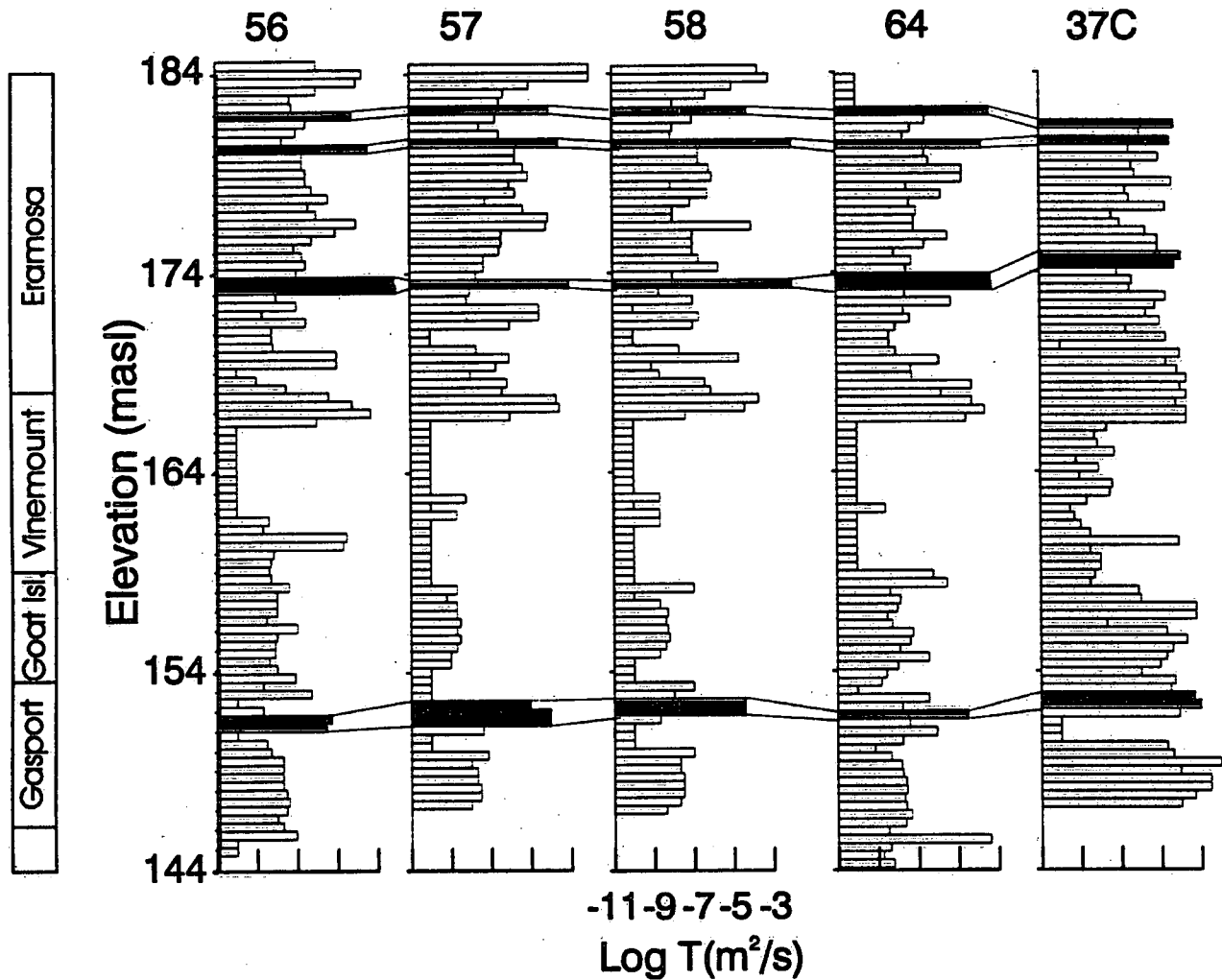


Figure 3.13 Vertical transmissivity profiles of several boreholes within an area of about 100 m² determined using constant head injection tests with a 0.5-m test interval and illustrating possible correlation of permeable features.

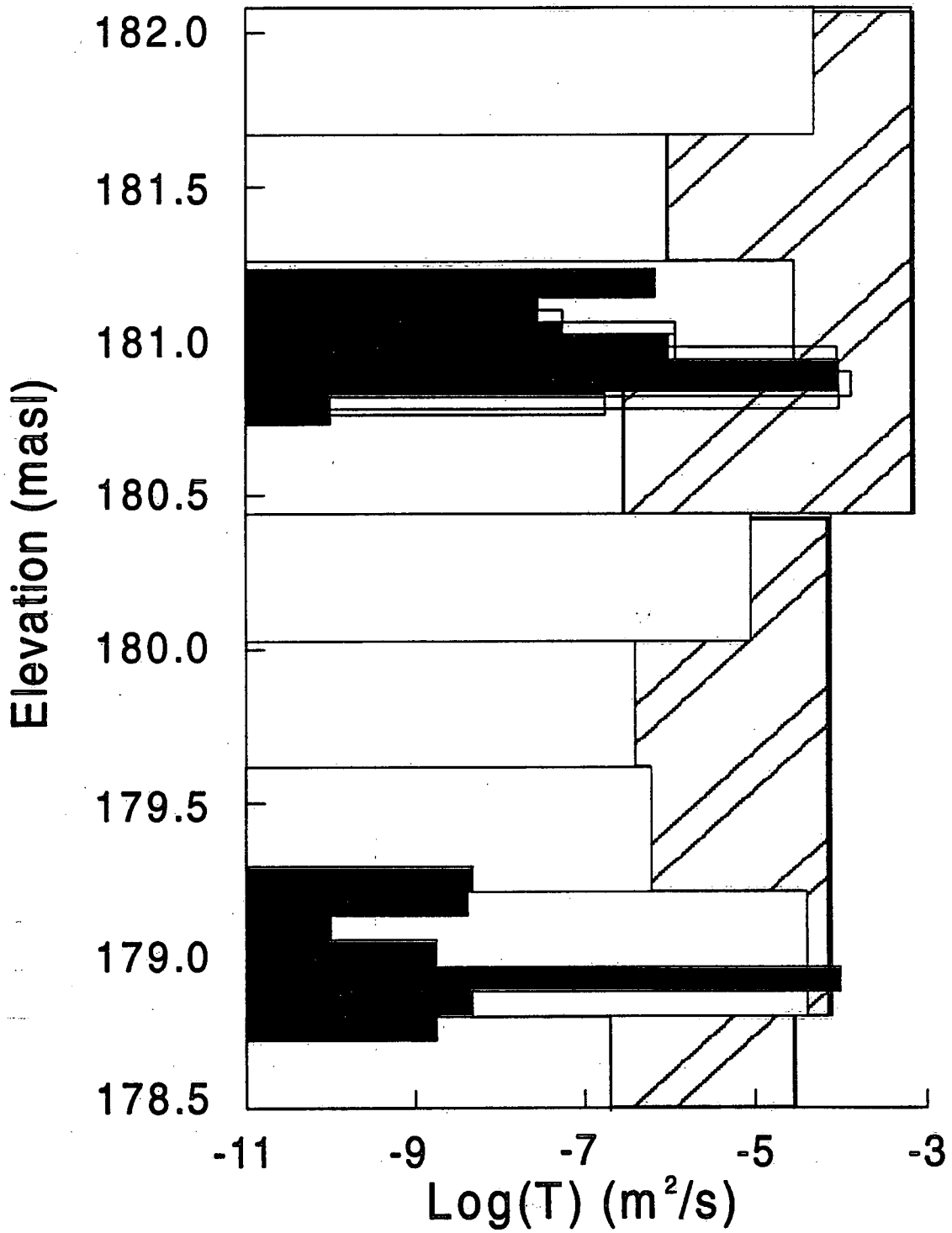


Figure 3.14 Comparison of T results for 2.0-m, 0.5-m and 0.1-m test intervals.

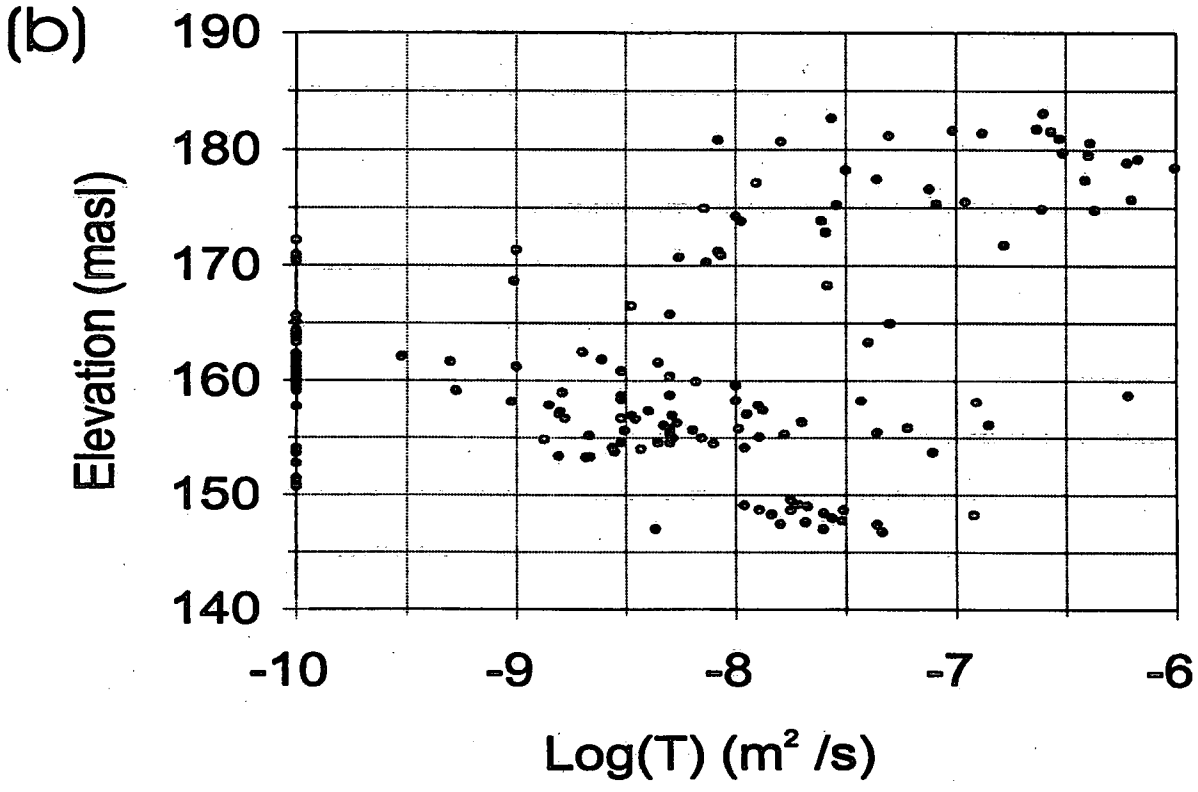
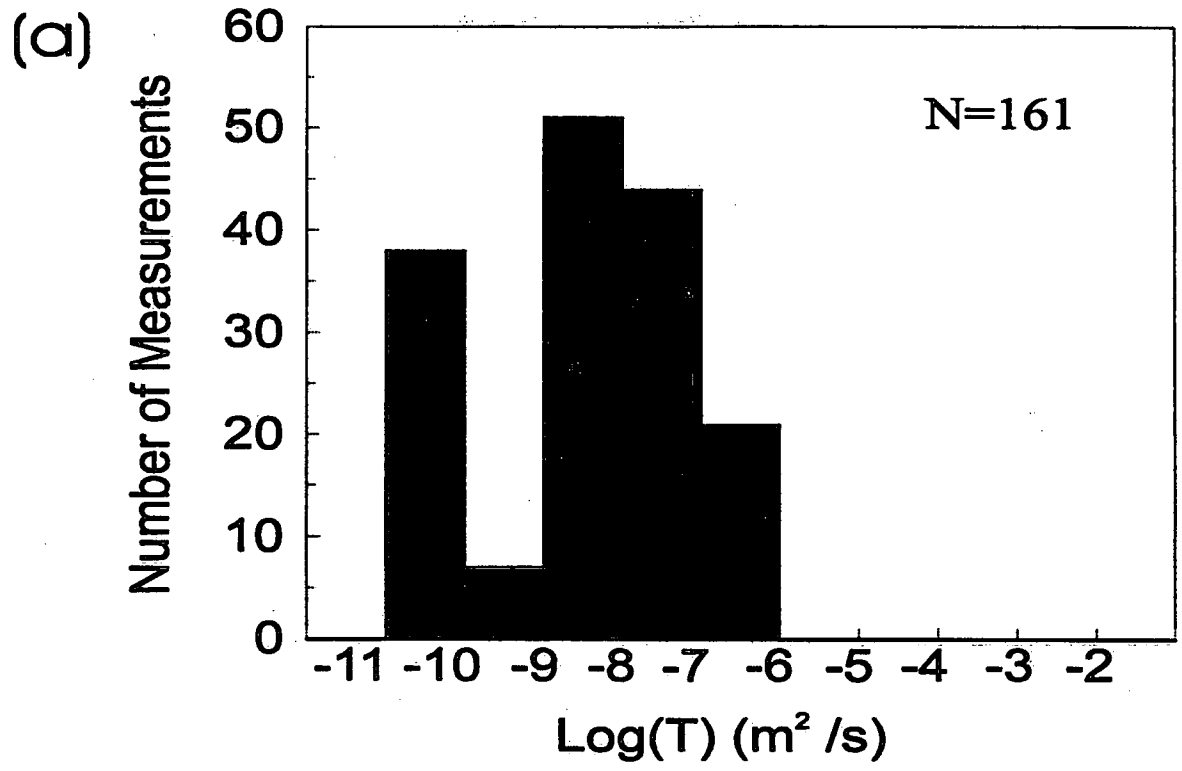


Figure 3.15 (a) Distributions of measured matrix transmissivities and (b) all measurements of matrix transmissivity relative to elevation.

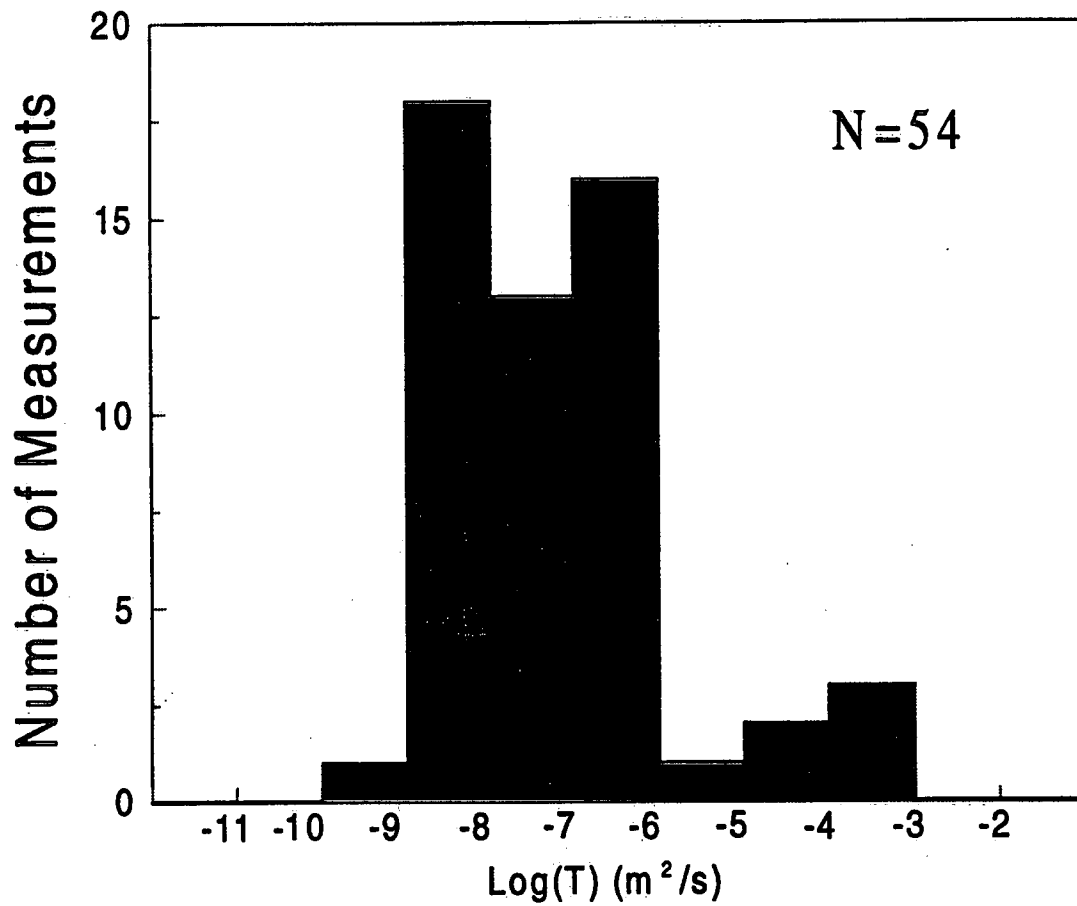


Figure 3.16 Distribution of measured transmissivities where only vertical fractures were identified in the core record.

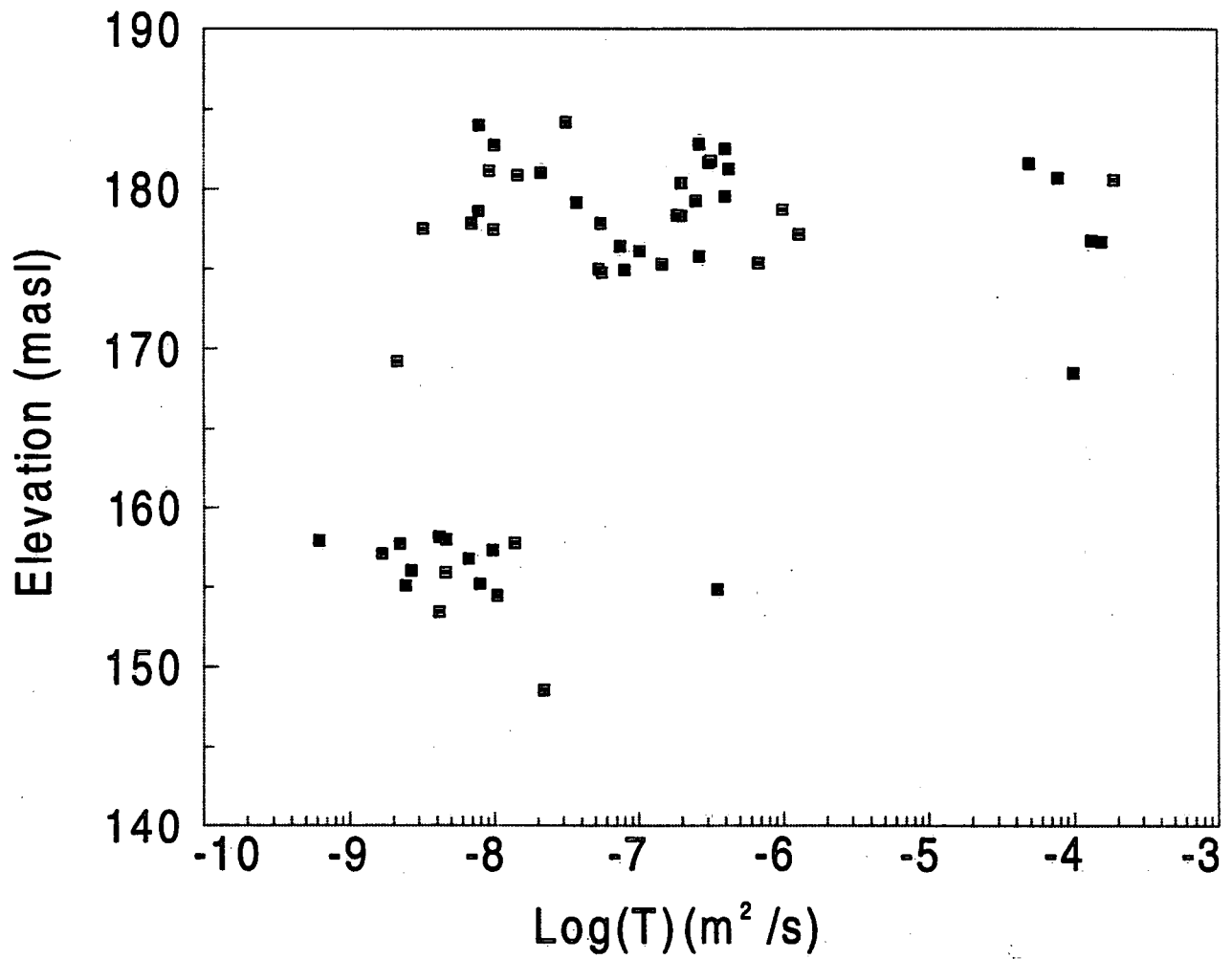


Figure 3.17 Transmissivity measurements in zones where only vertical fractures have been identified in the core record.

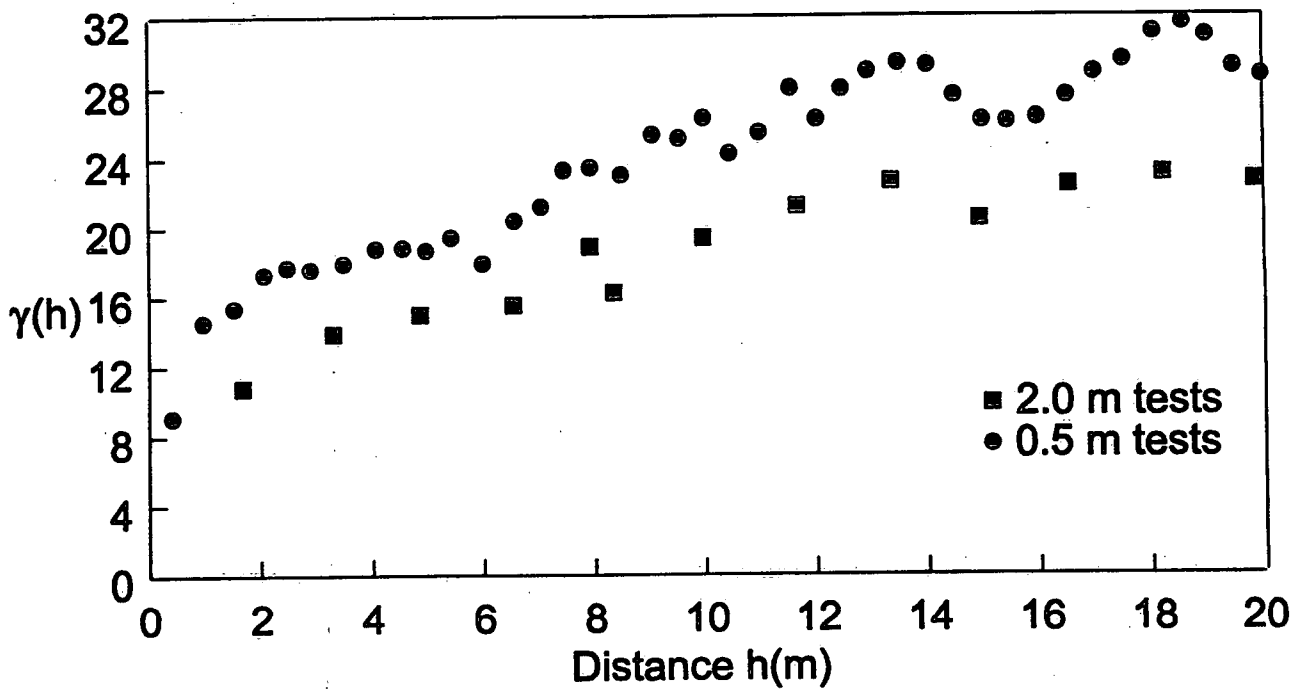


Figure 3.18 Variogram of transmissivity measurements using data from both 2.0-m and 0.5-m hydraulic tests.

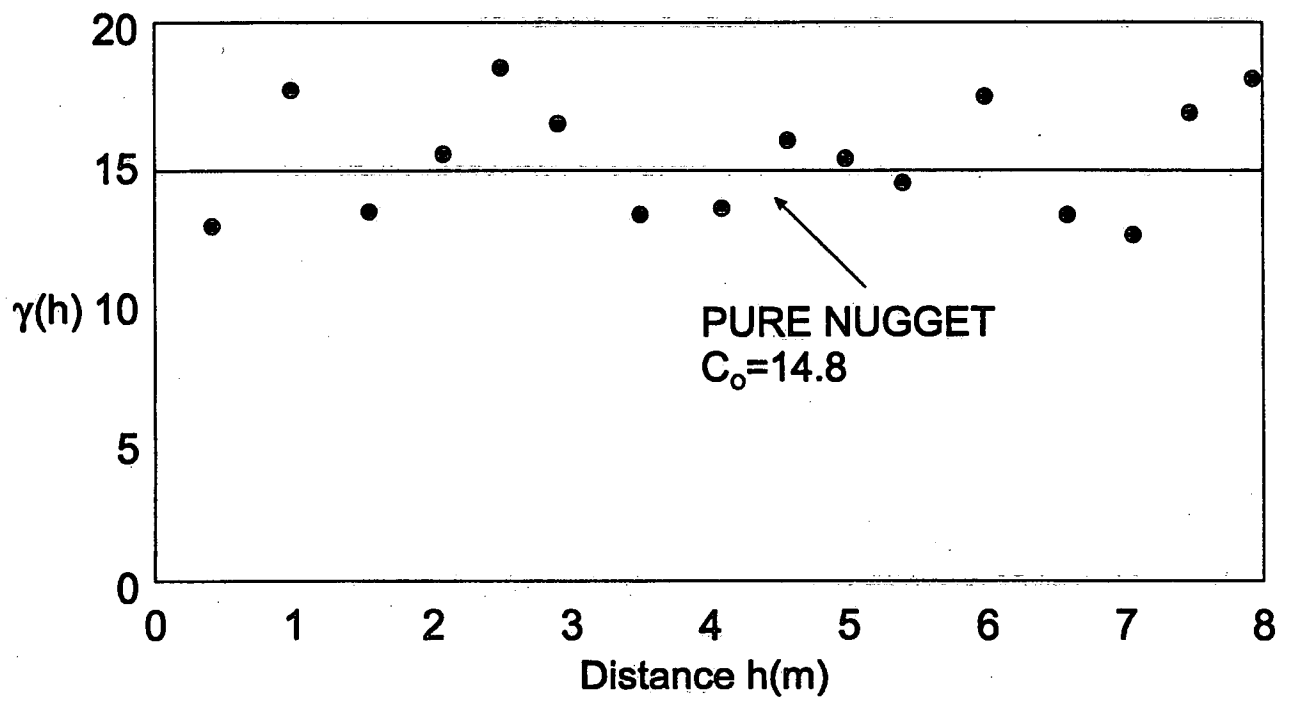


Figure 3.19 Variogram of Eramosa T measurements from south cluster site boreholes.

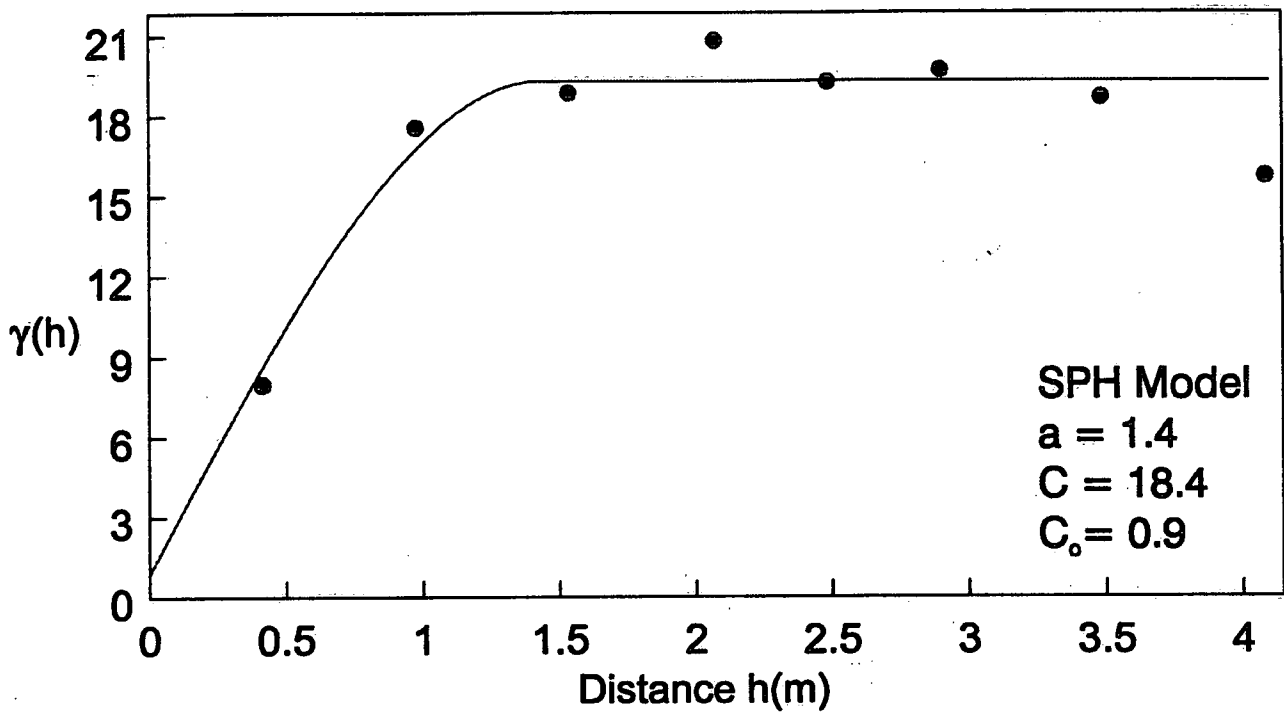


Figure 3.20 Variogram of Gasport T measurements from south cluster site boreholes.

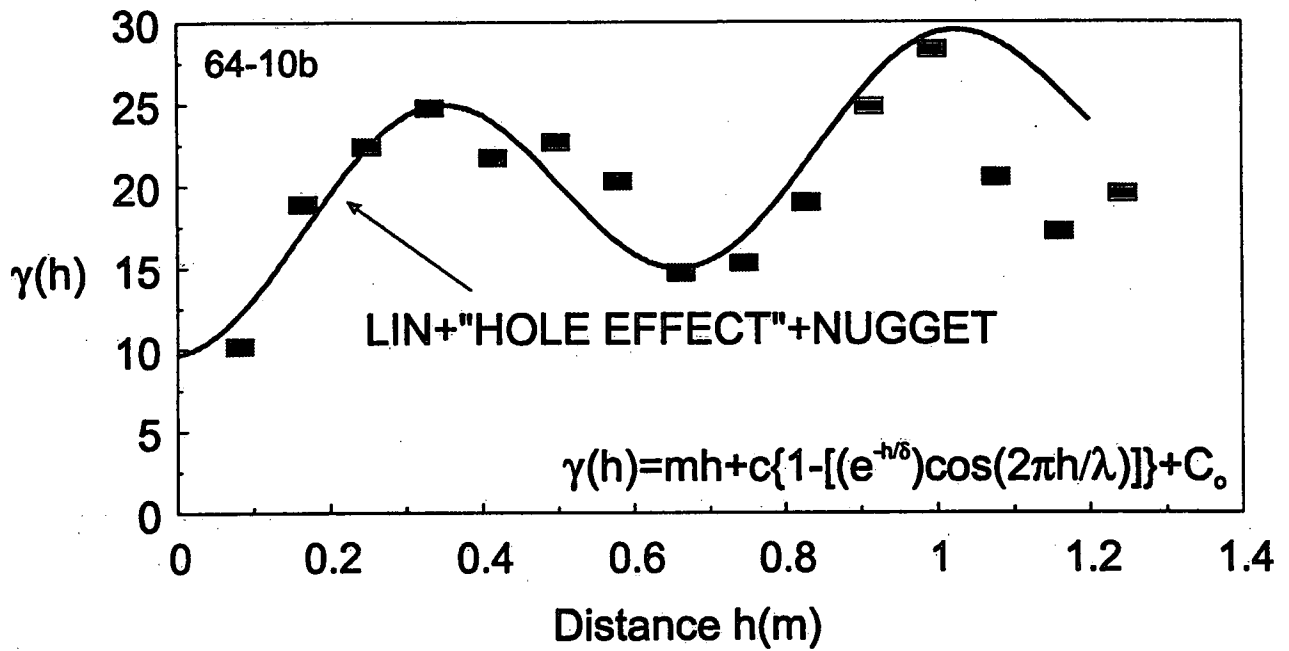


Figure 3.21 Variogram of 0-1m \bar{T} measurements over a continuous 3.4 m section of Eramosa dolostone.

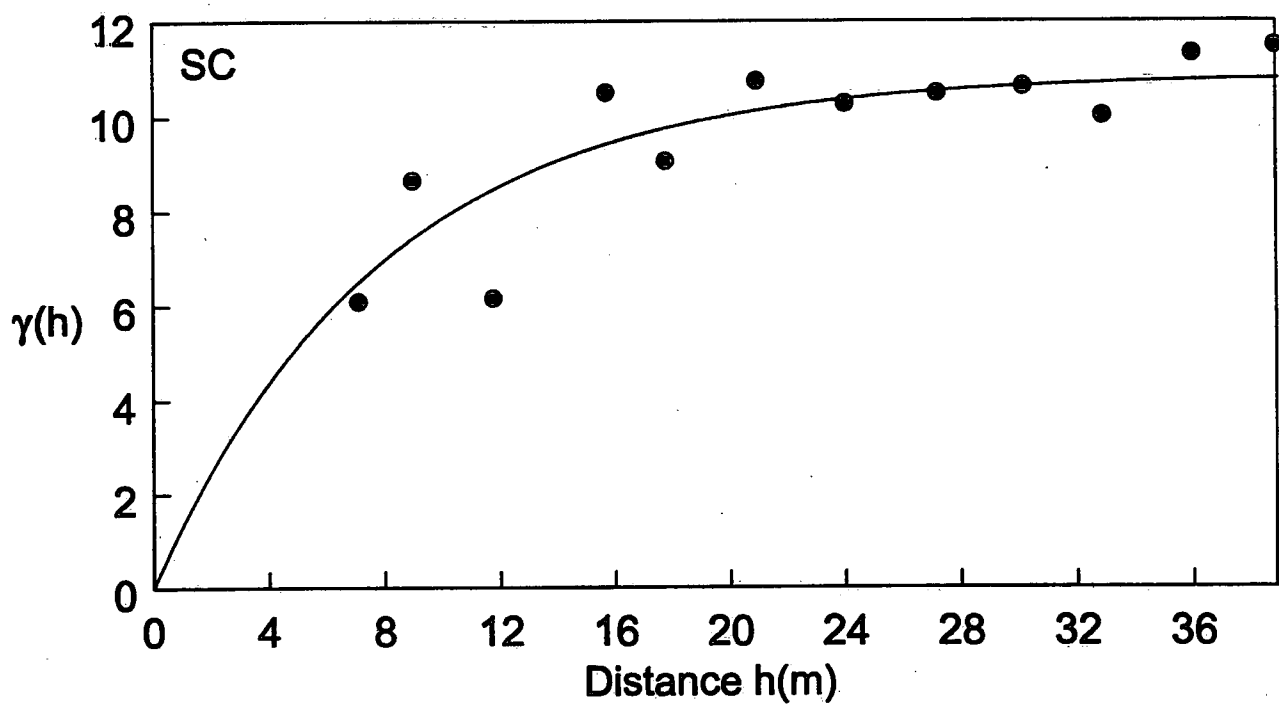


Figure 3.22 Variogram of T measurements in south cluster site. In this case, correlation is examined horizontally at all depths.

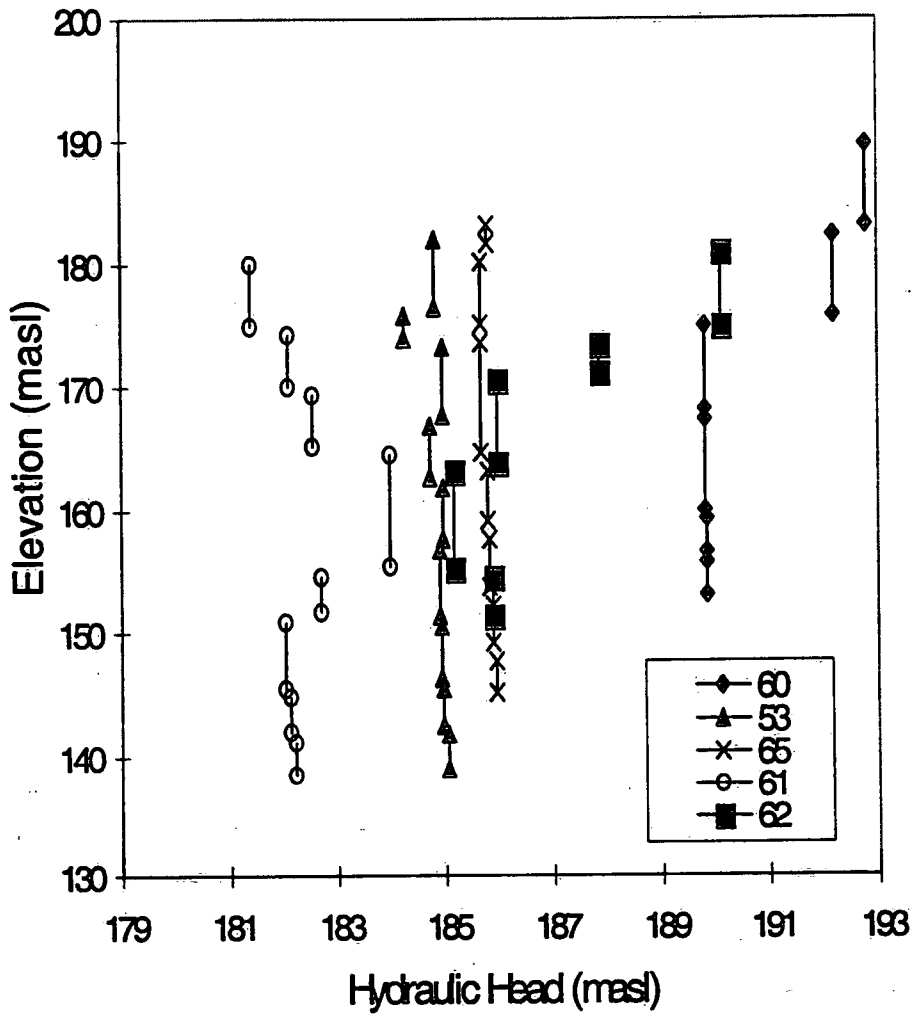


Figure 3.24 Spring hydraulic head distribution in boreholes 60, 65, 53, 61 & 62.

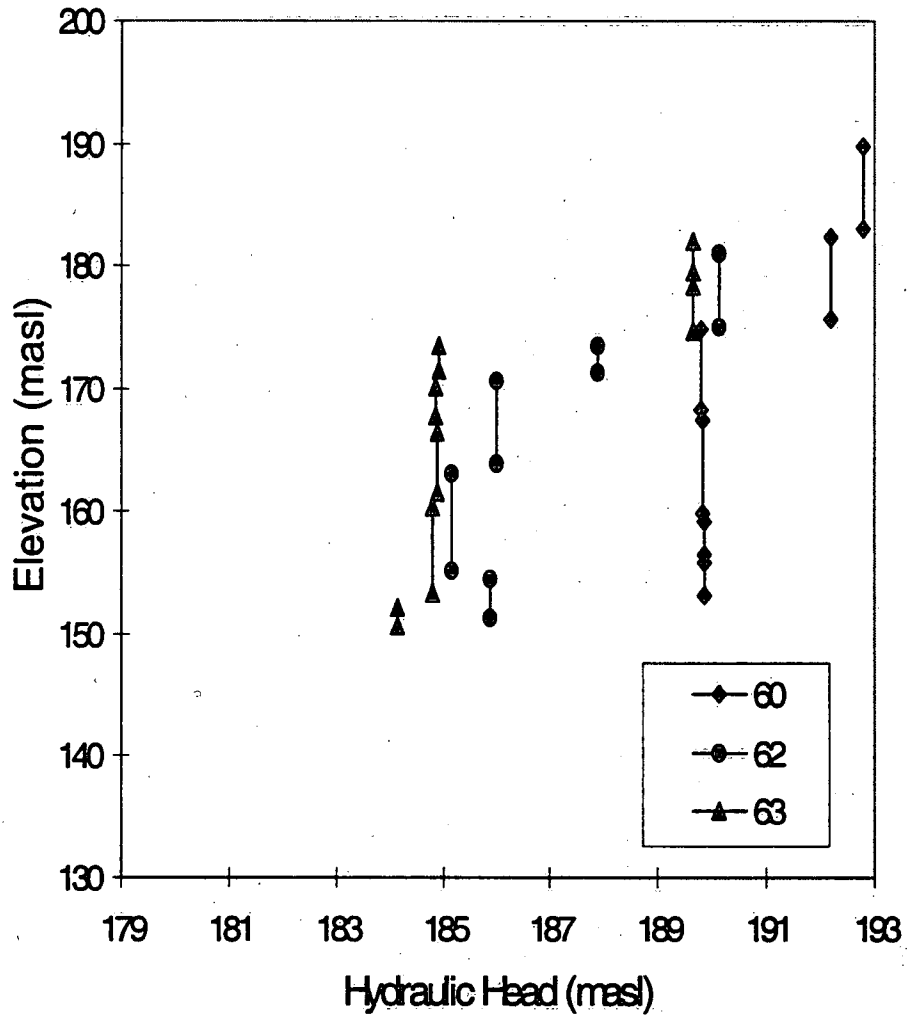


Figure 3.25 Spring hydraulic head distribution in boreholes 60, 62 & 63.

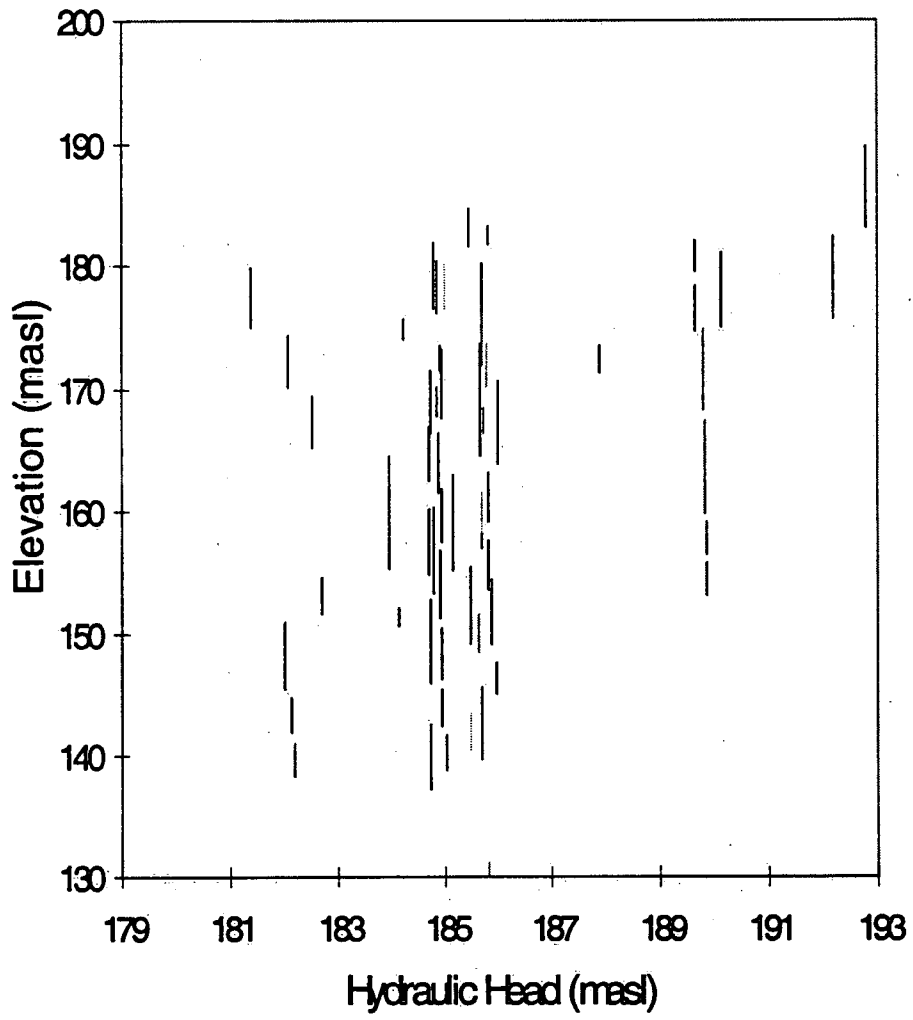


Figure 3.26 Spring hydraulic head distribution in all boreholes.

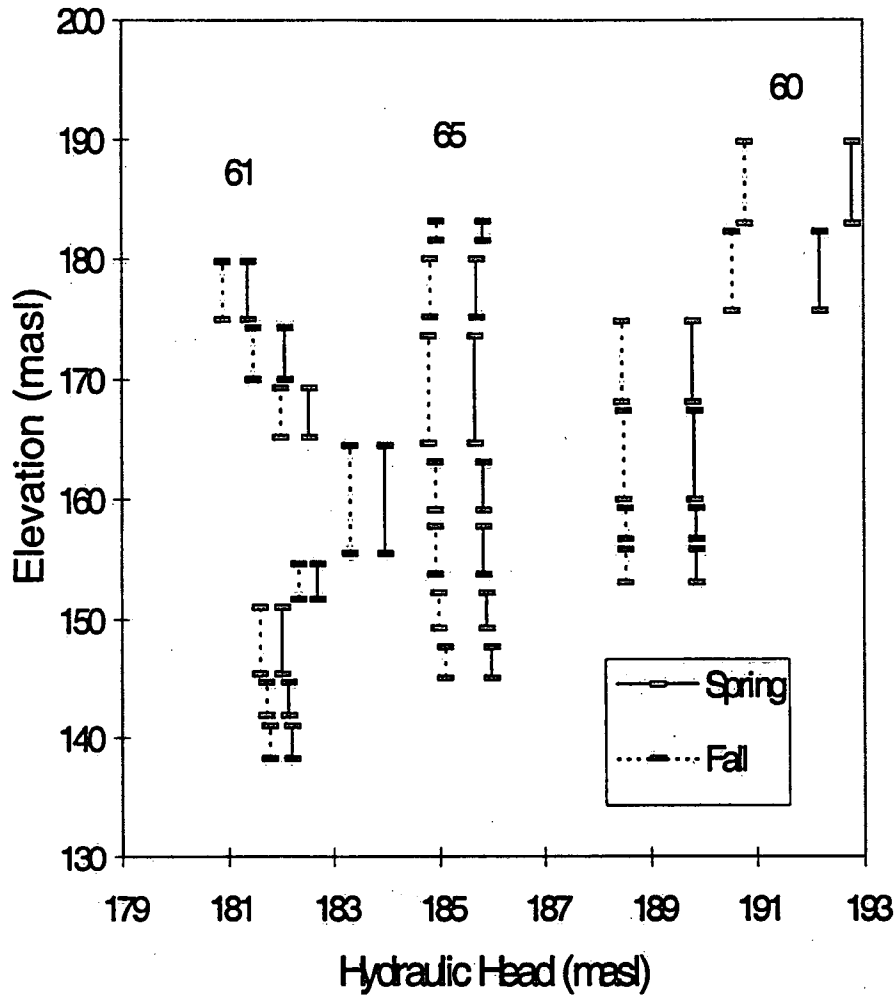


Figure 3.27 Spring and fall hydraulic head distribution in boreholes 60, 61 & 65.

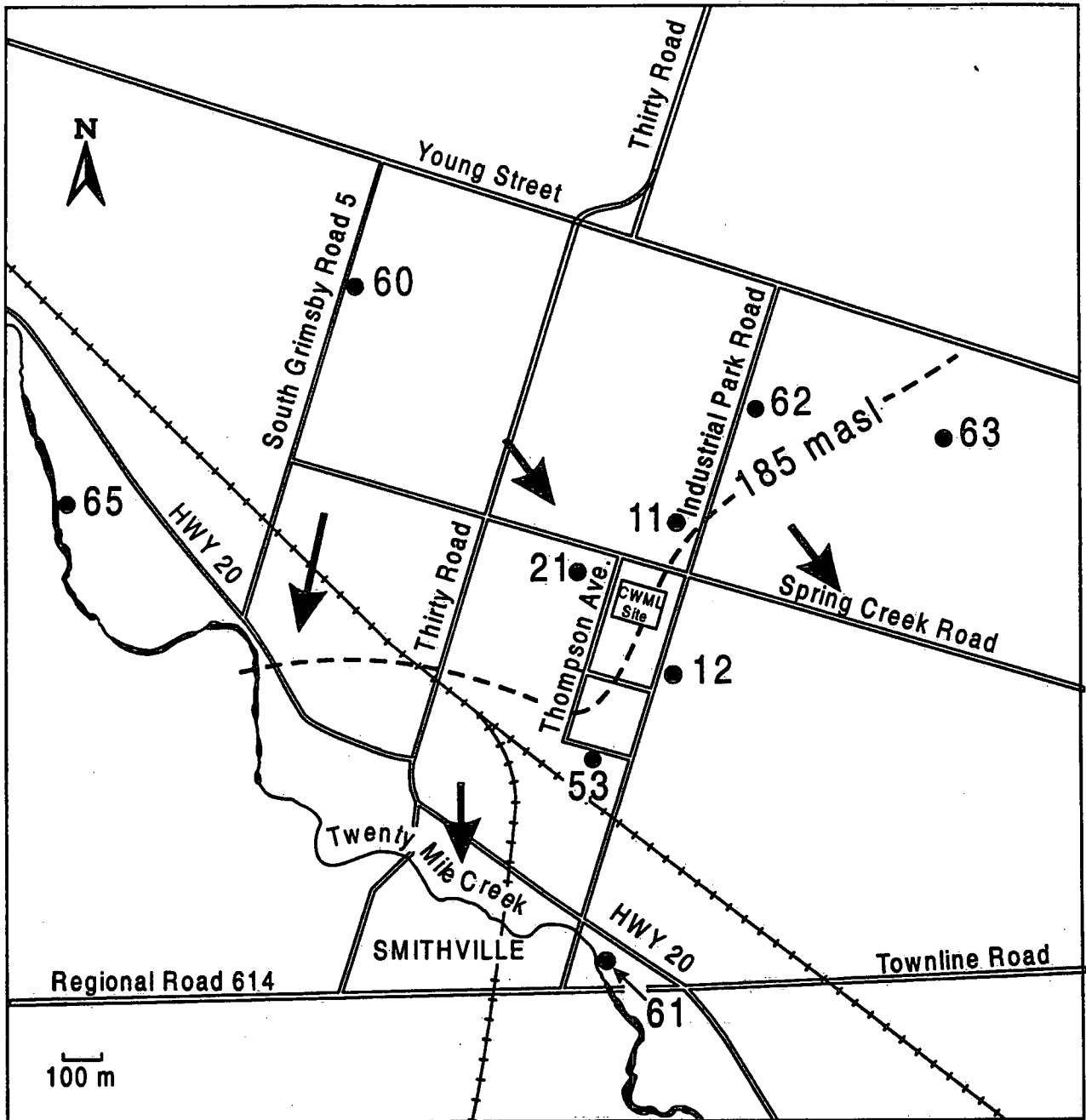


Figure 3.28 Directions of groundwater flow in most permeable and connected pathway.

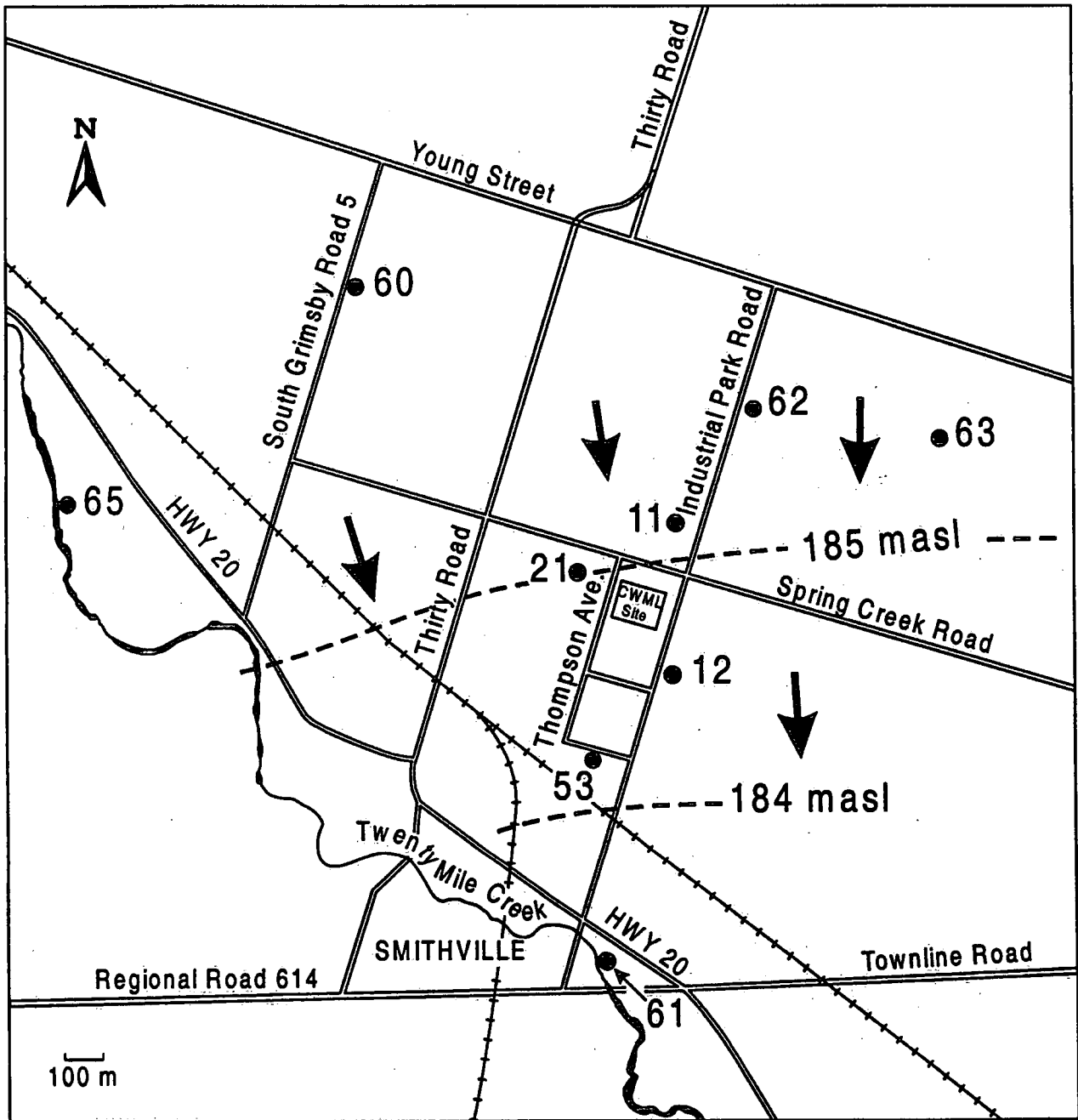


Figure 3.29 Groundwater flow directions in Upper Eramosa unit.

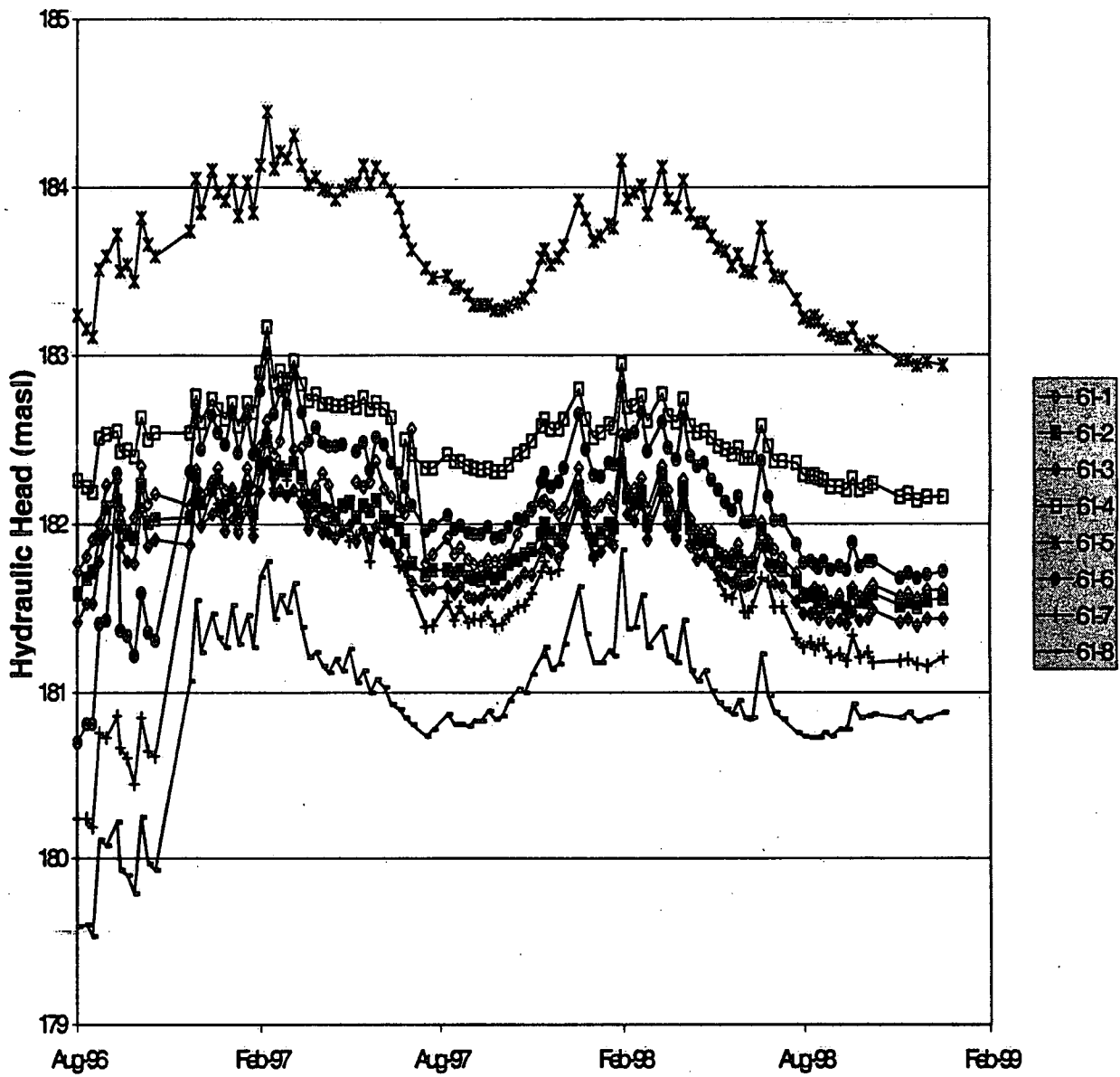


Figure 3.30 Hydrograph for monitoring intervals in borehole 61.

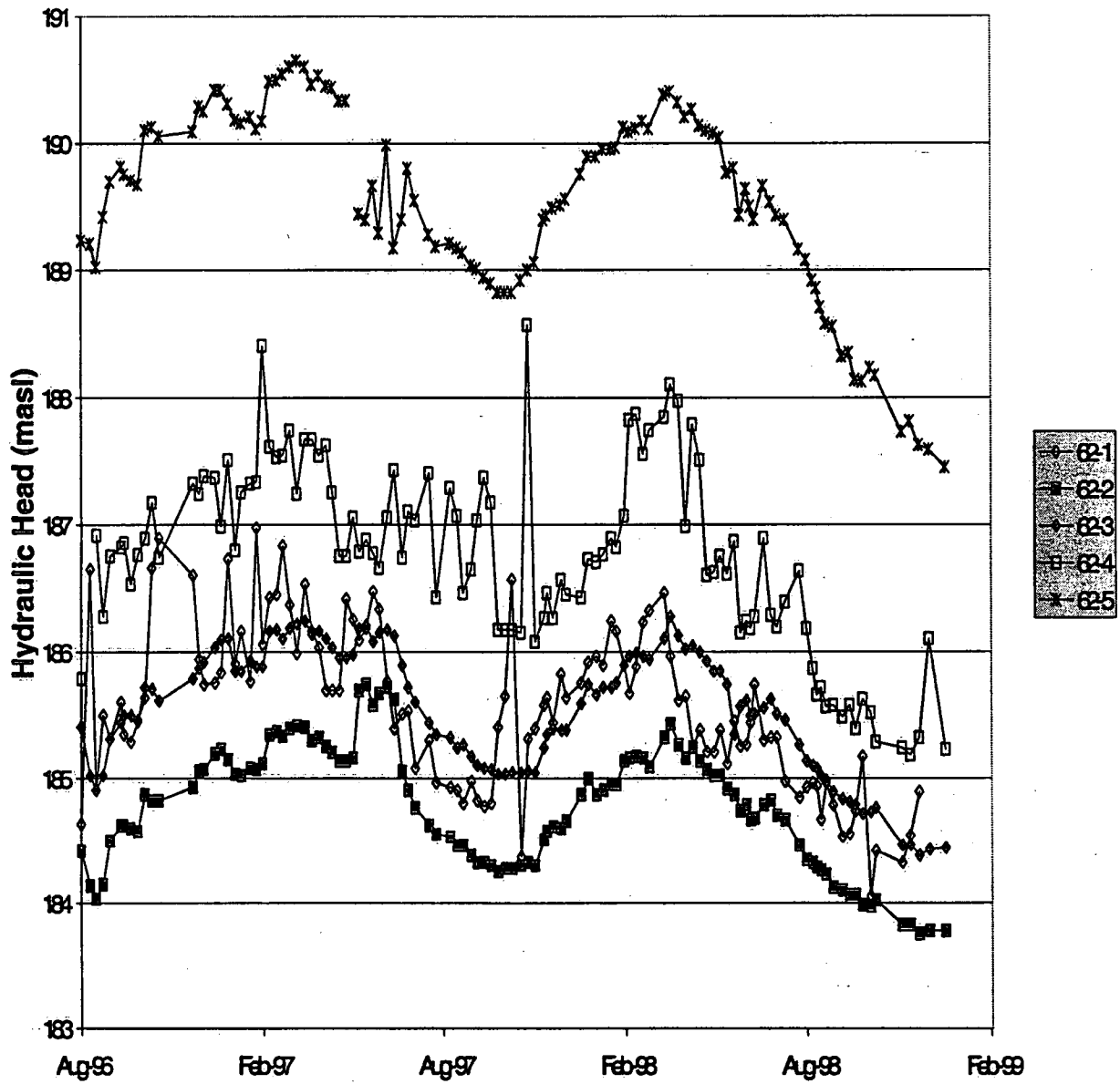


Figure 3.31 Hydrograph for monitoring intervals in borehole 62.

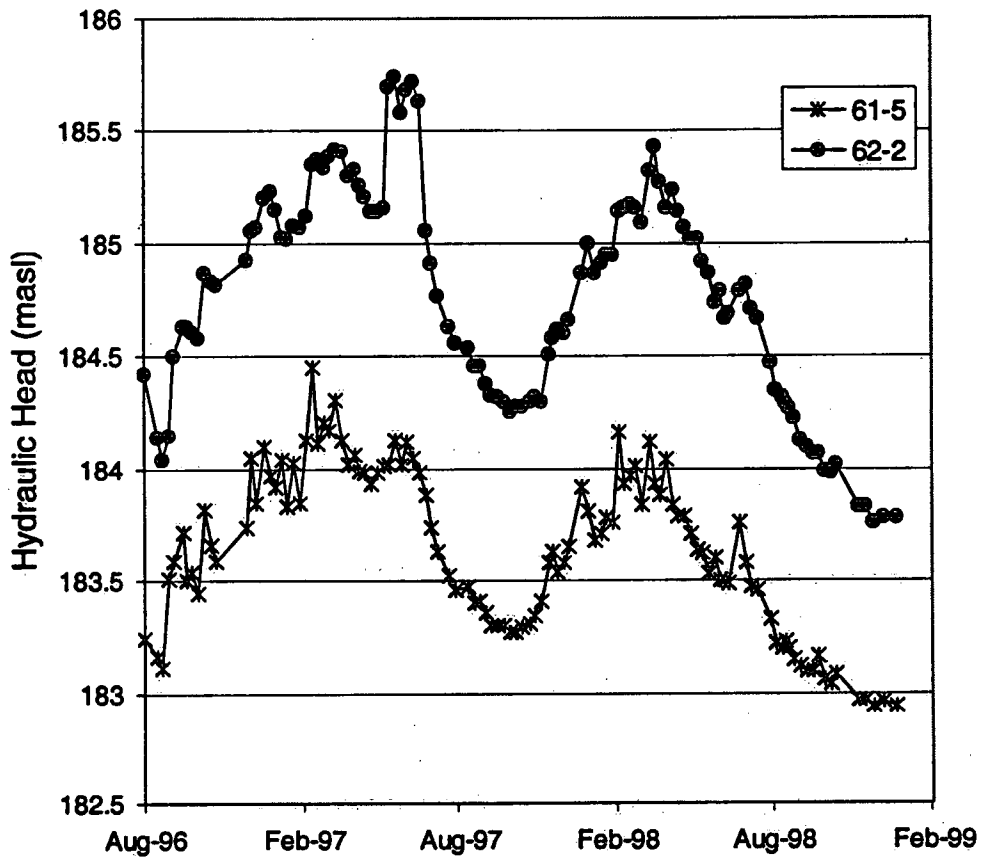


Figure 3.32 Hydrographs for two monitoring zones in boreholes 61 and 62. The two zones are connected and roughly up and down gradient of the site.

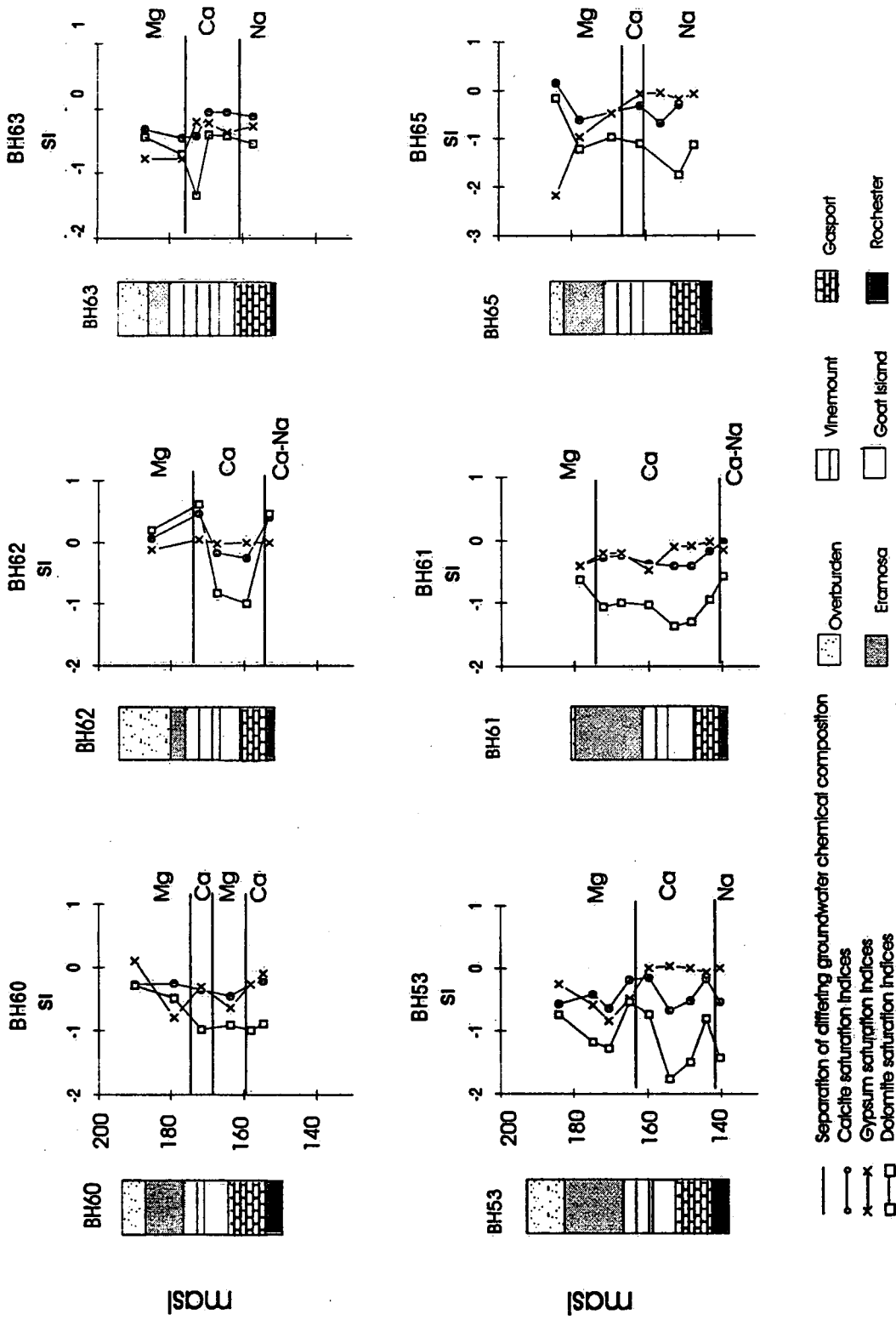


Figure 3.33 Calculated saturation indices using PHREEQC for dolomite, gypsum and calcite calculated with groundwater chemistry from Westbay monitoring zones.

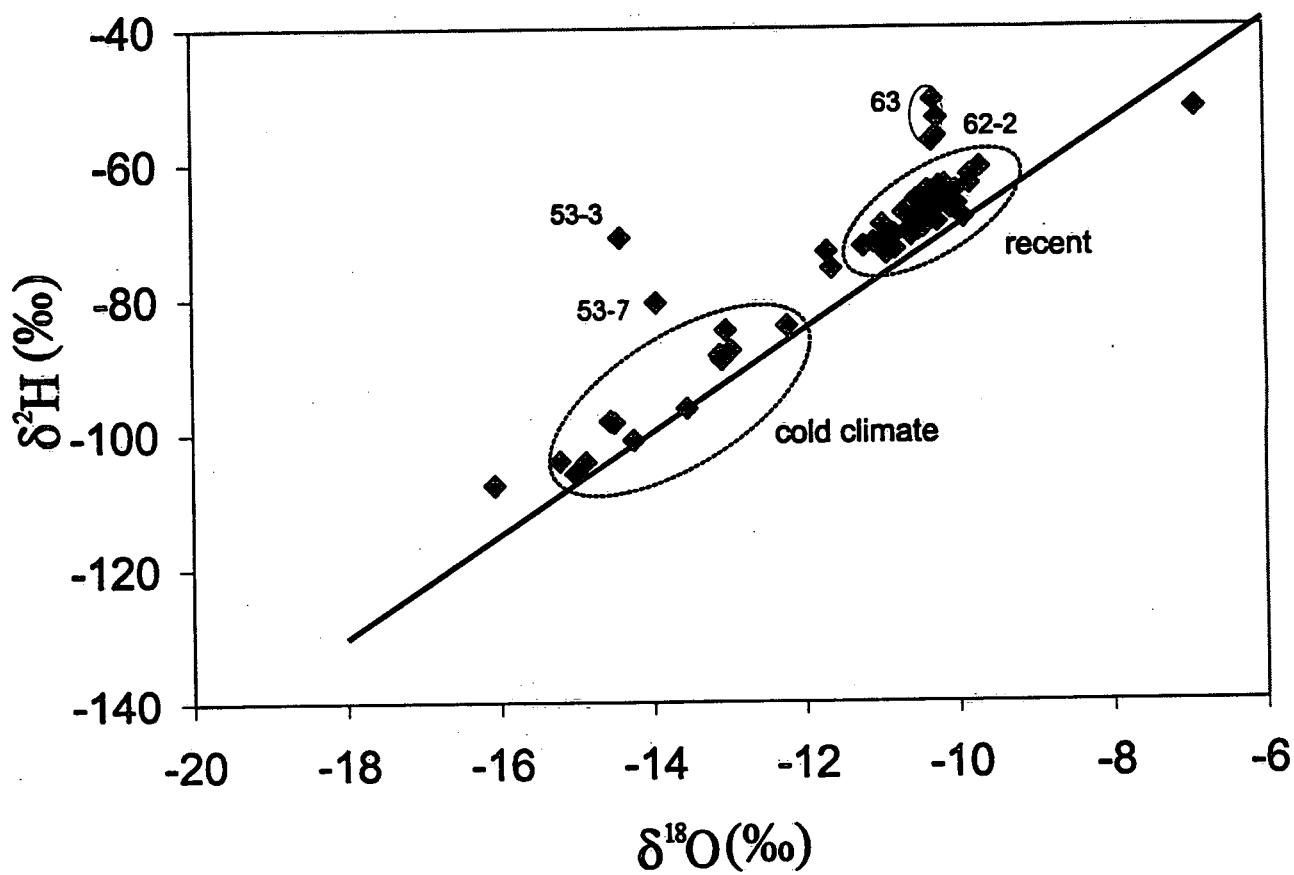


Figure 3.34 Isotope analyses from all monitoring zones sampled.

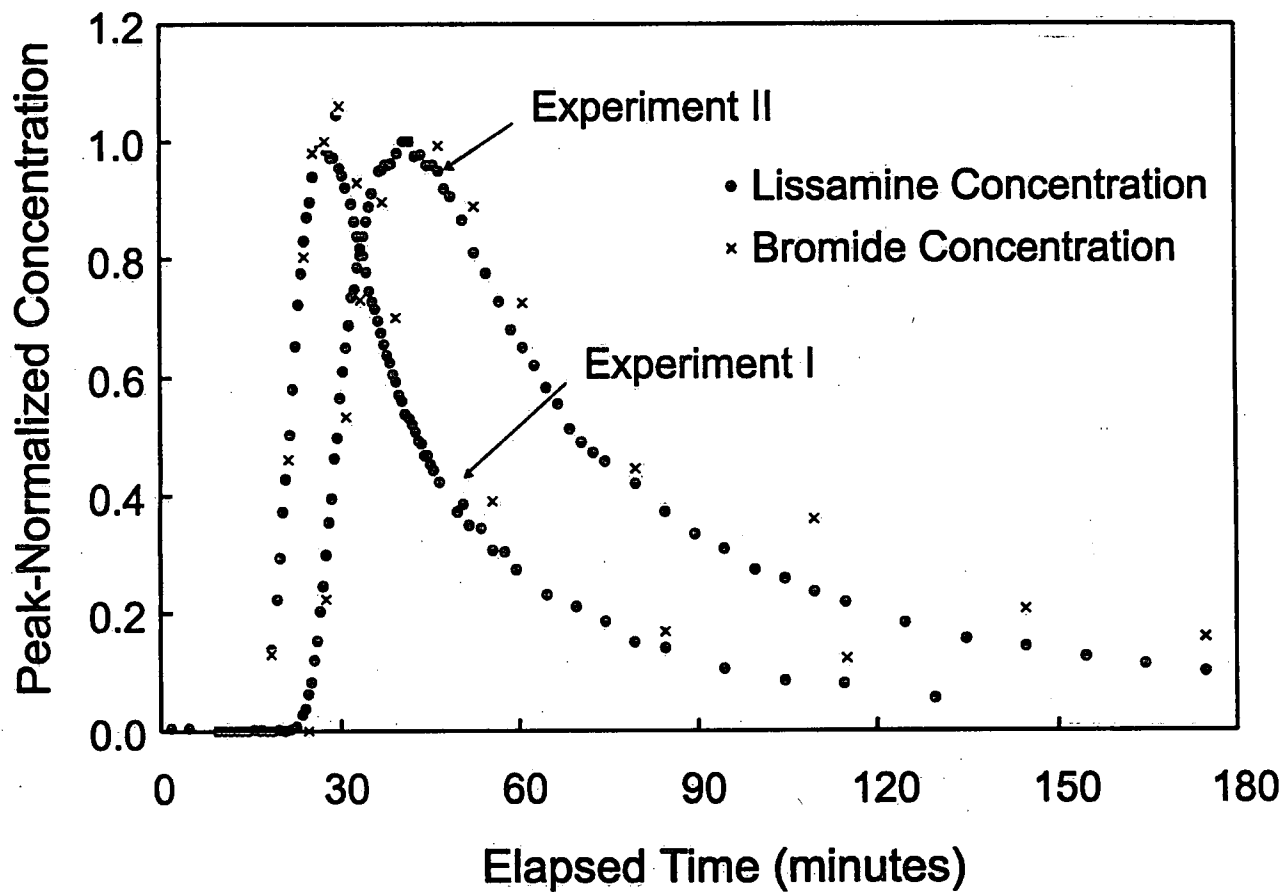


Figure 3.35 Breakthrough curves for the injection-withdrawal tracer experiments. Concentration in the withdrawal zone is normalized to peak concentration.

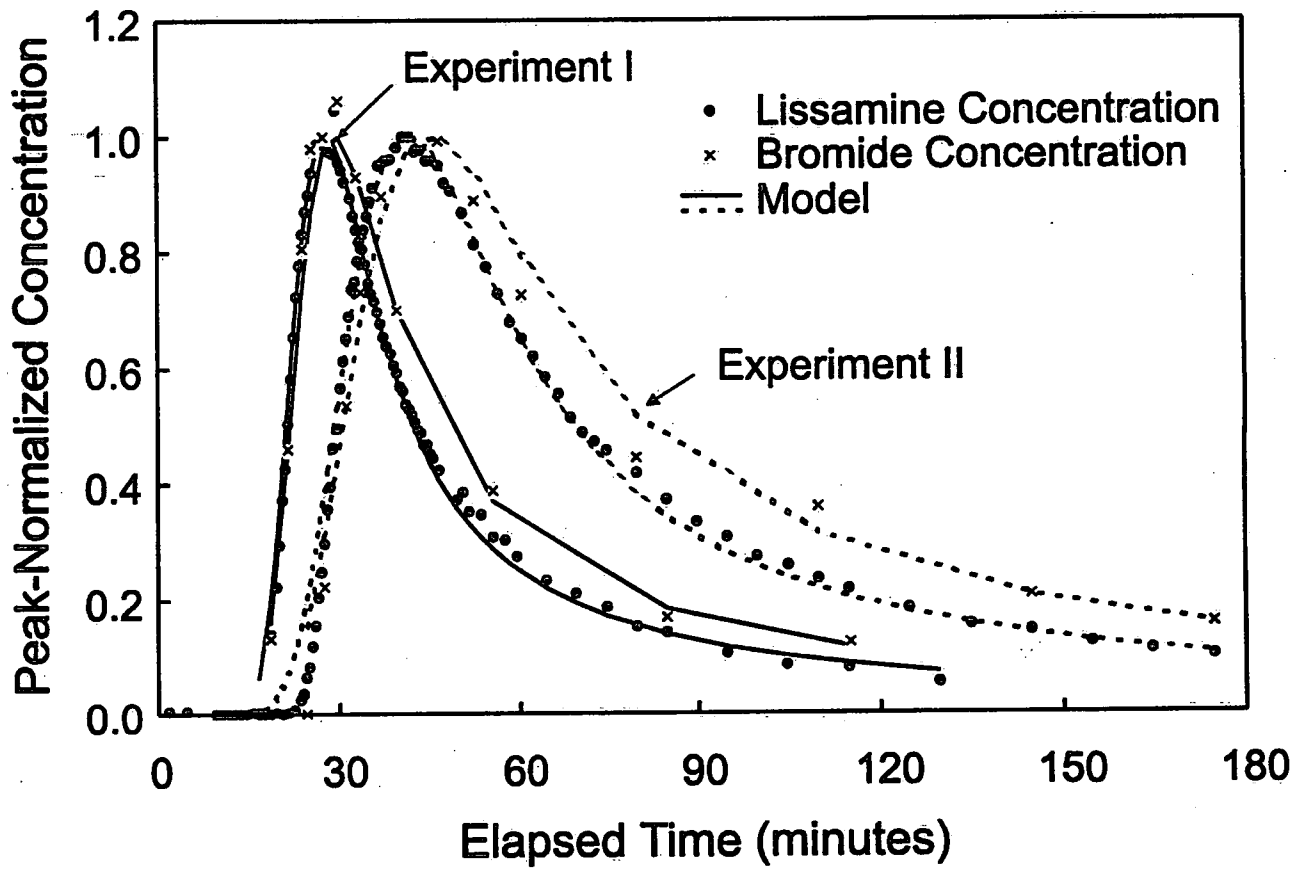


Figure 3.36 Model fit to field breakthrough curves.

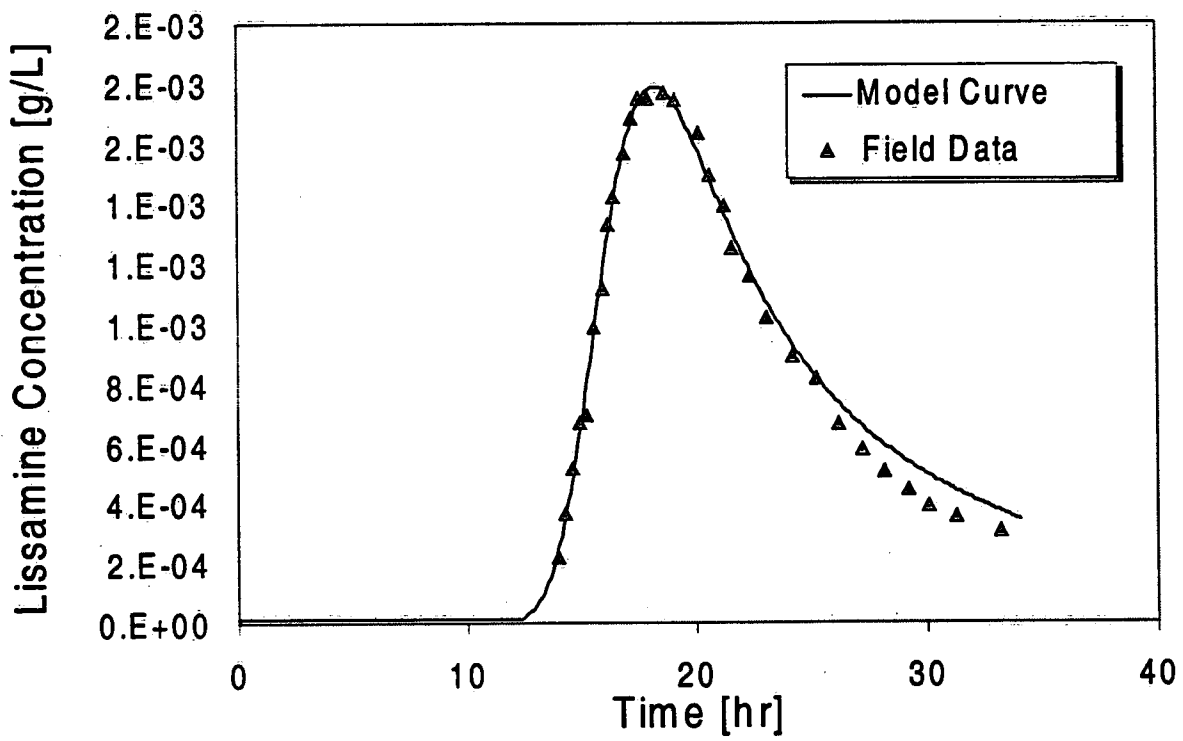


Figure 3.37 Tracer breakthrough and model fit in borehole 58 as results of radial-divergent tracer experiment.

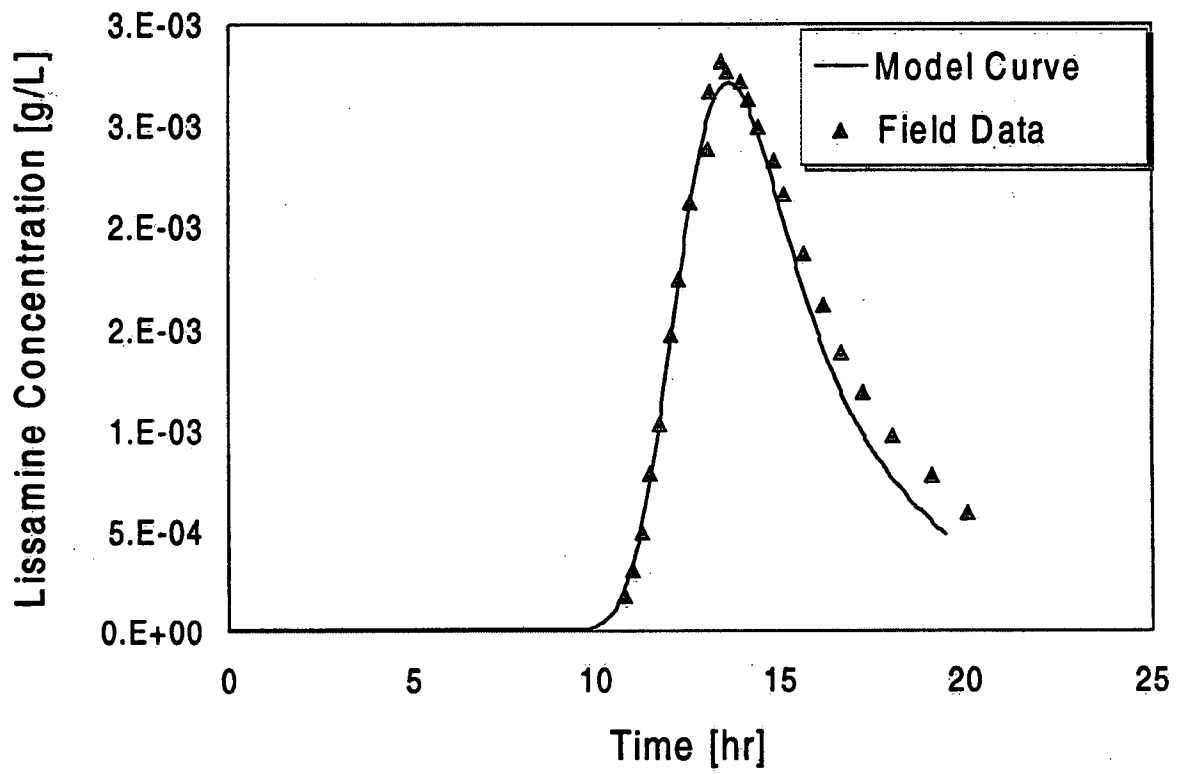


Figure 3.38 Tracer breakthrough and model fit in borehole 59 as results of radial-divergent tracer experiment.

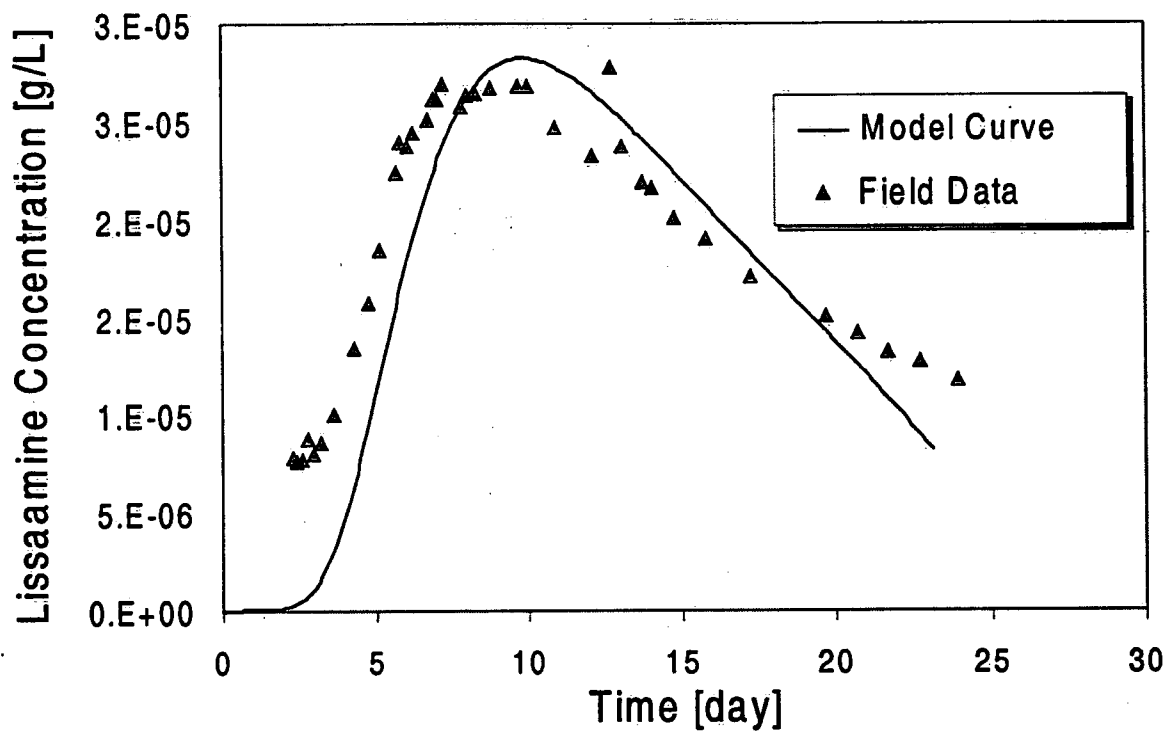


Figure 3.39 Tracer breakthrough and model fit in borehole 64 as results of radial-divergent tracer experiment.

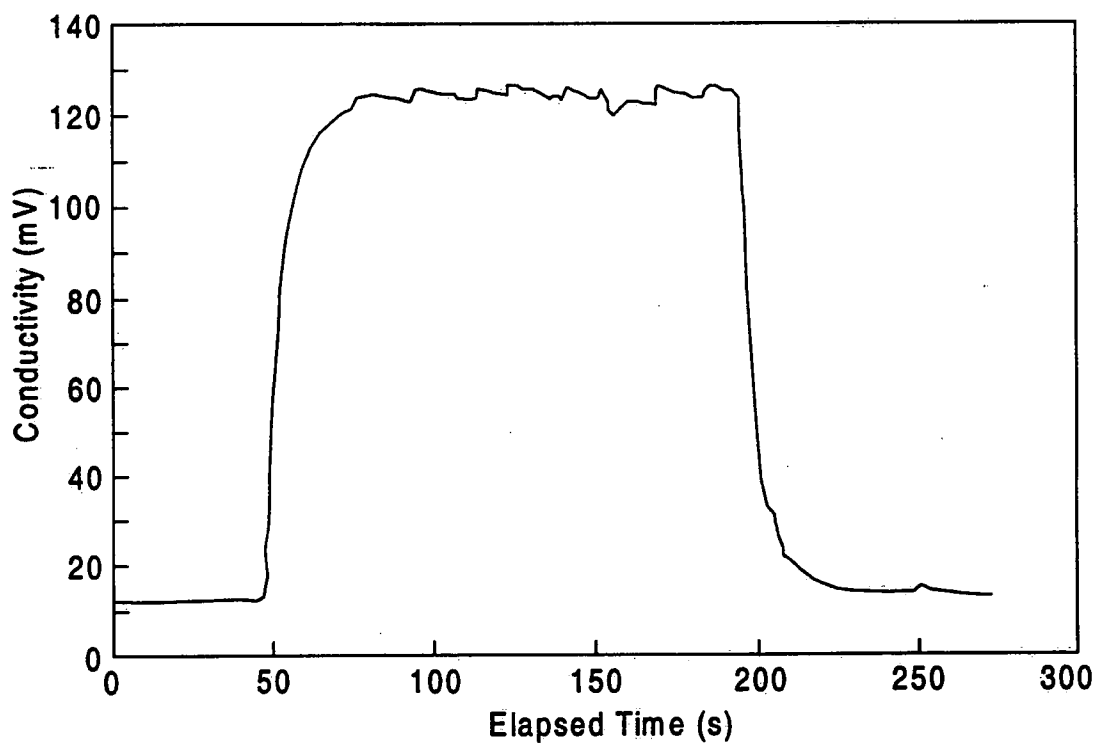


Figure 3.40 Conductivity measurements of tracer input approximating a Heavyside step function.

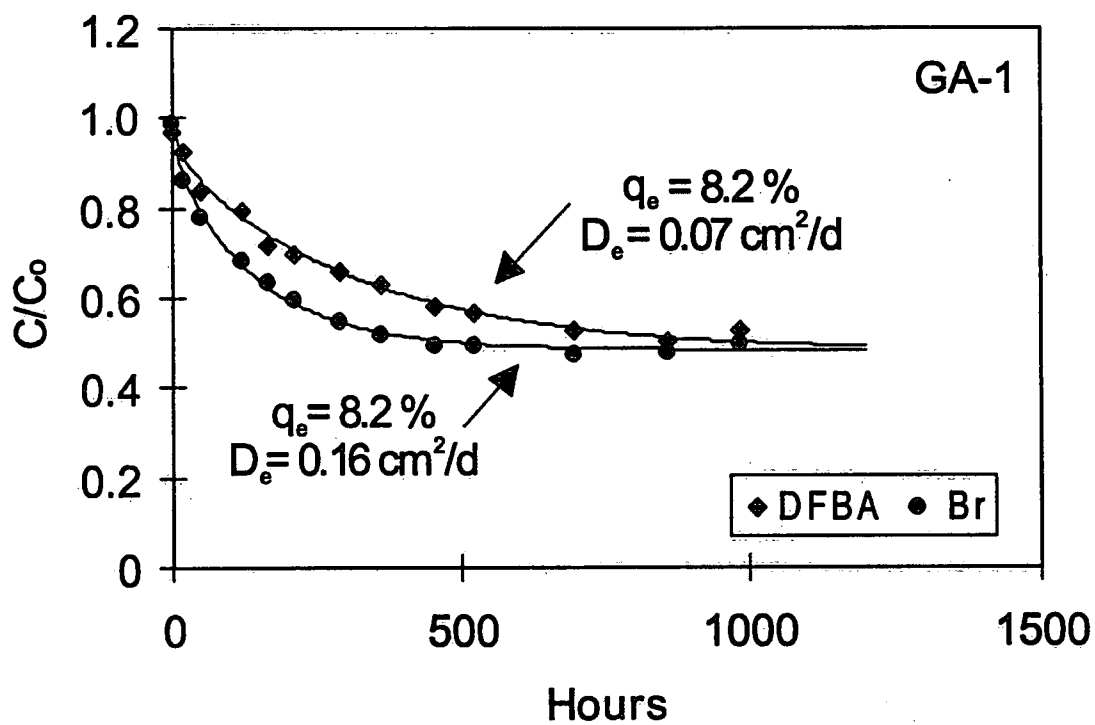


Figure 3.41 Modelling fit to diffusion experiment results for cell GA-1.

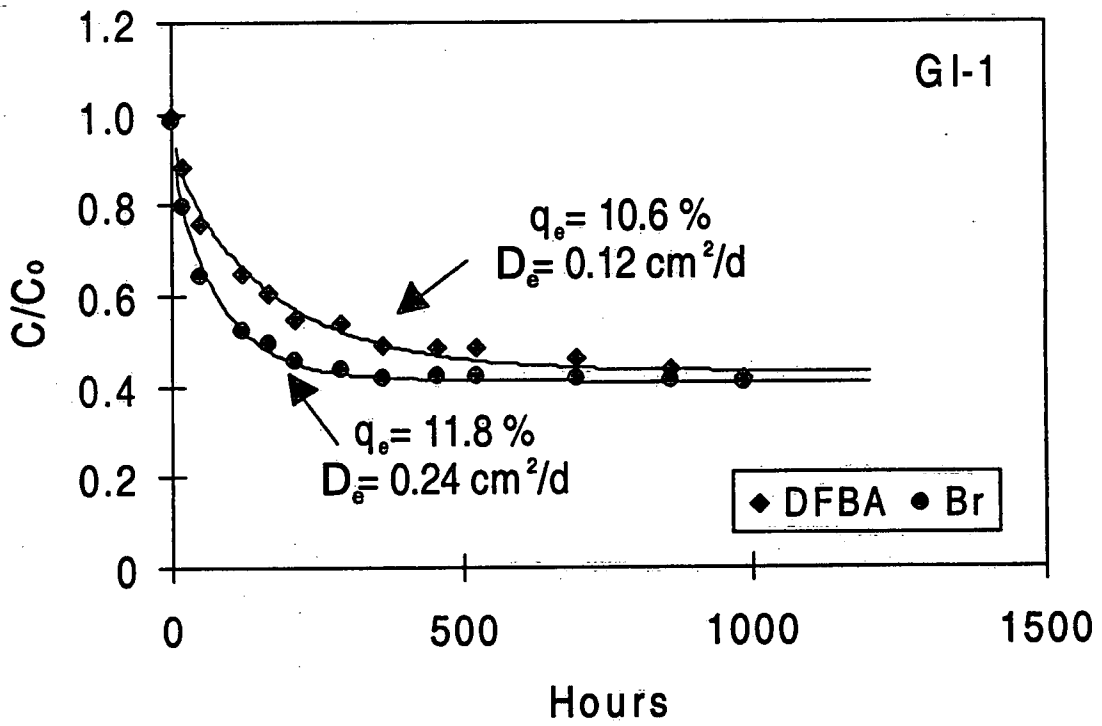


Figure 3.42 Modelling fit to diffusion experiment results for cell G1-1.

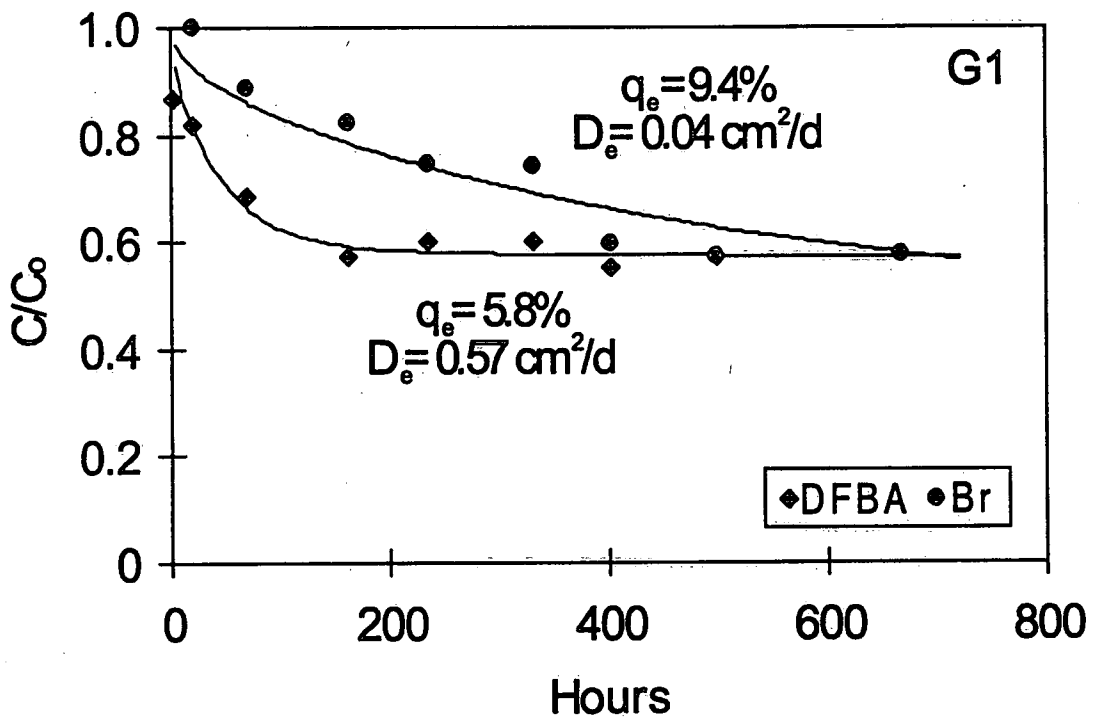


Figure 3.43 Modelling fit to diffusion experiment results for cell G1.

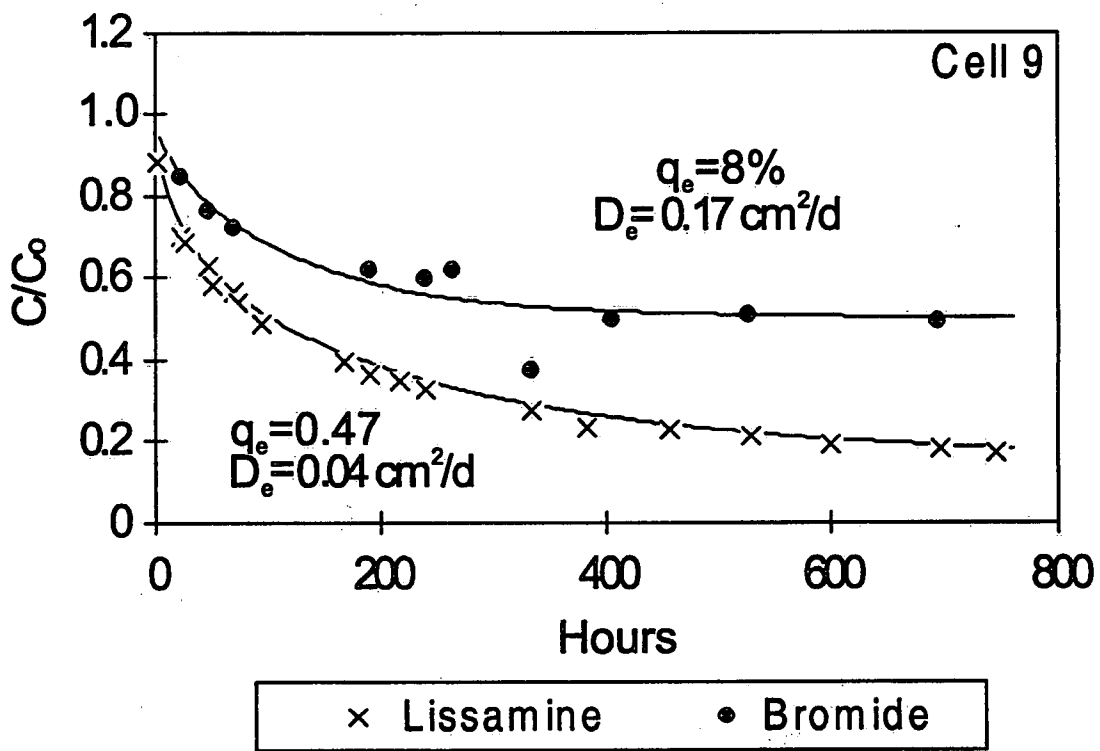


Figure 3.44 Modelling fit to diffusion experiment results for cell 9.

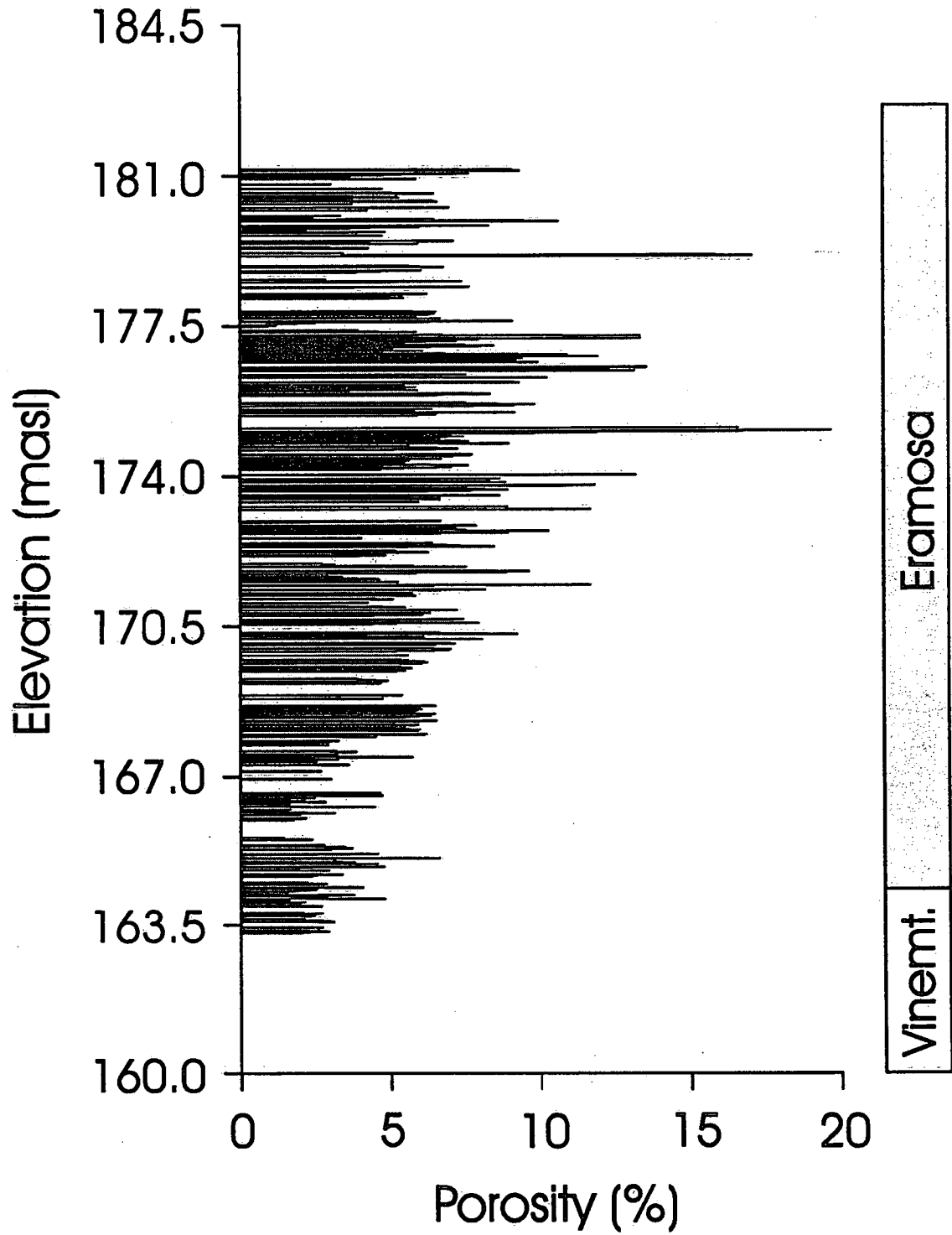


Figure 3.45 Gravimetric porosity measurements in borehole 64.

Table 2.1 Description of samples used in diffusion experiments.

Cell ID	Lithology	Borehole	Date Started	Date Ended	Sample Location (fbgs) ¹	Cell Height (cm)	Cell Radius (cm)	Reservoir Radius (cm)
1	Goat Island	54A	28/4/97	26/8/97	112.50	8.81	2.25	0.64
9	Vinemount	59	28/4/97	26/8/97	114.25	11.48	2.25	0.66
10	Gasport	59	28/4/97	26/8/97	136.58	6.85	2.25	0.65
D	Gasport	54B	28/4/97	26/8/97	124.42	9.42	2.24	0.61
OH3a	Ont. Hydro		14/4/97	06/09/97	-	6.48	3.16	0.64
C	Goat Island	54B	28/4/97	06/09/97	83.58	9.54	2.24	0.63
control 1	Stainless Steel		14/4/97	24/4/97	-	7.00	2.25	0.40
6	Eramosa	58	20/10/97	29/01/98	71.25	10.12	2.25	0.63
A	Vinemount	64	20/10/97	29/01/98	121.75	13.17	2.25	0.64
B	Vinemount	64	20/10/97	29/01/98	122.33	11.53	2.24	0.64
V1	Vinemount	54A	20/10/97	29/01/98	94.42	10.16	2.25	0.63
G1	Gasport	64	16/02/98	13/02/98	110.75	11.94	2.25	0.62
E1	Eramosa	64	16/02/98	13/02/98	15.00	13.99	2.25	0.64
E3	Eramosa	64	16/02/98	13/02/98	27.17	10.16	2.25	0.63
E2	Eramosa	64	16/02/98	13/02/98	26.58	14.11	2.25	0.63
G3	Gasport	64	16/02/98	13/02/98	121.83	12.89	2.25	0.62
Control 2	Stainless Steel	64	16/02/98	13/02/98	-	7.00	2.25	0.63
ER1	Eramosa	64	22/04/98	06/02/98	17.16	10.55	2.25	0.63
V2-1	Vinemount	64	22/04/98	06/02/98	55.67	12.16	2.25	0.63
GA-1	Gasport	64	22/04/98	06/02/98	112.00	11.97	2.25	0.63
E2-3	Eramosa	64	22/04/98	06/02/98	35.75	10.47	2.24	0.63
E2-2	Eramosa	64	22/04/98	06/02/98	25.42	11.66	2.25	0.64
GA-2	Gasport	64	22/04/98	06/02/98	110.75	12.45	2.25	0.63
GI-1	Goat Island	64	22/04/98	06/02/98	100.00	12.13	2.24	0.63
Control 2	Stainless Steel	-	22/04/98	06/02/98	-	7.00	2.25	0.63
jun4v21	Vinemount	64	27/06/98	16/09/98	54.75	11.85	2.24	0.64
jun4e1	Eramosa	64	27/06/98	16/09/98	27.75	12.15	2.19	0.63
jun4vi1	Vinemount	64	27/06/98	16/09/98	74.75	12.15	2.37	0.64
jun4e2	Eramosa	64	27/06/98	16/09/98	37.75	11.66	2.25	0.63
jun5gi1	Goat Island	64	27/06/98	16/09/98	102.00	11.53	2.24	0.63
jun5r1	Rochester	64	27/06/98	16/09/98	133.00	13.25	2.25	0.63
jun5gi2	Goat Island	64	27/06/98	16/09/98	95.33	12.50	2.26	0.63
jun5gal	Gasport	64	27/06/98	16/09/98	112.58	12.22	2.25	0.61
Control 2	Stainless Steel	-	27/06/98	16/09/98	-	7.00	2.25	0.63

¹refers to measurement along core axis.

Table 2.2 Hydraulic apertures (in μm) of the fractures used for the radial-divergent tracer experiments.

Fracture Depth (mbct)	56	58	59	64	37C
11.0	470	472	577	917	439
41.7	171	416	425	379	-

Table 2.3 Comparison of methods (and laboratories) of organic carbon analysis.

Sample	Leco CR12 Carbon Analyzer NWRI	Leco RC412 Carbon Analyzer Leco Ltd.	UIC C-Analyzer/ Pre-Acidification ¹ Wash. State Univ.
SMV-14 (Eramosa)	0.20%	—	0.09 - 0.11%
SMV-15 (Vinemount 1)	0.10%	—	0.12%
SMV-16 (Goat Island)	0.13%	—	0.11%
SMV-47 (Goat Island)	3.89 - 4.03%	2.66 - 2.68%	—
SMV-18 (Gasport)	0.00%	—	0.01%
SMV-19 (Rochester)	0.07%	—	0.12%

Table 2.4 List of samples used for the analysis of organic carbon.

Sample	Borehole	Sample Interval (mbgs)		Lithology	Description
SMV-45	53	57.09		Decew	arg./stylolite only
SMV-145	54C	53.79	53.84	Decew	
SMV-147	54A	53.67		Decew	
SMV-2	54A	13.33	13.44	Eramosa	
SMV-3	54A	16.30	16.48	Eramosa	
SMV-4	54A	19.82	20.00	Eramosa	
SMV-14	54B	17.75	17.92	Eramosa	
SMV-46	54A	9.40		Eramosa	dark horizon/petrol odour
SMV-53	53	23.09		Eramosa	
SMV-10	54A	46.59	46.75	Gasport	
SMV-18	54B	39.99	40.15	Gasport	
SMV-42	53	54.05		Gasport	arg./stylolite only
SMV-44	53	52.42		Gasport	arg./stylolite only
SMV-48	54A	48.62		Gasport	host rock without stylolite
SMV-49	54A	48.62		Gasport	host rock with stylolite
SMV-84	54B	40.00		Gasport	
SMV-154	65			Gasport	light grey stylolite w/clay
SMV-158	65			Gasport	light grey stylolite w/clay
SMV-159				Gasport	stylolite
SMV-161				Gasport	host rock aggregate sample (?)
SMV-7	54A	31.97	32.12	Goat Island	
SMV-8	54A	35.01	35.16	Goat Island	
SMV-9	54A	37.42	37.59	Goat Island	
SMV-16	54B	25.43	25.58	Goat Island	
SMV-43	53	40.48		Goat Island	arg. only
SMV-47	54A	33.89		Goat Island	arg. only
SMV-80	54B	25.58		Goat Island	
SMV-139	54B	29.15	29.18	Goat Island	stylolite
SMV-140	54B	28.90	28.92	Goat Island	
SMV-142	54C	33.26		Goat Island	argillaceous band
SMV-155				Goat Island	host rock aggregate sample (?)
SMV-160				Goat Island	stylolite
SMV-156	65			Vinemount	dark grey stylolite w/clay
SMV-157	65			Vinemount	dark grey stylolite w/clay
SMV-15	54B	22.03	22.16	Vinemount/Unit 1	
SMV-51	58	38.35		Vinemount/Unit 1	arg. only
SMV-78	54B	22.16		Vinemount/Unit 1	
SMV-133	54D	27.86	27.89	Vinemount/Unit 1	
SMV-134	54D	27.78		Vinemount/Unit 1	argillaceous band
SMV-137	54B	22.59	22.61	Vinemount/Unit 1	
SMV-144	54C	27.91	27.94	Vinemount/Unit 1	

Table 2.4 (Cont'd) List of samples used for the analysis of organic carbon.

Sample	Borehole	Sample Interval (mbgs)		Lithology	Description
SMV-149	54A	30.24	30.27	Vinemount/Unit 1	
SMV-150	54A	30.32		Vinemount/Unit 1	stylolite
SMV-39	53	30.77		Vinemount/Unit 2	host rock and arg./stylolite
SMV-40	53	30.77		Vinemount/Unit 2	host rock and arg./stylolite
SMV-41	53	30.77		Vinemount/Unit 2	arg./stylolite only
SMV-131	54D	23.37	23.40	Vinemount/Unit 2	
SMV-132	54D	24.74	24.77	Vinemount/Unit 2	
SMV-135	54D	23.45	23.47	Vinemount/Unit 2	thick arg. band, some matrix
SMV-136	54B	19.62	19.65	Vinemount/Unit 2	
SMV-143	54C	25.65	25.68	Vinemount/Unit 2	
SMV-148	54A	27.25	27.28	Vinemount/Unit 2	
SMV-19	54B	46.69	46.87	Rochester	
SMV-86	54B	46.69		Rochester	
SMV-138	54B	50.73	50.75	Rochester	
SMV-146	54C	55.59	55.62	Rochester	

Table 2.5 Cell reservoir volumes (all volumes are in mL)

Cell ID	Forward Lissamine	Reverse Lissamine	Forward Bromide	Reverse Bromide	Forward Nitrite	Forward dfba
1	11.5	11.5	11.5	11.5		
9	15	14.7	15	14.7		
10	8.8	8.8	8.8	8.8		
D	11.6	11.9	11.6	11.9		
OH3a	9		9			
C		12.1				
control 1	3.8					
6	12.6	12.8	12.6	12.8	12.8	11.8
A	16.9	16.6	16.9	16.6	16.6	
B	12.9	14.6	12.9	14.6	14.6	
V1	13.2	13.3	13.2	13.3	13.3	
G1			14.6			14.6
E1	17.1		17.1			
E3			17.7			17.7
E2			15.3			15.3
G3			16.7			16.7
Control 2			9			9
ER1			13.5			13.5
V2-1			16			16
GA-1			14.6			14.6
E2-3			13.2			13.2
E2-2			14.7			14.7
GA-2			15			15
GI-1			15.2			15.2
Control 2			8.2			8.2
jun4v21			13.43			13.43
jun4e1			15.03			15.03
jun4vi1			14.88			14.88
jun4e2			14.39			14.39
jun5gi1			14.56			14.56
jun5r1			16.23			16.23
jun5gi2			14.96			14.96
jun5ga1			15.22			15.22
Control 2			8.59			8.59

Table 2.6 Summary of tracers used in each cell.

Cell ID	Forward Lissamine	Reverse Lissamine	Forward Bromide	Reverse Bromide	Forward Nitrite	Forward dfba
1	x	x	x	x		
9	x	x	x	x		
10	x	x	x	x		
D	x	x	x	x		
OH3a	x		x			
C		x				
control 1	x					
6	x	x	x	x	x	x
A	x	x	x	x	x	
B	x	x	x	x	x	
V1	x	x	x	x	x	
G1			x			x
E1	x		x			
E3			x			x
E2			x			x
G3			x			x
Control 2			x			x
ER1			x			x
V2-1			x			x
GA-1			x			x
E2-3			x			x
E2-2			x			x
GA-2			x			x
GI-1			x			x
Control 2			x			x
jun4v21			x			x
jun4e1			x			x
jun4vi1			x			x
jun4e2			x			x
jun5gi1			x			x
jun5r1			x			x
jun5gi2			x			x
jun5ga1			x			x
Control 2			x			x

Table 3.1 Summary of vertical and bedding plane fracture spacings

Fracture Grouping	N	Total Length (m)	Mean Spacing (m)	Std. Dev (m)	Distribution ¹	α	β	R ²
BPF: Eramosa	588	252.20	0.39	0.46	Exponential	105.58	-1.98	0.93
BPF: Eramosa	588	252.20	0.39	0.46	Power	8.11	-1.77	0.90
BPF: Upper Vinemount	270	75.39	0.22	0.26	Power	2.55	-1.85	0.93
BPF: Lower Vinemount	204	66.39	0.27	0.3	Power	2.66	-1.62	0.84
BPF: Goat Island	92	107.29	0.7	0.8	Power	5.05	-1.18	0.93
BPF: Vine + Goat	566	249.07	0.31	0.45	Power	5.99	-1.83	0.94
BPF: Gasport	410	169.29	0.38	0.51	Power	5.82	-1.59	0.90
BPF: Eramosa-SC	190	82.03	0.41	0.49	Power	3.31	-1.44	0.84
BPF: Eramosa-NC	137	54.37	0.34	0.39	Power	2.89	-1.29	0.67
VF: Eramosa	127	252.20	0.77	1.03	Power	3.45	-0.94	0.75
VF: Eramosa	127	252.20	0.77	1.03	Exponential	11.59	-0.91	0.66
VF: Vinemount	4	141.78	1.1	1.4				
VF: Goat Island	11	107.29	0.7	0.5				
VF: Gasport	12	169.29	1.5	1.6				

¹Distributions defined as Exponential: $y = \alpha e^{\beta x}$ and Power: $y = \alpha x^{\beta}$

Table 3.2 Fracture sets measured in the Eramosa member.

Set	Range	Importance	Corresponding Set: Gartner Lee (1995)
I	95°-110°	Major	D (045°- 109°)
II	350°-5°	Major	C (003°- 44°)
III	60°-70°	Major	D (045°- 109°)
IV	145°-150°	Minor	B (140°- 182°)
V	40°-45°	Minor	C (003°- 44°)

Table 3.3 Summary of transmissivity measurements in the Lockport units using a 2-m test interval.

	N	T_{min} (m ² /s)	T_{max} (m ² /s)	T_G (m ² /s)	$S_{Ln(T)}$
Eramosa	129	1E-08	>1E-02	1E-05	2.7
Goat Island*	131	<1E-10	2E-03	2E-07	4.8
Gasport	79	3E-10	>1E-02	6E-06	4.6
Eramosa/Goat Island Contact	18	<1E-10	>1E-02	5E-05	3.8
Goat Island/Gasport Contact	18	6E-09	2E-04	4E-06	3.3

*Includes Vinemount Unit.

Table 3.4 Summary of transmissivity measurements in the Lockport units using a 0.5-m test interval.

	N	T_{min} (m ² /s)	T_{max} (m ² /s)	T_G (m ² /s)	$S_{Ln(T)}$	$2b_{eq-max}$ (μ m)	$\langle 2b_{eq} \rangle$ (μ m)	S_{2b}
Eramosa	385	<1E-10	>1E-02	6E-07	3.8	>2570	228	392
Upper Vinemount	105	<1E-10	5E-05	1E-07	6.5	434	308	484
Lower Vinemount	79	<1E-10	>1E-02	2E-09	3.5	>2570	38	83
Goat Island	126	<1E-10	6E-04	9E-09	3.6	1006	74	171
Gasport	129	<1E-10	>1E-02	2E-07	5.4	>2570	338	628

* $2b_{eq-min} = < 6 \mu$ m in all units.

Table 3.5 Summary of fracture porosity calculations using constant-head injection tests with 0-1 m and 0.5 m test intervals.

	Test Interval (m)	Total Length (m)	T_{total} (m ² /s)	$2b_{total}$ (μm)	Fracture Porosity
Eramosa	0.1	4.23	1E-02	2631	6E-04
Eramosa	0.5	157.85	8E-02	5211	3E-05
Upper Vinemount	0.5	43.05	4E-02	3937	9E-05
Lower Vinemount	0.5	32.39	1E-04	601	2E-05
Goat Island	0.5	52.07	2E-03	1480	3E-05
Gasport	0.1	2.82	4E-05	421	1E-04
Gasport	0.5	51.60	8E-02	5106	1E-04

Table 3.6 Summary of matrix transmissivity measurements in the Lockport units using a 0.5-m test interval.

	N	T_{min} (m ² /s)	T_{max} (m ² /s)	T_G (m ² /s)	$s_{Ln(T)}$	K_G (m/s)	K_A (m/s)
Eramosa	44	<1E-10	1E-06	3E-08	2.6	7E-08	4E-07
Vinemount	31	<1E-10	5E-08	4E-10	2.0	1E-09	1E-08
Goat Island	56	<1E-10	1E-07	4E-09	1.6	9E-09	3E-08
Gasport	22	<1E-10	1E-07	8E-09	2.2	2E-08	5E-08
All	161	<1E-10	1E-06	4E-09	2.6	1E-08	1E-07

Table 3.7(a) Summary of intervals tested using pulse interference tests.

Set	Test ID	Borehole	Distance	Position	Interval		2b _{ch}	Response
			(m)		(masl)		(um)	
1	Source	54D			180.70	180.29	510	N
1	PI-14	54A	9.4	+2.50	182.52	182.10	56	N
1	PI-13	54A	9.4	+2.00	182.10	181.69	175	N
1	PI-12	54A	9.4	+1.50	181.69	181.27	169	N
1	PI-11	54A	9.4	+1.00	181.27	180.85	40	N
1	PI-9/PI-10	54A	9.4	+0.50	180.85	180.43	51	Detected
1	PI-1/PI-2	54A	9.4	0.00	180.43	180.02	638	Y
1	PI-3	54A	9.4	-0.50	180.02	179.60	577	Y
1	PI-4/PI-5	54A	9.4	-1.00	179.60	179.18	93	N
1	PI-6	54A	9.4	-1.50	179.18	178.77	65	N
1	PI-7	54A	9.4	-2.00	178.77	178.35	138	N
1	PI-8	54A	9.4	-2.50	178.35	177.93	222	N
1	PI-14	54B	14.8	+2.50	183.12	182.62	50	N
1	PI-13	54B	14.8	+2.00	182.62	182.12	28	N
1	PI-12	54B	14.8	+1.50	182.12	181.62	34	N
1	PI-11	54B	14.8	+1.00	181.62	181.12	27	N
1	PI-9/PI-10	54B	14.8	+0.50	181.12	180.62	39	N
1	PI-1/PI-2	54B	14.8	0.00	180.62	180.12	320	Y
1	PI-3	54B	14.8	-0.50	180.12	179.62	34	Y
1	PI-4/PI-5	54B	14.8	-1.00	179.62	179.12	162	Detected
1	PI-6	54B	14.8	-1.50	179.12	178.62	167	N
1	PI-7	54B	14.8	-2.00	178.62	178.12	29	Detected
1	PI-8	54B	14.8	-2.50	178.12	177.62	25	N
1	PI-14	54C	11.3	+2.50	182.68	182.26	103	N
1	PI-13	54C	11.3	+2.00	182.26	181.85	43	N
1	PI-12	54C	11.3	+1.50	181.85	181.43	211	N
1	PI-11	54C	11.3	+1.00	181.43	181.02	23	N
1	PI-9/PI-10	54C	11.3	+0.50	181.02	180.61	47	Y
1	PI-1/PI-2	54C	11.3	0.00	180.61	180.19	391	Y
1	PI-3	54C	11.3	-0.50	180.19	179.78	30	N
1	PI-4/PI-5	54C	11.3	-1.00	179.78	179.36	98	N
1	PI-6	54C	11.3	-1.50	179.36	178.95	30	N
1	PI-7	54C	11.3	-2.00	178.95	178.53	200	N
1	PI-8	54C	11.3	-2.50	178.53	178.12	15	N

Table 3.7(b) Summary of intervals tested using pulse interference tests.

Set	Test ID	Borehole	Distance	Position	Interval		2b _{ch}	Response
			(m)		(masl)		(um)	
2	source	54D			178.65	178.24	227	N
2	PI-23	54A	7.80	+2.50	180.87	180.45		N
2	PI-22	54A	7.80	+2.00	180.45	180.03		N
2	PI-20/PI-21	54A	7.80	+1.50	180.03	179.62		N
2	PI-19	54A	7.80	+1.00	179.62	179.20		N
2	PI-17/PI-18	54A	7.80	+0.50	179.20	178.78		Y
2	PI-16	54A	7.80	0.00	178.78	178.37		Y
2	PI-24/PI-25	54A	7.80	-0.50	178.37	177.95		Y
2	PI-26	54A	7.80	-1.00	177.95	177.53		N
2	PI-27	54A	7.80	-1.50	177.53	177.12		N
2	PI-28	54A	7.80	-2.00	177.12	176.70		N
2	PI-29	54A	7.80	-2.50	176.70	176.28		N
2	PI-23	54B	15.19	+2.50	181.12	180.62		N
2	PI-22	54B	15.19	+2.00	180.62	180.12		N
2	PI-20/PI-21	54B	15.19	+1.50	180.12	179.62		N
2	PI-19	54B	15.19	+1.00	179.62	179.12		N
2	PI-17/PI-18	54B	15.19	+0.50	179.12	178.62		Y
2	PI-16	54B	15.19	0.00	178.62	178.12		Y
2	PI-24/PI-25	54B	15.19	-0.50	178.12	177.62		N
2	PI-26	54B	15.19	-1.00	177.62	177.12		N
2	PI-27	54B	15.19	-1.50	177.12	176.62		N
2	PI-28	54B	15.19	-2.00	176.62	176.12		N
2	PI-29	54B	15.19	-2.50	176.12	175.62		N
2	PI-23	54C	8.72	+2.50	180.61	180.19		N
2	PI-22	54C	8.72	+2.00	180.19	179.78		N
2	PI-20/PI-21	54C	8.72	+1.50	179.78	179.36		N
2	PI-19	54C	8.72	+1.00	179.36	178.95		N
2	PI-17/PI-18	54C	8.72	+0.50	178.95	178.53		Y
2	PI-16	54C	8.72	0.00	178.53	178.12		N
2	PI-24/PI-25	54C	8.72	-0.50	178.12	177.70		N
2	PI-26	54C	8.72	-1.00	177.70	177.29		N
2	PI-27	54C	8.72	-1.50	177.29	176.87		N
2	PI-28	54C	8.72	-2.00	176.87	176.46		N
2	PI-29	54C	8.72	-2.50	176.46	176.05		N

Table 3-7(c) Summary of intervals tested using pulse interference tests.

Set	Test ID	Borehole	Distance	Position	Interval		2b _{ch}	Response
			(m)		(masl)		(um)	
3	source				177.42	177.02		N
3	PI-31	54A	7.1	+0.50	177.95	177.53		N
3	PI-30	54A	7.1	0.00	177.53	177.12		N
3	PI-31	54B	15.5	+0.50	178.12	177.62		N
3	PI-30	54B	15.5	0.00	177.62	177.12		N
3	PI-31	54C	7.2	+0.50	177.70	177.29		N
3	PI-30	54C	7.2	0.00	177.29	176.87		N
4	source				168.41	168.00		N
4	PI-41	54A	10.1	+3.0	169.61	169.19		N
4	PI-40	54A	10.1	+2.50	169.19	168.78		N
4	PI-39	54A	10.1	+2.00	168.78	168.36		N
4	PI-38	54A	10.1	+1.50	168.36	167.94		N
4	PI-37	54A	10.1	+1.00	167.94	167.53		N
4	PI-32	54A	10.1	0.00	167.11	166.69		N
4	PI-33	54A	10.1	-0.50	166.69	166.27		N
4	PI-34	54A	10.1	-1.00	166.27	165.86		N
4	PI-35	54A	10.1	-1.50	165.86	165.44		N
4	PI-36	54A	10.1	-2.00	165.44	165.02		N
4	PI-39,40,41	54B	18.7	+2.00	170.12	169.62		N
4	PI-38	54B	18.7	+1.50	169.62	169.12		N
4	PI-37	54B	18.7	+1.00	169.12	168.62		N
4	PI-36	54B	18.7	+0.50	168.62	168.12		N
4	PI-32	54B	18.7	0.00	168.12	167.62		N
4	PI-33	54B	18.7	-1.00	167.12	166.62		N
4	PI-34	54B	18.7	-1.50	166.62	166.12		N
4	PI-35	54B	18.7	-2.00	166.12	165.62		N
4	PI-40,41	54C	6.0	+0.50	170.66	170.24		N
4	PI-32	54C	6.0	0.00	170.24	169.83		N
4	PI-39	54C	6.0	-0.50	169.83	169.41		N
4	PI-38	54C	6.0	-1.00	169.41	169.00		N
4	PI-37	54C	6.0	-1.50	169.00	168.58		N
4	PI-36	54C	6.0	-2.00	168.58	168.17		N
4	PI-35	54C	6.0	-2.50	168.17	167.76		N
4	PI-33	54C	6.0	-3.0	167.76	167.34		N
4	PI-34	54C	6.0	-3.5	167.34	166.93		N

Table 3.7(d) Summary of intervals tested using pulse interference tests.

Set	Test ID	Borehole	Distance (m)	Position	Interval (masl)		$2b_{ch}$ (μm)	Response
5	Source				167.59	167.19		N
5	PI-42	54A	10.9	+3.0	169.61	169.19		N
5	PI-43	54A	10.9	+2.50	169.19	168.78		N
5	PI-44	54A	10.9	+2.00	168.78	168.36		N
5	PI-45	54A	10.9	+1.50	168.36	167.94		N
5	PI-46	54A	10.9	+1.00	167.94	167.53		N
5	PI-47	54A	10.9	+0.5	167.53	167.11		N
5	PI-48	54A	10.9	0.00	167.11	166.69		N
5	PI-49	54A	10.9	-0.50	166.69	166.27		N
5	PI-50	54A	10.9	-1.00	166.27	165.86		N
5	PI-51	54A	10.9	-1.50	165.86	165.44		N
5	PI-42	54B	19.1	+2.00	170.12	169.62		N
5	PI-43	54B	19.1	+1.50	169.62	169.12		N
5	PI-44	54B	19.1	+1.00	169.12	168.62		N
5	PI-45	54B	19.1	+0.50	168.62	168.12		N
5	PI-46	54B	19.1	0.00	168.12	167.62		N
5	PI-47	54B	19.1	-0.50	167.62	167.12		N
5	PI-48	54B	19.1	-1.00	167.12	166.62		N
5	PI-49	54B	19.1	-1.50	166.62	166.12		N
5	PI-50	54B	19.1	-2.00	166.12	165.62		N
5	PI-51	54B	19.1	-2.50	165.62	165.12		N
5	PI-42	54C	7.0	+0.50	170.66	170.24		N
5	PI-43	54C	7.0	0.00	170.24	169.83		N
5	PI-44	54C	7.0	-0.50	169.83	169.41		N
5	PI-45	54C	7.0	-1.00	169.41	169.00		N
5	PI-46	54C	7.0	-1.50	169.00	168.58		N
5	PI-47	54C	7.0	-2.00	168.58	168.17		N
5	PI-48	54C	7.0	-2.50	168.17	167.76		N
5	PI-49	54C	7.0	-3.0	167.76	167.34		N
5	PI-50	54C	7.0	-3.5	167.34	166.93		N
5	PI-51	54C	7.0	-4.0	166.93	166.51		N

Table 3.8 Results of time-lag interpretation of pulse interference tests.

Set #	Test ID	Source Interval	$2b_{ch}$	T_{ch}	Observation Interval	$2b_{ch}$ (μm)	T_{ch} (m^2/s)	Distance (m)	t_{peak} (s)	Δh_{DO}	T_{pulse} (m^2/s)	$2b_{pulse}$ (μm)	S		
1	PI-1	180.70 180.29	510	8.E-05	54B	180.62	180.12	320	2.E-05	14.8	7	0.02707	6.E-04	993	3.E-05
	PI-1	180.70 180.29	510	8.E-05	54A	180.43	180.02	638	2.E-04	9.4	13	0.00264			
	PI-1	180.70 180.29	510	8.E-05	54C	180.61	180.19	391	4.E-05	11.3	15	0.00842	6.E-04	1020	2.E-04
	PI-3	180.70 180.29	510	8.E-05	54A	180.02	179.60	577	1.E-04	9.4	10	0.01613	6.E-04	986	1.E-04
	PI-3	180.70 180.29	510	8.E-05	54B	180.12	179.62	34	2.E-08	14.8	25	0.00063			
	PI-9	180.70 180.29	510	8.E-05	54C	181.02	180.61	47	6.E-08	11.3	22	0.0145	3.E-04	779	1.E-04
2	PI-17	178.65 178.24	227	7.E-06	54A	179.20	178.78	65	2.E-07	7.8	636	0.01151	1.E-05	271	3.E-04
		178.65 178.24	227	7.E-06	54B	179.12	178.62	167	3.E-06	15.2	335	0.08697	4.E-06	184	2.E-06
		178.65 178.24	227	7.E-06	54C	178.95	178.53	200	5.E-06	8.7	432	0.03978	6.E-06	216	4.E-05
2	PI-16	178.65 178.24	227	7.E-06	54A	178.78	178.37	138	2.E-06	7.8	715	0.0125	8.E-06	243	3.E-04
		178.65 178.24	227	7.E-06	54B	178.62	178.12	29	1.E-08	15.2	364	0.08479	4.E-06	187	3.E-06
2	PI-25	178.65 178.24	227	7.E-06	54A	178.37	177.95	222	6.E-06	7.8	525	0.02536	6.E-07	101	1.E-05

Table 3.9 Summary of results of pumping tests conducted at south cluster site.

Test ID	Bore-hole	Date	Interval (masl)		Q (L/min)	r (m)	r/L	T (m ² /s)	S	T _v (m ² /s)
1	55	28-Oct-97	178.29	176.36	6.2	30.41	0.08	5.E-05	3.E-06	5.E-09
1	56	28-Oct-97	176.77	175.55	6.2					
1	57	28-Oct-97	177.03	175.25	6.2	17.16	0.07	5.E-05	5.E-06	1.E-08
1	58	28-Oct-97	176.54	175.29	6.2	36.1	0.07	5.E-05	1.E-06	3.E-09
1	59	28-Oct-97	177.10	175.32	6.2	36.73	0.08	5.E-05	2.E-06	4.E-09
2	55	03-Nov-97	178.29	176.36	8	22.33	0.05	5.E-05	4.E-06	4.E-09
2	56	03-Nov-97	176.77	175.52	8	26.09	0.05	5.E-05	3.E-06	3.E-09
2	57	03-Nov-97	177.03	175.25	8	20.27	0.08	5.E-05	5.E-06	1.E-08
2	58	03-Nov-97	176.54	175.33	8					
2	59	03-Nov-97	177.10	175.32	8	7.01	0.06	5.E-05	3.E-05	6.E-08

Table 3.10(a) Summary of Westbay monitoring intervals.

Monitor	Installation Date	Interval (masl)	Length (m)	Monitor	Installation Date	Interval (masl)	Length (m)		
53-1	Aug-96	141.73	138.96	2.77	62-1	Aug-96	154.49	151.36	3.13
53-2	Aug-96	145.50	142.48	3.02	62-2	Aug-96	163.14	155.23	7.91
53-3	Aug-96	150.53	146.26	4.28	62-3	Aug-96	170.56	163.88	6.67
53-4	Aug-96	156.82	151.29	5.54	62-4	Aug-96	173.44	171.30	2.14
53-5	Aug-96	161.85	157.58	4.28	62-5	Aug-96	195.45	175.01	20.44
53-6	Aug-96	166.89	162.61	4.28	63-1	Jul-97	152.20	150.70	1.50
53-7	Aug-96	173.18	167.64	5.54	63-2	Jul-97	160.60	153.39	7.21
53-8	Aug-96	175.69	173.93	1.76	63-3	Jul-97	166.74	161.58	5.16
53-9	Aug-96	191.75	176.45	15.30	63-4	Jul-97	170.43	167.73	2.70
60-1	Aug-96	155.84	153.02	2.82	63-5	Jul-97	173.71	171.41	2.29
60-2	Aug-96	159.15	156.58	2.57	63-6	Jul-97	178.62	174.69	3.93
60-3	Aug-96	167.44	159.90	7.54	63-7	Jul-97	194.35	179.60	14.75
60-4	Aug-96	174.91	168.19	6.72	65-1	Jul-97	147.96	145.59	2.37
60-5	Aug-96	182.37	175.65	6.72	65-2	Jul-97	152.46	149.16	3.30
60-6	Aug-96	197.04	183.11	13.93	65-3	Jul-97	157.96	153.66	4.30
61-1	Aug-96	141.12	138.41	2.70	65-4	Jul-97	163.46	159.16	4.30
61-2	Aug-96	144.80	141.85	2.95	65-5	Jul-97	173.96	164.66	9.30
61-3	Aug-96	150.95	145.54	5.41	65-6	Jul-97	180.46	175.16	5.30
61-4	Aug-96	154.63	151.68	2.95	65-7	Jul-97	187.16	181.66	5.50
61-5	Aug-96	164.46	155.37	9.09					
61-6	Aug-96	169.38	165.20	4.18					
61-7	Aug-96	174.29	170.12	4.18					
61-8	Aug-96	182.24	175.03	7.21					

Table 3.10(b) Summary of multi-level monitoring intervals.

Monitor	Borehole	Installation Date	Interval (masl)		Length (m)
11A	11	Jun-87	145.62	139.79	5.83
11B	11	Jun-87	155.42	149.22	6.20
11C	11	Jun-87	160.42	157.02	3.40
11D	11	Jun-87	168.32	166.52	1.80
11E	11	Jun-87	176.82	172.02	4.80
11F	11	Jun-87	184.72	181.62	3.10
12A	12	Jul-87	142.6	137.27	5.33
12B	12	Jul-87	152.8	145.9	6.90
12C	12	Jul-87	160.2	154.5	5.70
12D	12	Jul-87	171.4	166.5	4.90
12E	12	Jul-87	180.3	176.2	4.10
21A	21	Jul-87	131.15	128.08	3.07
21B	21	Jul-87	144.45	140.25	4.20
21C	21	Jul-87	154.35	148.35	6.00
21D	21	Jul-87	164.55	158.15	6.40
21E	21	Jul-87	173.35	169.95	3.40
21F	21	Jul-87	180.05	176.35	3.70

Table 3.11 Summary of temporary monitors in new boreholes.

Monitor	Borehole	Installation Date ¹	Status ²	Interval ³ (masl)		Length (m)
34C-TL	34C	Jan-97	N	173.33	165.07	8.26
37C-TL	37C	May-96	N	173.06	164.99	8.07
37C-TU	37C	Jan-97	N	182.39	173.88	8.51
53-TL	53	May-96	N	172.17	163.91	8.26
54A-TL	54A	May-96	Y	175.44	167.22	8.21
54A-TU	54A	May-96	Y	188.66	176.27	12.38
54B-TL	54B	May-96	Y	171.22	161.37	9.85
54B-TU	54B	Oct-97	Y	188.51	172.22	16.29
54C-TL	54C	May-96	Y	175.30	167.13	8.17
54C-TU	54C	Jan-97	Y	188.80	176.13	12.67
54D-TL	54D	May-96	Y	175.46	167.39	8.07
54D-TU	54D	Oct-97	Y	188.06	176.28	11.78
55-TL	55	May-96	Y	173.34	165.08	8.26
56-TL	56	May-96	Y	173.31	165.05	8.26
57-TL	57	Jan-97	Y	173.38	165.21	8.17
58-TL	58	Jan-97	Y	173.73	165.61	8.12
59-TL	59	Jan-97	Y	173.45	165.28	8.17
59-TU	59	Dec-97	N	184.29	174.28	10.01

¹Approximate date of installation

²Status at time of completion of study. Y-monitor still installed, N-monitor not installed

³For upper zones (ie. TU) bedrock contact taken as top of interval.

Table 3.12 Summary of inorganic analyses in groundwater obtained from Westbay monitoring intervals.

Monitor	pH	Eh (mV)	Alkalinity (mg/L CaCO ₃)	Ca (mg/L)	Mg (mg/L)	Na (mg/L)	K (mg/L)	Fe (mg/L)	SO ₄ (mg/L)	Cl (mg/L)	HS (mg/L)	SiO ₂ (mg/L)
53-9	6.9	320	300	268	477	127	7.00	1.67	2810	64.2	0.00	16.3
53-8	7.2	259	160	214	72	32.2	2.40	0.35	628	6.70	0.02	12.7
53-7	7.2	195	125	132	97	41.0	2.60	0.46	519	16.2	0.00	13.3
53-6	7.2	29	257	250	125	53	4.20	0.16	847	34.7	0.79	12.9
53-5	7.3	-30	138	662	178	451	25.3	0.13	1840	1290	3.42	7.46
53-4	6.6	-100	209	558	154	116	12.5	0.09	2105	216	4.48	7.06
53-3	7.0	-80	127	575	153	206	10.5	0.07	1920	514	5.86	8.32
53-2	6.9	-94	292	663	164	407	5.91	0.05	1495	1061	5.56	8.50
53-1	6.3	-103	180	2900	847	7000	137	0.05	1457	18917	5.68	26.4
60-6	6.9	98	400	400	520	260	5.70	10.60	2943	19.4	0.09	15.9
60-5	7.2	155	291	140	110	31.3	2.20	0.01	616	11.4	0.04	13.0
60-4	7.0	-78	234	338	136	119	8.10	0.05	1185	315	5.81	10.2
60-3	7.1	-53	248	173	122	51.9	5.20	0.09	794	72.5	2.31	12.7
60-2	7.0	93	268	342	90	45.1	5.40	1.13	1172	80.6	0.27	13.7
60-1	7.0	-62	255	507	127	370	19.3	0.06	1679	864	3.64	11.7
61-8	7.0	-9	300	248	285	92.9	6.20	1.00	1430	34.8	0.29	14.9
61-7	6.9	-13	310	387	83	44.4	4.40	0.09	1265	58.0	3.35	12.5
61-6	7.0	-25	218	447	103	56	3.80	0.06	1120	56.5	3.07	12.3
61-5	7.0	-22	237	278	112	51.7	4.00	0.03	763	38.7	1.77	12.8
61-4	6.9	-65	204	465	91	70.8	6.50	0.06	1443	163	6.13	9.83
61-3	6.8	-63	232	538	121	127	6.90	0.07	1450	373	5.81	9.38
61-2	7.0	-28	230	562	107	100	6.70	0.09	1678	224	2.13	11.0
61-1	7.1	10	231	600	125	324	13.7	2.08	1196	1025	0.13	9.42
62-5	7.4	118	285	392	341	129	5.00	9.69	2270	164	0.00	12.7
62-4	7.7	47	245	551	197	85.0	10.2	5.20	2350	75.2	0.00	7.46
62-3	7.1	-92	206	537	127	36.0	10.2	0.05	1745	44.5	5.35	7.90
62-2	7.1	-95	176	520	120	30.4	7.70	0.06	1933	67.5	5.11	7.41
62-1	7.6	28	204	710	238	704	25.5	4.52	1903	1654	-	7.42

Table 3.12. (Cont'd) Summary of inorganic analyses in groundwater obtained from Westbay monitoring intervals

Monitor	pH	Eh (mV)	Alkalinity (mg/L CaCO ₃)	Ca (mg/L)	Mg (mg/L)	Na (mg/L)	K (mg/L)	Fe (mg/L)	SO ₄ (mg/L)	Cl (mg/L)	HS (mg/L)	SiO ₂ (mg/L)
63-6	7.3	162	214	149	177	65	2.80	1.83	672	11.1	0.01	14.5
63-5	7.3	153	204	139	167	53.9	2.60	1.7	742	14.3	0.00	13.9
63-4	6.9	103	224	376	88.7	32.4	4.50	1.77	1310	17.4	0.02	13.0
63-3	7.3	92	231	352	129	43.1	4.40	5.95	1334	31.1	0.12	11.8
63-2	7.3	101	216	323	117	39.1	4.50	5.43	923	37.4	0.10	11.9
63-1	7.3	94	193	359	134	43.5	4.30	3.38	1176	31.0	0.22	11.1
65-6	7.1	14	204	114	86	32.0	2.60	0.232	418	8.2	0.76	15.6
65-5	7.0	179	229	268	170	72.0	5.40	2.98	912	70.0	0.49	12.9
65-4	6.9	-115	177	753	191	624	32.0	0.053	1390	1410	4.93	6.84
65-3	6.9	-80	-	1010	273	1500	31.6	0.045	1440	1300	4.42	6.24
65-2	6.7	-105	145	798	225	2190	42.6	0.049	1450	5490	3.56	6.27
65-1	6.8	-105	144	1650	340	2900	57.1	0.051	1280	7700	-	6.65

Table 3.13 Summary of isotope analyses in Westbay monitoring intervals.

Sample I.D.	Monitor	$\delta^{18}\text{O}$ (‰)	$\delta^2\text{H}$ (‰)	^3H (direct) (TU +/-8)	^3H (enriched) (TU)
BH60-15	60-6	-9.82	-61.92	22	-
BH60-18	60-5	-10.26	-66.82	10	-
BH60-27	60-4	-11.08	-71.87	6	3.3 +/-0.6
BH60-36	60-3	-10.61	-69.98	29	0.8 +/- 0.5
BH60-46	60-2	-10.33	-67.01	<6	-
BH60-50	60-1	-10.98	-71.92	8	4.4 +/-0.6
BH62-23	62-5	-9.7	-60.8	18	-
BH62-26	62-4	-10.26	-56.12	-	5.0 +/-0.7
BH62-30.5	62-3	-10.8	-70.75	8	1.5 +/-1.0
BH62-39.5	62-2	-9.99	-66.21	10	1.6 +/-1.0
BH62-50	62-1	-10.96	-69.32	<6	-
BH53-16.5	53-9	-9.83	-63.23	<6	-
BH53-19.5	53-8	-10.51	-69.47	<6	-
BH53-22.5	53-7	-14.4	-70.97	<6	6.5 +/- 0.7
BH53-30	53-6	-10.25	-68.89	<6	6.3 +/-0.8
BH53-36	53-5	-13.03	-84.83	-	1.6 +/-0.6
BH53-42	53-4	-14.87	-104.29	<6	1.3 +/- 0.5
BH53-49.5	53-3	-13.94	-80.63	<6	31.0 +/- 2.2
BH53-55.5	53-2	-12.22	-84.22	<6	<0.8 +/-0.5
BH53-60	53-1	-13.54	-96.37	<6	-
BH61-7	61-8	-10.01	-64.22	17	-
BH61-10	61-7	-10.52	-65.63	<6	-
BH61-16	61-6	-10.5	-70.09	<6	1.6 +/-0.5
BH61-22	61-5	-10.38	-64.27	15	-
BH61-34	61-4	-10.91	-73.53	<6	-
BH61-37.5	61-3	-10.59	-70.92	<6	<0.8 +/-0.6
BH61-46	61-2	-10.8	-72.88	<6	2.4 +/- 0.6
BH61-51	61-1	-10.86	-72.21	<6	-
BH63-15	63-6	-10.32	-56.92	<6	1.4 +/-0.5
BH63-19.5	63-5	-10.15	-63.44	7	2.4 +/-1.1
BH63-25.5	63-4	-10.18	-64.66	15	4.8 +/-1.3
BH63-29.5	63-3	-10.17	-65.94	7	3.4 +/-1.1
BH63-34	63-2	-10.3	-50.73	<6	2.6 +/-0.5
BH63-41.5	63-1	-10.25	-53.43	<6	-
BH65-4	65-7	-6.9	-52.08	65	-
BH65-7	65-6	-9.91	-68.27	<6	-
BH65-13.5	65-5	-10.08	-66.91	<6	6.9 +/-0.7
BH65-24	65-4	-16.07	-107.72	<6	-
BH65-29.5	65-3	-15.21	-104.15	-	0.9 +/- 0.5
BH65-35	65-2	-15.01	-105.97	8	3.8 +/-1.3
BH65-39	65-1	-14.24	-101.05	<6	-

Table 3.14 Summary of isotopic analyses from multilevel monitoring intervals.

Sample I.D.	Monitor	$\delta^{18}\text{O}$ (‰)	$\delta^2\text{H}$ (‰)	^3H (direct) (TU +/-8)
BH11a	11A	-11.63	-75.69	<6
BH11c	11B	-11.21	-72.43	<6
BH11d	11C	-10.55	-68.94	<6
BH11e	11D	-10.68	-67.56	11
BH11f	11E	-10.33	-64.5	10
BH21a	21A	-13.08	-89.19	<6
BH21b	21B	-13.11	-88.47	<6
BH21c	21C	-12.96	-87.77	<6
BH21d	21D	-11.69	-73.23	<6
BH21e	21E	-10.43	-69.74	9
BH21f	21F	-10.39	-67.95	<6
BH12a	12A	-14.54	-98.19	<6
BH12b	12B	-14.49	-98.44	<6
BH12c	12C	-10.97	-71.63	<6
BH12d	12D	-10.5	-67.43	<6
BH12e	12E	-10.23	-63.69	<6
River Water by 61		-12.39	-87.31	16
River Water by 65		-8.6	-62.78	10
Injection Water during tracer test, Oct 98 (hydrant water)				68

Table 3.15 Results of point dilution experiments.

Borehole Test ID	Date	Interval* (masl)	Midpoint (masl)	Fracture Geometry	2b (μm)	v_{pd} (m/day)		
37C	3.5	10-Mar-96	178.5	Single	425	33		
37C	3.6	17-Oct-96	178.5	Single	425	35.2		
37C	3.8	16-Dec-96	180.4	Dual	544/ 606	10.5 & 10.5 [#]		
37C	3.11b	17-Dec-96	180.4	Dual	544/ 606	6.6 & 6.6 [#]		
56	1	09-Jun-98	182.12	181.91	182.02	Single	1095	8
54A	2	08-Oct-98	180.13	179.92	180.03	Single	909	40
59	3	14-Oct-98	182.1	181.9	182.00	Single	1400	3
59	4	19-Oct-98	181.9	181.69	181.80	Single	136	4
59	5	21-Oct-98	180.45	180.24	180.35	Single	2444	21

*Intervals used in 37C are not known (only fracture location recorded).

[#]Assumes equal velocity in each of the two fractures.

Table 3.16 Summary of parameter values obtained for final fits to model. The fits were obtained under the constraint of a natural flow field oriented parallel to the trajectory between the two boreholes.

Experiment	2b (μm)	α_L	$\theta_m(D^*)^{1/2}$ ($\text{m}/\text{t}^{1/2}$)	θ_m^{-1}	v (m/day)
I (Peak Normalized)	697	0.18	1.5e-6	0.11	30
II (Peak Normalized)	918	0.31	1.5e-6	0.11	30

Table 3.17 Calculated parameters determined from the radial-divergent tracer experiments.

Borehole	Radial Distance (m)	Aperture (μm)	Dispersivity (m)	Matrix Porosity
59	30.9	1026	0.09	0.07
58	38.4	810	0.13	0.09
64	126.7	730	3.95	0.06

Table 3.18 Results of analyses of organic carbon on bulk rock samples.

	Organic Carbon (%) Range	Number of samples	Mean (%)
Eramosa	0.000 - 0.200	7	0.072
Vinemount	0.010 - 0.116	12	0.035
Goat Island	0.000 - 0.126	6	0.038
Gasport	0.000 - 0.040	5	0.027
Decew	0.014 - 0.041	2	0.028
Rochester	0.021 - 0.070	3	0.041
Glass Beads	0.001 - 0.014	4	0.005

Table 3.19 Results of analyses of organic carbon on stylolite samples.

	Organic Carbon (%) Range	Number of samples	Mean (%)
Vinemount	0.000 - 0.050	3	0.020
Goat Island	0.004 - 0.071	3	0.048
Gasport	0.000 - 0.045	6	0.014
Decew	0.000	1	0.000
Quarry Samples	.004 - 0.070	4	0.026

Table 3.20 Results of analyses of organic carbon on samples of argillaceous layers.

	Organic Carbon (%) Range	Number of samples	Mean (%)
Vinemount	0.016 - 4.001	3	2.545
Goat Island	0.026 - 5.261	3	3.104

Table 3.21 Calculated retardation factors for the matrix and example fracture (2b=500 μm).

	f_{oc}	Porosity	Gamma	TCE			TCB			TCE		TCB	
				LogK _{ow} ²	K _d (mL/g)	K _r (cm)	LogK _{ow} ²	K _d (mL/g)	K _r (cm)	R	R _r	R	R _r
Eramosa	0.00072	0.060	0.47	2.6	0.166	0.355	4.1	1.992	4.267	8	15	86	172
Vinemount	0.00035	0.048	0.37	2.6	0.081	0.216	4.1	0.968	2.593	5	10	53	105
Goat Island	0.00038	0.082	0.64	2.6	0.087	0.137	4.1	1.051	1.648	4	6	34	67
Gasport	0.00027	0.088	0.68	2.6	0.062	0.091	4.1	0.747	1.091	3	5	23	45
Arg. Bands ¹	0.03104	0.060	0.47	2.6	7.144	15.299	4.1	85.886	183.939	307	613	3680	7359

¹Porosity assumed

² Average value from Montgomery and Welkom, 1990.

A bulk density of 2.57 g/cm³ and a geometric factor of 0.1 were used for all calculations.

Table 3.22 Summary of diffusion experiment results.

Lithology	Cell	Bromide			Second Tracer			Gravimetric Porosity	Calculated Porosity
		Effective Porosity	Effective Diffusivity (cm ² /day)	Geometric Factor	Effective Porosity	Effective Diffusivity (cm ² /day)	Geometric Factor		
Eramosa	cell 6	0.090	0.14	0.078	0.090	0.11	0.067	0.078	0.080
	ER-1	0.046	0.14	0.078	0.046	0.07	0.107	0.045	0.040
	E2-3	0.082	0.65	0.362	0.094	0.20	0.304	0.078	0.073
	E2-2	0.058	0.15	0.083	0.046	0.15	0.228	0.057	0.053
	jun4e1	0.094	0.09	0.050	0.082	0.07	0.107	0.076	0.086
	jun4e2	0.070	0.09	0.050	0.058	0.09	0.137	0.055	0.062
Vinemount	cell 9	0.080	0.17	0.095				0.102	0.073
	cell A	0.050	0.13	0.072	0.050	0.10	0.100	0.037	0.045
	cell B	0.060	0.16	0.089	0.050	0.09	0.090	0.032	0.054
	V1	0.040	0.19	0.106	0.064	0.08	0.080	0.026	0.036
	jun4v21	0.070	0.10	0.056	0.058	0.09	0.137	0.065	0.064
	jun4vi1	0.058	0.15	0.083	0.046	0.18	0.274	0.055	0.053
Goat island	cell 1	0.110	0.18	0.100				0.082	0.099
	GI-1	0.118	0.24	0.134	0.106	0.12	0.183	0.114	0.108
	jun5gi1	0.094	0.11	0.061	0.094	0.06	0.091	0.081	0.087
	jun5gi2	0.094	0.18	0.100	0.094	0.10	0.152	0.082	0.084
Gasport	cell 10	0.110	0.58	0.323				0.157	0.100
	G3	0.094	0.08	0.045	0.082	0.22	0.335	0.068	0.080
	GA-1	0.082	0.16	0.089	0.082	0.07	0.107	0.089	0.075
	GA-2	0.046	0.12	0.067	0.046	0.06	0.091	0.060	0.042
	jun5ga1	0.082	0.08	0.045	0.082	0.04	0.061	0.068	0.075
	Mean		0.078		0.103	0.071		0.147	0.072

Table 3.23. Summary of all measured porosity values

	N	porosity		
		minimum	maximum	mean
Eramosa	358	0.010	0.197	0.065
Vinemount	9	0.024	0.102	0.048
Goat Island	10	0.061	0.114	0.082
Gasport	12	0.058	0.157	0.088
Rochester	4	0.053	0.073	0.061

Table 3.24 Summary of all bulk density measurements.

	N	bulk density (g/cm ³)		
		minimum	maximum	mean
Eramosa	7	2.46	2.69	2.59
Vinemount Unit 1	2	2.55	2.78	2.68
Goat Island	5	2.35	2.61	2.51
Gasport	5	2.35	2.58	2.51
Rochester	3	2.46	2.63	2.57
Mean	22			2.57

Appendix A
Site Chronology of Events

**CWML SITE
SMITHVILLE, ONTARIO
CHRONOLOGY OF EVENTS**

Date	Description
1966	The site is purchased by the Township of South Grimsby (which later became the Township of West Lincoln). The site is part of the Smithville Industrial Park Development.
November 1969	Municipal Well No. 2 installed on south side of London Road about 500 m south of the present CWML facility.
1970	The Corporation of the Township of West Lincoln is formed.
1978	The site is purchased by Master Industrial and Engineered Services Ltd. (presumed owner of Chemical Waste Management Ltd.).
pre-1978	Air photographs indicate the site is agricultural and has not been actively farmed for at least 30 years.
June 1978	MOE awarded a Certificate of Approval to Chemical Waste Management Ltd. (CWML) for storage and transfer of PCB contaminated wastes at the site. CWML is a subsidiary of the D & D Group Ltd., run by Thomas (Rusty) Drew.
June 1978	McGlone & Associates Ltd. conducted a soils permeability investigation at the site, consisting of a single test pit at the location of a proposed storage tank.
1978-1985	Site received approximately 434,000 L of liquid wastes, including 266,000 L of PCB wastes, 57,000 L organic and chlorinated solvents, as well as acids, alkalis, other inorganic wastes, sludges. This information is from the MOE Transfers of Liquid Industrial Wastes Report.
April 1979	McGlone & Associates Ltd. conducted a brief geotechnical/hydrogeological investigation (3 boreholes) on-site.
1980	MOE installed 5 test wells (TW1/80 - TW5/80) to the base of the overburden, located north and south of the fenced compound. Soil and water samples from the wells were tested for PCBs and contained no detectable levels.
May 1980	The United States EPA effectively banned the import/export of PCBs.
Nov. 1983	The site is reported as being full, and then is maintained as a transfer station for PCBs shipped to Alberta.

**CWML SITE
SMITHVILLE, ONTARIO
CHRONOLOGY OF EVENTS**

Date	Description
May 1984	A PCB spill is reported in the parking lot west of the fenced compound. The spill was partly cleaned up, and the recovered waste stored in barrels on-site.
September 1984	A three member commission of the Environmental Assessment Board is established to hear briefings on a mobile incinerator for the site.
Spring 1985	The site Certificate of Approval is revised to permit only storage of wastes then located on the site.
March 1985	The St. Catharines Standard reports that D & D Group Ltd. has another abandoned site in Edmonton.
April 1985	The Globe and Mail reports that 180,000 L of PCBs are stored at the site.
July 1985	Local environmentalists (Help Eliminate Landfill Pollution) discover PCB oil in a shallow storm water lagoon at the site. (Sample obtained using a pail on a rope, thrown over the site fence). HELP chairman is Ken Durham, and Dr. Brindle from Brock University is involved with the group.
August 1985	MOE tested soil and water in the onsite retention lagoon. PCBs are detected in on-site and off-site soils. The St. Catharines Standard reports that the MOE has tested the municipal water supply and found no detection of PCBs.
September 1985	MOE announces the approval of PCB destruction using a mobile incineration unit.
October 1985	14 domestic wells north of the CWML site were sampled by the MOE, no PCBs were detected.
November/December 1985	72,000 L of PCB-contaminated sludge, oily water, and soil is removed from the on-site lagoon under MOE direction. (MOE subcontractors were Sanexen and Chemisolv).
December 1985	Gartner Lee Ltd. is retained by MOE to investigate potential off-site migration of contaminants. Seismic refraction survey conducted at site by Gartner Lee Ltd. to map the buried bedrock upper surface. Proctor and Redfern is retained by MOE as the project manager for site decommissioning.

**CWML SITE
SMITHVILLE, ONTARIO
CHRONOLOGY OF EVENTS**

Date	Description
December 1985 - ?	Proctor and Redfern made detailed inventory of wastes/materials on the site.
by March 1987	All remaining wastes at the site are placed in on-site secure storage; the south portion of the site covered by synthetic membrane.
March 1986	A conviction for the May 1984 spill is announced.
April 1986	A geophysical (seismic) survey is carried out to delineate the bedrock surface in site area, by Gartner Lee Ltd. Subsequently, an expanded seismic refraction survey is conducted at the site by Gartner Lee Ltd.
April 1986	Site reported to contain 2 upright tanks holding an estimated 180,000 L of PCBs, empty PCB contaminated drums, PCB solids, drained transformers.
May 1986	MOE and the Township of West Lincoln sign an agreement to clean up the site: start of the Phase II activities.
May - Aug 1986	Test pit investigation of gravel driveway on-site to investigate potential PCB spill area. Supervised by Gartner Lee Ltd.
June 1986	7 boreholes (GL1 to GL7) drilled under supervision by Gartner Lee Ltd. and grouted on completion of drilling.
July 1986	The original 5 MOE test wells (TW1/80 - TW5/80) are abandoned (overdrilled and grouted), under MOE supervision.
August 1986	A warehouse is constructed on site to store PCB wastes and materials.
November 1986 - April 1987	A deep bedrock drilling program at site (Boreholes 1 to 9) is conducted under supervision by Gartner Lee Ltd. Boreholes 1 - 4 instrumented with monitoring wells.
early February 1987	NAPL (30 - 50% PCB) is discovered in the open hole of Borehole 3, immediately east of the site.
February 1987	Detection of NAPL in the bedrock immediately east of the site (Borehole 3). Regional Municipality of Niagara Municipal Well #2 (located about 500 m south of site) is shut off as a precaution. No contamination detected at the well at that time.

**CWML SITE
SMITHVILLE, ONTARIO
CHRONOLOGY OF EVENTS**

Date	Description
March 1987	<p>Dissolved PCBs and TCBs are detected in deeper bedrock zones at locations between the site and RMON Municipal Well #2.</p> <p>Well #2 is ordered "permanently" shutdown.</p> <p>Impermeable synthetic membrane is temporarily placed on site.</p>
April - Dec 1987	<p>Regular meetings of the Citizen's Liaison Committee with MOE project team.</p>
May - December 1987	<p>Golder Associates Ltd. (GAL) field program GAL Phase I May - July 1987 GAL Phase II Oct - Dec 1987</p> <ul style="list-style-type: none"> • Installation of boreholes/wells: L1-L3, 3A-3C, 5B-5D, 7C, 7D, 10 - 32, P1-P20 • 2 short-term (2 hr) pumping tests at Municipal Well 2 • Pumping tests at wells 16,18,19,23 • Packer tests at boreholes 11, 12, 21 • Abandoned BH1 nest and installed new shallow well at BH1
June 1987	<p>The three "McGlone" boreholes are abandoned (overdrilled and grouted) under Golder Associates Ltd. supervision to ensure no downward contaminant movement through the boreholes. GAL reports no degradation of the integrity of the original borehole seals.</p> <p>Boreholes 5 - 9 (previously drilled under supervision of Gartner Lee Ltd.) are instrumented with monitoring wells under Golder Associates Ltd. supervision.</p>
April 1988	<p>Phase 4 program opened.</p> <p>Proctor and Redfern Ltd. assumes responsibility for monitoring private residences (sampling) from MOE.</p>

**CWML SITE
SMITHVILLE, ONTARIO
CHRONOLOGY OF EVENTS**

Date	Description
May - December 1988	<p>Golder Associates Ltd. Phase III field program:</p> <ul style="list-style-type: none"> • Construction and testing of: well nest 33; a shallow aquifer monitoring well network forming a ring around the study area (wells 30, 34, 36-40); deep aquifer monitoring wells beyond the limits of the study area (wells 45-48); "infill" monitoring wells for plume delineation (wells 41-44). • Drilling, packer testing, and construction of deep well nest 35. • Investigation of DNAPL contamination beneath the Quonset hut on-site. • pilot-scale pumping of four shallow monitoring wells, 3C, 14, 19, 23 (35 L of DNAPL recovered). Pumping through the summer and fall of 1988 removed 104,000 L of water from these wells. • 24 hr aquifer pumping test of the deep (Vinemount) aquifer (December 1988).
October 1988	ENSCO Inc. is awarded contract for on-site incineration of PCB wastes.
November 1988	<p>Presentation to MOE by Proctor and Redfern for installation of test shafts into the bedrock at the site. (This project never implemented).</p> <p>McGlone and Associates Ltd. perform a geotechnical investigation for an elevated tank on site, consisting of two boreholes (one borehole to bedrock surface, one borehole to three metres below bedrock surface.) Boreholes filled with concrete to 6.1 m below grade, then backfilled with cuttings. Two soil samples analyzed contained no detectable PCBs.</p>
January 1989 - September 1989	<p>Golder Associates Ltd. Phase IV field investigation:</p> <ul style="list-style-type: none"> • 3-day aquifer pumping test of the shallow (Eramosa) aquifer (pre-design studies for the shallow recovery well network) (January 1989). • construction of permanent shallow recovery well network, recovery wells RW1-RW8 (April 1989). • construction and testing of well nests south of municipal well #2 and west of Thompson Road (wells 49-52).
February 1989	Formation and initial meeting of the Smithville Bedrock Remediation Advisory Panel.

**CWML SITE
SMITHVILLE, ONTARIO
CHRONOLOGY OF EVENTS**

Date	Description
May 1989	Continuous operation of the shallow recovery well network begins.
June 1989	Smithville Bedrock Remediation Advisory Panel submits its report with two recommendations: immediate installation of containment pump and treat system, and managed program to evaluate containment and remedial strategies.
July 1989	The property is acquired by the Ontario Ministry of the Environment.
October 1989	8 recovery wells added to regular test well sampling program.
December 1989	Phase 1 and 2 programs officially closed.
April 1990	Transfer of site management to MOE from Proctor and Redfern Ltd. Ongoing activities supervised by MOE include: - groundwater monitoring program (samples collected from "early warning wells" and domestic wells) - surface water monitoring - maintenance of groundwater pumping program
Sept - November 1990	Upgrade of site groundwater collection system to permanent system. Thomas Environmental Ltd. under contract to operate the system.
October 1990	Field (drilling) investigation of contaminated soil underlying the lagoon area, conducted by Golder Associates Ltd. Site preparation activities for on-site PCB incineration begin.
February 1991 - December 1992	Continuous on-site incineration of PCBs. (Start of Phase III activities).
June 1991	Under MOE supervision, a test pit to the bedrock surface is excavated approximately 120 metres northeast of the site, and soil and bedrock surface are mapped.
July 1991 - October 1992	Approximately 2880 cubic metres of soil from the former lagoon area and 5320 cubic metres of surface soil are excavated and incinerated. The lagoon excavation is shored and left open to the bedrock surface. (Lagoon excavation size is 20.5 metres by 17.5 metres by 6 metres deep).

**CWML SITE
SMITHVILLE, ONTARIO
CHRONOLOGY OF EVENTS**

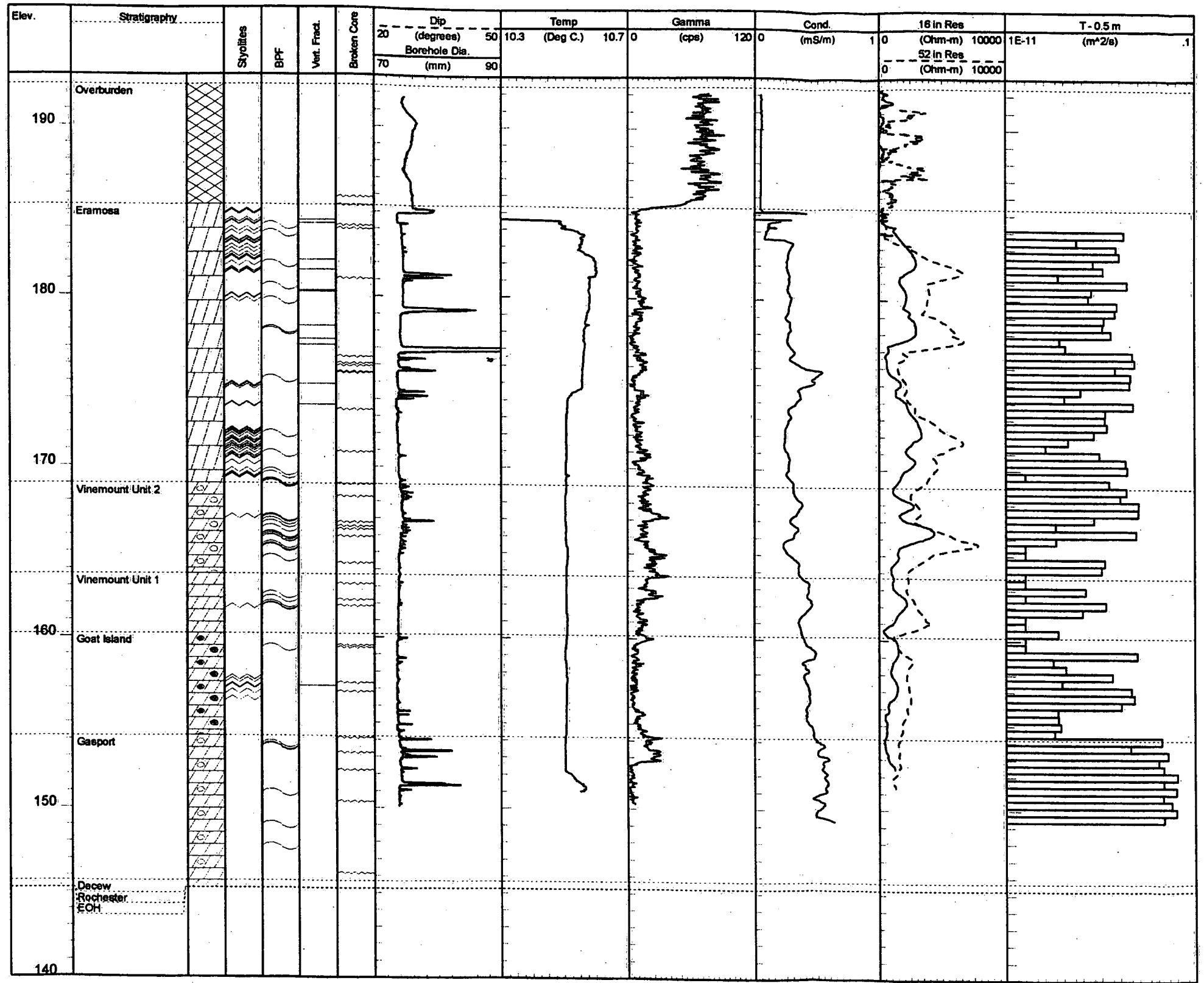
Page 7 of 7

Date	Description
December 1991 - December 1992	Decontamination of the onsite tank farm and the containment building.
July 1993	Formation of the Managing Board of Directors for the site is established by agreement between the MOEE and the Township of West Lincoln.
August 1993	Ground surface restoration at the site is complete.
November 1993	The Ontario Clean Water Agency is retained by the MOEE as the operating authority for site maintenance and monitoring activities.
1994	Smithville Phase IV Bedrock Remediation Program staff are appointed.
October 1994	Sanaxen is awarded a contract to operate the site water treatment system.

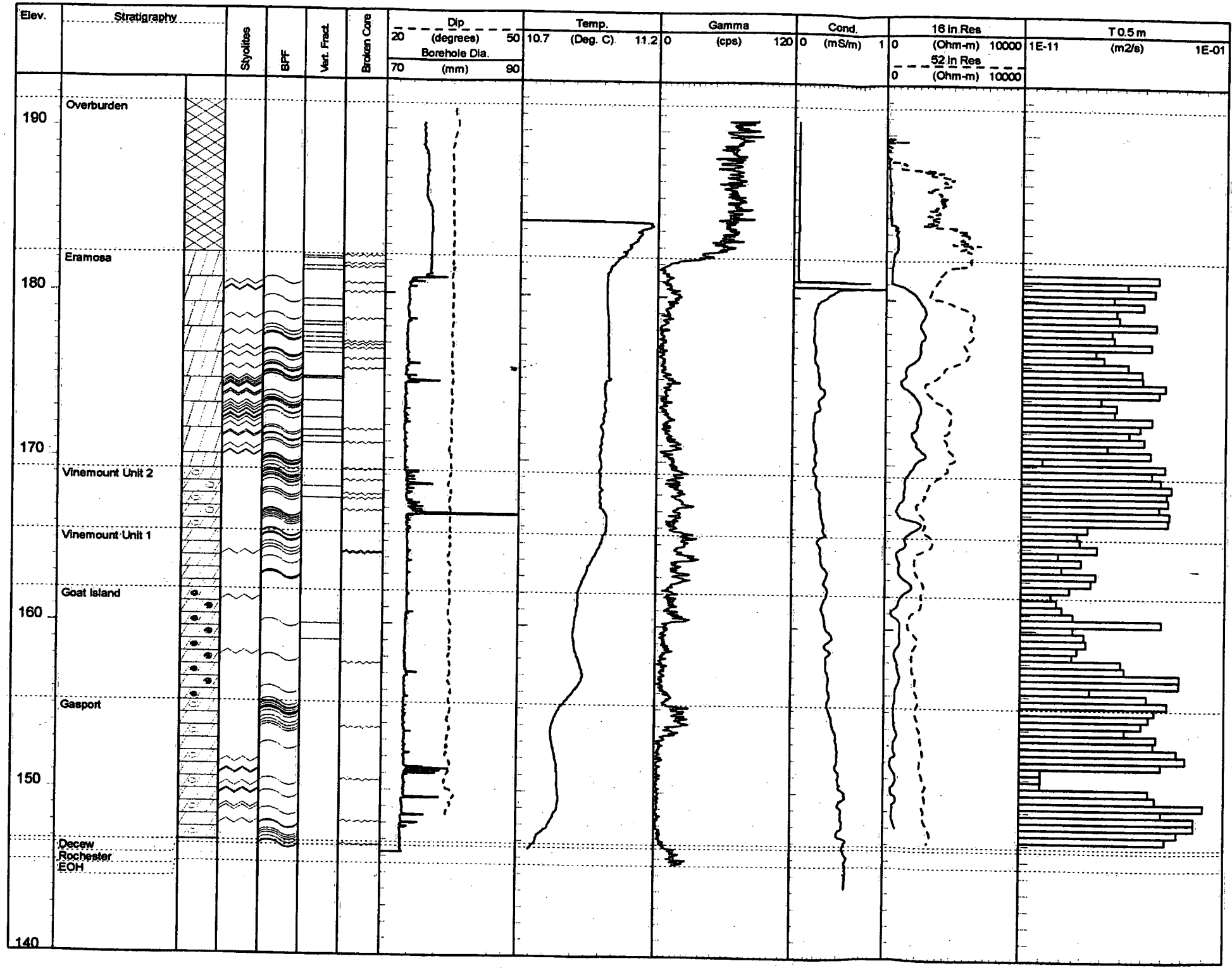
May 1995

941-9033

Appendix B
Composite Borehole Logs

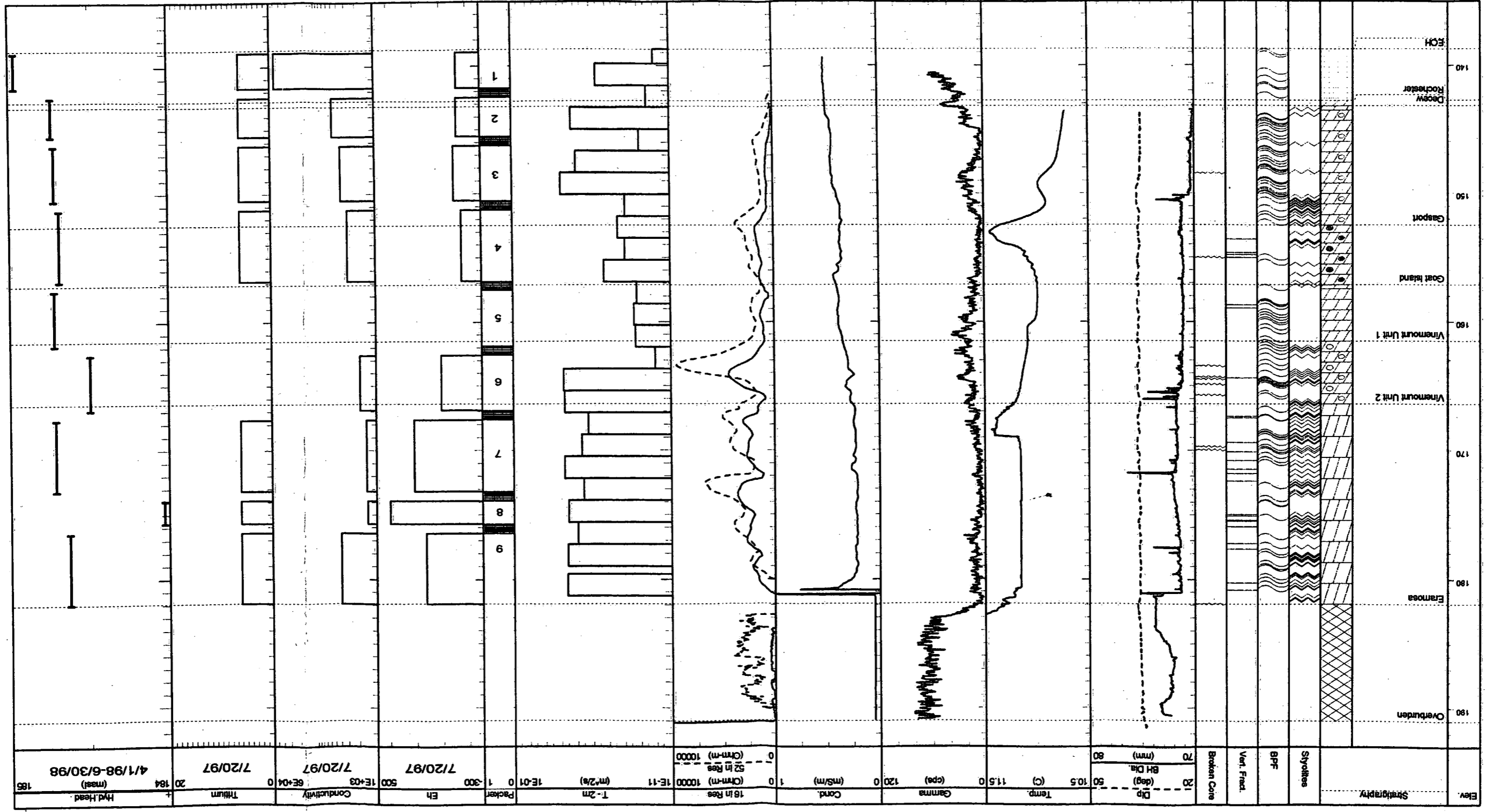


Borehole 34C
Reference Elevation: Top of Steel Casing - 192.94 masl
Borehole Azimuth: 115 deg. Borehole Dip: 57 deg.

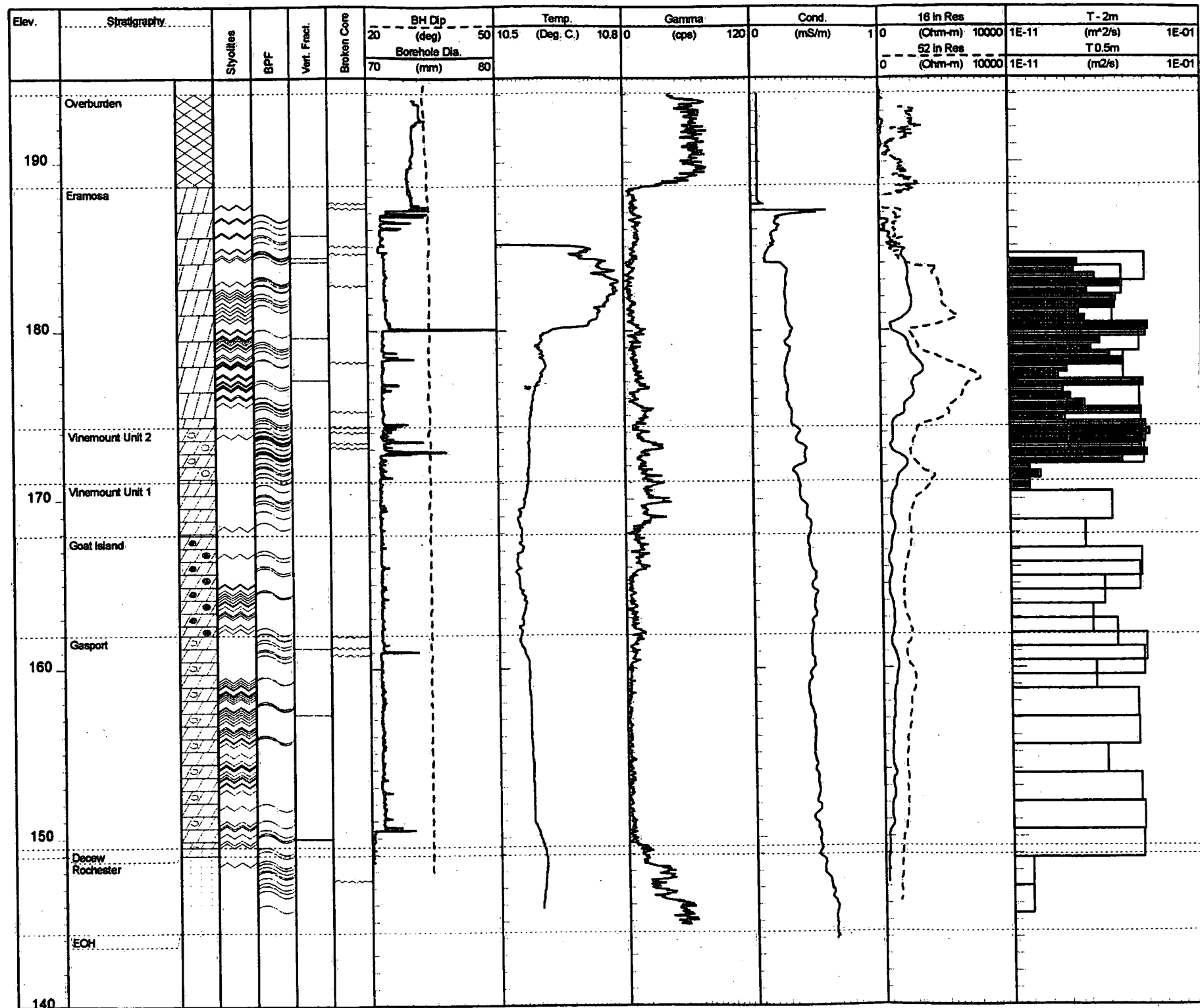


Borehole 37C
 Reference Elevation: Top of Steel Casing - 192.23 masl
 Borehole Azimuth: 0 deg. Borehole Dip: 55 deg.

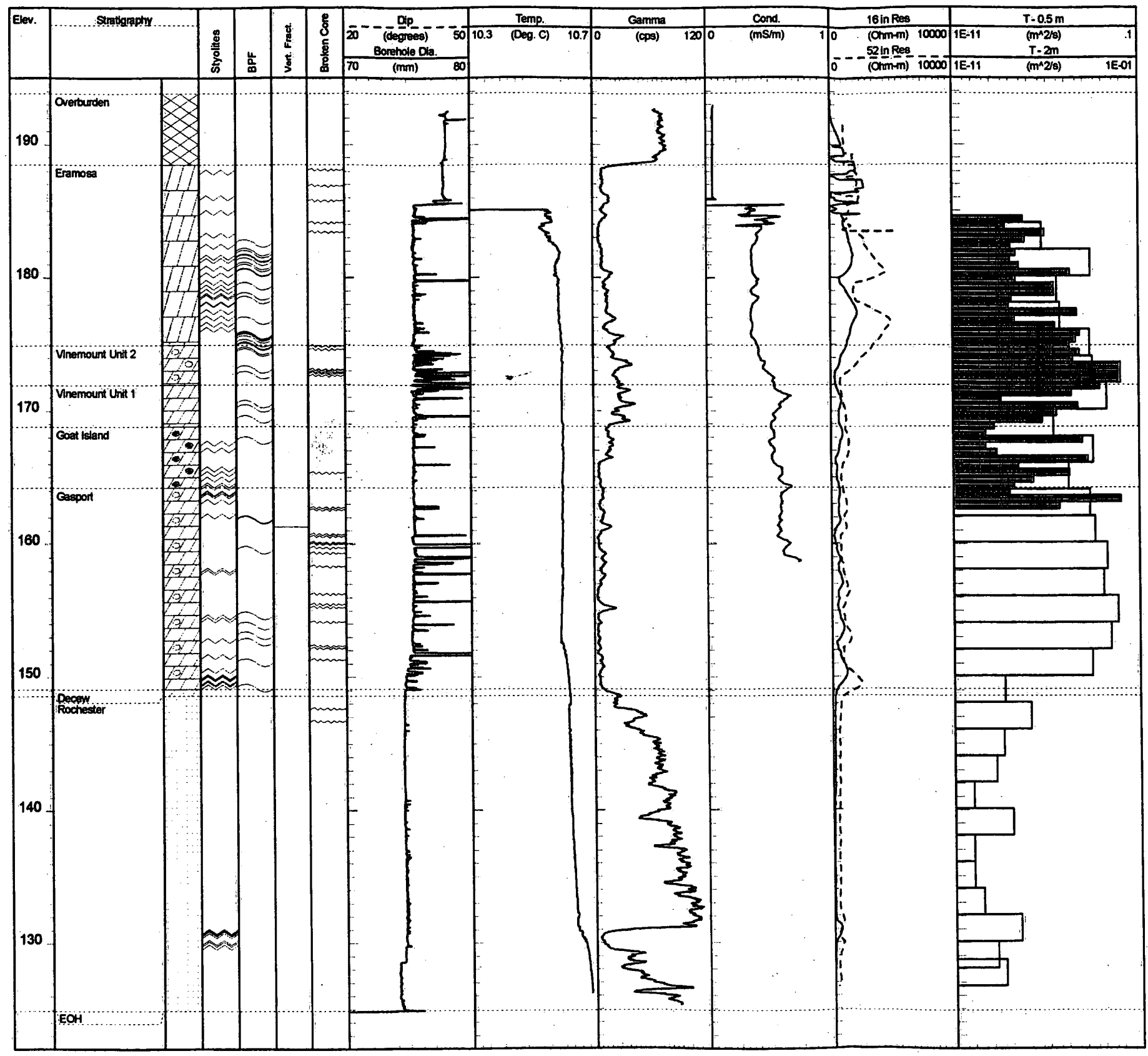
Borehole 53
 Reference Elevation: Top of Steel Casing - 191.76 masl
 Borehole Azimuth: 15 deg.
 Borehole Dip: 57 deg.



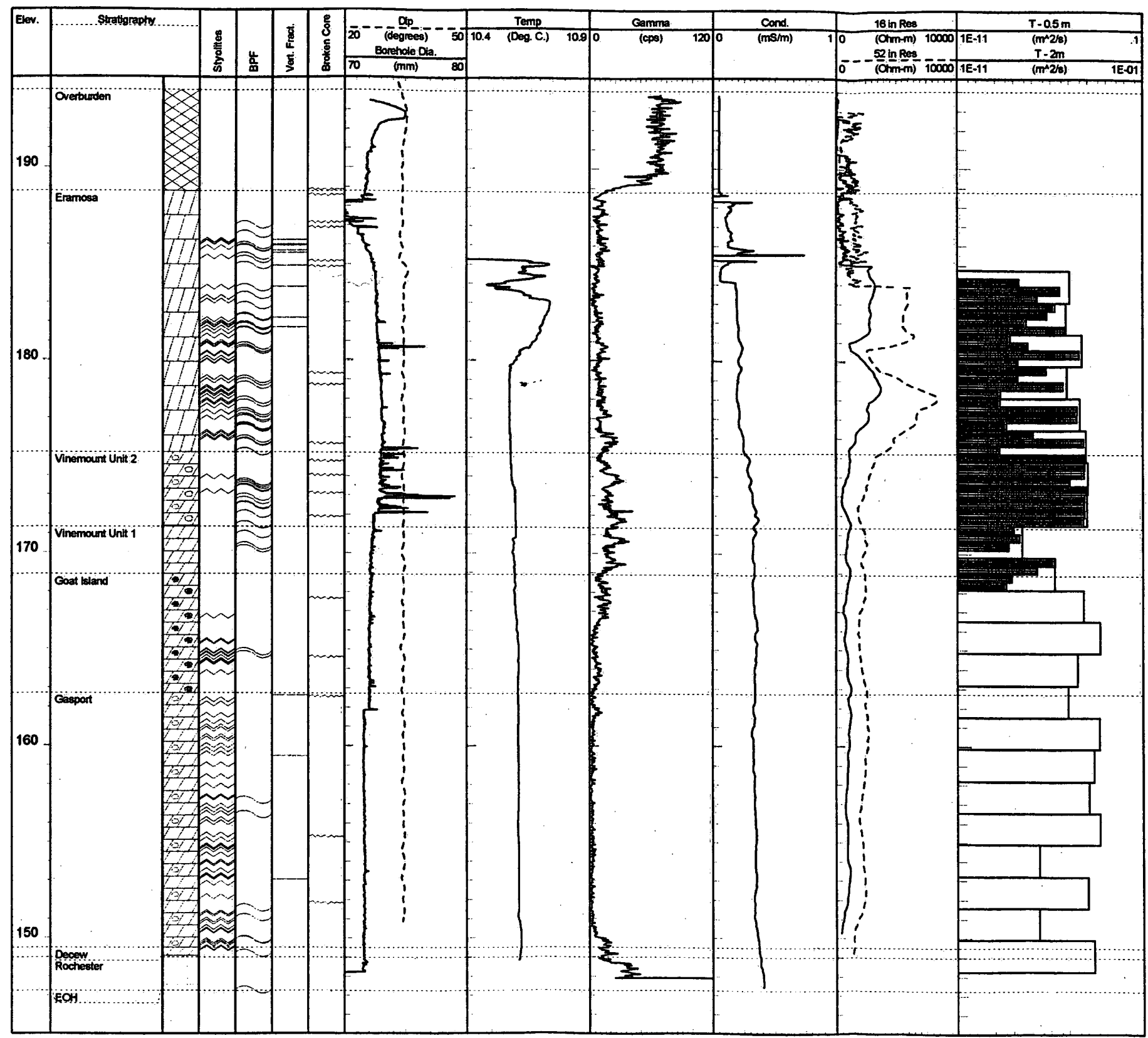
Elev.	Stratigraphy	Syolites	BPF	Vert. Fract.	Broken Core	Dip (deg)	BH Dia (mm)	Temp. (C)	Gamma (cps)	Cond. (ms/m)	18 In Res (Ohm-m)	10000	1E-11	T-2m (m ² /s)	1E-01	0	1-300	Eh	7/20/97	500	1E+03	Conductivity	6E+04	0	20	184	Ttium	7/20/97	4/1/98-6/30/98	Hyd Head	185
-------	--------------	----------	-----	--------------	-------------	-----------	-------------	-----------	-------------	--------------	-------------------	-------	-------	--------------------------	-------	---	-------	----	---------	-----	-------	--------------	-------	---	----	-----	-------	---------	----------------	----------	-----



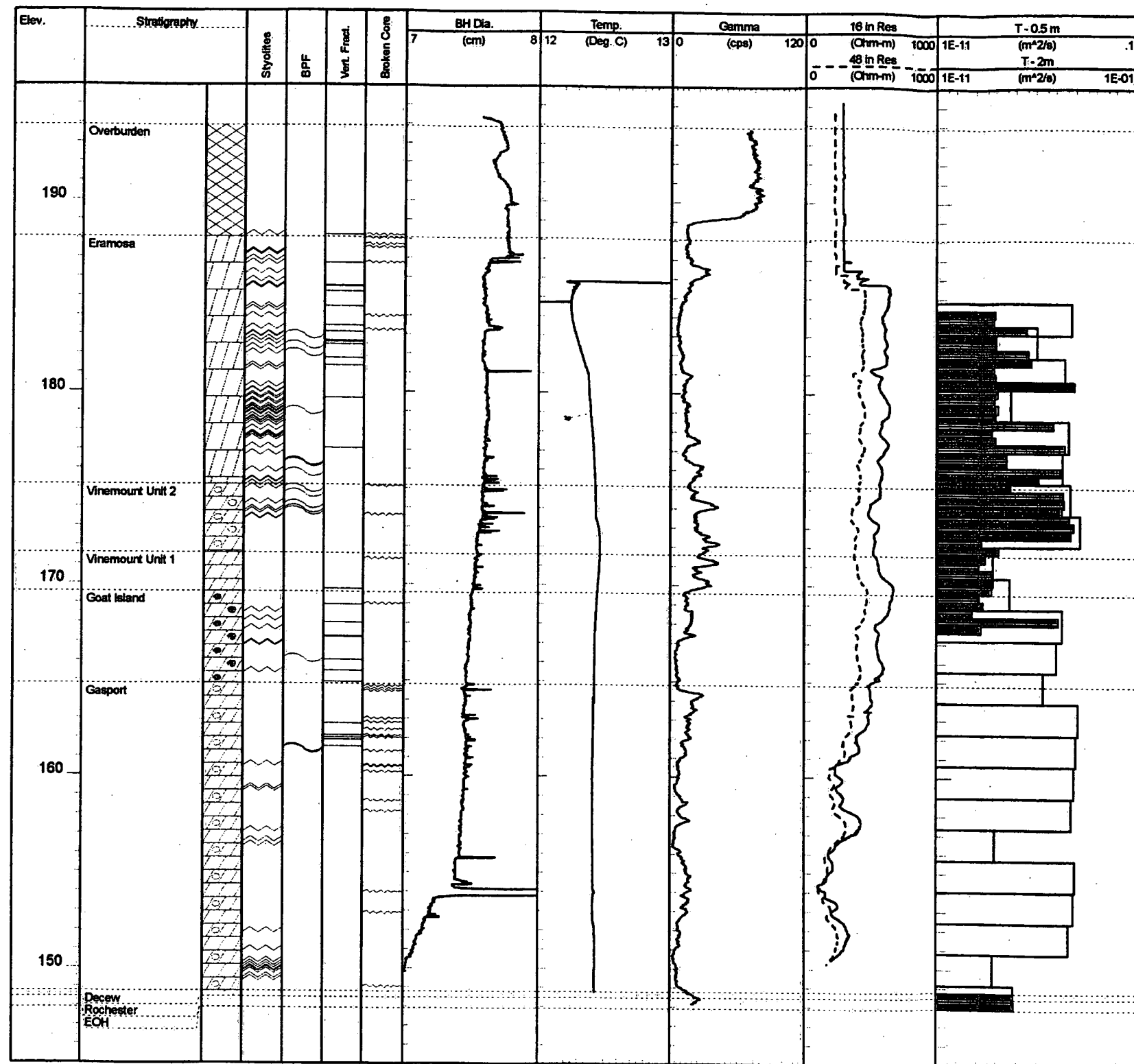
Borehole 54A
 Reference Elevation: Top of Steel Casing - 194.94 masl
 Borehole Azimuth: 128 deg. Borehole Dip: 56.5 deg.



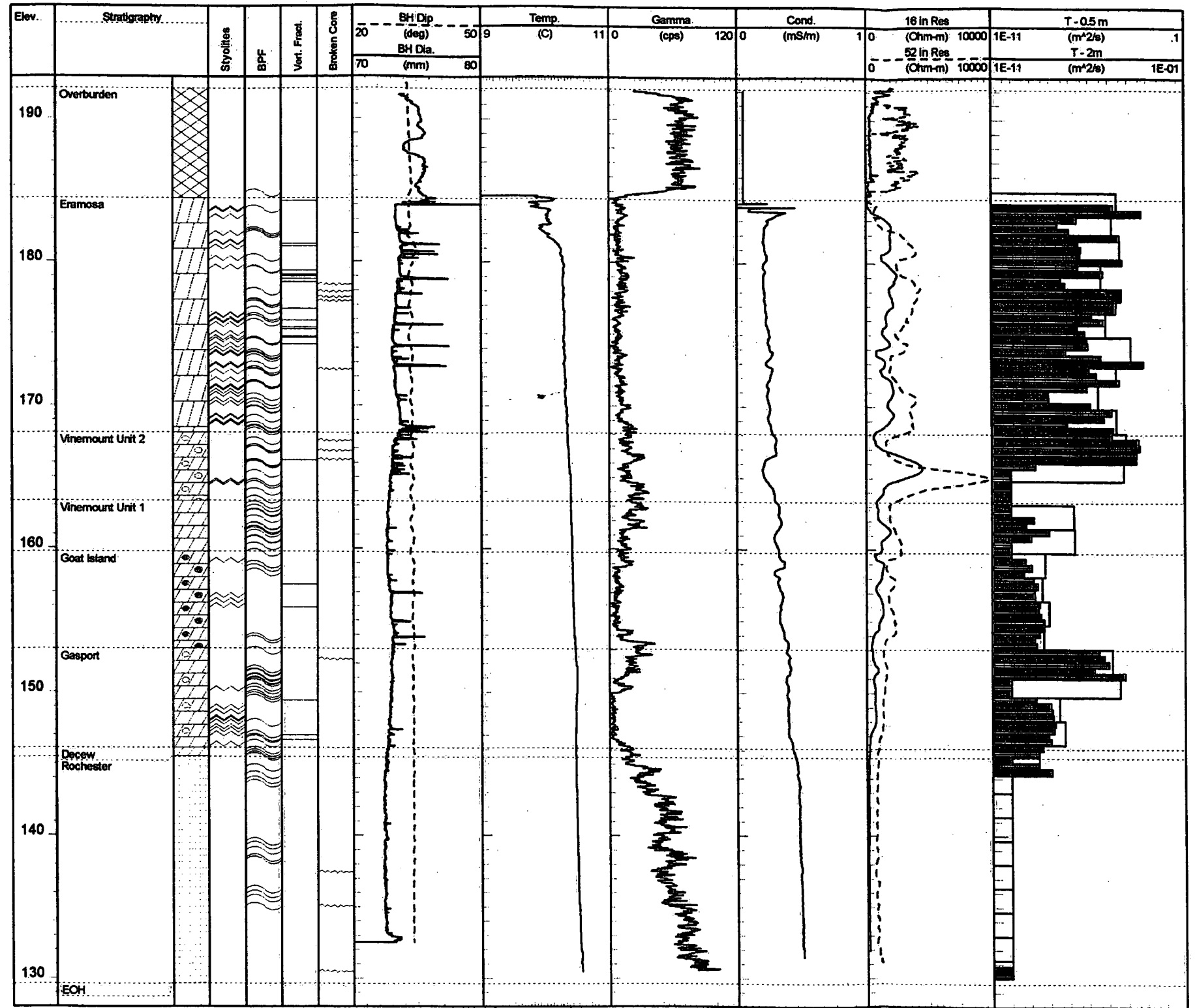
Borehole 54B
 Reference Elevation: Top of Steel Casing - 194.62 masl
 Borehole Azimuth: 0 deg. Borehole Dip: 90 deg.



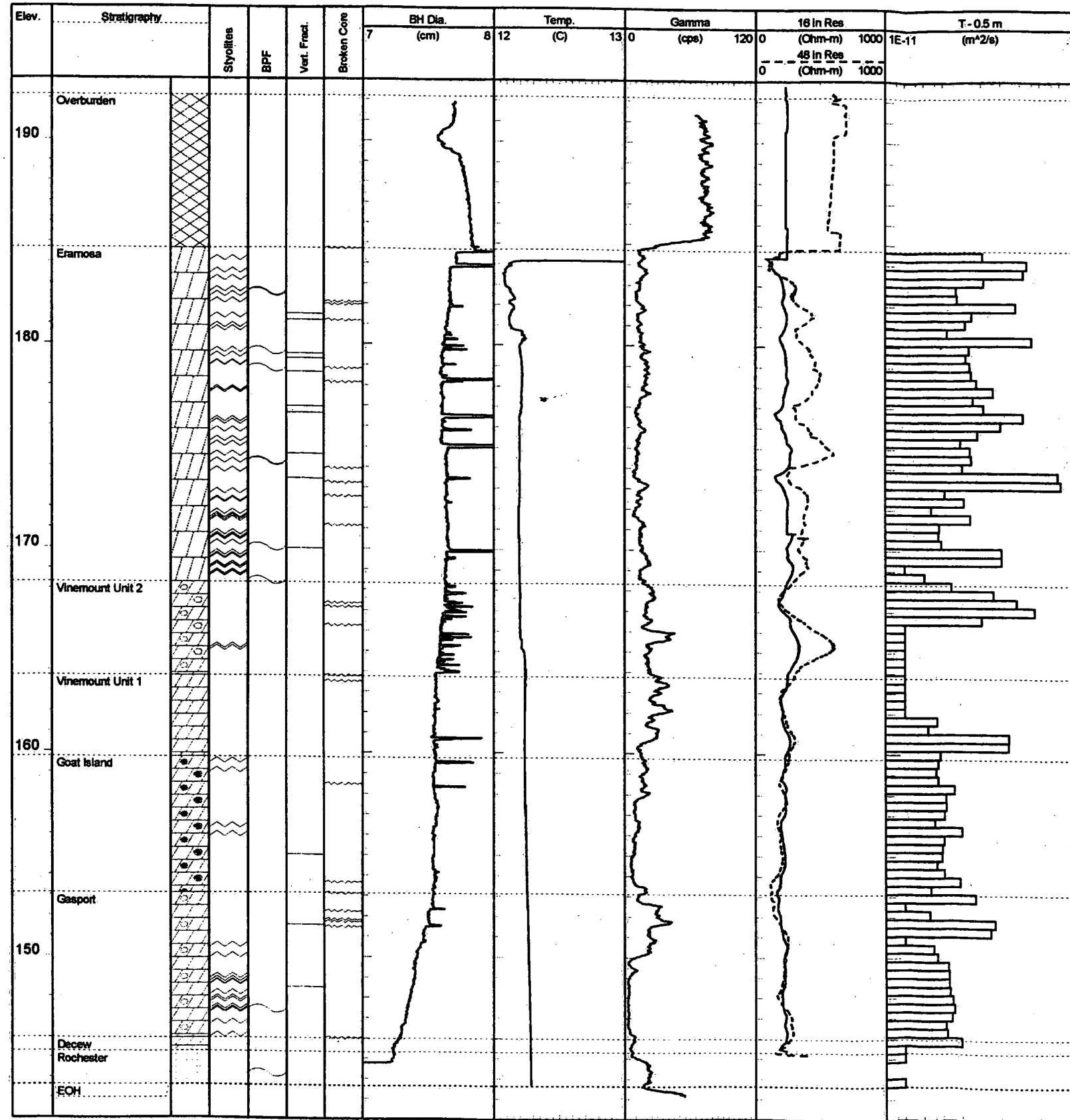
Borehole 54C
Reference Elevation: Top of Steel Casing - 194.70 masl
Borehole Azimuth: 45 deg. Borehole Dip: 56 deg.



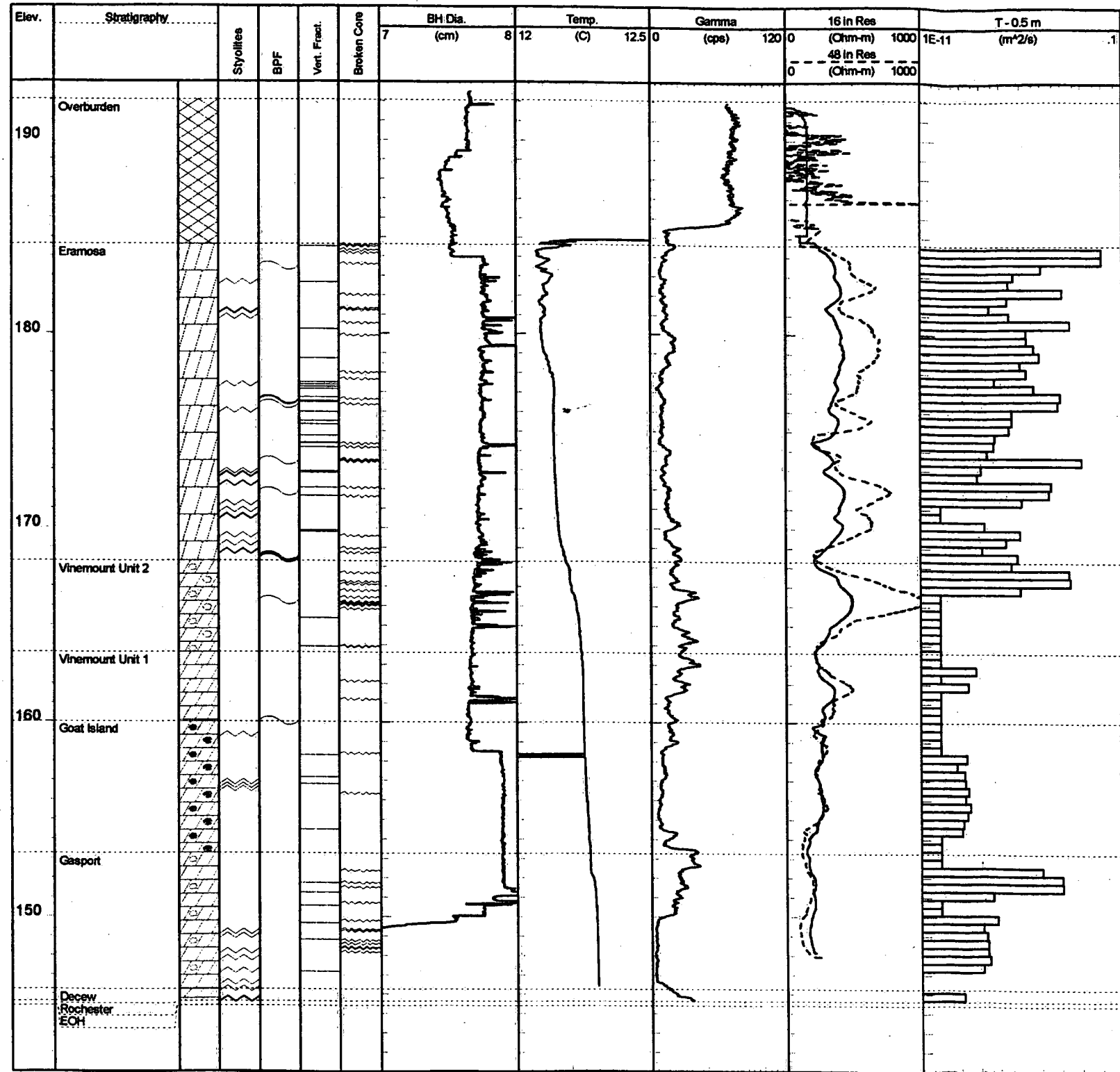
Borehole 54D
Reference Elevation: Top of Steel Casing - 194.63 masl
Borehole Azimuth: 259 deg. Borehole Dip: 55 deg.



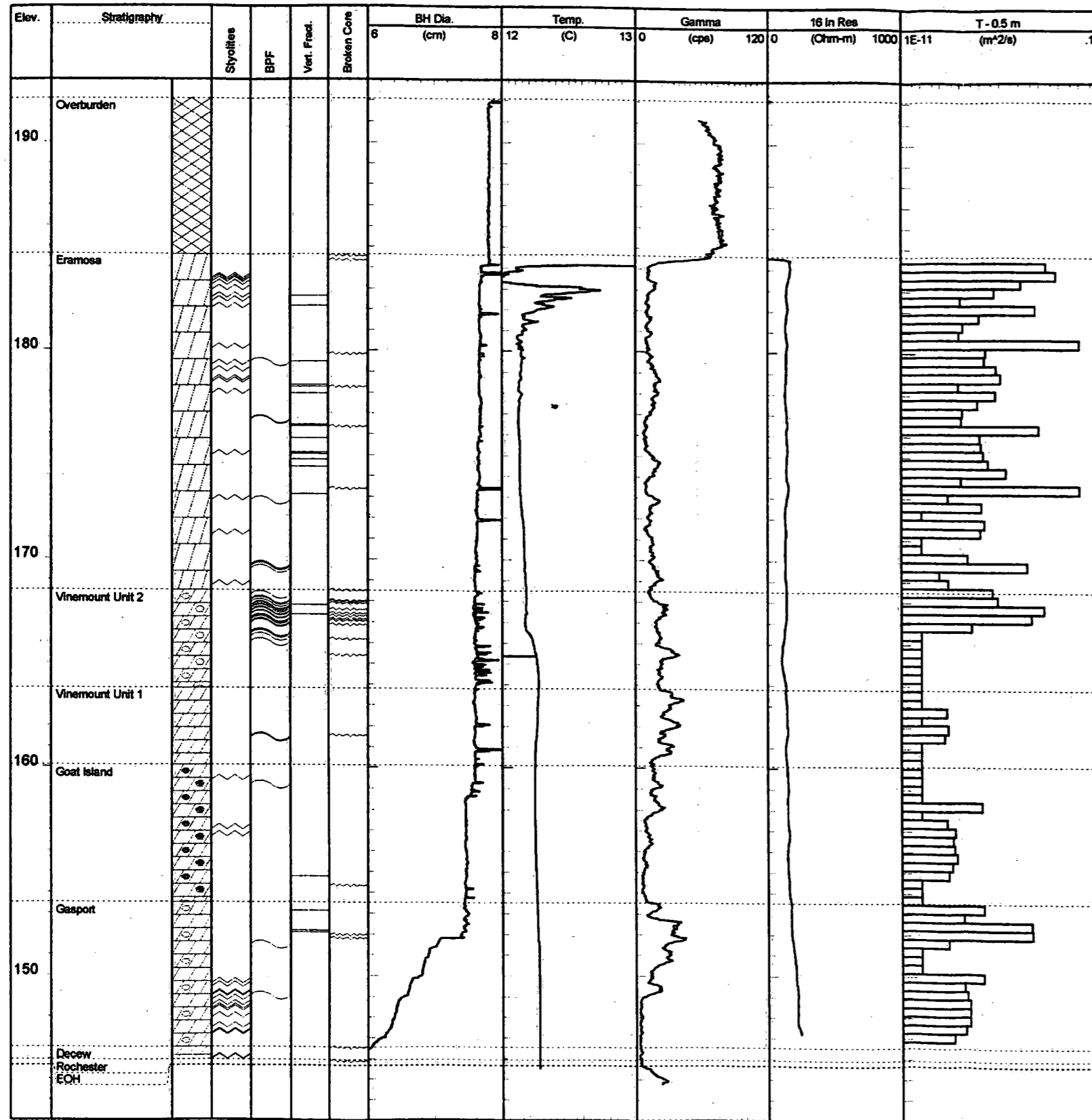
Borehole 55
Reference Elevation: Top of Steel Casing - 192.93 masl
Borehole Azimuth: 265 deg. Borehole Dip: 57 deg.



Borehole 56
Reference Elevation: Top of Steel Casing - 192.94 masl
Borehole Azimuth: 257 deg. Borehole Dip: 56 deg.



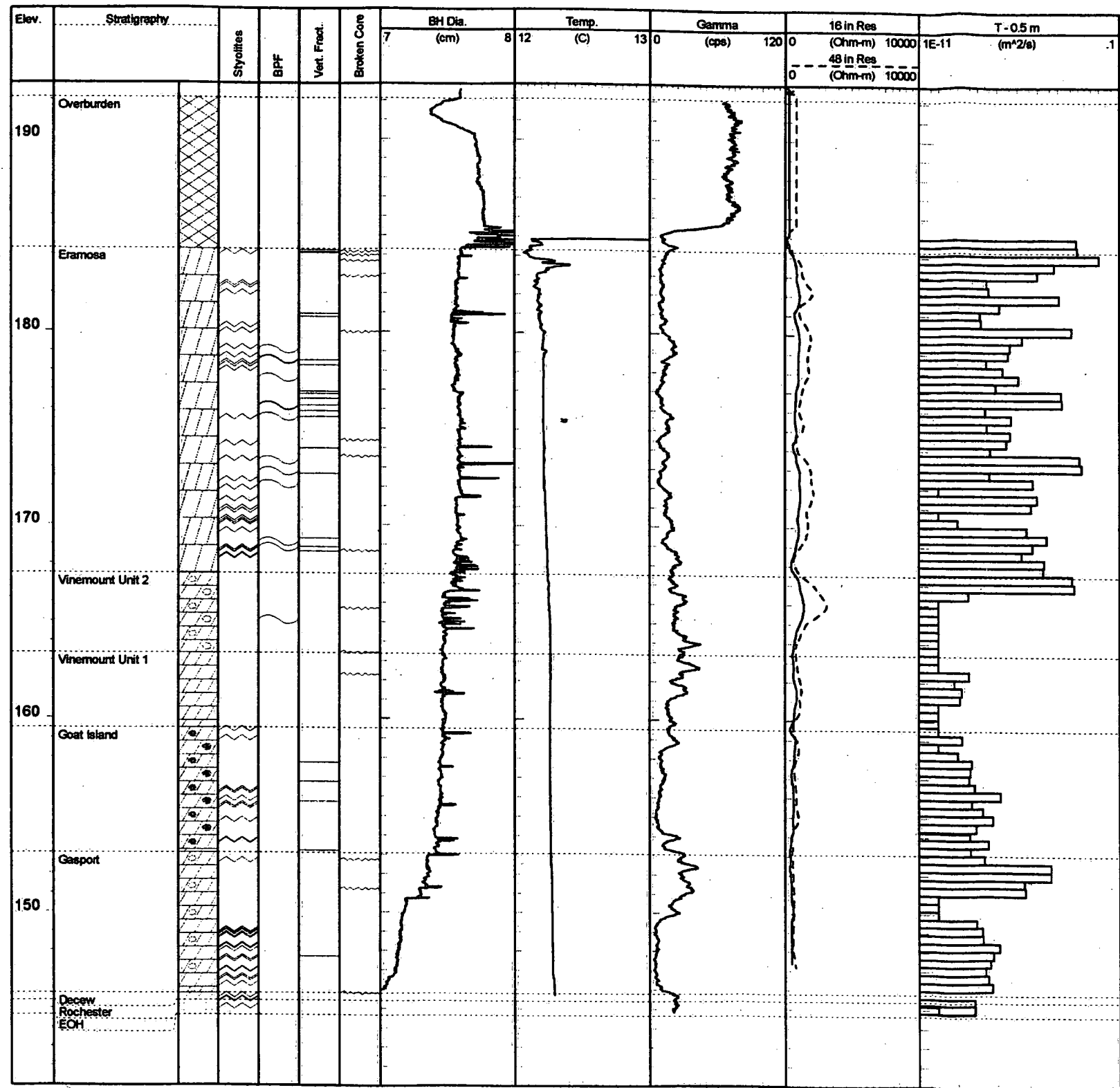
Borehole 57
Reference Elevation: Top of Steel Casing - 192.78 masl
Borehole Azimuth: 20 deg. Borehole Dip: 56 deg.



Borehole 58

Reference Elevation: Top of Steel Casing - 193.02 masl

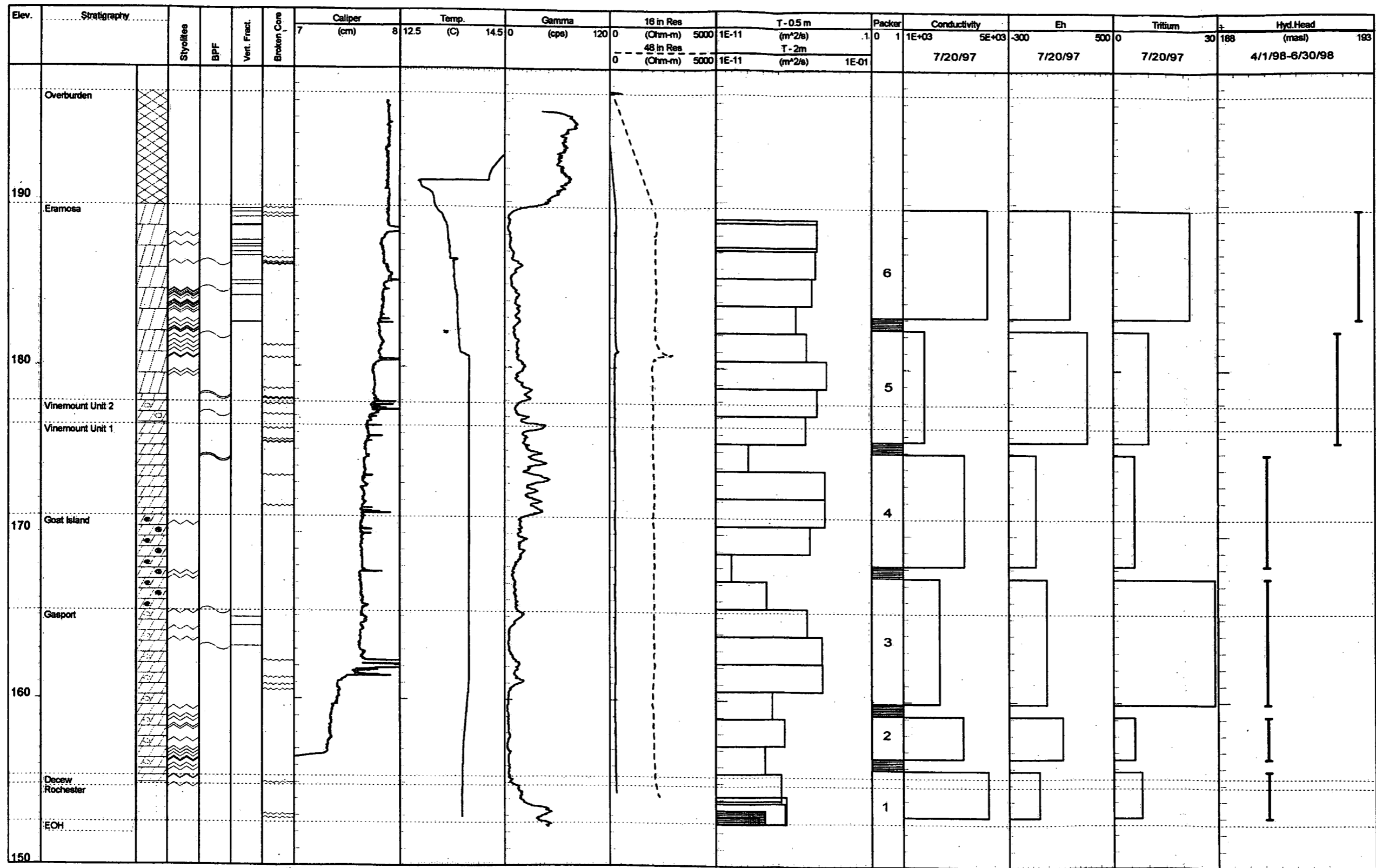
Borehole Azimuth: 306 deg. Borehole Dip: 55.5 deg.



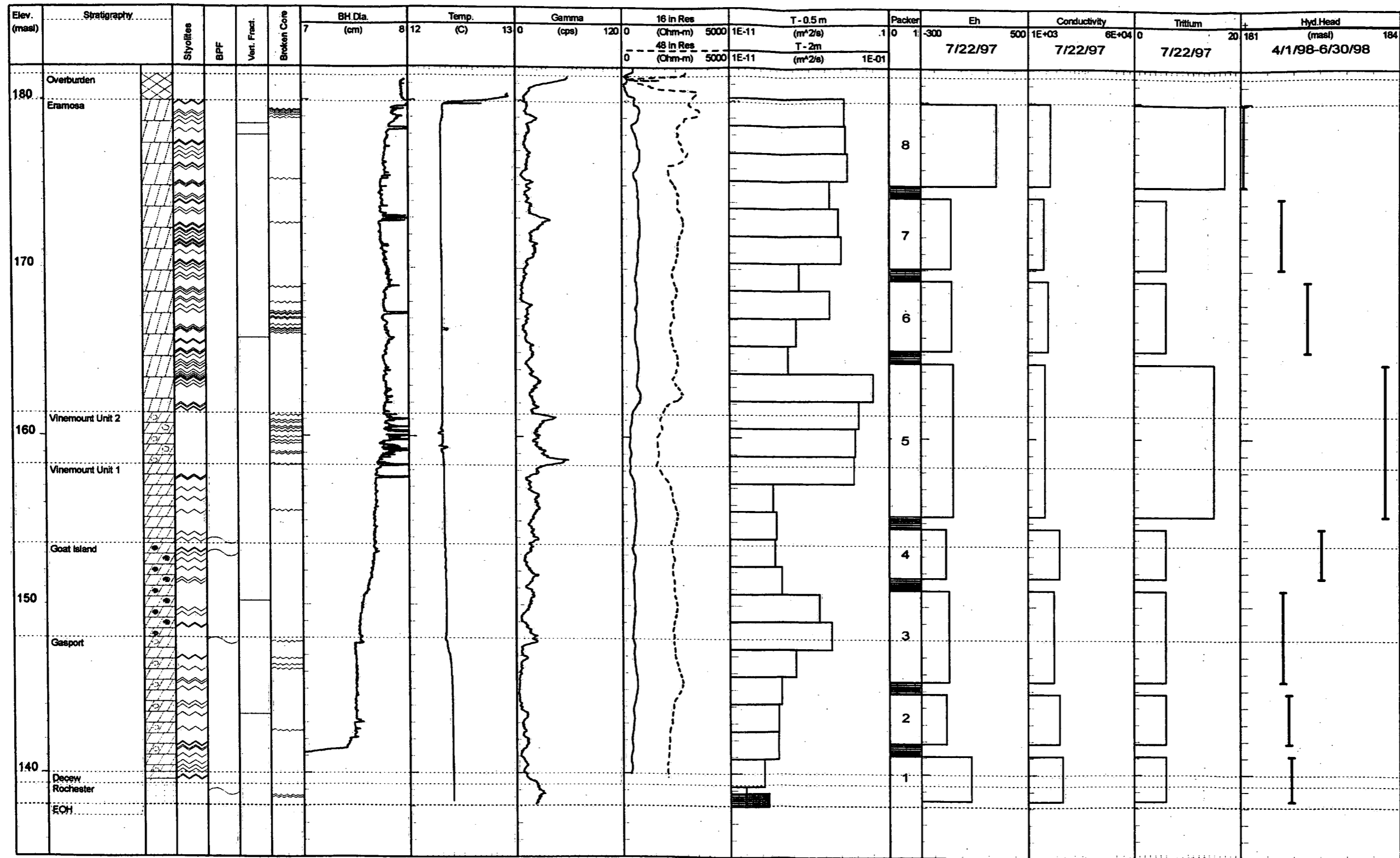
Borehole 59

Reference Elevation: Top of Steel Casing - 192.85 masl

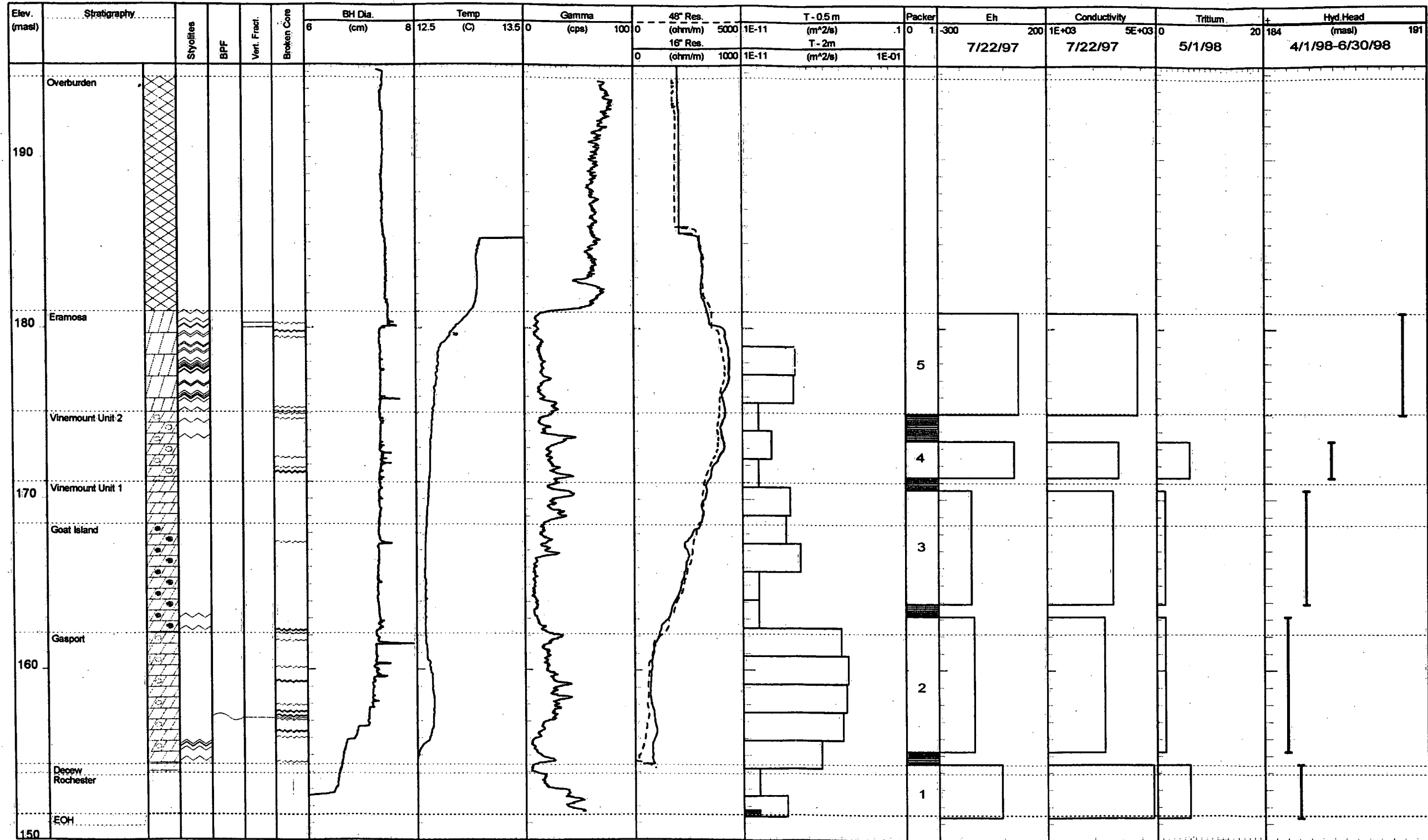
Borehole Azimuth: 143 deg. Borehole Dip: 56 deg.



Borehole 60
Reference Elevation: Top of Steel Casing - 197.04 masl
Borehole Azimuth: 15 deg. Borehole Dip: 56 deg.



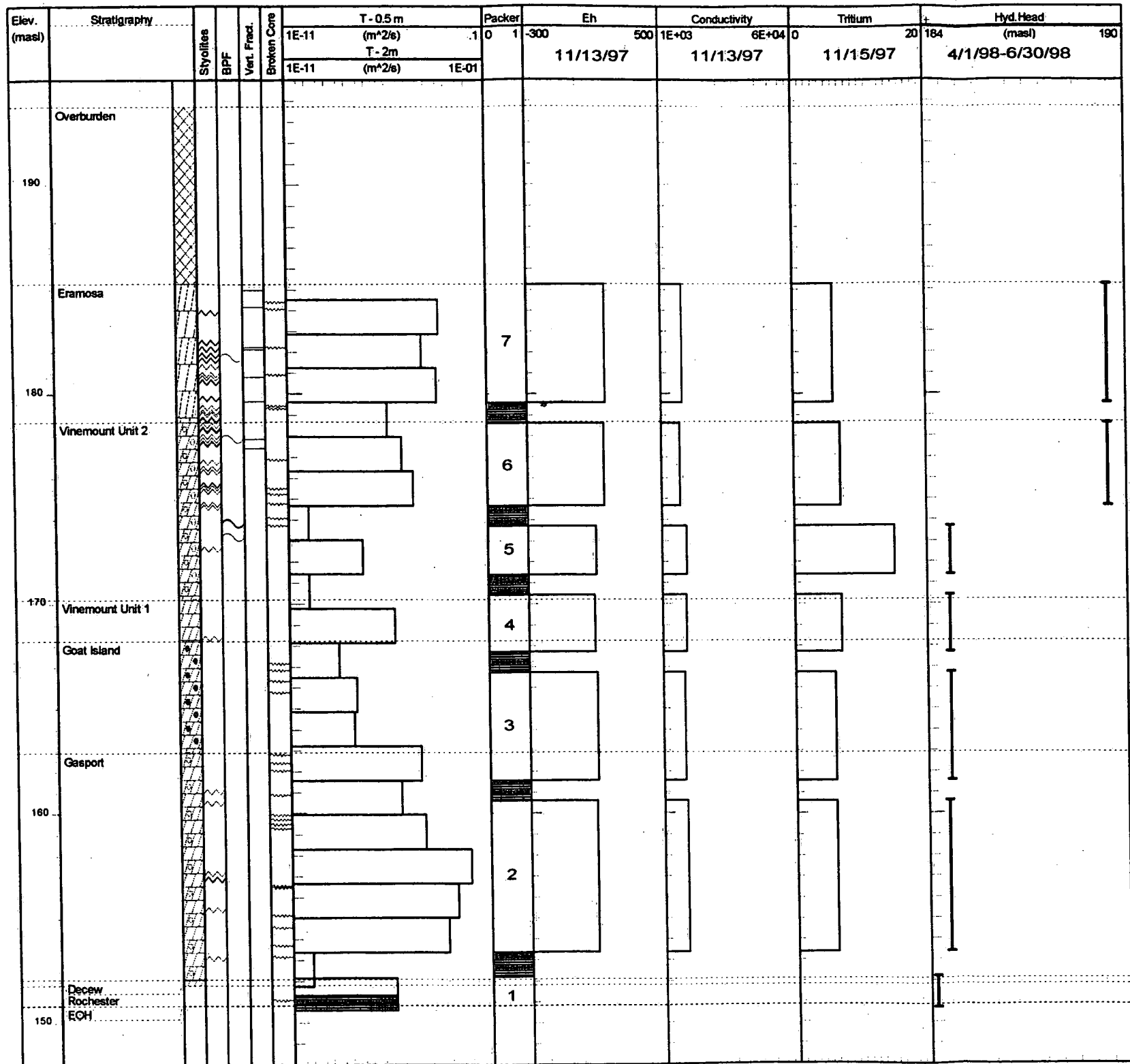
Borehole 61
Reference Elevation: Top of Steel Casing - 182.24 masl
Borehole Azimuth: 234 deg. Borehole Dip: 55 deg.



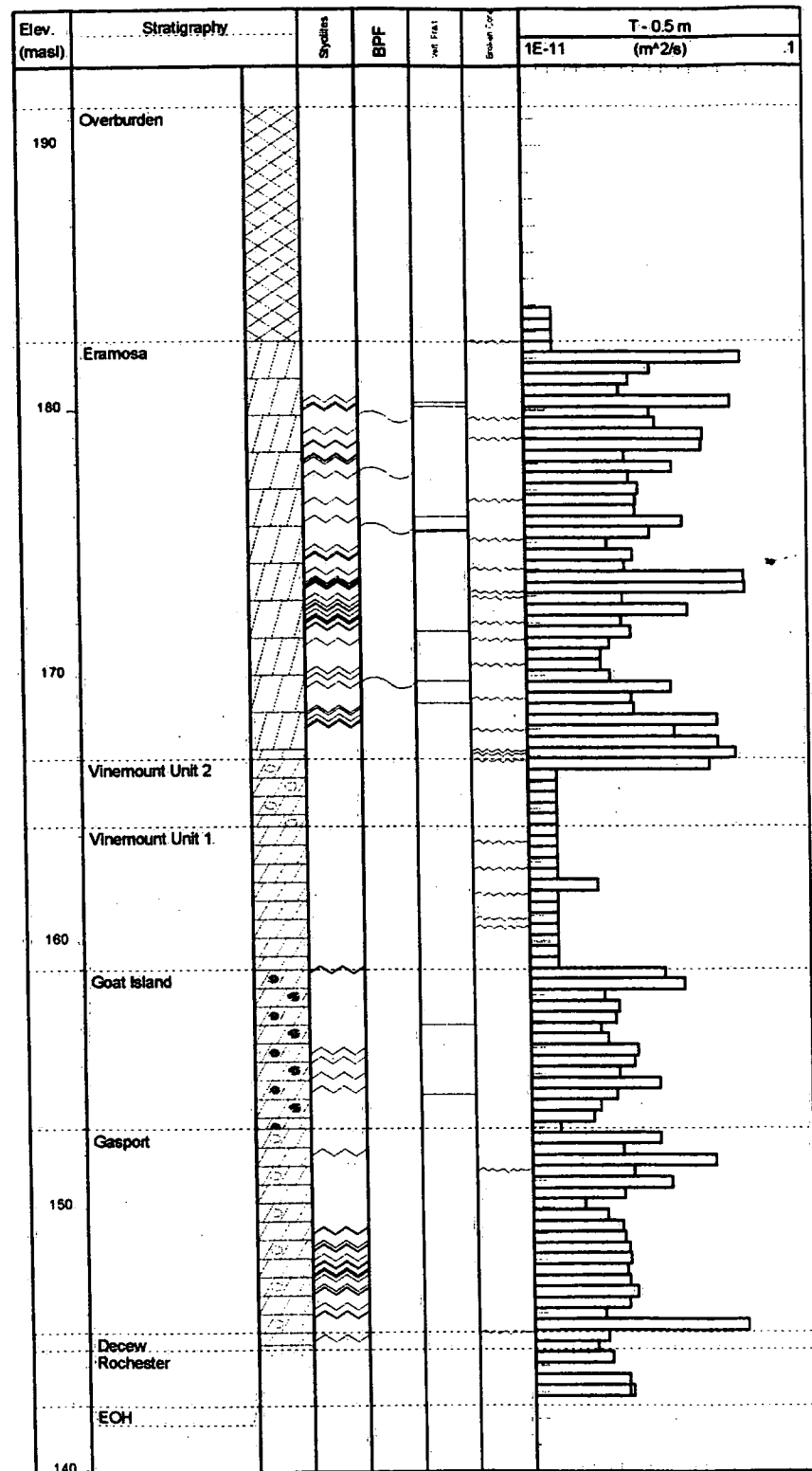
Borehole 62

Reference Elevation: Top of Steel Casing - 195.45 masl

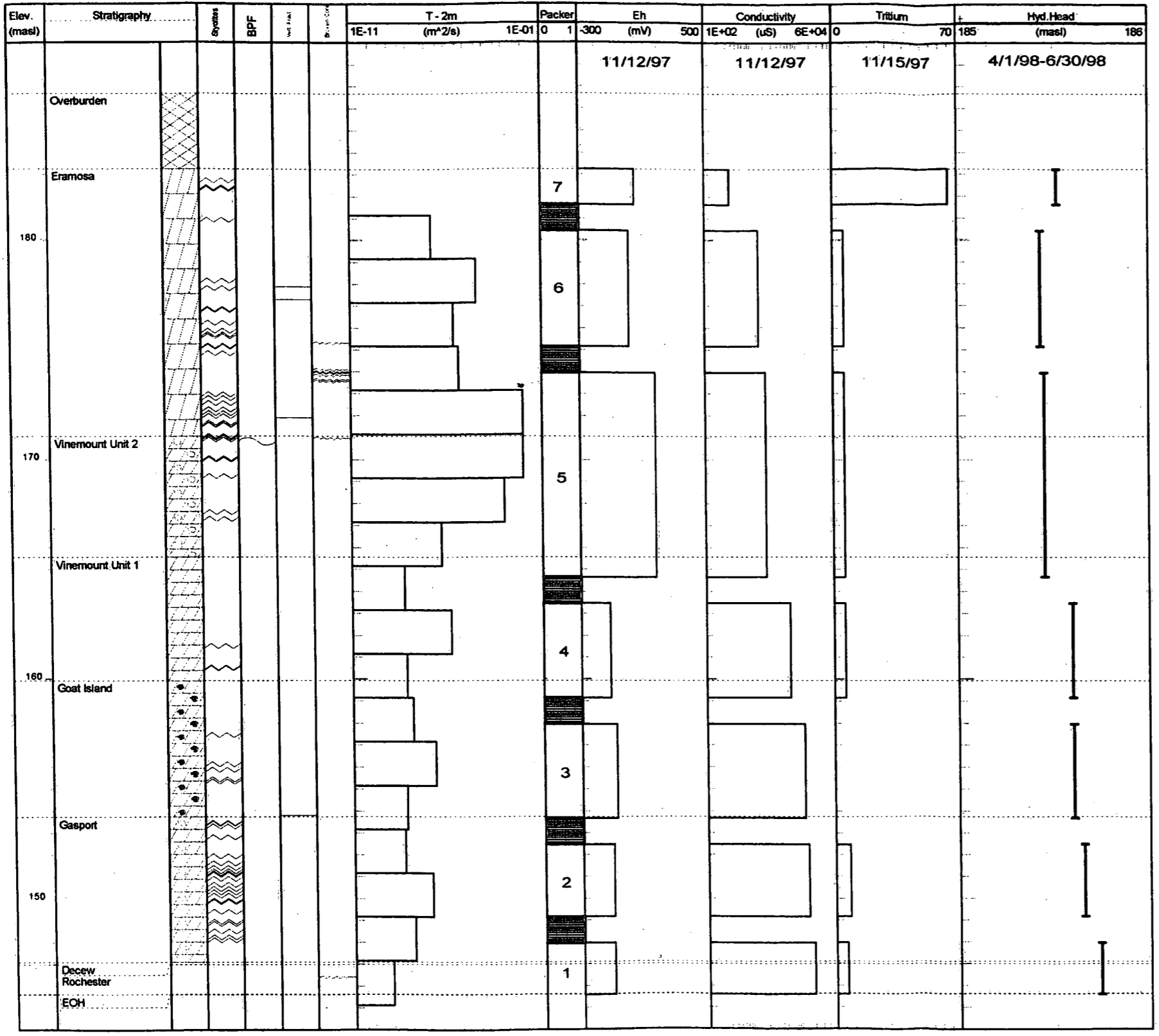
Borehole Azimuth: 213 deg. Borehole Dip: 55.5 deg.



Borehole 63
Reference Elevation: Top of Steel Casing - 194.35 masl
Borehole Azimuth: 284 deg. Borehole Dip: 55 deg.



Borehole 64
 Reference Elevation: Top of Steel Casing - 192.60 masl
 Borehole Azimuth: 341.5 deg. | Borehole Dip: 56 deg.



11/12/97

11/12/97

11/15/97

4/1/98-6/30/98

7

6

5

4

3

2

1

Borehole 65
 Reference Elevation: Top of Steel Casing - 187.16 masl
 Borehole Azimuth: 0 deg. Borehole Dip: 90 deg.

Appendix C
Transmissivity profiles using 0.1 m data

37C

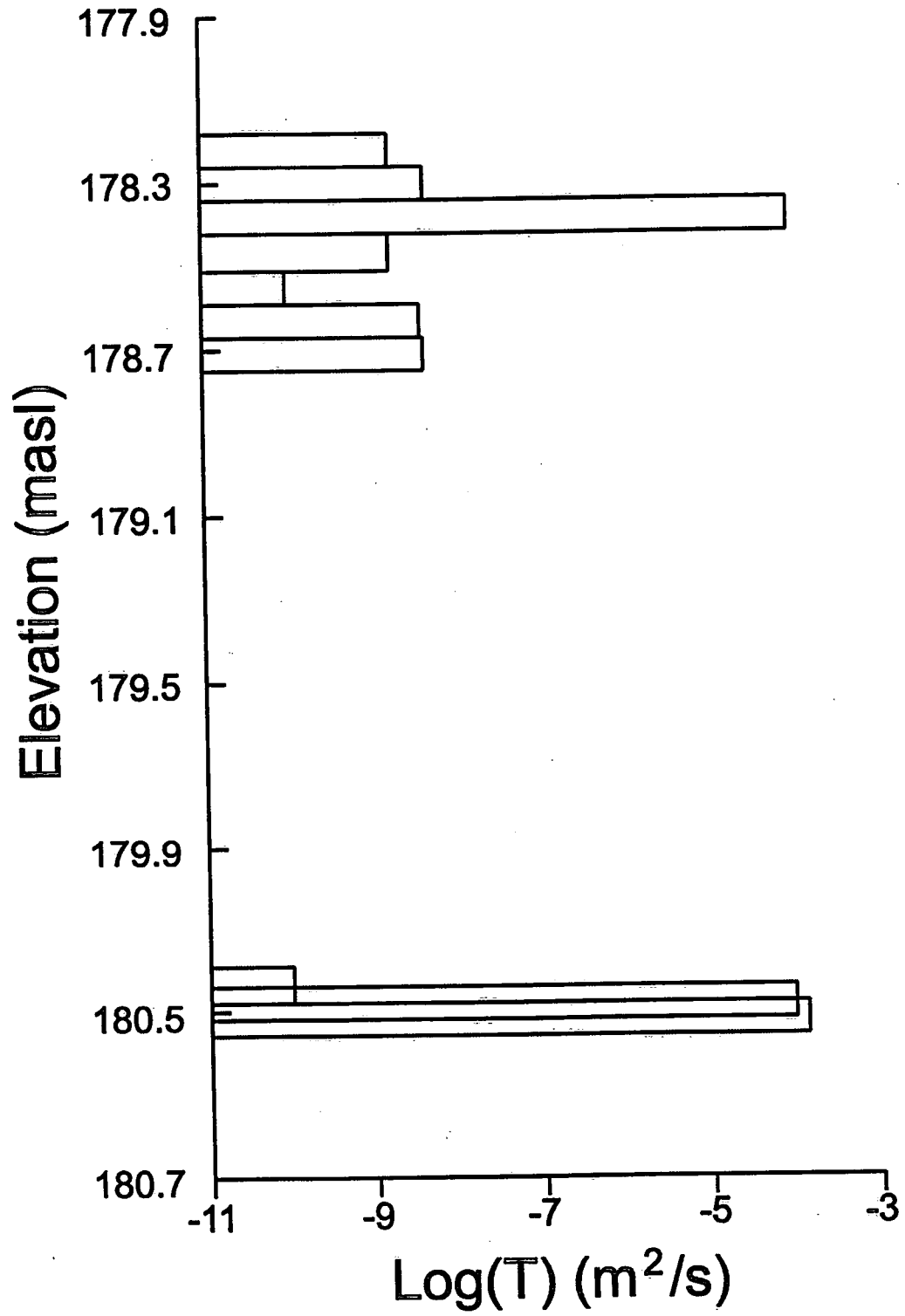


Figure C1. Transmissivity measurements using a 0.1 m test interval in 37C (part 1).

37C

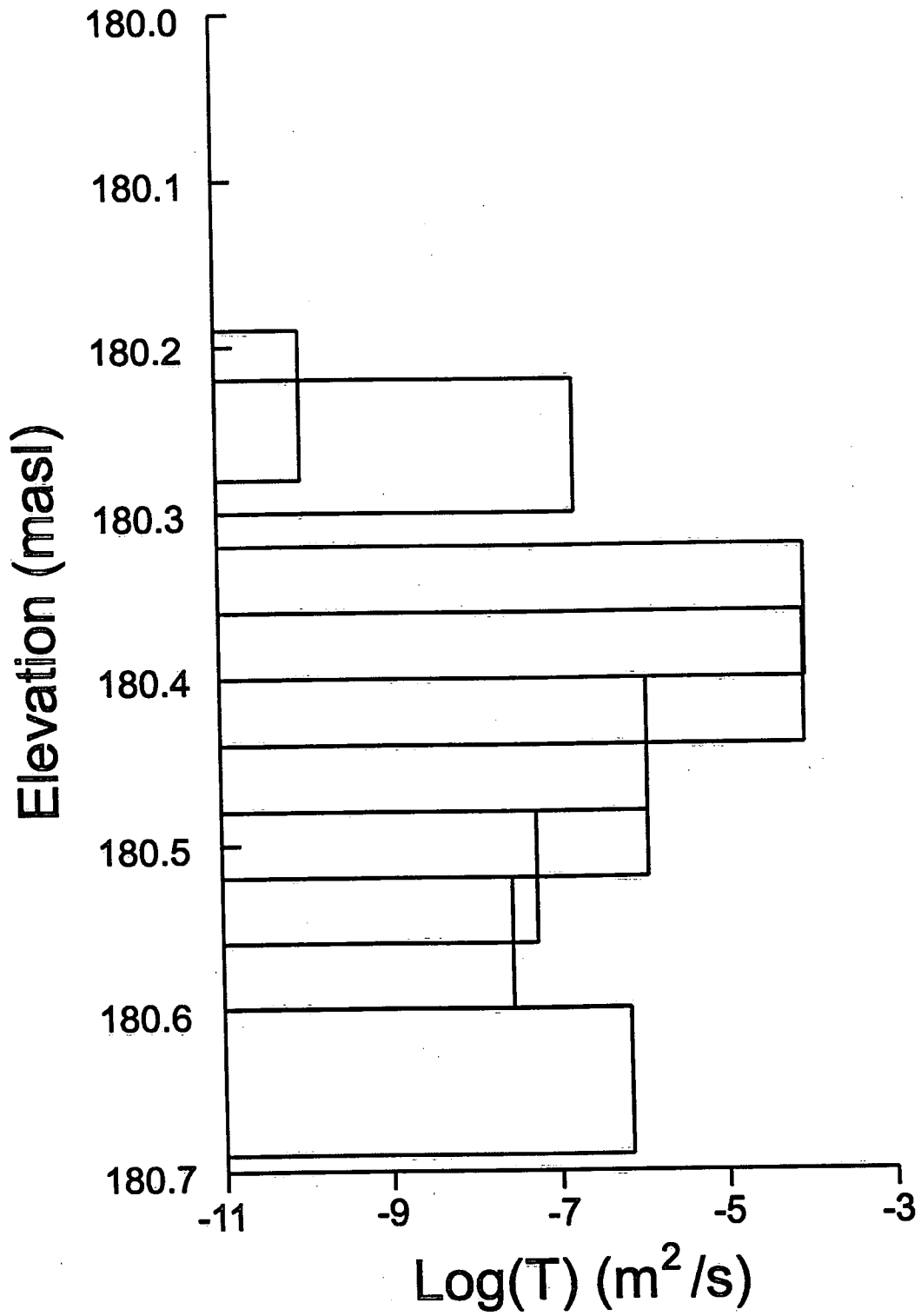


Figure C2. Transmissivity measurements using a 0.1 m test interval in 37C (part 2).

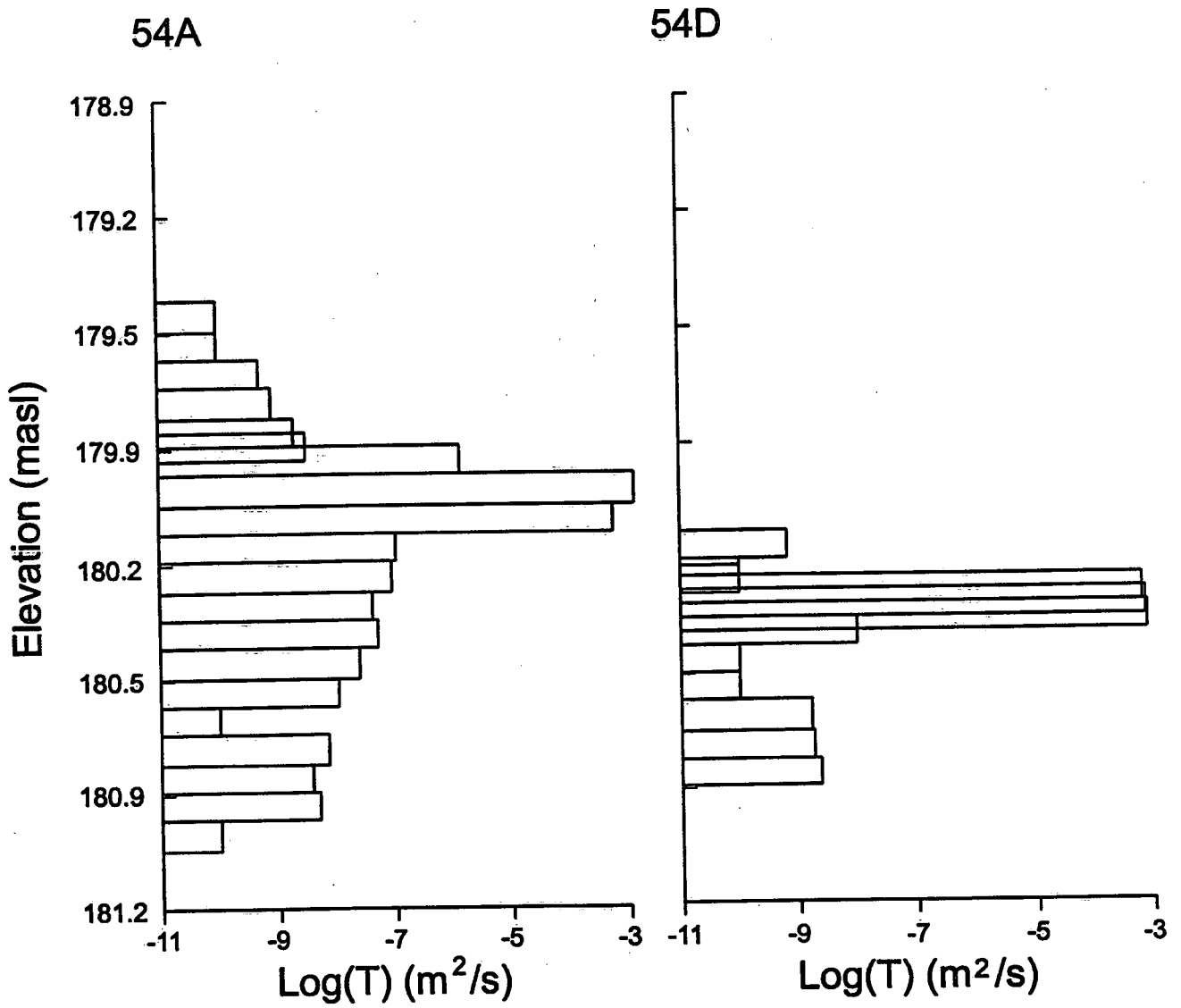


Figure C3. Transmissivity measurements using a 0.1 m test interval in 54A and 54D.

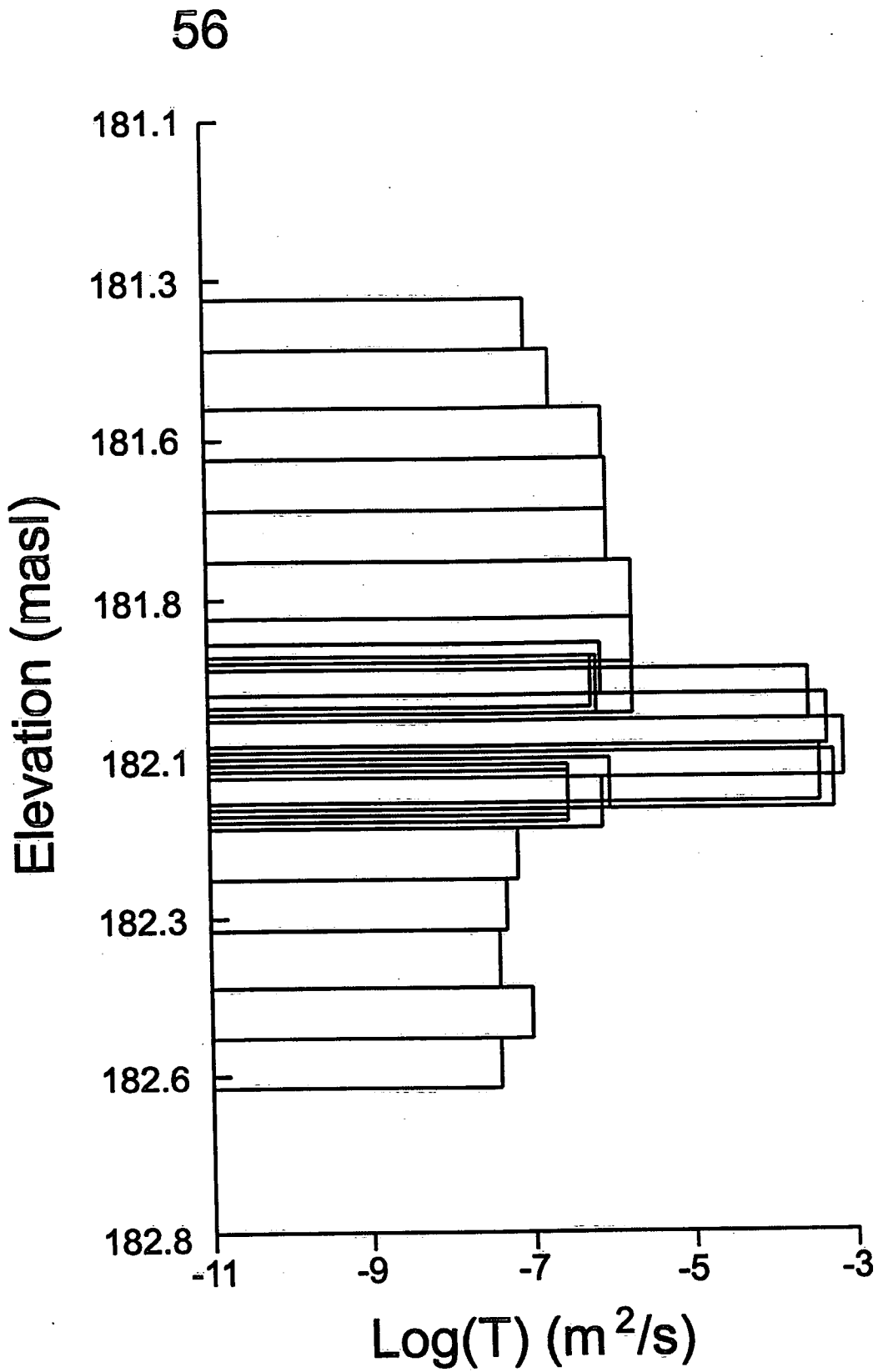
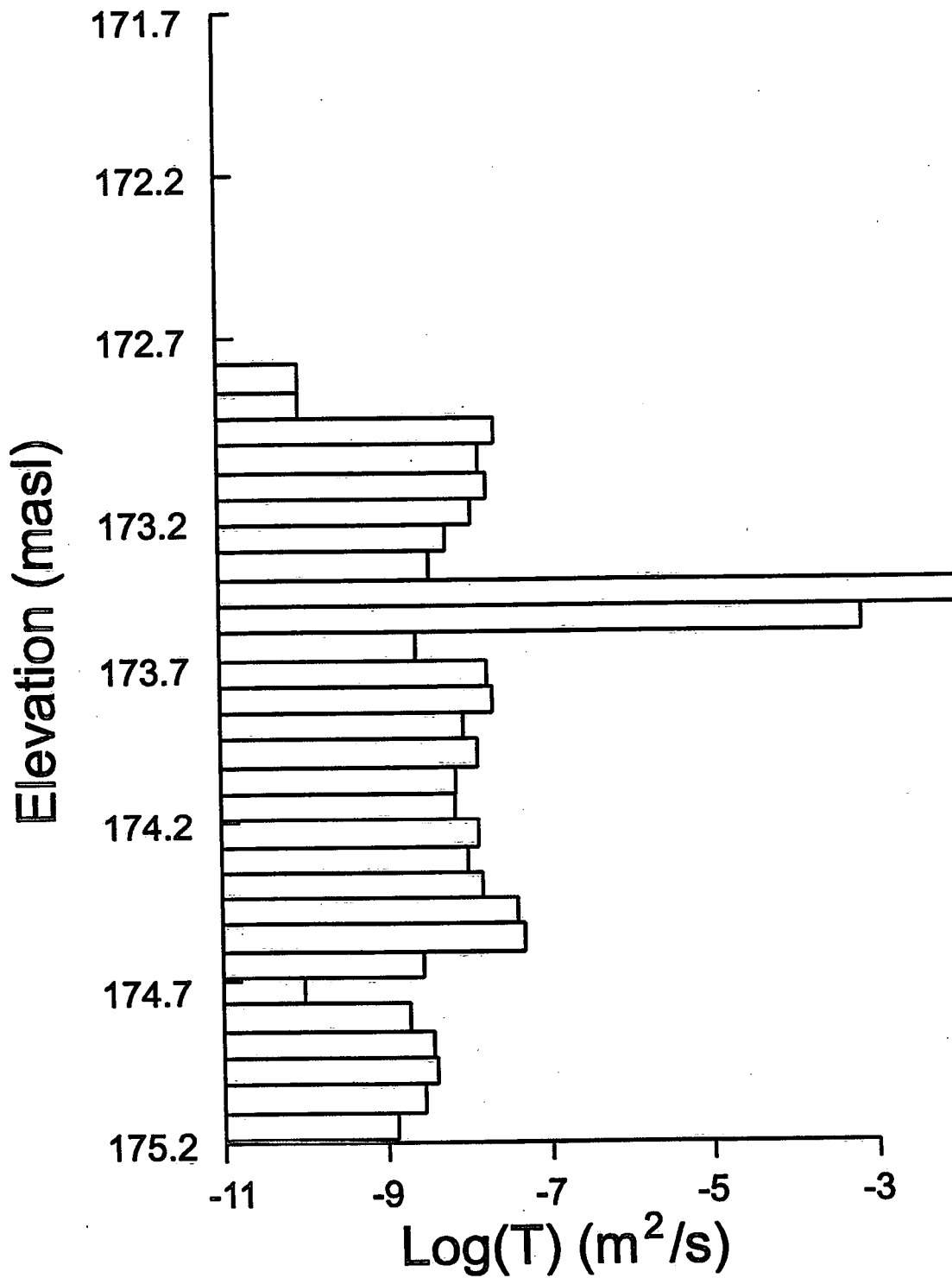


Figure C4. Transmissivity measurements using a 0.1 m test interval in 56.



64

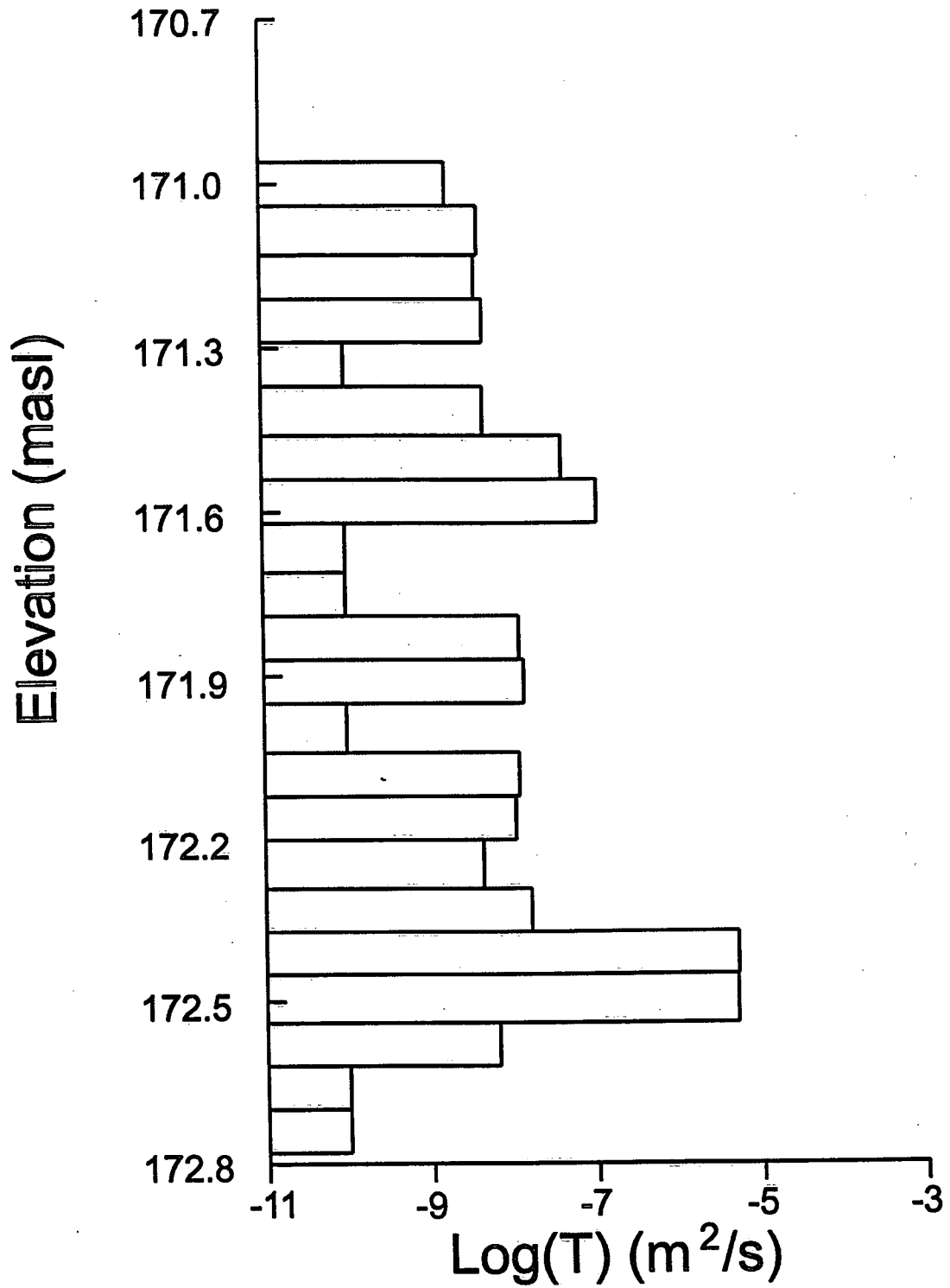


Figure C6. Transmissivity measurements using a 0.1 m test interval in 64 (part 2).

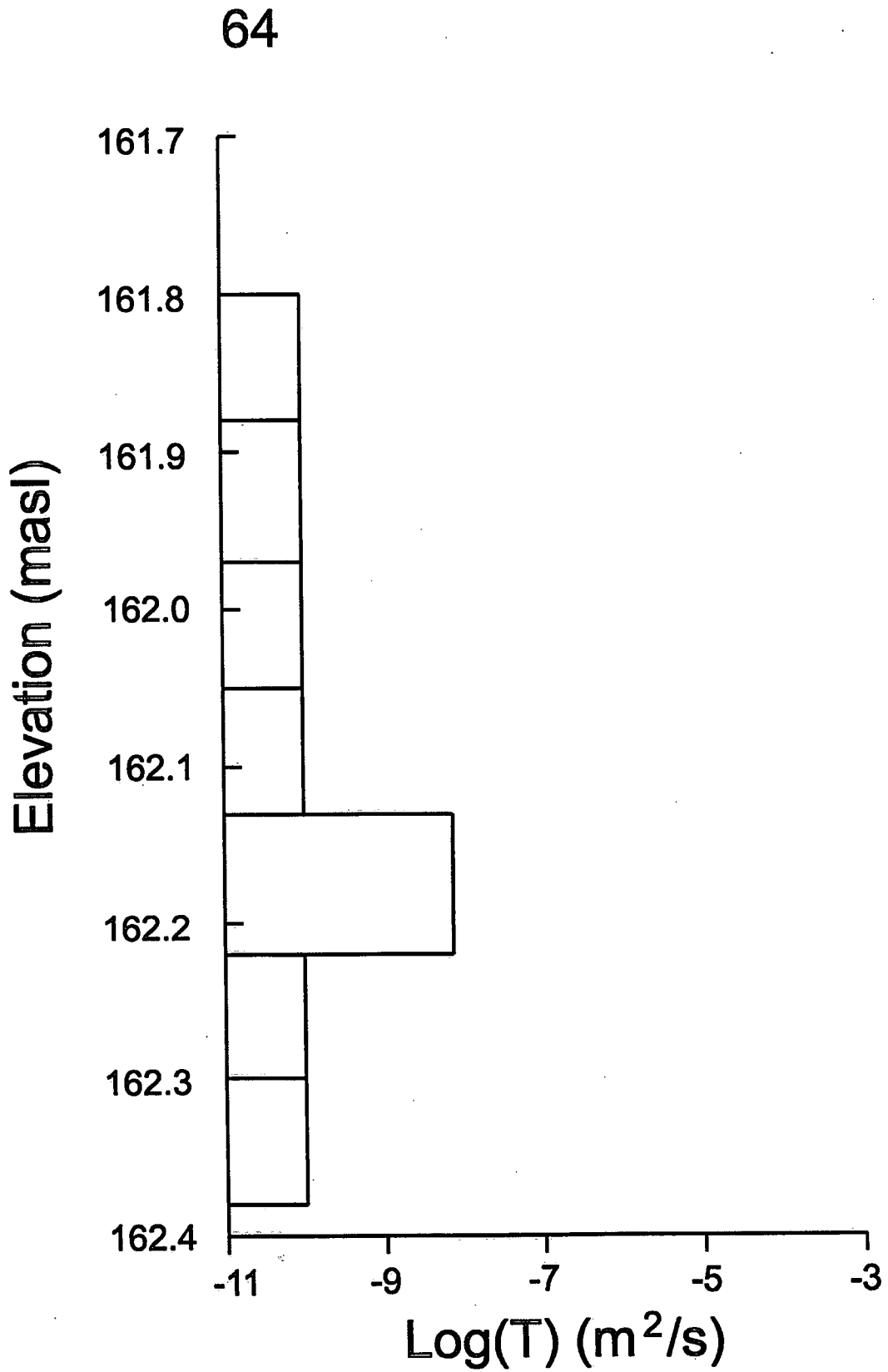


Figure C7. Transmissivity measurements using a 0.1 m test interval in 64 (part 3).

64

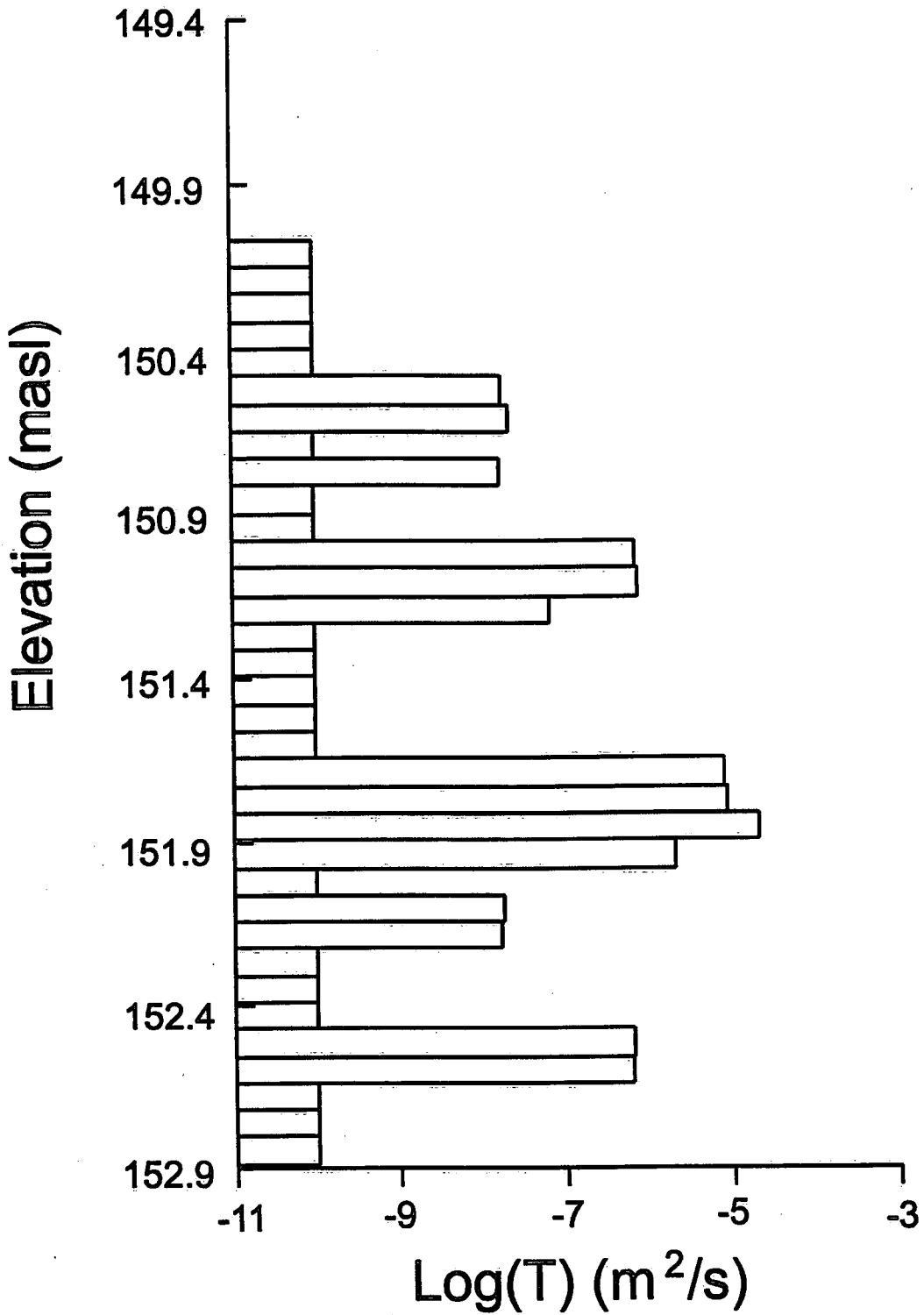


Figure C8. Transmissivity measurements using a 0.1 m test interval in 64 (part 4).

Appendix D
Pumping Test Response Curves

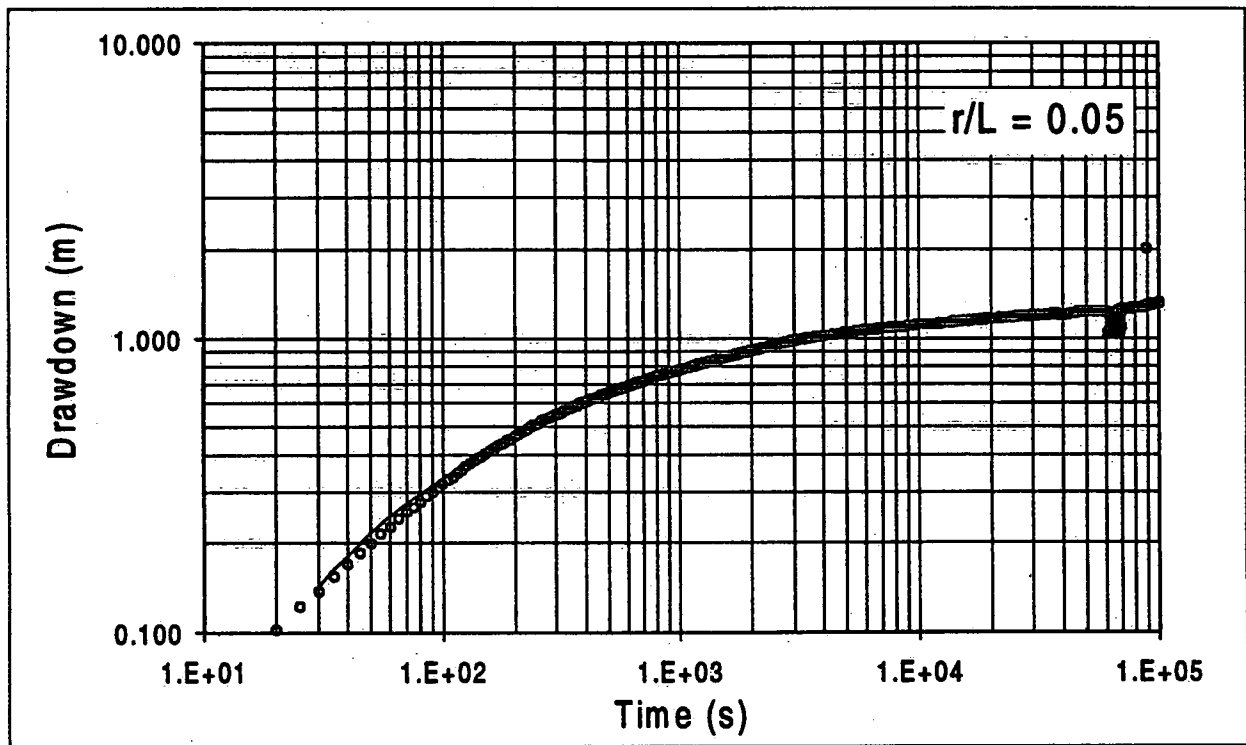


Figure D1 Pumping test 2: Response and type curve match in borehole 55 to pumping in borehole 58.

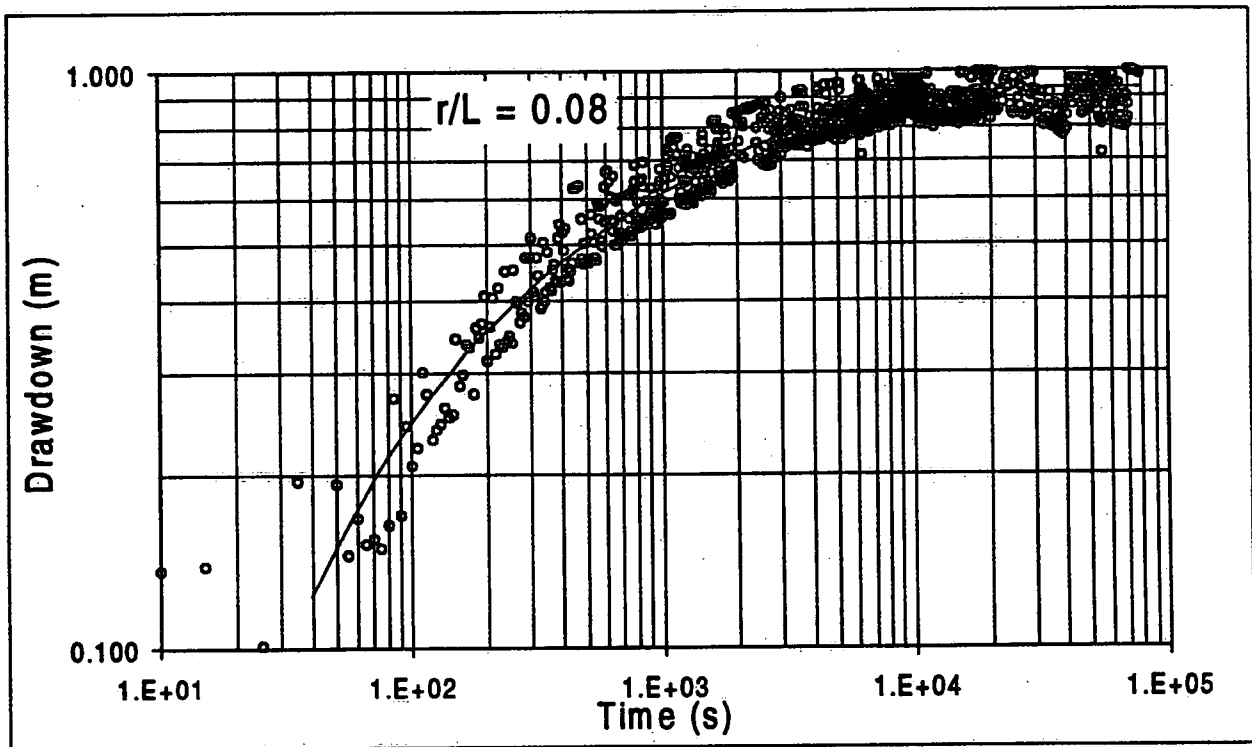


Figure D2 Pumping test 1: Response and type curve match in borehole 55 to pumping in borehole 56.

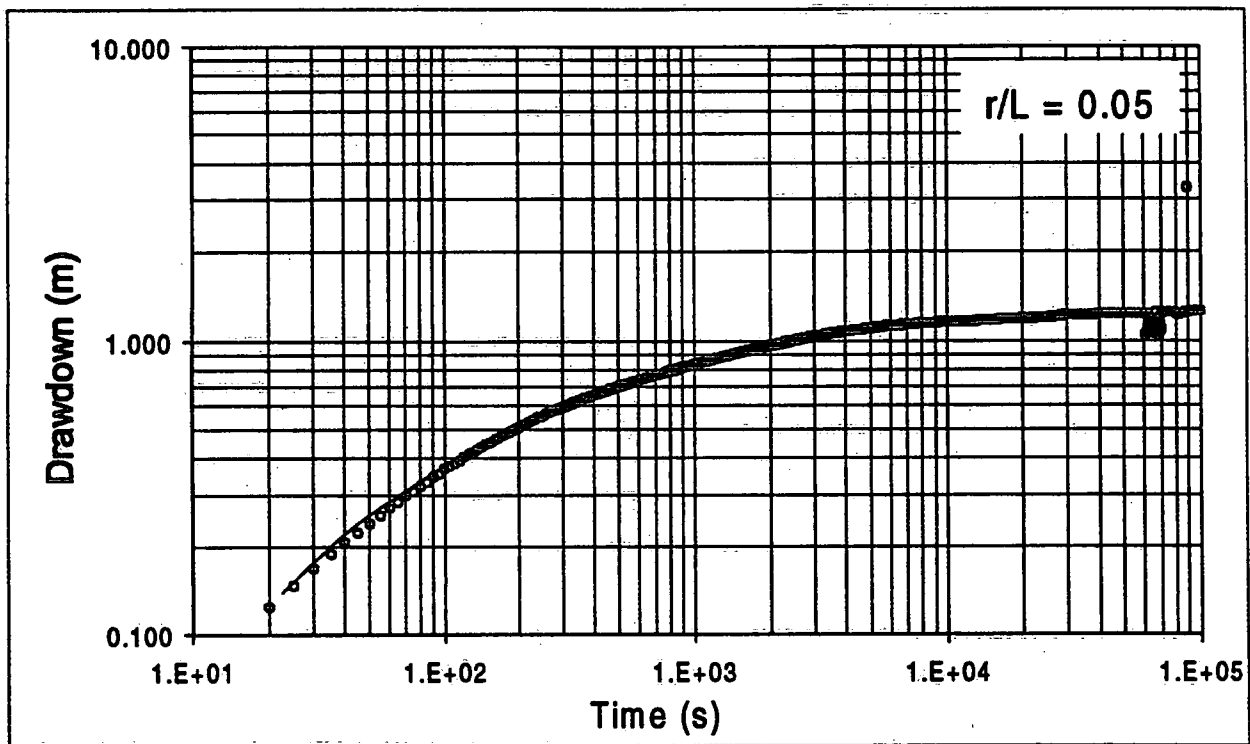


Figure D3 Pumping test 2: Response and type curve match in borehole 56 to pumping in borehole 58.

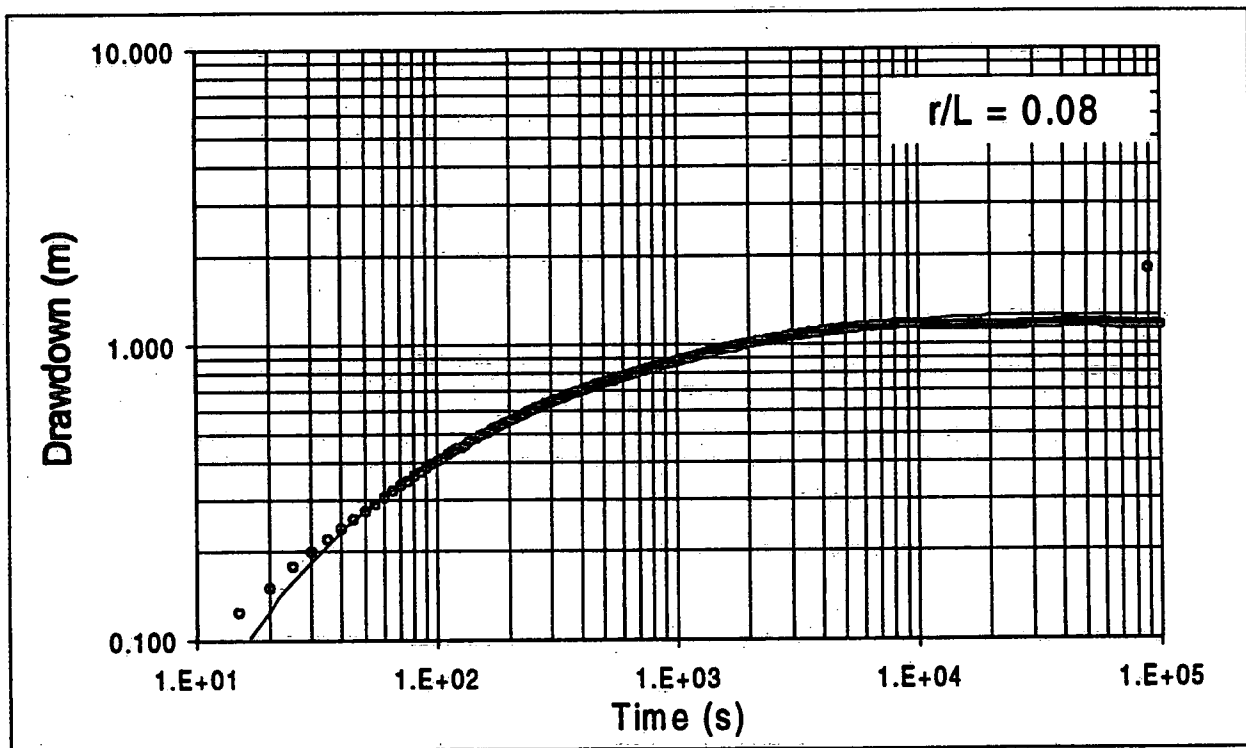


Figure D4 Pumping test 2: Response and type curve match in borehole 57 to pumping in borehole 58.

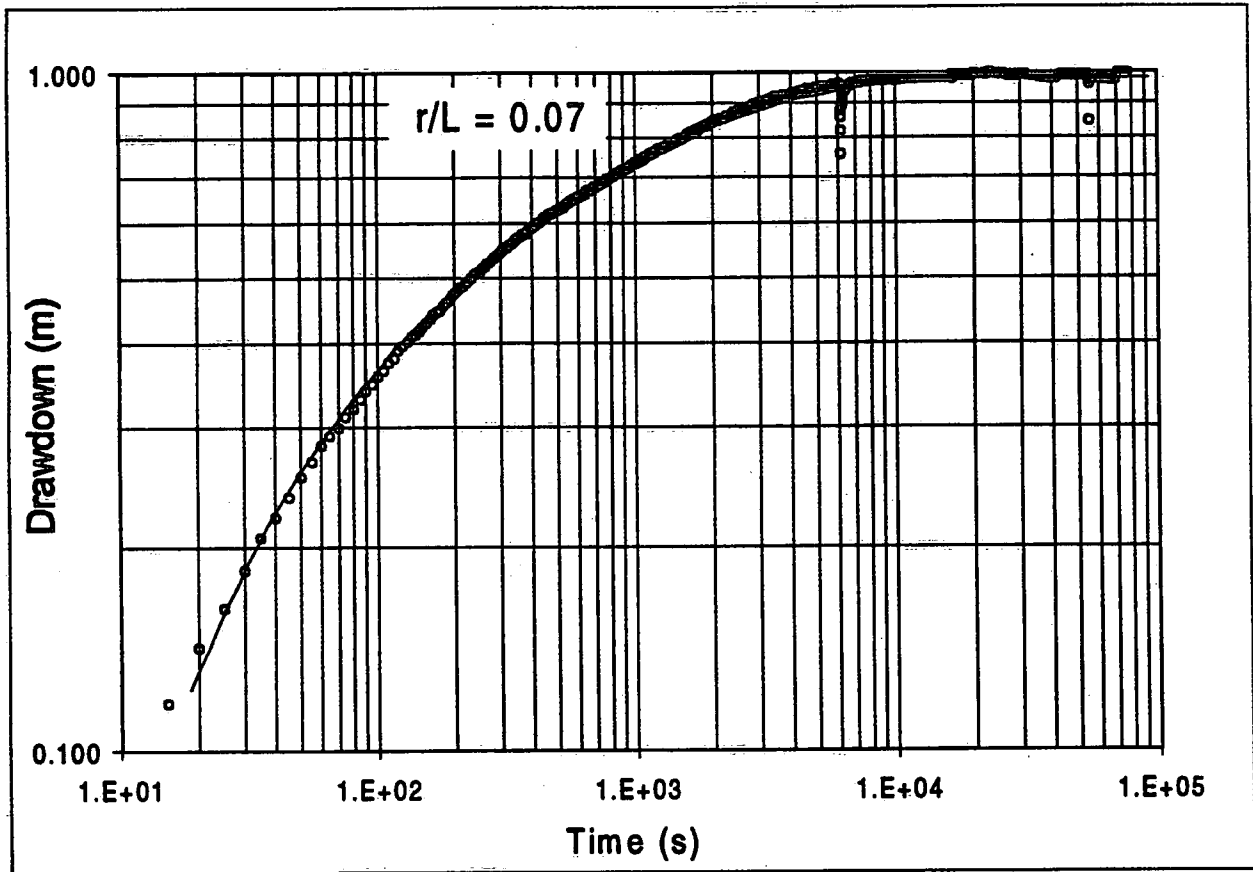


Figure D5 Pumping test 1: Response and type curve match in borehole 57 to pumping in borehole 56.

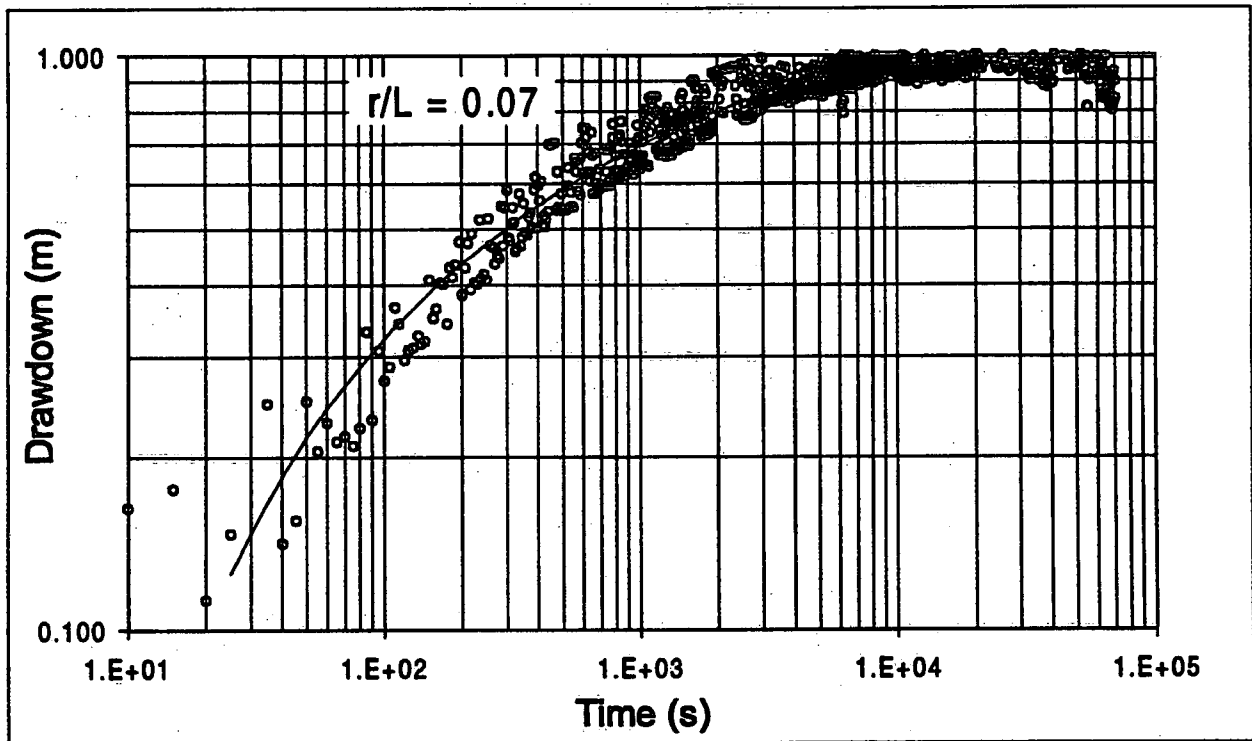


Figure D6 Pumping test 1: Response and type curve match in borehole 58 to pumping in borehole 56.

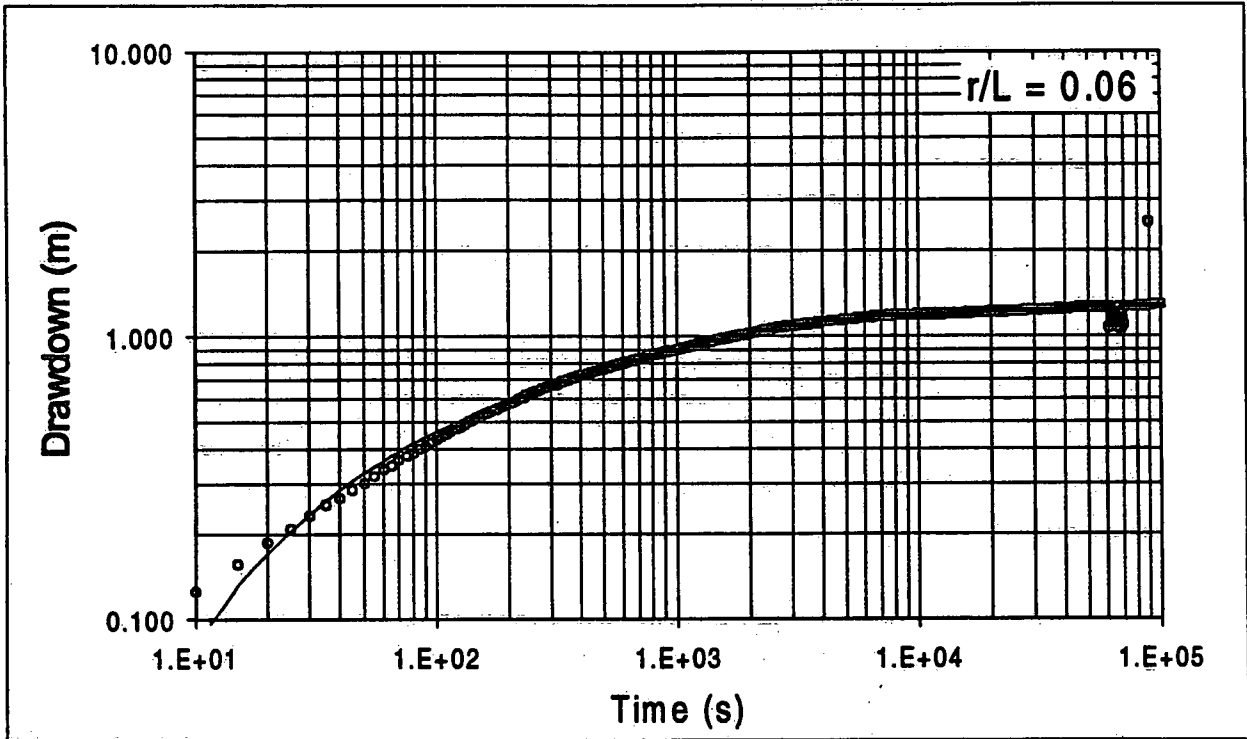


Figure D7 Pumping test 2: Response and type curve match in borehole 59 to pumping in borehole 58.

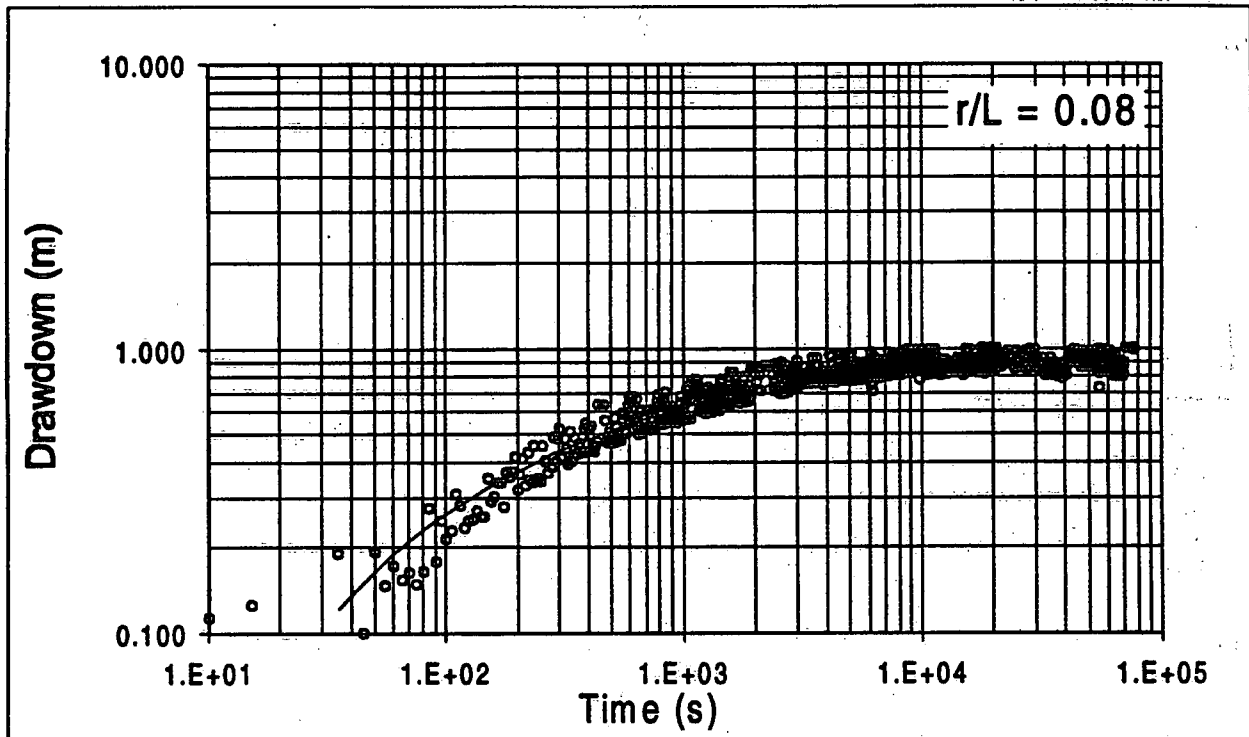


Figure D8 Pumping test 1: Response and type curve match in borehole 59 to pumping in borehole 56.

12529

**DATE DUE
REMINDER**

25 FEB 2004

**Please do not remove
this date due slip.**